DEVELOPMENT OF AN OPTIMIZED DELIVERY METHOD OF SURFACE IRRADIATION USING AN ELECTRON BEAM

A Dissertation

by

MATTHEW BLAKE FITZMAURICE

Submitted to the Office of Graduate and Professional Studies of
Texas A&M University
in partial fulfillment of the requirements for the degree of

DOCTOR OF PHILOSOPHY

Chair of Committee,	Leslie A. Braby
Committee Members,	John R. Ford
	John W. Poston, Sr.
	Rosana G. Moreira
Head of Department,	Yassin A Hassan

May 2015

Major Subject: Nuclear Engineering

ABSTRACT

Food safety has long been a nationwide concern. In 2011 alone, 731 outbreaks of foodborne illness were documented in the United States. These outbreaks resulted in over 13,000 illnesses, almost 900 people hospitalized and 45 deaths. The FDA has approved food irradiation as one method to combat foodborne illness.

This research aims to develop a method, using electron scattering, to reduce the maximum to minimum dose ratio over the surface of a cantaloupe while also maintaining the electron penetration depth sufficient to provide an adequate dose throughout the rind. This research utilized a set of Monte Carlo N-Particle eXtended (MCNPX) decks to calculate the dose received by a cantaloupe passing under a 10 MeV electron beam. The decks also included metallic reflectors, to scatter the electron beam, to achieve a more uniform surface dose distribution. Dose distributions as a function of surface position and depth were obtained, and a surface dose map and dose depth curves were generated for each reflector plate model.

It was shown that the surface dose ratio can be reduced from 83505 to 2.176 with the use of metallic reflectors. Additionally, the scattered electrons have sufficient energy to provide adequate dose throughout the rind to combat bacteria internalization without delivering a dose that might damage the texture of the interior of the cantaloupe. This technique could be easily extended to irradiate the surface of other medium-sized objects.

DEDICATION

To my family, for all the support and encouragement over the years. Also to all the friends along the way that have made the journey a memorable one.

ACKNOWLEDGEMENTS

I would like to thank my committee chair, Dr. Leslie Braby for all his time, help, and patience in doing this research. His comments and suggestions have aided this work along the way to completion. Thanks are also due to my committee members, Drs John Ford, John Poston, and Rosana Moreira, for their additional guidance and support. Finally, thanks to my friends and colleagues for making my time at Texas A&M University a great experience.

NOMENCLATURE

CDC	Centers for Disease Control
DNA	Deoxyribonucleic Acid
DSB	Double Strand Breaks
EGS	Electron Gamma Shower
ETRAN	Electron Transport through Extended Media
GEANT	Geometry and Tracking
ITS	Integrated Tiger Series
LET	Linear Energy Transfer
LINAC	Linear Accelerators
MCNP	Monte Carlo N-Particle
MCNPX	Monte Carlo N-Particle Extended
PENELOPE	Penetration and Energy Loss of Positrons and Electrons
RNA	Ribonucleic Acid
ROS	Reactive Oxygen Species
SSB	Single Strand Breaks
USDA	United States Department of Agriculture
WHO	World Health Organization
Z	Atomic Number

TABLE OF CONTENTS

LIST OF FIGURES

LIST OF TABLES

1. INTRODUCTION

1.A. Motivation

Food safety has long been a nationwide concern and in recent years this concern has intensified as the number of deaths and hospitalizations from foodborne illness have risen. In 2011 alone, 731 outbreaks of foodborne illness were documented in the United States. These outbreaks resulted in over 13,000 illnesses, almost 900 hospitalizations and 45 deaths (CDC, 2013). 2011 also saw the second most deadly foodborne illness outbreak when 33 people died from eating cantaloupes infected with listeria (Allen, 2011). These numbers represent only the reported cases of foodborne illness; in total, the CDC estimates that each year roughly 48 million people (1 in 6 Americans) get sick, 128,000 are hospitalized, and 3000 die of foodborne diseases in the United States (CDC, 2014).

In addition to the number of people affected by foodborne illnesses, Scharff has estimated that the cost of foodborne illness in the United States is as high as $152 billion annually when considering quality-adjusted life years as well as the illnesses' impact on daily activities (2010). According to other studies, fourteen major pathogens account for $14.1-16.3 billion direct cost-of-illness estimate for non-fatal outcomes (Hoffmann et al, 2012; Scharff, 2012). These fourteen pathogens account for over 95% of the illnesses, hospitalizations, and deaths caused by all 31 pathogens identified by the CDC.

1.B. Present Status of the Question

Currently, the USDA allows the irradiation of fresh or frozen pork, poultry, shellfish and mollusks; refrigerated or frozen beef; fresh eggs; dry or dehydrated spices; and seeds used for sprouting; for microbial disinfection, either with gamma or electron beam (e-beam) sources. Additionally, irradiation is allowed for delayed maturation and arthropod disinfection of fruits and vegetables. The USDA approved the use of irradiation after a thorough scientific review of a substantial number of studies on the effects of irradiation on a wide variety of products. This included the examination of the chemical effects of irradiation on food, the impact on nutrient content of irradiated products, and the potential toxicity concerns and effects on microorganisms in or on irradiated products. The FDA concluded that irradiation can safely and effectively reduce disease-causing microbes and that it does not compromise the nutritional quality of treated products. Additionally, a study by the World Health Organization (1999) on food irradiation concluded that "food irradiated to any dose appropriate to achieve the intended technological objective is both safe to consume and nutritionally adequate." Furthermore, the Codex Alimentarius Commission, American Medical Association, Health Canada, European Commission's Scientific Committee on Food, and various other health organizations have endorsed the process.

Many other agencies have also reached the same conclusions, even though numerous volatile compounds have been isolated from irradiated products (Smith and Pillai, 2004; Sommers, 2013). The USDA's approval for use of food irradiation technology comes from the observation that the vast majority (more than 70%) of the

radiolytic volatile compounds found in irradiated foods are hydrocarbons. These compounds also commonly appear in unprocessed and thermally processed foods; additionally, the levels produced create little concern for health (Smith and Pillai, 2004). In addition to volatile compound production, irradiation reduces vitamin levels in treated food. While measurable, these reductions are not substantial or concerning. The most noticeable and likely adverse effect of irradiation is the production of undesirable odors, flavors, and texture changes (WHO, 1999). Although minor, these adverse effects can be minimized—in the case of cantaloupe—by reducing the dose to the interior of the fruit and concentrating it on the surface.

1.C. Objective

The objective of this research is to develop a method, using electron scattering, to reduce the maximum to minimum dose ratio over the surface of a cantaloupe while also maintaining the electron penetration depth sufficient to provide adequate dose throughout the rind. To accomplish this objective, a set of Monte Carlo N-Particle extended (MCNPX) decks were used to calculate the dose received by a cantaloupe passing under a 10 MeV electron beam, dose distributions as a function of surface position and depth were obtained, and a 3D spherical mesh was centered on the cantaloupe to determine the dose in each voxel. First, an initial model of only the cantaloupe and electron beam was run. After the initial run, a basic metallic reflector plate setup was added to the model. After running the model with reflectors, a 3D dose map of both single and double beam irradiation was created and evaluated to determine

how to alter the design, which allowed for a more uniform irradiation of the cantaloupe. The shape, positioning, and material of the reflective plates were all altered to further optimize the dose uniformity on the surface of the cantaloupe by shielding hot spots from the electron beam while reflecting electrons toward cold spots. To determine the optimal design, the variation in maximum and minimum surface dose was calculated from the MCNPX mesh tally. The dose map and variation were compared for each design to better develop the next reflector plate setup. Lastly, to determine the electron penetration and confirm the dose is concentrated on the surface, a dose-depth curve was created at representative surface locations for each design.

2. BACKGROUND

2.A. Food Irradiation Biology

The primary method of inactivating microorganisms with radiation is by damaging the deoxyribonucleic acid (DNA) and/or ribonucleic acid (RNA) of the microorganism. Alteration or destruction of a DNA/RNA molecule, which contains genetic information necessary for self-replication and cell division, can cause the cell to lose its ability to produce viable daughters. Other methods include damaging other cellular components: membranes, enzymes, etc.; however, many of these components can be quickly synthesized and replaced. Both of these types of damage can be caused by direct or indirect effects.

The deposition of energy in the target biological molecule causes the direct effects whereas interaction with free radicals and toxic oxygen derivatives, or Reactive Oxygen Species (ROS), formed by the radiation causes the indirect effects. Low linear energy transfer (LET) radiation, such as gamma and electrons, will more than likely generate direct effects; however, both direct and indirect effects play an important role in irradiation. At lower doses, the indirect effects are more important, while at higher doses direct effects are more important. This occurs because more ROS gets created closer together at higher doses, which results in the ROS reacting with each other rather than reacting with vital cell components.

DNA has a diameter of approximately 20 Å with the base pairs stacked 3.4 Å apart. (Nelson & Cox, 2005) Due to the large size of DNA, it is the easiest to damage by

direct effects. This damage comes in many forms: most often Single (SSB) and Double Strand Breaks (DSB) as well as crosslinks from being directly hit by the radiation. Each strand of the double-helical DNA complements its opposing strand and can be used as a template for DNA replication. When at least one strand still remains intact, as in a SSB, the DNA can carry out the repair process with high fidelity. Conversely, a DSB results in a loss of some genetic information. Therefore, DSBs are the most crucial DNA lesion that determines the fate of the cell. (Alpen, 1998) Many methods do exist to repair DNA damage and the ability of any organism to accommodate these damages depends largely on the cell's innate DNA repair systems. When these methods fail, the unrepaired breaks often result in the reproductive death of the cell.

The ROS formed during irradiation damage the DNA/RNA by causing SSBs, creating abasic sites, adding to the DNA, or creating lesions (for example 8-oxo-2′deoxyguanosine). These forms of DNA damage affect the cell in the same manner as direct damage to the DNA; however, SSBs are more likely to be repaired correctly than DSBs and crosslinks.

2.A.1. Bacteria Internalization

While most bacteria reside on the surface of a food product, the bacteria can internalize themselves. Bacteria internalization occurs when bacteria enter into the flesh of a product; it can become internalized through multiple pathways, most of which occur before a food product is harvested. It can enter fruits and vegetables through stomata, stem scar, calyx, abiotic wounds, or phyropathogenic penetrations. Additionally, the

roots of a plant can take up contaminated water. After the produce has been harvested, bacteria can penetrate the surface of produce through soaking it in contaminated water or by entering through cuts or punctures. Bacteria internalization poses a problem greater than surface contamination because it is very difficult to remove through chemical means and is only effectively removed through heat or radiation treatment. Of the two viable methods, heat degrades the quality of the produce, while at low doses radiation does not.

Cantaloupes have a low probability of root uptake and soil transport of bacteria. Bacteria can also internalize through openings in the rind (cuts, fissures, ground spot, stem scar), prolonged submersion, or soft rot. These methods also have a low probability of occurrence and can be detected during packing (Lopez-Velasco et al, 2012). Experiments soaking cantaloupes in contaminated water have shown that when internalization happens, bacteria can be internalized up to 5mm (Suslow, 2004). This short internalization depth is within the electron beam penetration depth.

2.B. Food Irradiation Technologies

Food irradiation is a non-thermal treatment used to enhance food safety and preservation through the use of either gamma (γ) rays, X-rays, or an electron beam to render the microbial population unable to grow and reproduce. Gamma and X-rays are both types of electromagnetic radiation called photons; they are used to irradiate relatively thick and dense foods to achieve acceptable dose uniformity since they have greater penetrating capability than electrons. In contrast, electron beams have the ability

to penetrate the product to a limited depth depending on the density and characteristics of the product. Beams of 1-10 MeV electrons have less penetration power, higher efficiency, and relatively lower cost than gamma rays, and provide an excellent alternative for fruit and vegetable surface pasteurization compared to gamma rays.

Gamma rays are produced by large radioactive sources such as ^{60}Co and ^{137}Cs while electron or X-ray beams come from electron accelerator systems to deliver ionizing doses to food products. An electron accelerator system consists of two essential features: an electron generator and accelerator. The electron gun generates electrons by raising a cathode to a sufficiently high temperature to result in electrons being emitted from the surface. Two categories of electron accelerators exist: utilizing direct methods and radio frequency methods. Direct acceleration methods establish a large potential difference by physically transferring charge to a high voltage terminal. Radio frequency linear accelerators (LINAC) use electric fields alternating at radio frequencies to accelerate particles as a substitute for high voltage acceleration (Humphries, 1986). This makes LINACs more powerful and efficient than electrostatic accelerators. Upon entering the interior of a hollow cylindrical electrode, electrons drift in a field-free tube, the polarity of the voltage in the tube is reversed, and the electrons are then accelerated as they cross the gap between successive tubes. Figure 2.1 shows the principle of a linear accelerator. A typical 10 MeV LINAC, such as the one at the National Electron Beam Research facility, produces beam currents of 10 mA, which gives a beam power of 100 kW.

X-rays are generated using an electron accelerator to propel the particles into a metallic target, generating bremsstrahlung photons. The X-ray energy production increases with the kinetic energy of the electron and the atomic number (Z) of the target, making it desirable to use a high Z material with good thermal conductivity and a high melting point; such materials include tantalum, tungsten, or gold.

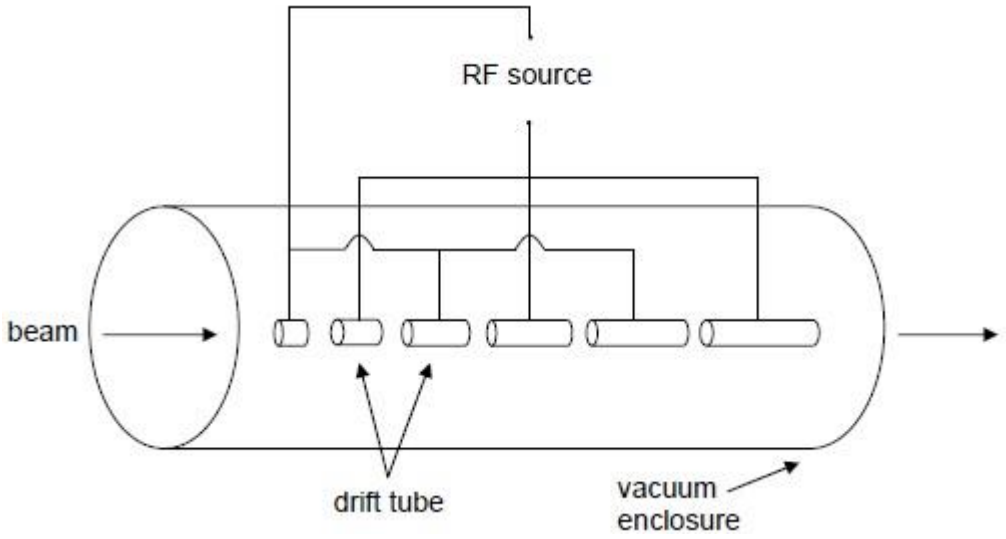

Figure 2.1: Principles of a LINAC (Hellborg, 2005).

2.C. Election Interaction & Scattering

As electrons pass through matter, they undergo collisions with atomic electrons and nuclei, each of which results in many possible energy losses and angular changes (Evans, 1955). If the change in angle is greater than 90 degrees, the electron is said to be backscattered or reflected. An electron can be scattered by various mechanisms; the most common mechanism of interaction is when the incident electron interacts with

electrons in the material. On average, this type of collision results in the majority of energy lost by electrons, and causes the ejection of the target electron from its atomic orbitals. The ejected electrons, known as secondary electrons or delta rays, can also undergo collisions. This can result in any of the secondary electrons, as well as the primary, being scattered out of the material. This interaction method generally results in a production of multiple lower energy electrons after multiple collisions. This method can also result in the primary electron losing all its energy; however, since one electron cannot be differentiated from another, the electron with more energy is considered the primary. This means at most the primary can lose one half of its energy. The second method of electron reflection is by the incident electron directly hitting a nucleus in the material; this results in energy transfer, an appreciable alteration in trajectory, and the possible producing of x-ray radiation. While much less probable, this method of interaction generally results in the electron retaining most of its energy and getting reflected after only one collision. Both of these methods can be elastic in nature, but are more commonly inelastic and result in bremsstrahlung x-rays being produced. The physics and cross sections for single as well as multiple scattering events are represented mathematical by probability functions. These probability functions are well sampled and followed in MCNPX.

2.C.1. Electron Dosimetry

Most of the energy lost by an electron while it passes through matter is transferred to other electrons; this is referred to as collision energy transfer. Some of the

energy lost is converted to bremsstrahlung; this is also known as radiative energy transfer. The average rate of energy transferred per unit path length of an electron is quantified by its stopping power or LET. The stopping power depends on the electron's kinetic energy and the atomic number of the material it interacts with. The total stopping power equals the sum of the collision and radiative stopping powers (Attix, 1986). The collision stopping power is the rate of energy loss resulting from soft collisions, energy transferred by columbic forces causing interaction, and hard collisions (one electron directly hitting another), and the radiative stopping power is the rate of energy loss resulting from radiative processes, almost exclusively bremsstrahlung.

While easily calculable, LET is hard to directly measure. Instead, the absorbed dose is the primary quantity used in dosimetry due to its easy measurability. Absorbed dose is defined as the energy absorbed per mass from any kind of ionizing radiation. The SI unit for absorbed dose is the gray (Gy) where one Gy represents one joule deposited per kilogram of material. Additionally, the dose rate can also be quantified and expressed as the dose per unit time.

The absorbed dose is not homogenous throughout a target such as an irradiated food product. Dose uniformity, or the ratio between the maximum and the minimum absorbed dose, is an important quantity to control for food irradiation purposes; this ratio is often desired to be low. The dose distribution and uniformity can be obtained empirically by the dose-mapping technique; Monte Carlo simulations are one method to calculate the dose distribution inside the food product.

2.D. Electron Reflectors

Plates of almost any material can be used to reflect electrons. Most of the incident electron beam energy can be deposited in the plates, conservatively all 100 kW of incident beam energy, so the plate material should have good thermal conductivity. Because complex shapes may be required, it should also be easily worked and shaped. Also the Z value and density affect x-ray production and plate thickness. Thermal conductivity is important because the plates will receive considerable energy from the electron beam, therefore heating the plates up. This heat must be removed or it will be dissipated by infrared radiation and air convection and the plates will reach a high temperature. Table 2.1 shows the Z_{eff}, density, thermal conductivity, melting point, and heat capacity of various materials that could be used to create electron reflectors.

The data in Table 2.1 shows that graphite and ceramics are poor thermal conductors, but have high melting points and heat capacities. This means that they would only be able to withstand the heat generated by short radiation pulses of the electron beam, while making it hard to remove the heat through an active cooling system. Additionally, these materials are all more difficult to shape than a metal. The table also shows that the metals all vary in their thermal properties. Aluminum, copper, silver, gold, and tungsten provide acceptable thermal conductivity to allow for heat removal. Of these, aluminum has the lowest melting point, but its heat capacitance allows it to absorb more heat energy than the other metals. Copper provides both a high melting point and large heat capacitance. Silver, gold, and tungsten have high melting points—extremely high in the case of tungsten—but all have low heat capacities. Of these five metals, gold

is far too expensive to be used, silver and tungsten are both moderately priced, but copper is inexpensive and aluminum is very inexpensive. Aluminum, copper, silver, and gold are all easy to shape, while tungsten is difficult.

Table 2.1: Material properties of selected reflector materials.

Material Type	Material	Zeff	Density	Thermal Conductivity	Melting Point	Heat Capacity
			g/cm3	W/m*C	C	J/kg*C
Metals	Aluminum	13	2.7	237	660.323	790
	Brass - Red	38.01	8.75	1.6	1000	380
	Brass - Yellow	29.34	8.47	1.2	930	380
	Bronze (68% Cu, 32% Zn)	29.33	8.4	110	~ 950	435
	Copper	29	8.96	401	1084.62	385
	Gold	79	19.3	317	1064.18	129
	Iron	26	7.87	80.2	1538	450
	Lead	82	11.3	35.3	327.462	129
	Nickel	28	8.9	90.7	1455	445
	Silver	47	10.5	429	961.78	235
	SS-302	25.61	7.9	16.2	~1400	500
	Tin	50	7.265	66.6	231.928	217
	Titanium	22	4.506	21.9	1670	736
	Tungsten	74	19.3	174	3414	132
	Zinc	30	7.14	116	419.527	389
Carbon	Graphite - Parallel	6	1.7	19.5	5530	715
	Graphite - Perpendicular	6	1.7	0.057	5530	715
Ceramics	Alumina	10.57	3.8	30	2072	779
	Concrete	9.527	2.3	0.8	> 1000	880
	Glass - Borosilicate	10.29	2.23	1	~ 1650	750
	Rock - Granite	11.55	2.8	2.2	> 900	790
	Rock - Limestone	11.80	2.0	1	> 825	851
	Titanium Dioxide - Parallel	15.65	4.26	13	1843	168
	Titanium Dioxide - Perpendicular	15.65	4.26	9	1843	168

2.E. Computational Tools

Computational tools were used to aid in this research; relative to experimental methods, they allowed for the extension of the scope and complexity of the problems that can be addressed. The two computational tools used for this research were MCNPX and the MatLab® computing environment. These two tools have the capacity to handle extremely large data sets and solve complex problems with uncertainties in a short amount of time.

2.E.1. Monte Carlo Methods

The Monte Carlo method is a technique of numerical analysis that employs random sampling to solve a mathematical problem (Turner, 2007). It simulates the paths of particles and estimates dose by summing and averaging the histories of many particles.

There are several codes available to calculate the transport of electrons and photons: Electron Transport through extended media (ETRAN), Integrated Tiger Series (ITS), Electron Gamma Shower (EGS), Monte Carlo N-Particle (MCNP), Penetration and Energy Loss of Positrons and Electrons (PENELOPE), Geometry and Tracking (GEANT).

MCNPX, a version of MCNP, was used because it allowed for a complex, 3D model of the actual system. This included the use of a distributed source term along with particle tallies over multiple volumes. Additionally, MCNPX has built-in access to tens of thousands of continuous-energy nuclear and atomic data cross sections, which allows

necessary information to be obtained for a variety of inputs. MCNPX also allows for a large number of variance reduction methods that when employed can lower the computational time and improve relative errors (MCNP X-5 Monte Carlo Team, 2003). For this research, it was possible to model a cantaloupe, e-beam, and set of reflectors and easily modify the reflectors. This model then provided the dose in each voxel of the cantaloupe.

2.E.2. MatLab®

MatLab®, by MathWorks, was used to manipulate the large complex matrices of data and plot the relevant data points. For this research MatLab® made it possible to input the voxel dose values from MCNPX and output data plots. The two types of plots used for this research were 3D surface plots of the dose, and line plots of the voxel dose versus depth along various axes.

3. EXPERIMENTS AND SIMULATIONS

3.A. Procedure

The objective of this research is to develop a method, using electron reflection, to reduce the surface dose ratio for a cantaloupe while also maintaining the electron penetration depth and adequate product flow through the system. This method required using MCNPX to model a cantaloupe passing under a 10 MeV electron beam and tallying the dose received by the cantaloupe. After a control run--a cantaloupe and beam alone—a basic metallic reflector plate setup was added to the model. The designs of these plates were then altered in many ways, which included the thickness, size, shape, positioning, and material of the reflective plates as well as adding holes and/or dimples to the plates and changing the shape, size and angle of the holes and dimples.

After each reflector plate design model was run, a surface dose map and set of dose depth curves were created. Additionally, the surface dose uniformity ratio was calculated. These three tools were used to compare reflector designs and determine how to change the design in the hope of achieving an optimal one. The final goal is to achieve a dose uniformity ratio of three or less.

3.B. Cantaloupe Model for MCNPX

To begin, an MCNPX control deck was created; this deck modeled a cantaloupe passing under a 10 MeV electron beam and measured the absorbed dose. Three cantaloupes were modeled as 15 cm diameter spheres of water with a smooth surface

with a 15 cm gap between each. A smooth surface sphere model is used to minimize computer time requirements. The electron beam was initially modeled as a 70 cm wide by 2 cm deep beam, which centered over the conveyor belt. To again minimize the computer time, the initial control deck extended the length of the beam to 62 cm to simulate the cantaloupe passing under the beam, instead of running the deck at multiple steps. Figure 3.1 gives a graphical representation of this assumption.

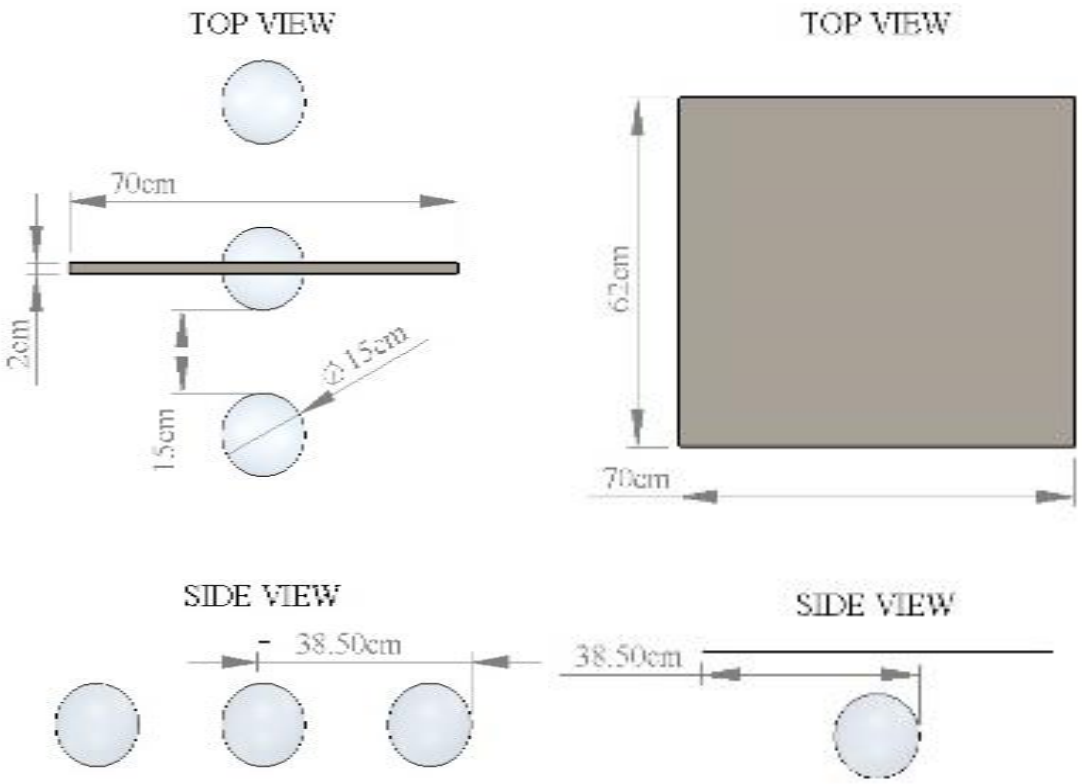

Figure 3.1. A graphical representation of the ebeam extension. Left shows the actual configuration, right shows the configuration for optimized computing time.

To determine the absorbed dose in the cantaloupe, a 3D spherical mesh was centered on the cantaloupe. The mesh was set to create voxel sizes of 1 degree by 1

degree by 0.535714 cm. A PEDEP mesh tally was used to record the average energy deposition per unit volume (MeV/cm^3/source particle). This initial model was run assuming a single beam irradiation configuration resulting in multiple surface voxels receiving a zero dose. For this reason, it was decided to use a double beam irradiation configuration for the control case. These new dose values were calculated using MatLab® to combine the dose received from the upward and downward beams. For the double beam configuration, the maximum dose was found to be 1.55×10^{-21} Gy/source particle and the minimum dose 1.86×10^{-26} Gy/source particle.

3.C. Reflector Models

After the initial control model was created and run, a basic metallic reflector plate setup was added to the model. The simplest set or reflectors consisted of four stainless steel plates: a flat, solid, rectangle above and below; and an angled, solid, rectangle on either side, parallel to the conveyor (see Figure 3.1.) In addition to the plates being added to the deck, two more changes were made to simulate move under an e-beam. The first change was returning the e-beam dimensions to 70 cm wide by 2 cm deep centered over the conveyor belt. The simplification of extending the beam was not valid in the case of reflectors, as both the beam and reflectors remain stationary while the cantaloupe moves. Furthermore, the deck had to simulate moving by using five discrete stops for the cantaloupe: directly under the beam, ±15 cm offset from the center of the beam, and ±30 cm offset from the center of the beam. To achieve the final absorbed dose values, the sum of all five stops was found using MatLab®. Additionally,

the absorbed dose from a single beam, a pure double beam, and a double beam with a 90 degree rotation of the cantaloupe about its vertical axis between the two beam locations was calculated. As with the control MCNPX deck results, the dose from the two double beam configurations was determined through a simple summation in MatLab®. Figure 3.2 shows the initial reflector plate design (Design A), e-beams, and three cantaloupes traveling along the conveyor belt.

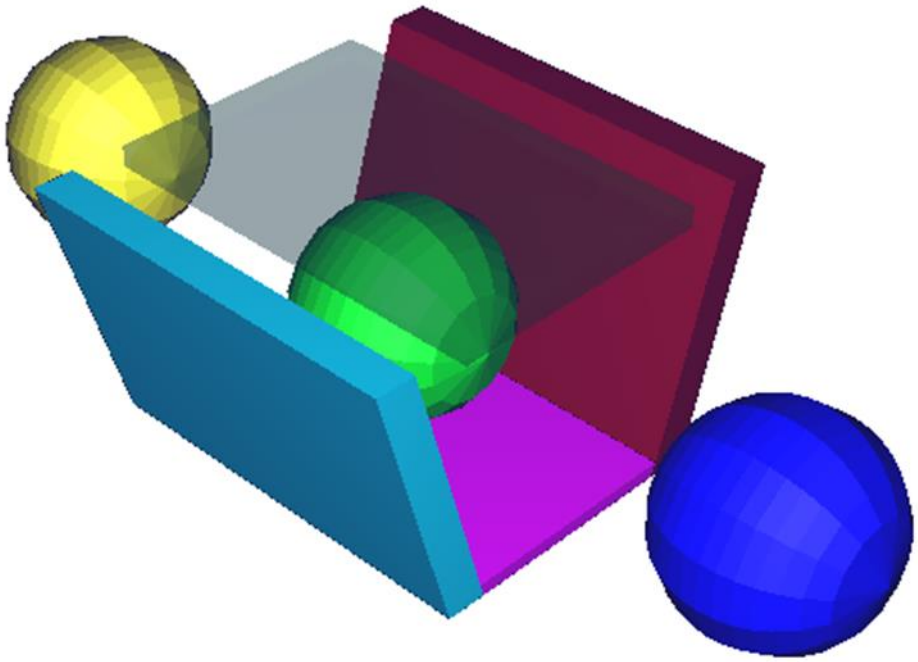

Figure 3.2. A model of initial reflector plate design (Design A), and three cantaloupes traveling along the conveyor belt.

After the first set of reflectors was modeled, the reflectors were altered. Initially, the reflector plate design was changed by making the upper and lower plates thicker with a stair step design. The design of the reflective plates was changed and simulated

multiple times; the various changes included the thickness, size, shape, positioning, and material of the reflective plates as well as adding holes and/or dimples to the plates and changing the shape, size and angle of the holes and dimples. The reasoning behind each change in design can be found in Appendix A. A list of the designs modeled and simulated along with the characteristics of each is shown in Table 3.1.

Each new reflector plate design was created based upon the dose uniformity of the previous designs. The changes were made with the intent to minimize hotspots while directing particles towards the low-dose areas.

In addition to changing the reflector plate design, after design G, it was decided to increase the number of discrete stops at which the cantaloupe's dose is calculated to 15. The ten additional stops were: ±2.5 cm, ±5 cm, ±7.5 cm, ±10 cm, and ±12.5 cm offset from the center of the beam. With the new change in distance between the stops, a simple summation was no longer valid. Instead, a weighted summation was used; this gave each stop a weight equal to the distance between the midpoints of the following and previous stops.

In an effort to determine the reflector material's effect on the reflector design, the material was changed for certain models. The assumption was that the material affected the optimal thickness of the upper plate. Testing showed that for the most favorable design, the density of the material was inversely proportional to the upper plate's thickness.

Table 3.1. Reflective plate design characteristics.

Design	Material	Upper Plate					Side Plate					
		Design	Thickness	Width	Length	Holes	Design	Upper Slope	Lower Slope	Thickness	Length	Dimples
			cm	cm	cm	cm				cm	cm	
A	SS-302	slab	1	15	4	N/A	Constant	2	N/A	1	30	No
B	SS-302	3 steps	1	15, 10, 5	4	N/A	Constant	2	N/A	1	30	No
C	SS-302	2 steps	1	32	4, 2	N/A	Constant	2	N/A	1	30	No
D	SS-302	2 steps	1	15	30, 2	N/A	Constant	2	N/A	1	30	No
E	SS-302	2 steps	1	20	30, 4	.176777	Constant	2	N/A	1	30	No
F	SS-302	2 steps	2, 1	20	30, 4	.176777	Constant	2	N/A	1	30	No
G	SS-302	slab	1	20	30	.176777	Constant	2	N/A	1	30	No
H	SS-302	slab	1	20	30	.176777	Constant	3.33	N/A	1	30	No
I	SS-302	slab	0.5	20	30	.176777	Constant	3.33	N/A	1	30	No
J	SS-302	slab	0.5	20	30	.125	Constant	3.33	N/A	1	30	No
K	SS-302	slab	0.5	20	30	.176777	Varied	10	3.33	1	30	No
L	SS-302	slab	0.5	20	30	.176777	Constant	2	N/A	1	30	No
M	Al	slab	1.5	20	30	.176777	Constant	3.33	N/A	1	30	No
N	Al	slab	1.5	20	30	.176777	Constant	3.33	N/A	3	30	No
O	Pb	slab (Al)	0.36	20	30	.176777	Constant	3.33	N/A	1	30	No
P	Pb	slab (Al)	0.18	20	30	.176777	Constant	3.33	N/A	1	30	No
Q	Al	slab	1.5	20	30	.176777	Constant	3.33	N/A	3	30	Yes
R	Al	slab	2.5	20	30	.176777	Constant	3.33	N/A	3	30	Yes
S	Al	slab	1.5	20	30	.176777	Constant	2.5	N/A	3	30	Yes
T	Al	slab	2	20	30	.176777	Constant	3.33	N/A	3	30	Yes
U	Al	slab	1.5	20	30	.176777	Constant	2	N/A	3	30	Yes
V	Al	slab	1.7	20	30	.176777	Constant	3.33	N/A	3	30	Yes
W	Al	slab	1.6	20	30	.176777	Constant	3.33	N/A	3	30	Yes
X	Al	slab	1.55	20	30	.176777	Constant	3.33	N/A	3	30	Yes
Y	Al	slab	1.55	20	30	.17677	Constant	3.33	N/A	3	30	Yes

3.D. Generation of Dose Map and Dose Depth Curve

After each reflector plate design was run, a surface dose map and set of dose depth curves were created. The dose map was created by importing the 3D PEDEP mesh tally data into MatLab®. A 3D shaded surface plot was then used to show the values of the absorbed dose for the outer shell of voxels (surface voxels); then, the dose data was plotted logarithmically. As the reflector plate designs distributed the dose more effectively, the scale of the plots had to be decreased. With each decrease in plot scale, all subsequent plots were done in the current and all previous scales, including the original. This was done to allow side by side comparison of all designs, while ensuring dose uniformity discrepancies could still be seen.

Secondarily, a set of dose depth curves was plotted for each reflector plate design using the 3D PEDEP mesh tally data. MatLab® took the tally data and pulled the values for each voxel along a specific diameter chord through the cantaloupe and plotted the absorbed dose versus the distance from the center of the cantaloupe. The following chords, expressed as (r,φ,θ), were plotted: (r,0,0), (r,45,0), (r,45,45), (r,45,90), (r,45,135), (r,45,180), (r,45,225), (r,45,270), (r,45,315), (r,90,0), (r,90,45), (r,90,90), and (r,90,135), where every point on the chord has the same polar, θ, and azimuthal angle, φ. Each dose depth curve was plotted with different scales to clearly show the relative change in dose.

3.E. Surface Dose Uniformity Ratio

In addition to the surface dose maps and dose depth curves for each reflector plate design, the surface dose uniformity ratio was calculated. The surface dose uniformity ratio was calculated using the following formula:

$$R = \frac{D_{max}}{D_{min}} \qquad (3.1)$$

where: R is the variation in surface dose, or surface dose uniformity ratio, in the MCNPX model;
D_{max} is the maximum surface dose in the MCNPX model; and
D_{min} is the minimum surface dose in the MCNPX model.

Both the maximum and minimum surface doses are determined from the MCNPX mesh tally output. The variation in dose, from the MCNPX results, was calculated and compared for each design to compare the effectiveness of each design and determine the optimal one. The goal is to achieve a dose uniformity ratio of three or less, which is on par with most current large scale irradiation facilities (typically between two and three (WHO, 1999; Hallman, 2001).).

4. RESULTS AND DISCUSSION

4.A. Calculated Dose Ratio

The surface dose uniformity ratios for each reflector plate design, as well as the initial control, are given in Table 4.1.

Table 4.1: Surface dose uniformity ratios for all designs and configurations.

Design	Single Beam	Double Beam	Double Beam w/ 90° rotation about the vertical axis
Control	N/A	83505	36239
A	649.2	45.78	3349
B	1066	95.83	103.3
C	47645	17.06	23.00
D	938.3	30.79	47.86
E	619.8	55.79	38.72
F	869.4	61.46	65.69
G	510.9	38.54	50.50
H	18.73	6.217	6.296
I	44.46	2.723	2.814
J	43.65	2.850	3.128
K	50.24	3.279	3.520
L	58.31	3.339	3.477
M	138.9	2.945	3.061
N	116.3	2.917	3.047
O	22.70	3.375	3.323
P	24.20	4.105	4.381
Q	93.42	2.895	3.086
R	26.24	11.87	11.54
S	107.8	2.949	2.997
T	28.77	8.838	7.630
U	145.5	2.922	3.002
V	69.74	2.326	2.270
W	94.40	2.224	2.281
X	103.58	2.354	2.176
Y	115.02	2.558	2.535

Based on these results, double beam irradiation setups lead to better ratios in every case. Additionally, the data shows that the ratio came out below three with many different designs. Furthermore, the data show that while small changes do impact the ratio, the general reflector plate design is the most important factor present in the experimentation. The data shows that upper reflector plate thickness, side reflector plate angle, and reflector plate material are the three important characteristics, and can be optimized together. The final design, Design X, attempted to optimize the thickness of the reflector plates as if they were made from aluminum. The data supports optimized characteristics for the initial design.

4.B. Final Model

After altering the reflector plate design multiple times, a final design—Design X—was achieved; a diagram of this design can be seen in Figure 4.1. This design was comprised of an upper reflective plate of aluminum, which had dimensions of 20 cm perpendicular to the conveyor, 30 cm parallel to the conveyor, and 1.55 cm thickness. The upper plate also contained a matrix of streaming holes; the holes had a circular cross sectional radius of $32^{-1/2}$ cm, and were angled 45° through the plate.

The lower reflective plate of aluminum had dimensions of 20 cm perpendicular to the conveyor, 30 cm parallel to the conveyor, and 1 cm thickness.

The side reflective plate of aluminum had dimensions of $436^{1/2}$ cm long, 30 cm parallel to the conveyor, and $2^{-1/2}$ cm thickness. The side plates were oriented to have a slope of 10/3; in other words, the plates rose 10 cm for every 3 cm it traveled laterally.

The side plate also was finished with dimples; the dimples were created by 0.5 cm spheres 0.167 cm from the surface, making them 0.333 cm deep.

All the reflector plates were composed of pure aluminum, with a density of 2.6989 g/cm^3.

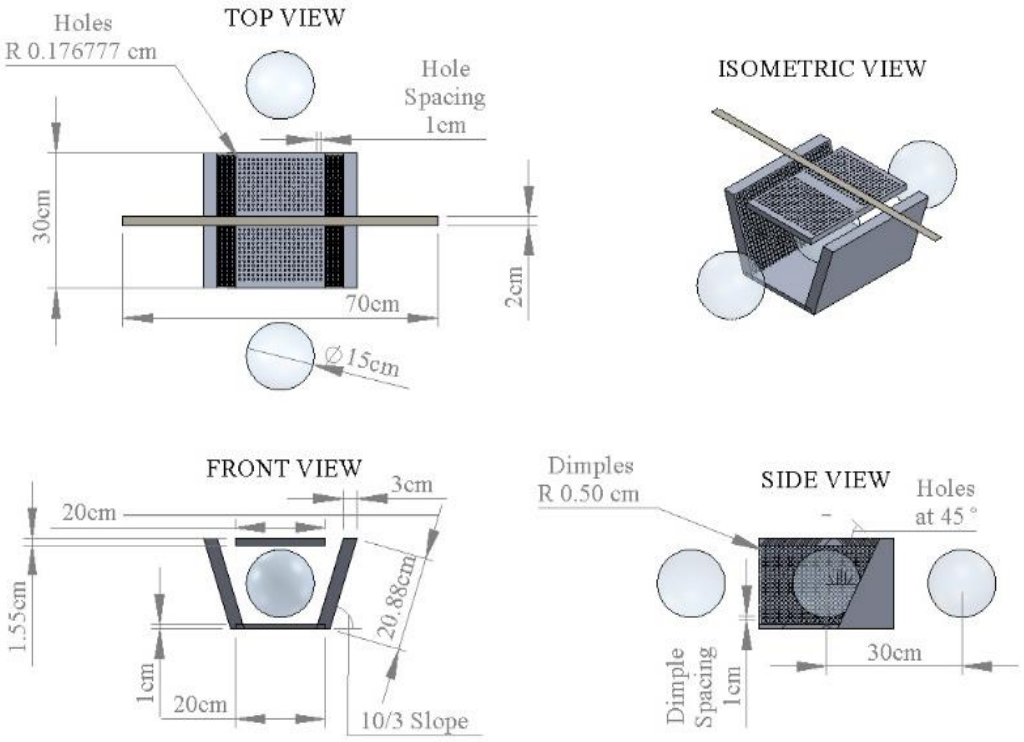

Figure 4.1. A model of Design X including the e-beam, and 3 cantaloupes traveling along the conveyor belt.

4.B.1. Dose Map

The surface dose maps generated by MatLab® for the control model and Design X are shown in Figures 4.2 - 4.5. The surface dose maps for these, every other design, and every scale zoom, can be found in Appendix B. The dose maps represent the

logarithm of the dose in each voxel expressed in MeV/g/source particle, viewed from a polar direction of (∞,θ,φ) and (∞,θ,-φ).

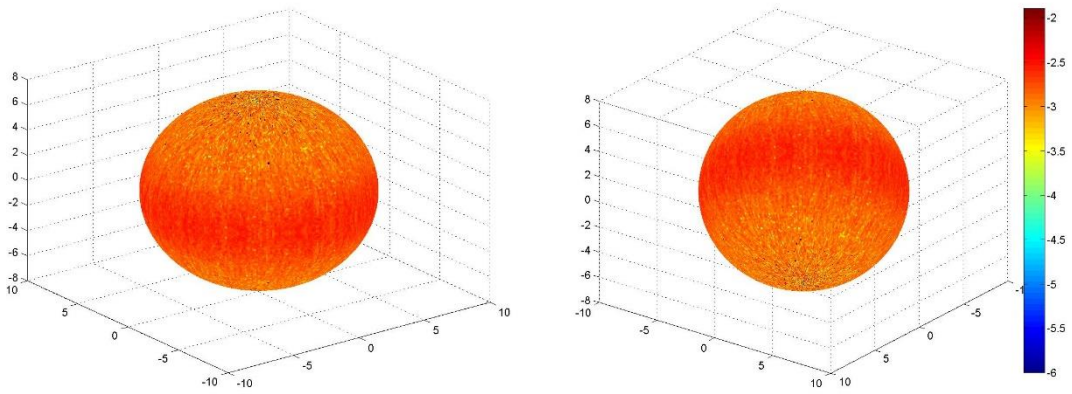

Figure 4.2: Surface dose map for control model, double beam irradiation.

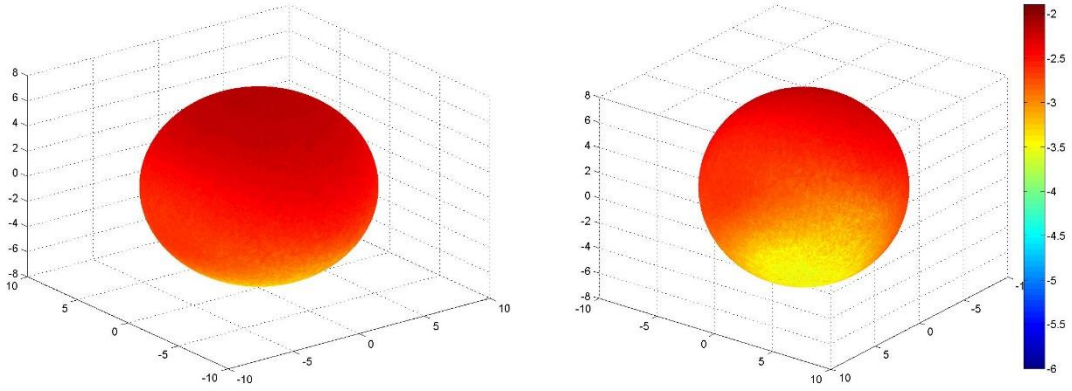

Figure 4.3: Surface dose map for Design X, single beam irradiation.

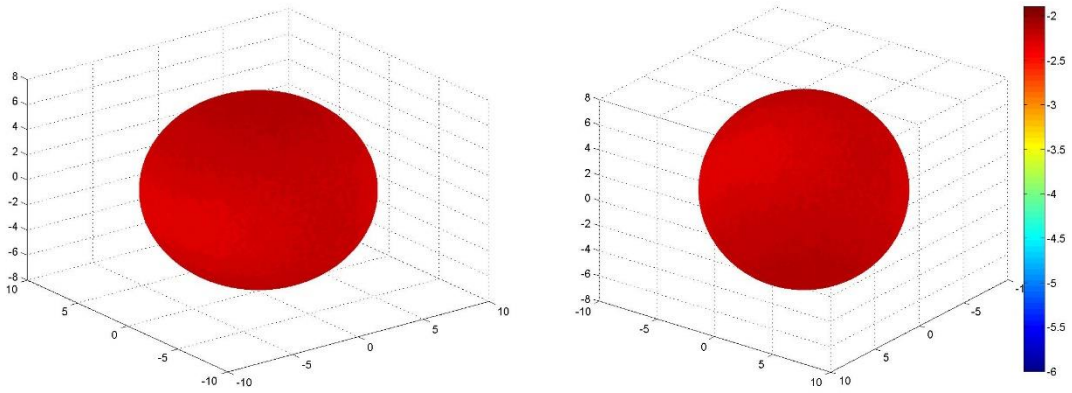

Figure 4.4: Surface dose map for Design X, double beam irradiation.

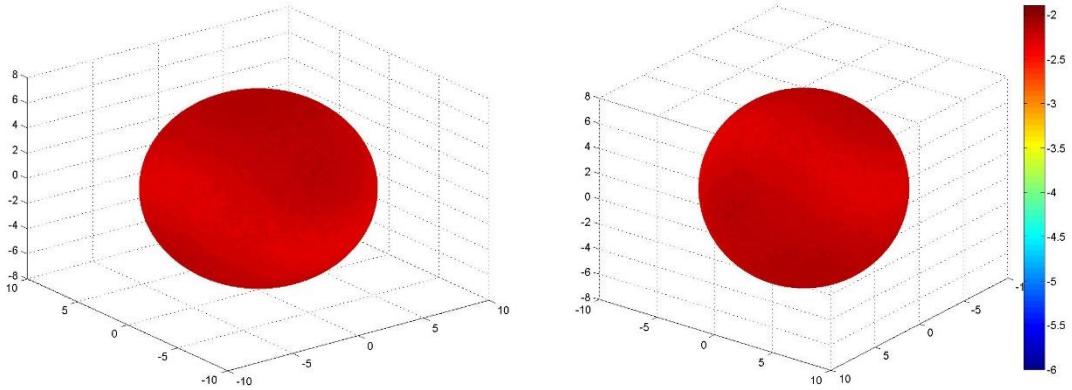

Figure 4.5: Surface dose map for Design X, double beam irradiation with a 90° rotation about the vertical axis.

It can be seen in Figures 4.2 - 4.5 that the surface dose uniformity is greatly improved. Additionally, the plots show that both double beam configurations are comparable, while they are both more uniform than the single beam.

4.B.2. Dose Depth Curve

The dose depth curves generated by MatLab® for the control model and Design X are shown in Figures 4.6 – 4.9. For simplicity, it was chosen to only include the plots

for the (r,90,0), (r,90,90), (r,0,0) chords, or the chords along the x, y, and z, axis, respectively. These plots show the dose in each voxel expressed in MeV/g/source particle for a constant φ and θ plotted against the voxel's radial value. The dose depth curves for these, every other design, and every diameter chord, can be found in Appendix C.

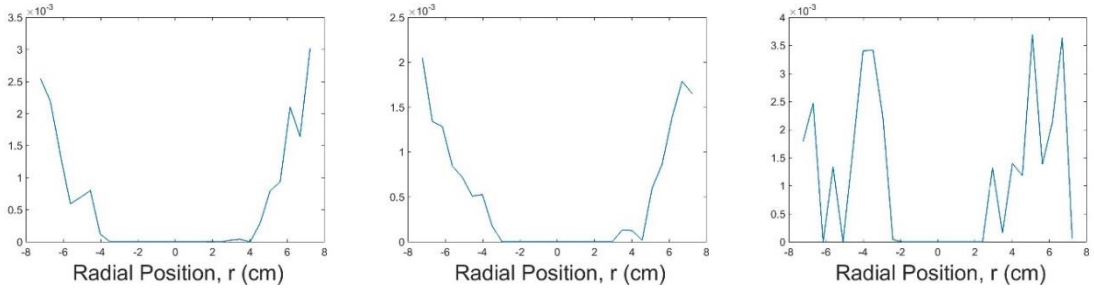

(r, φ = 90, θ = 0) (r, φ = 90, θ = 90) (r, φ = 0, θ = 0)

Figure 4.6: Dose depth curve for control model, double beam irradiation.

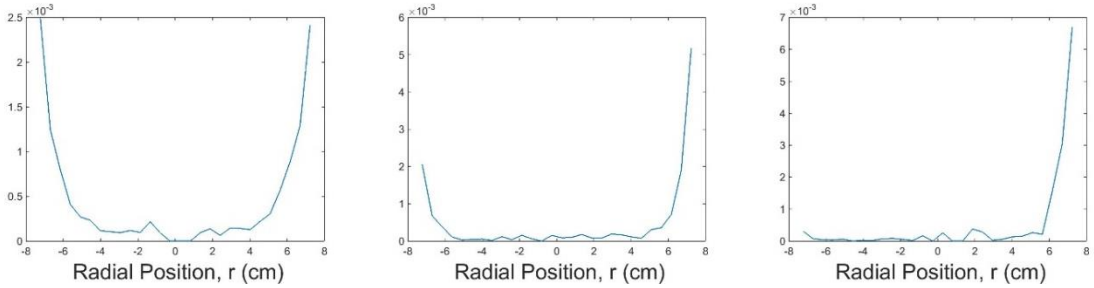

(r, φ = 90, θ = 0) (r, φ = 90, θ = 90) (r, φ = 0, θ = 0)

Figure 4.7: Dose depth curve for Design X, single beam irradiation.

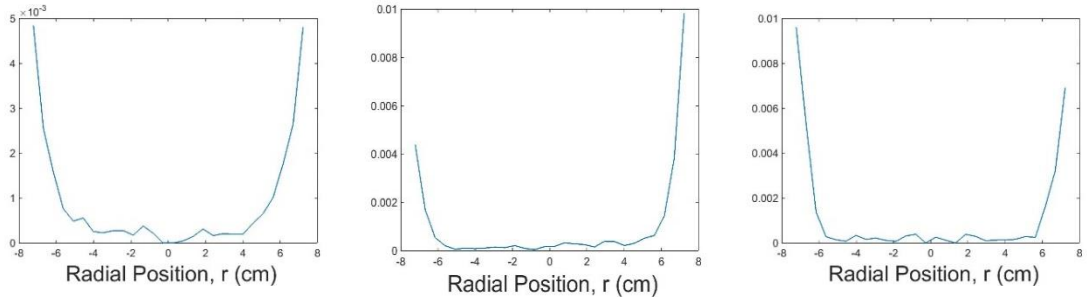

(r, φ = 90, θ = 0) (r, φ = 90, θ = 90) (r, φ = 0, θ = 0)

Figure 4.8: Dose depth curve for Design X, double beam irradiation.

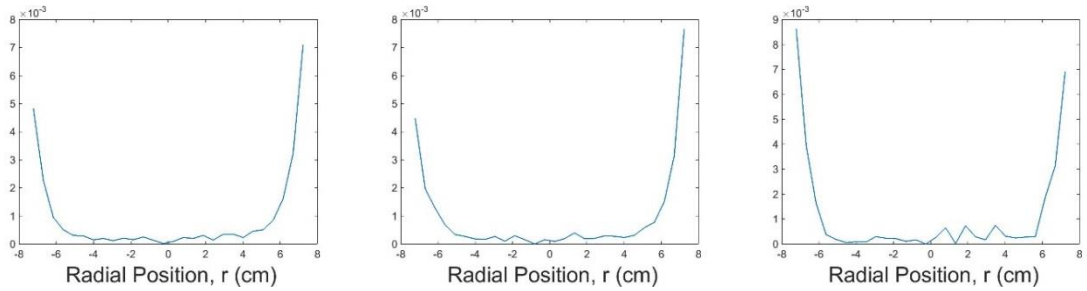

(r, φ = 90, θ = 0) (r, φ = 90, θ = 90) (r, φ = 0, θ = 0)

Figure 4.9: Dose depth curve for Design X, double beam irradiation with a 90° rotation about the vertical axis.

It can be seen in Figures 4.5 - 4.8 that the dose depth curve along the (r,90,0), (r,90,90), chords, x and y axes respectively, maintains its shape. This also shows that the electron penetration is greater than the distance bacteria have been found to internalize into cantaloupes. Additionally, the data along the (r,0,0) chord (the beam direction) develops an exponential shape like the other two directions, as opposed to peaking at a deeper penetration. This is because the top reflective plate scatters the beam, which results in almost no direct irradiation, while the control has the electrons directly hitting the cantaloupe. The direct irradiation results in a dose depth curve that resembles the energy deposition vs depth for direct electrons.

5. SUMMARY & CONCLUSIONS

5.A. Summary & Conclusions

An MCNPX deck was created to calculate the dose received by a cantaloupe passing under a 10 MeV electron beam. This deck included metallic reflectors to scatter the electron beam, which created a more uniform surface dose distribution. From the results of each deck, a surface dose map and dose depth curves were generated.

It was shown that the surface dose ratio can be reduced to 2.18 from 83500 by using metallic reflectors. Additionally, the plates concentrate the dose on the surface of the cantaloupe while achieving a penetration depth sufficient to combat bacteria internalization.

This means that using electron beam and metallic reflectors for the processing of cantaloupes is technologically feasible. Furthermore, this study can serve as a guide for developing similar reflector plates for other products, beam energies, and loading geometries.

5.B. Practicality & Limitations

While the MCNPX simulations showed that it is possible to distribute the surface dose more uniformly, there are still a few practical issues that must be addressed before full implementation. These issues include heat removal, product variation, product loading, and conveyor speed.

Heat removal is the most important limitation because the plates will receive considerable energy from the electron beam. This energy will manifest as heat and if not removed, it will cause the plates to lose shape and integrity; if the amount of heat energy is severe enough, it might melt the plates. As stated in Section II.D, aluminum was chosen due to its ability to easily conduct heat. This heat will need to be dissipated and removed by an active cooling system, such as water flowing through the plates. The details of this system would need to be worked out before implementing the design. Primary results from Design X show that the plates receive 22.97, 9.037, 9.032, & 1.207 kW of energy. This would require water flowing at 1.740, 0.6847, 0.6843, & 0.09148 gallons/minute to limit the temperature rise in the plates to 50 degrees C.

Product variation and loading also need to be addressed. Product variations such as size and shape are natural in all food, including cantaloupes. While usually minor, these variations can affect the surface dose distribution. Preliminary results show a max/min ratio of 2.33 for a cantaloupe of radius of 8.25 cm and 2.24 for a radius of 6.75 cm. Product loading variables, such as spacing between cantaloupes and lateral positioning of the cantaloupes also will affect dose distribution.

Conveyor speed is also an important feasibility factor that needs to be addressed. Conveyor speed directly affects the dose delivered, as the time spent under the electron beam dictates the dose delivered to the cantaloupe. This is important as the dose delivered not only must be low enough to meet legal regulations, but also high enough to provide microbial inactivation. Preliminary modeling of Design X shows a conveyor speed of 12.3 cm/s is required to keep the absorbed dose below the 1 kGy limit for fresh

fruits. This would allow for processing 1481 cantaloupes per hour with a double accelerator facility. These values were calculated using the following equations:

$$s_c = \frac{60\ cm}{\frac{1\ \text{kGy}}{D_{max}}} \qquad (5.1)$$

where: s_c is the conveyor belt speed;
60 cm is the distance traveled under the beam
1 kGy is the maximum allowed surface dose; and
D_{max} is the maximum surface dose in the MCNPX model.

$$T = \frac{s_c}{30\ \text{cm}} \qquad (5.2)$$

where: T is the cantaloupe throughput;
s_c is the conveyor belt speed; and
30 cm is the distance between cantaloupes. While these feasibility issues can be simulated and calculated from MCNPX simulations, physical experiments of the system would need to be performed to confirm the simulated results. This would ultimately determine the final feasibility of this surface dose optimization method. It is also recommended that reflector plate systems are simulated and optimized for other food products to further provide credence to this method of surface dose distribution.

REFERENCES

Allen, J.E., 2011. Tainted Cantaloupes Behind Deadliest Food-Borne Outbreak. ABC News Medical Unit. Retrieved 6/17/14 from http://abcnews.go.com/Health/Health/cantaloupes-tied-deadliest-food-outbreak/story?id=14874373#.TrQcKoReO-o.

Alpen, E.L.,1998. Radiation Biophysics. Academic Press, San Diego, CA. isbn: 9780120530854

Attix, F.H., 1986. Introduction to Radiological Physics and Radiation Dosimetry. John Wiley & Sons, New York, NY. isbn: 9780471011460

Centers for Disease Control and Prevention (CDC), 2013. Foodborne Outbreak Online Database. Centers for Disease Control and Prevention. Retrieved 6/17/14 from http://wwwn.cdc.gov/foodborneoutbreaks.

Centers for Disease Control and Prevention (CDC), 2014. CDC Estimates of Foodborne Illness in the United States: CDC 2011 Estimates. National Center for Emerging and Zoonotic Infectious Diseases (NCEZID), Division of Foodborne, Waterborne, and Environmental Diseases (DFWED). Retrieved 6/17/14 from http://www.cdc.gov/foodborneburden/2011-foodborne-estimates.html.

Evans, R.D., 1955. The Atomic Nucleus (1982 reprint). McGraw-Hill, New York, NY. isbn: 9780898744149.

Hallman, G.J., 2001. Irradiation as Quarintine Treatment. In R. Molins (Ed.), Food Irradiation: Principles and Applications (pp. 113-211) John Wiley & Sons, New York, NY. isbn: 9780471356349

Haynes, W.M. ed., 2014. CRC Handbook of Chemistry and Physics. 95th ed. CRC Press, Boca Raton, FL. isbn: 9781482208672.

Hellborg, R. ed., 2005. Electrostatic Accelerators: Fundamentals and Applications. Springer, New York, NY. isbn: 9783540239833

Hoffmann, S., and Anekwe T.D., 2013. Making Sence of Recent Cost-of-Foodborne-Illness Estimates. Economic Information Bulletin 118. U.S. Department of Agriculture, Economic Research Service. Retrieved 6/17/14 from www.ers.usda.gov/publications/eib-economic-information-bulletin/eib118.aspx.

Hoffmann, S., Batz, M.B., and Morris Jr, J.G., 2012. Annual Cost of Illness and Quality-Adjusted Life Year Losses in the United States Due to 14 Foodborne Pathogens. Journal of Food Protection. 75 (7), 1291-1302. 10.4315/0362-028X.JFP-11-417.

Humphries, S., 1986. Principles of Charged Particle Acceleration. Wiley-Interscience, New York, NY. isbn: 9780471878780

Lopez-Velasco, G., Sbodio, A., Tomás-Callejas, A., Wei, P., Tan, K.H., Suslow T.V., 2012. Assessment of root uptake and systemic vine-transport of Salmonella enterica sv. Typhimurium by melon (Cucumis melo) during field production. International Journal of Food Microbiology. 158 (2012) 65–72. 10.1016/j.ijfoodmicro.2012.07.005.

MCNP X-5 Monte Carlo Team, 2003. MCNP—A General Purpose Monte Carlo N Particle Transport Code, Version 5. LA UR 03 1987. Los Alamos National Laboratory.

Nelson, D.L., and Cox, M.M., 2005. Lehninger Principles of Biochemistry. W.H. Freeman, New York, NY. isbn: 9780716771081

Scharff, R., 2012. Economic Burden from Health Losses Due to Foodborne Illness in the United States. Journal of Food Protection. 75(1): 123-31. 10.4315/0362-028X.JFP-11-058.

Scharff, R., 2010. Health-related Costs from Foodborne Illness in the United States. Produce Safety Project. Georgetown University, Washington, DC. Retrieved 9/29/14 from http://www.marlerblog.com/uploads/image/PSP-Scharff%20v9.pdf.

Suslow, T. V., 2004. Minimizing the risk of foodborne illness associated with cantaloupe production and handling in California. California Cantaloupe Advisory Board, University of California, Davis Agricultural and Natural Resources Publication. Retrieved 1/4/15 from http://col.st/1bdyO9c

Smith, J.S., and Pillai, S.D., 2004. Irradiation and Food Safety. Food Technology. 58 (11), 48-55.

Sommers, C.H., Delincée, H., Smith, J.S., and Marchioni, E., 2013. Toxicological Safety of Irradiated Foods. In Food Irradiation Research and Technology 2nd ed., ed. X. Fan and C.H. Sommers, p. 43-61, Wiley-Blackwell Publishing, Ames, IA. isbn: 9780813802091.

Turner, J. E.,2007. Atoms, Radiation, and Radiation Protection. Wiley-VCH, Weinheim, Germany. isbn: 9783527406067

World Health Organization (WHO), 1999. High-dose irradiation: Wholesomeness of food irradiated with doses above 10 kGy. Report of a Joint FAO/IAEA/WHO Study Group. World Health Organization Technical Report Series 890. World Health Organization, Geneva, Switzerland.

APPENDIX A

DESIGN CHANGE REASONING

Design A consisted of four solid stainless steel plates: flat top and bottom plates, and a sloped side plate on either side of the conveyor belt. Design A resulted in a hot spot on top of the cantaloupe.

The changes in the model were to add two additional plates above the top attenuator and below the bottom reflector. This was in hopes to provide more shielding around the poles of the cantaloupe to diminish the hotspots there. (Design B) This design still had a hot spot on top of the cantaloupe.

To improve, two designs were tested: Design C extended the upper plates across the conveyor belt to the side reflectors. Design D extended the lowest attenuating plate along the direction of the conveyor belt. These two designs are different approaches to increase the dose on the leading and trailing faces of the cantaloupe. Design C reduced the dose reflected to the sides, while Design D didn't significantly alter the dose map.

It was decided that using a wider version of Design C was optimal. This was due to the ability for electrons to reach the side reflectors while causing a slight increase in the leading and tailing faces. At this point it was determined to place holes in the upper attenuator to aim the electrons toward the leading and tailing edges. (Design E) These holes had a circular cross sectional radius of $32^{-1/2}$ cm, and were angled 45° through the plate. They were arranged in a square matrix 28x19 with 1 cm between center points. This design increased the dose to the leading and tailing edges of the cantaloupe.

After running the simulation with holes in the top bar, it was noted that the upper hot spot increased. It was then decided the holes reduced the apparent thickness of the bar, and to increase the thickness of the upper bar. (Design F) This design slightly reduced the upper hotspot.

It was discovered that MCNP was already dividing by volume, and therefore dividing again by volume was giving false results. All the old data was replotted and a composite design was determined. This design applied all the changes from Design B to E (holes and wider) to Design A. This is because the apparent hotspot on the top does not exist and the top needs more dose while the reflectors are causing a much higher dose on the lower regions of the cantaloupes facing the reflectors. (Design G) This resulted in a high dose under the beam, and hotspots where the side plates reflect electrons onto the sides.

It was decided to increase the slope of the side plates in an effort to move the dose further under the cantaloupe. (Design H) The change in slope moved the side hot spots lower on the cantaloupe.

It was decided to add more stops under the beam. Bring the total from 5 to 15. Design H was rerun with the new stops. This resulted in the side hotspots disappearing, as with more stops closer to the beam, the reflected side dose as the cantaloupe approaches is accounted for.

It was decided to reduce the thickness of the top plate in an effort to increase the dose to the top of the cantaloupe. (Design I) This allowed more electrons to reach the top of the cantaloupe, resulting a more uniform dose distribution.

It was decided to reduce the cross sectional area of the upper holes by half. This is in an effort to decrease the dose to the leading and tailing faces of the cantaloupe. (Design J) This design showed that the dose was also reduced to the top of the cantaloupe, causing an increase in dose uniformity ratio.

It was decided to return the upper holes to the original cross sectional area. Instead the slope of the top half of the side reflecting plates was changed. This is in an effort to increase the dose to the sides on the top half of the cantaloupe. (Design K) This design resulted in less particles reaching the upper half of the sides of the cantaloupe

It was decided to return to single sloped side reflectors. The slope of the reflectors was then changed to a shallower slope than in Designs H-J. (Design L) This design resulted in the electrons being reflected too high up the sides of the cantaloupe.

It was decided to return to Design I, but change the metal to Aluminum instead of 302 Stainless Steel. Due to the 3x lower density the thickness of the top plates was increased 3x. (Design M) The material changes showed that plate thickness was roughly proportional to Z value.

It was decided that the side plates also needed to be increased in thickness by 3 due to the decrease in density. (Design N) This reiterated the proportionality of plate thickness and Z.

It was decided to try Design N, but change the metal to lead. The upper plate thickness was reduced by the ratio of the densities. (Design O) This reiterated the proportionality of plate thickness and Z.

It was decided to reduce the thickness of the upper and lower lead plates, in an attempt to increase the dose to the top and bottom of the cantaloupe. (Design P) This reiterated the proportionality of plate thickness and Z.

It was decided to return back to Design N, but dimple the face of the side reflector plates. (Design Q) The dimples resulted in a slight improvement of surface dose uniformity.

It was decided to optimize the upper plate thickness vs the dose distribution ratio of

Design Q (Designs R, T, & V-X). Each design's upper plate thickness was plotted vs. dose uniformity ratio. In the end it showed an optimum thickness of 1.65 cm.

Simultaneously it was decided to test the effect of side reflector slopes on dose distribution ratio. (Design S & U) Each design's slope was plotted vs. dose uniformity ratio. In the end it showed the initial 10/3 slope was best.

It was noticed that the holes in Design X were not centered. So this was rectified to create Design Y.

APPENDIX B

DOSE MAPS

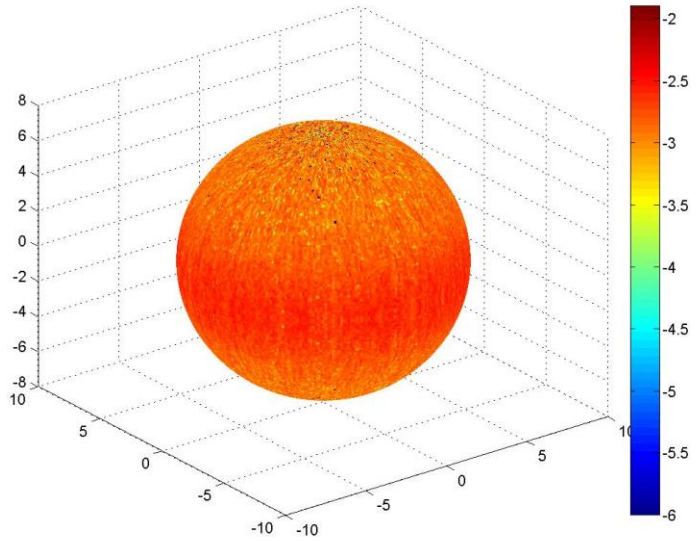

Figure B.1: Surface dose map for control model, double beam irradiation, from 30 degrees above the equatorial plane, original scale.

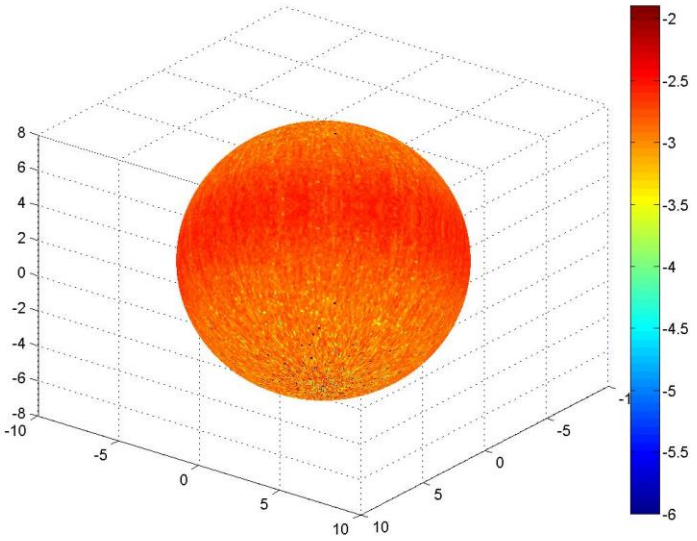

Figure B.2: Surface dose map for control model, double beam irradiation, from 30 degrees below the equatorial plane, original scale.

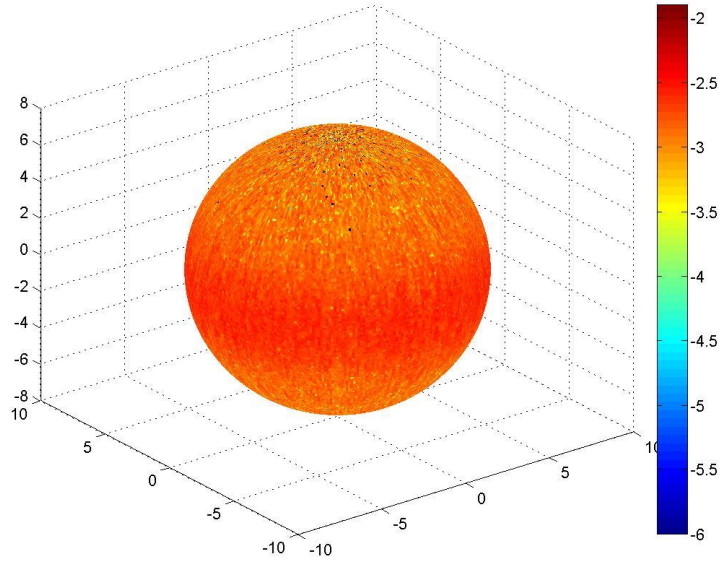

Figure B.3: Surface dose map for control model, double beam irradiation with a 90° rotation about the vertical axis, from 30 degrees above the equatorial plane, original scale.

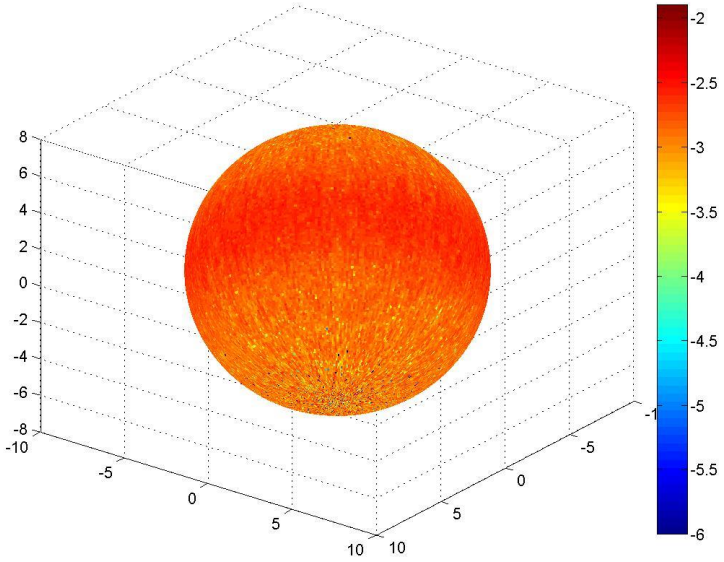

Figure B.4: Surface dose map for control model, double beam irradiation with a 90° rotation about the vertical axis, from 30 degrees below the equatorial plane, original scale.

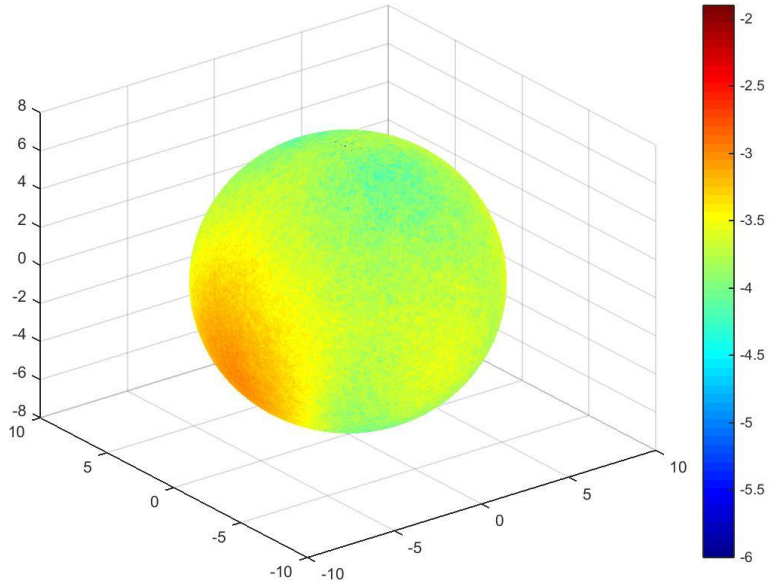

Figure B.5: Surface dose map for Design A, single beam irradiation, from 30 degrees above the equatorial plane, original scale.

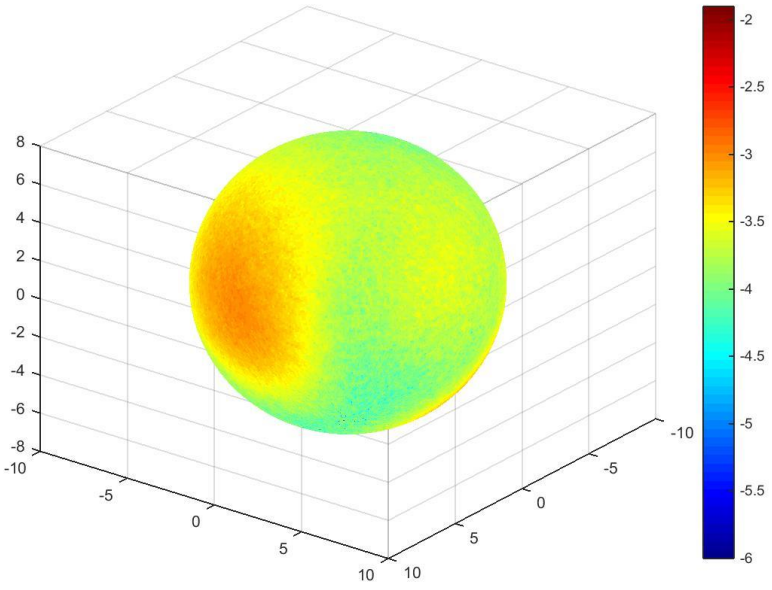

Figure B.6: Surface dose map for Design A, single beam irradiation, from 30 degrees below the equatorial plane, original scale.

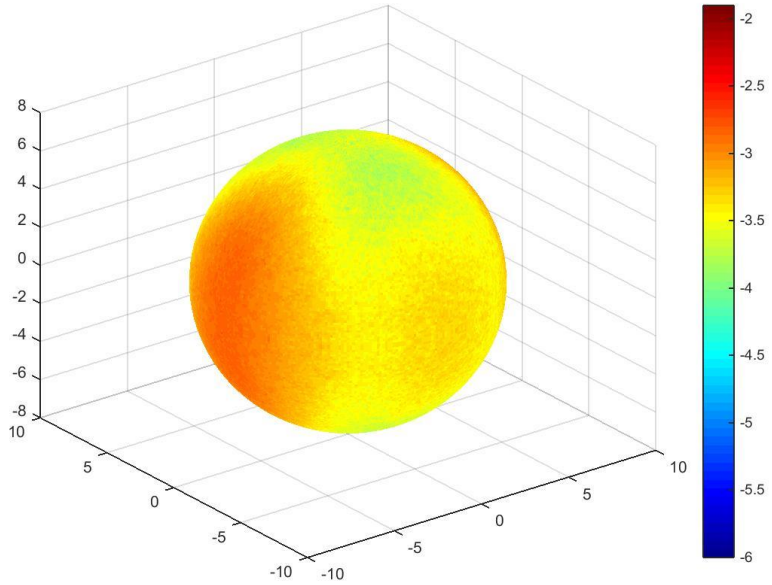

Figure B.7: Surface dose map for Design A, double beam irradiation, from 30 degrees above the equatorial plane, original scale.

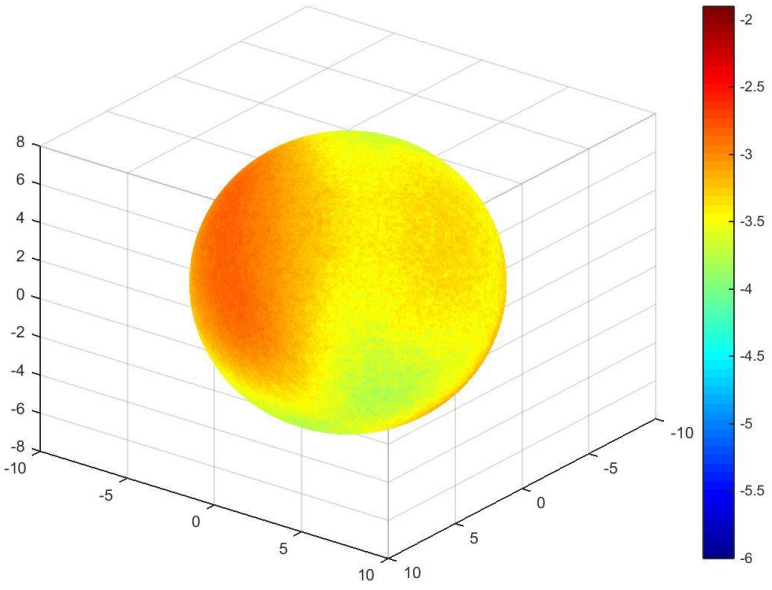

Figure B.8: Surface dose map for Design A, double beam irradiation, from 30 degrees below the equatorial plane, original scale.

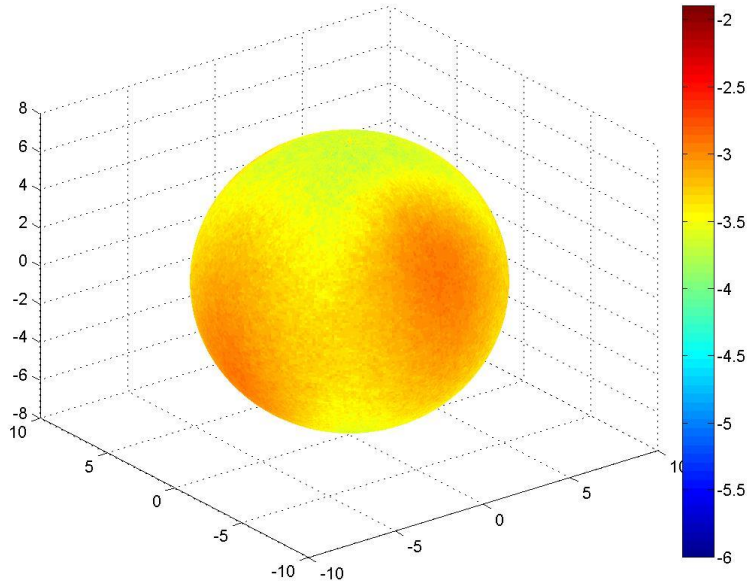

Figure B.9: Surface dose map for Design A, double beam irradiation with a 90° rotation about the vertical axis, from 30 degrees above the equatorial plane, original scale.

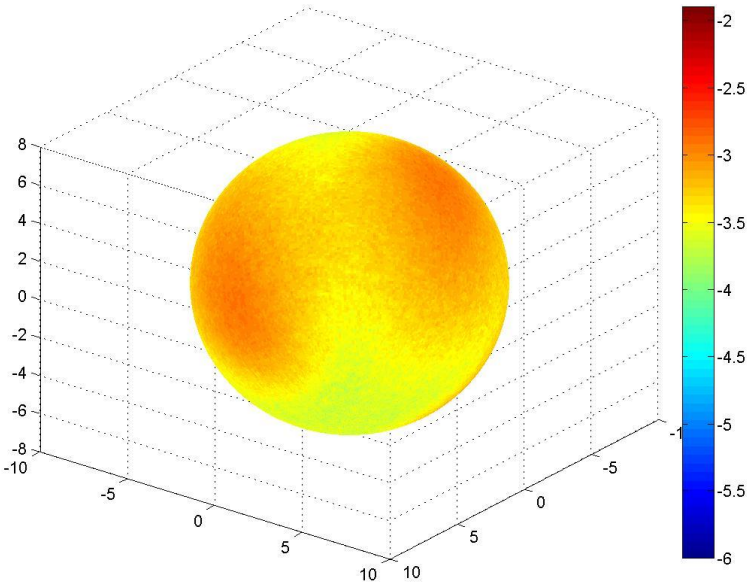

Figure B.10: Surface dose map for Design A, double beam irradiation with a 90° rotation about the vertical axis, from 30 degrees below the equatorial plane, original scale.

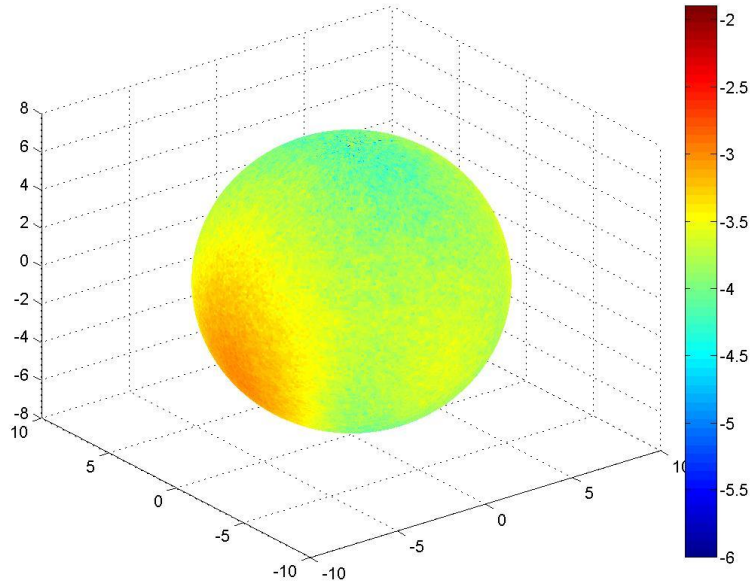

Figure B.11: Surface dose map for Design B, single beam irradiation, from 30 degrees above the equatorial plane, original scale.

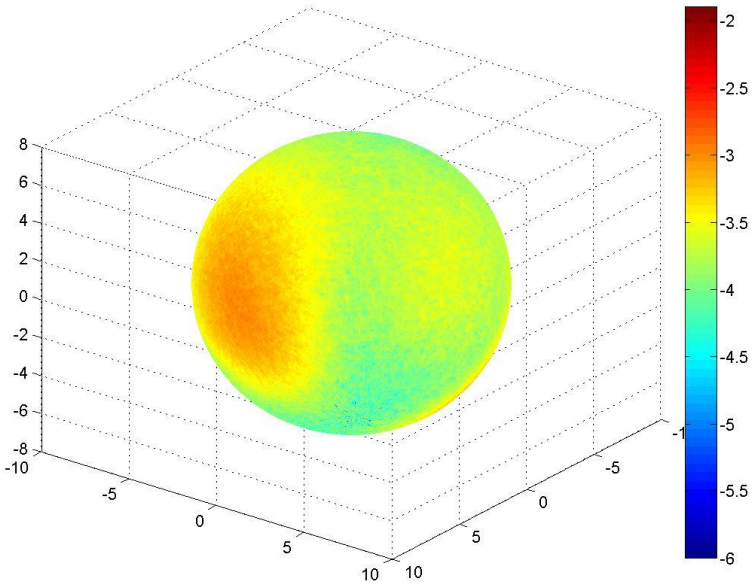

Figure B.12: Surface dose map for Design B, single beam irradiation, from 30 degrees below the equatorial plane, original scale.

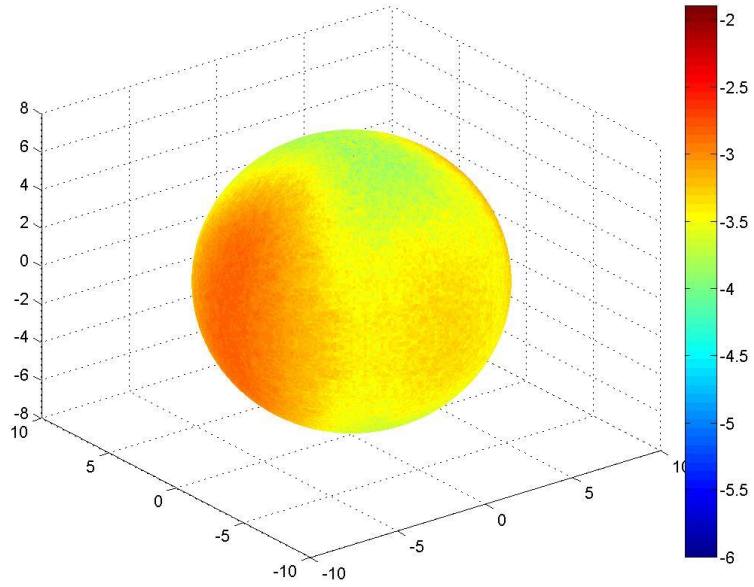

Figure B.13: Surface dose map for Design B, double beam irradiation, from 30 degrees above the equatorial plane, original scale.

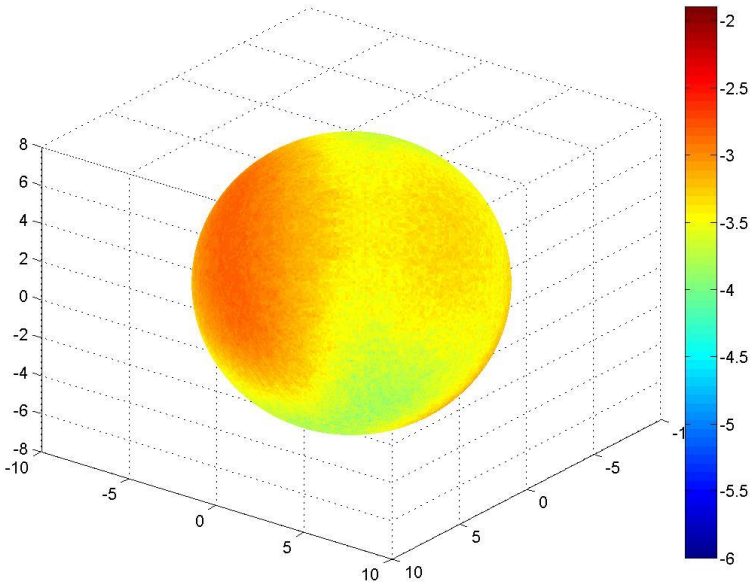

Figure B.14: Surface dose map for Design B, double beam irradiation, from 30 degrees below the equatorial plane, original scale.

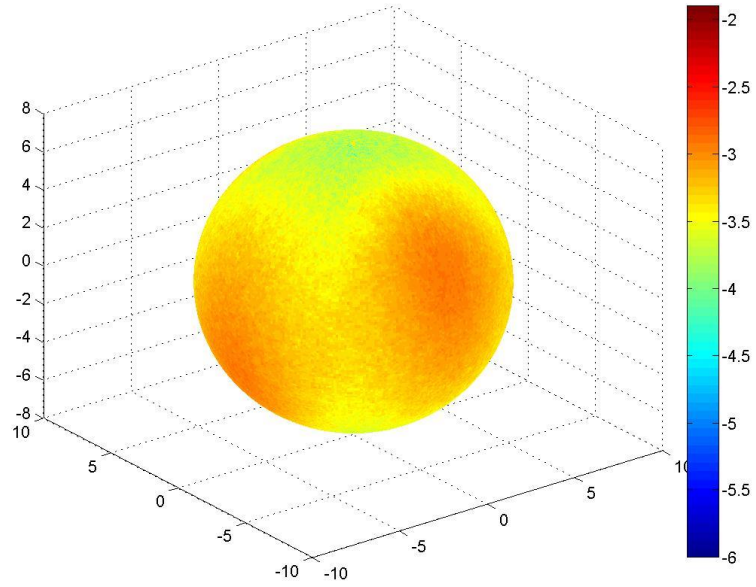

Figure B.15: Surface dose map for Design B, double beam irradiation with a 90° rotation about the vertical axis, from 30 degrees above the equatorial plane, original scale.

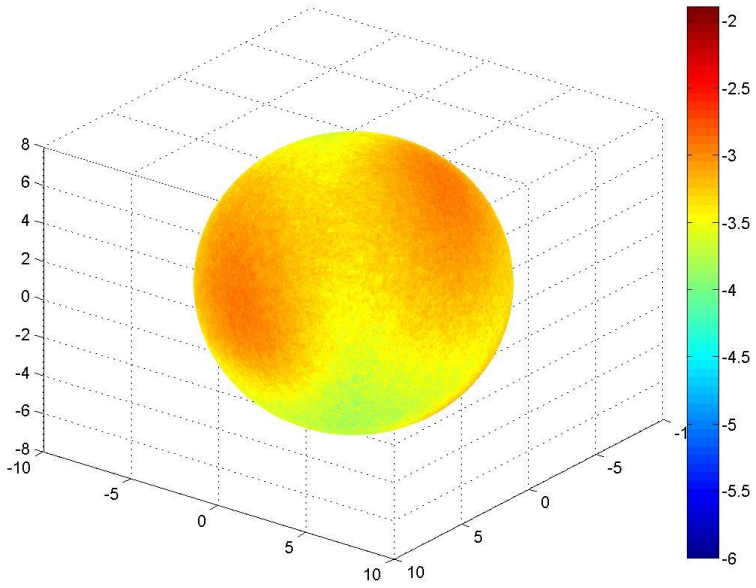

Figure B.16: Surface dose map for Design B, double beam irradiation with a 90° rotation about the vertical axis, from 30 degrees below the equatorial plane, original scale.

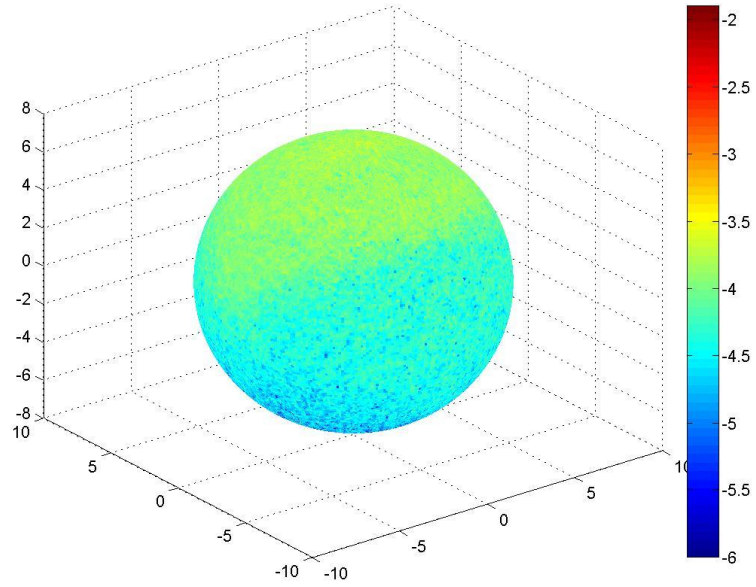

Figure B.17: Surface dose map for Design C, single beam irradiation, from 30 degrees above the equatorial plane, original scale.

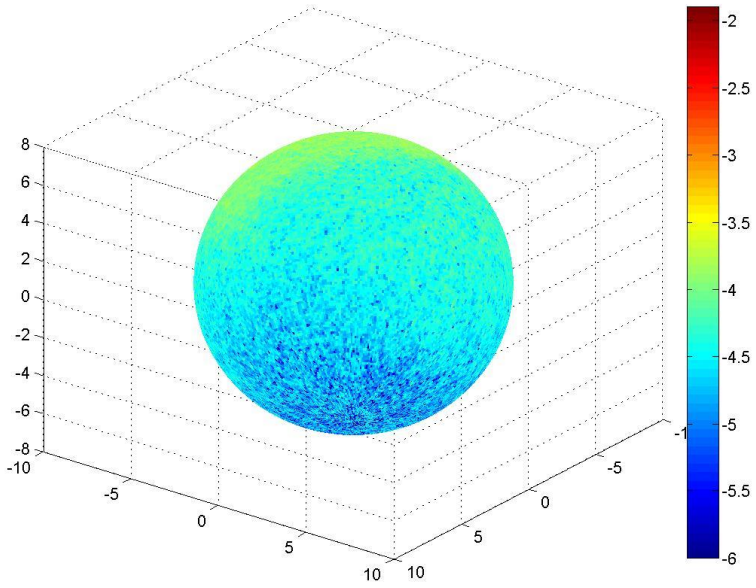

Figure B.18: Surface dose map for Design C, single beam irradiation, from 30 degrees below the equatorial plane, original scale.

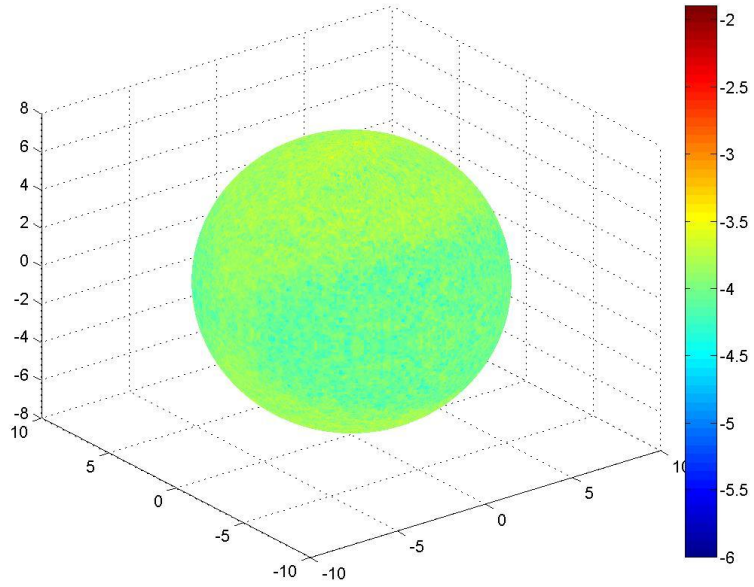

Figure B.19: Surface dose map for Design C, double beam irradiation, from 30 degrees above the equatorial plane, original scale.

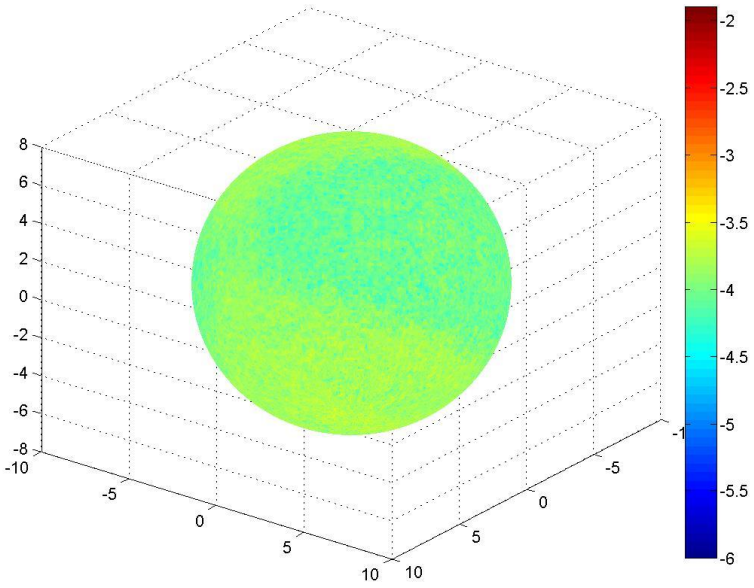

Figure B.20: Surface dose map for Design C, double beam irradiation, from 30 degrees below the equatorial plane, original scale.

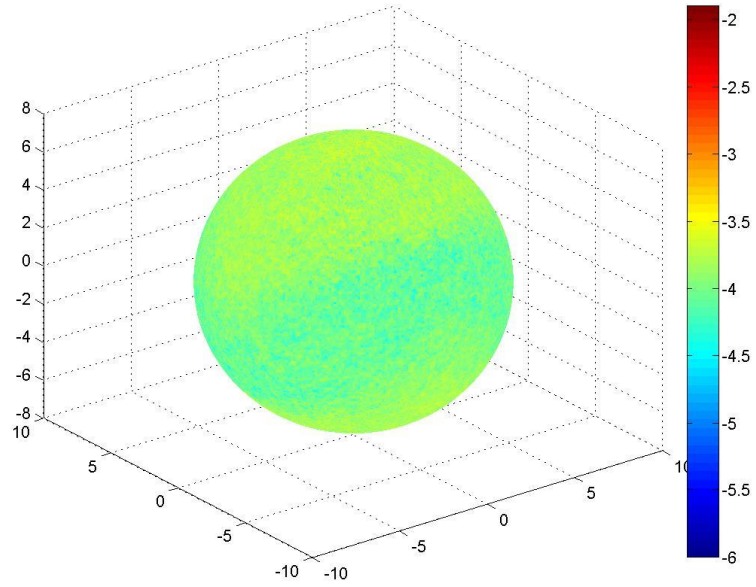

Figure B.21: Surface dose map for Design C, double beam irradiation with a 90° rotation about the vertical axis, from 30 degrees above the equatorial plane, original scale.

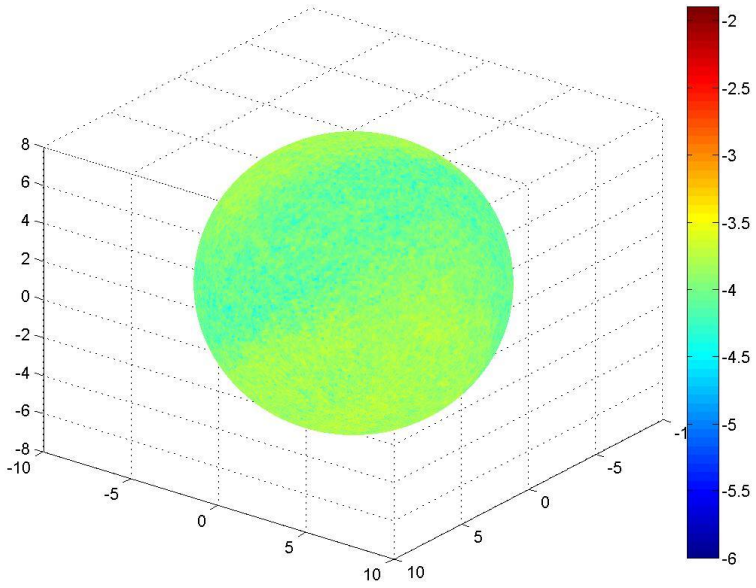

Figure B.22: Surface dose map for Design C, double beam irradiation with a 90° rotation about the vertical axis, from 30 degrees below the equatorial plane, original scale.

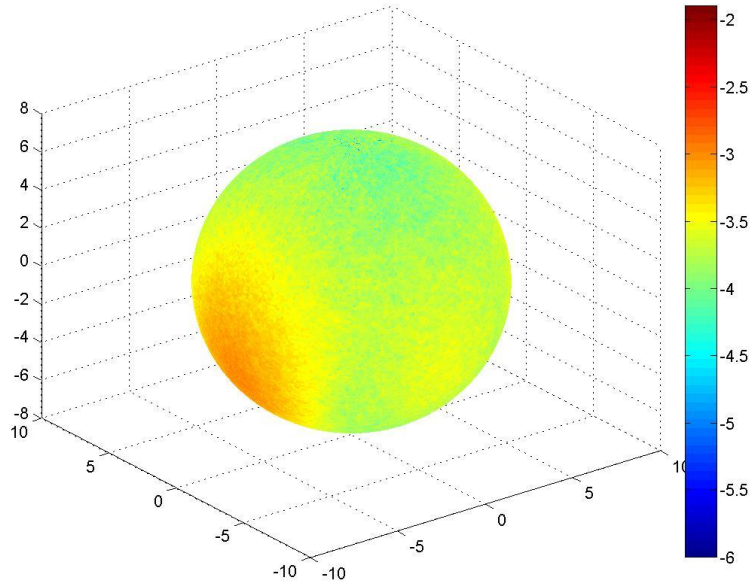

Figure B.23: Surface dose map for Design D, single beam irradiation, from 30 degrees above the equatorial plane, original scale.

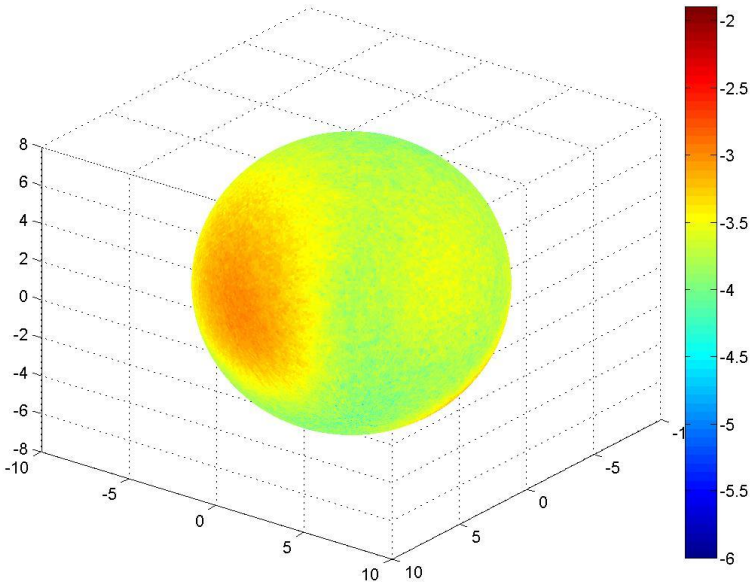

Figure B.24: Surface dose map for Design D, single beam irradiation, from 30 degrees below the equatorial plane, original scale.

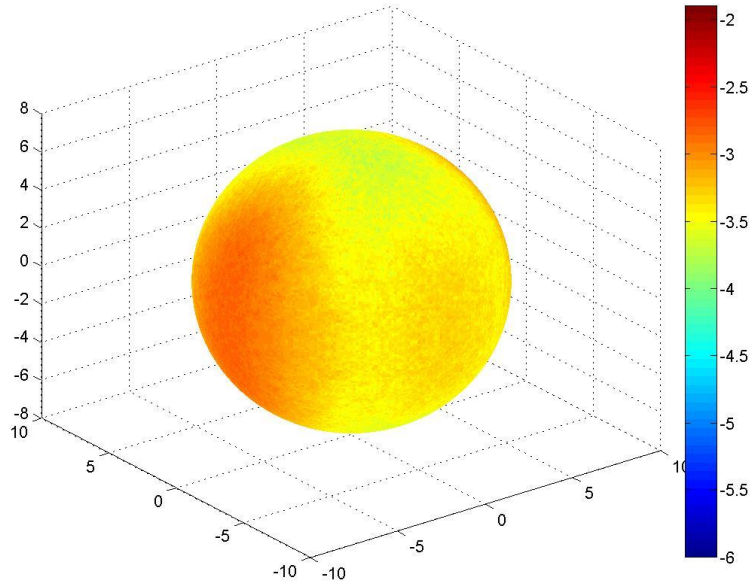

Figure B.25: Surface dose map for Design D, double beam irradiation, from 30 degrees above the equatorial plane, original scale.

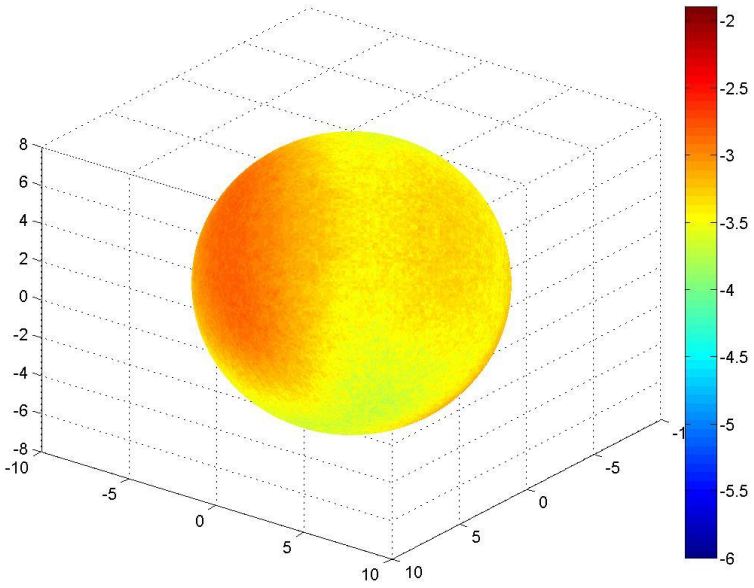

Figure B.26: Surface dose map for Design D, double beam irradiation, from 30 degrees below the equatorial plane, original scale.

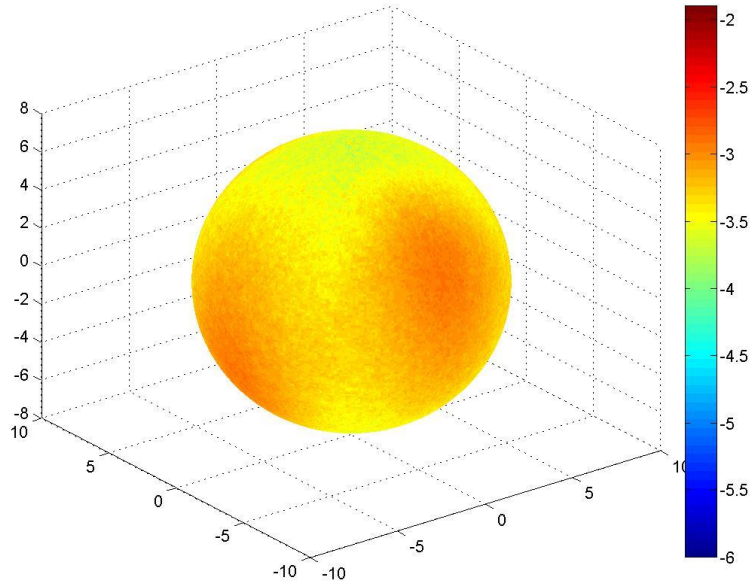

Figure B.27: Surface dose map for Design D, double beam irradiation with a 90° rotation about the vertical axis, from 30 degrees above the equatorial plane, original scale.

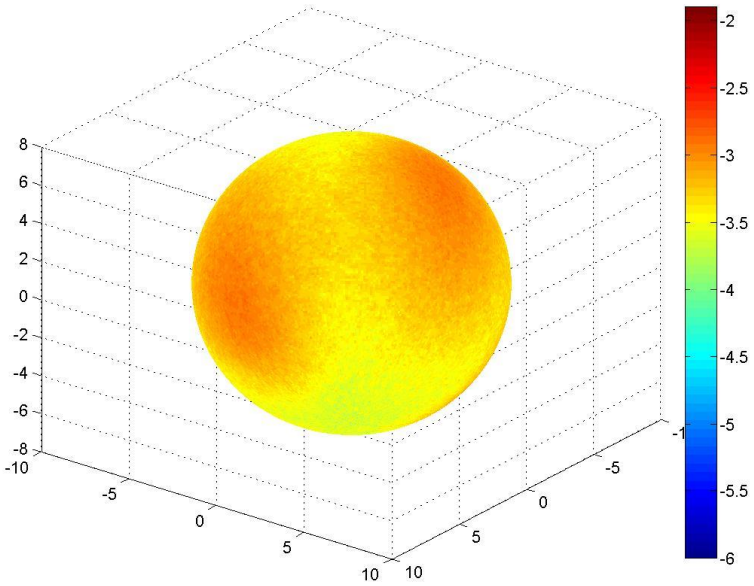

Figure B.28: Surface dose map for Design D, double beam irradiation with a 90° rotation about the vertical axis, from 30 degrees below the equatorial plane, original scale.

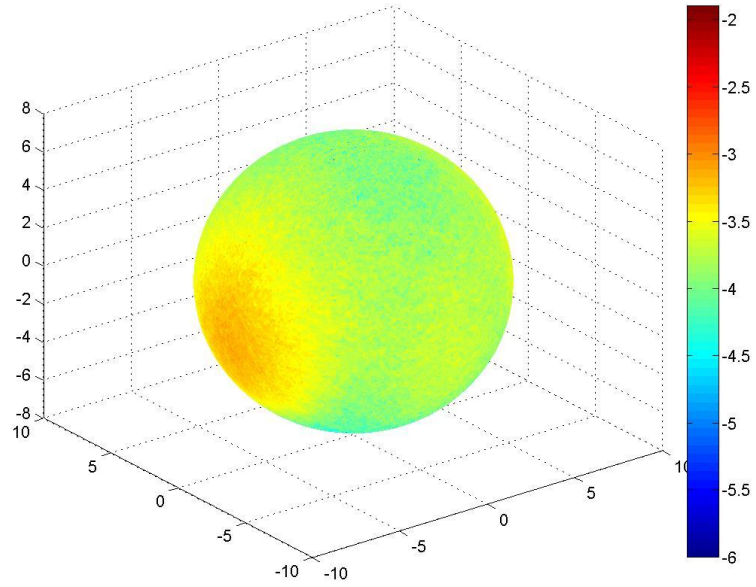

Figure B.29: Surface dose map for Design E, single beam irradiation, from 30 degrees above the equatorial plane, original scale.

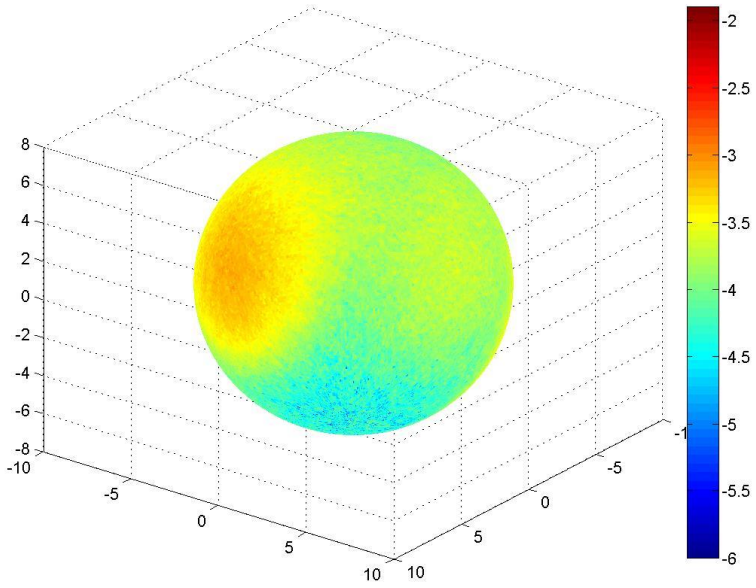

Figure B.30: Surface dose map for Design E, single beam irradiation, from 30 degrees below the equatorial plane, original scale.

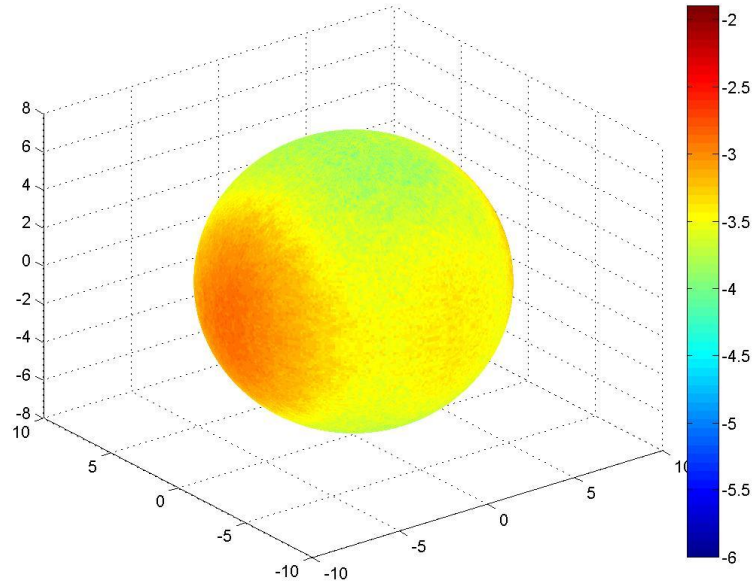

Figure B.31: Surface dose map for Design E, double beam irradiation, from 30 degrees above the equatorial plane, original scale.

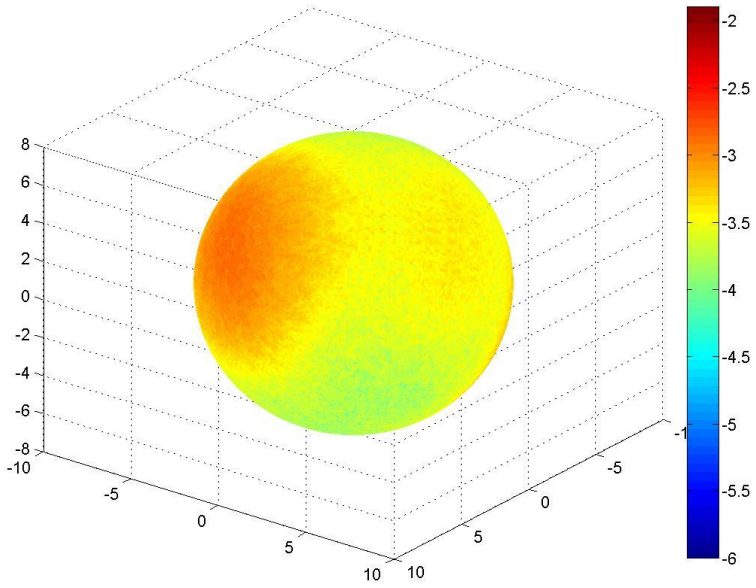

Figure B.32: Surface dose map for Design E, double beam irradiation, from 30 degrees below the equatorial plane, original scale.

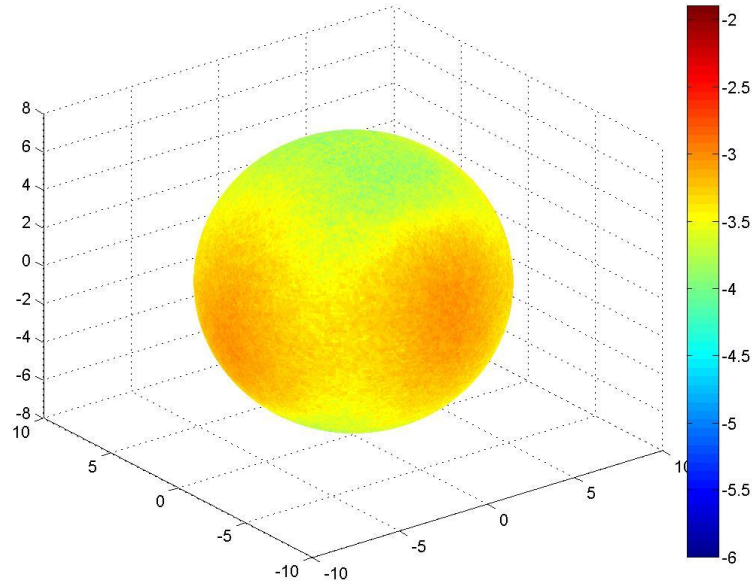

Figure B.33: Surface dose map for Design E, double beam irradiation with a 90° rotation about the vertical axis, from 30 degrees above the equatorial plane, original scale.

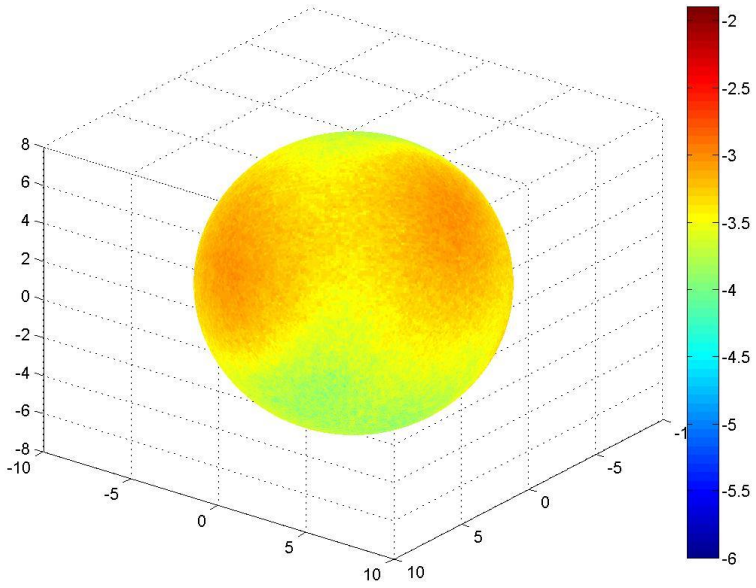

Figure B.34: Surface dose map for Design E, double beam irradiation with a 90° rotation about the vertical axis, from 30 degrees below the equatorial plane, original scale.

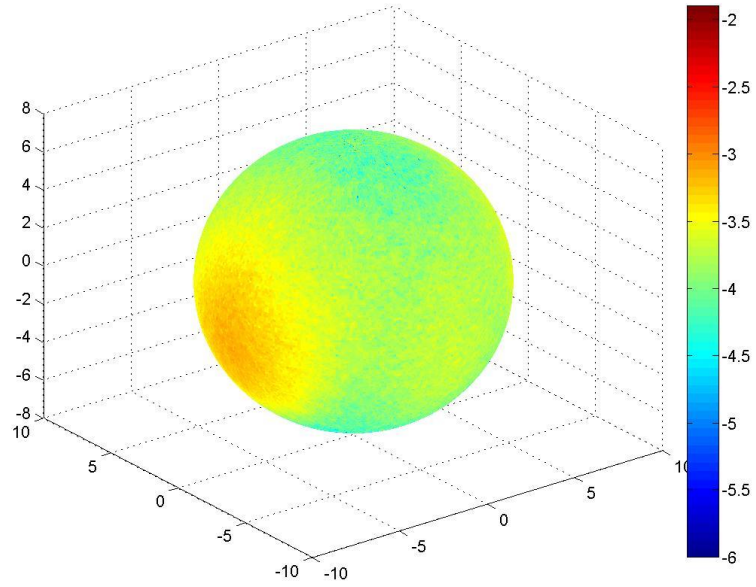

Figure B.35: Surface dose map for Design F, single beam irradiation, from 30 degrees above the equatorial plane, original scale.

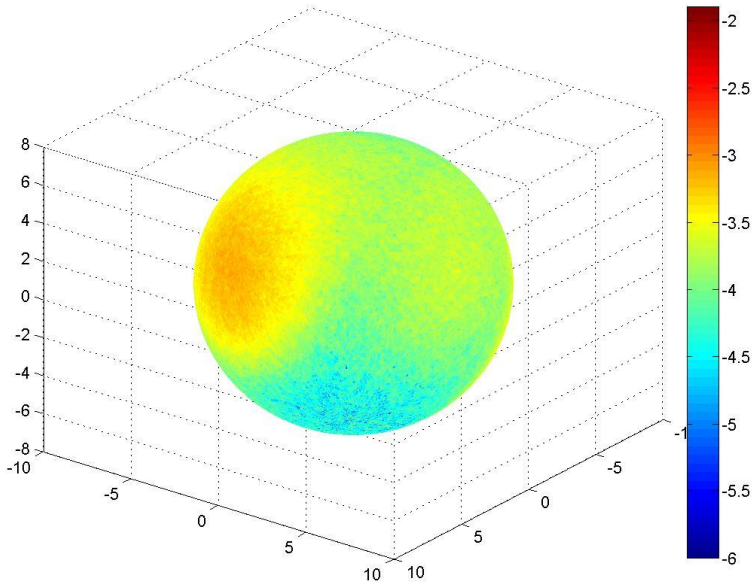

Figure B.36: Surface dose map for Design F, single beam irradiation, from 30 degrees below the equatorial plane, original scale.

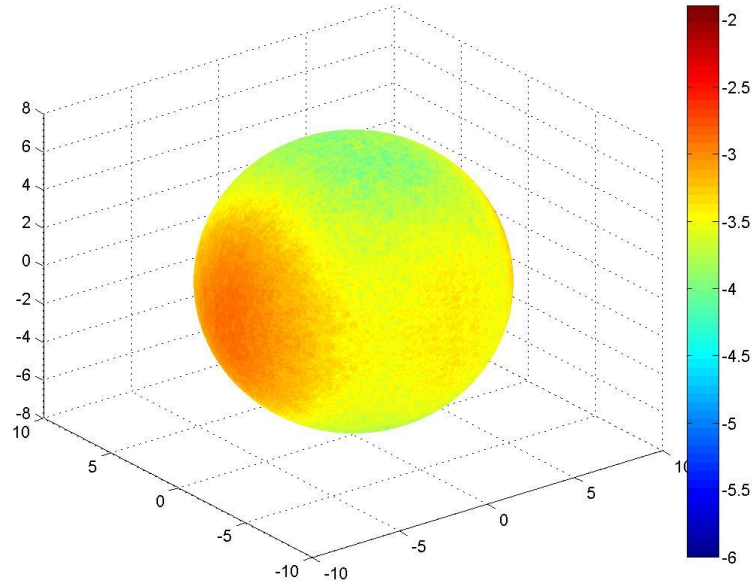

Figure B.37: Surface dose map for Design F, double beam irradiation, from 30 degrees above the equatorial plane, original scale.

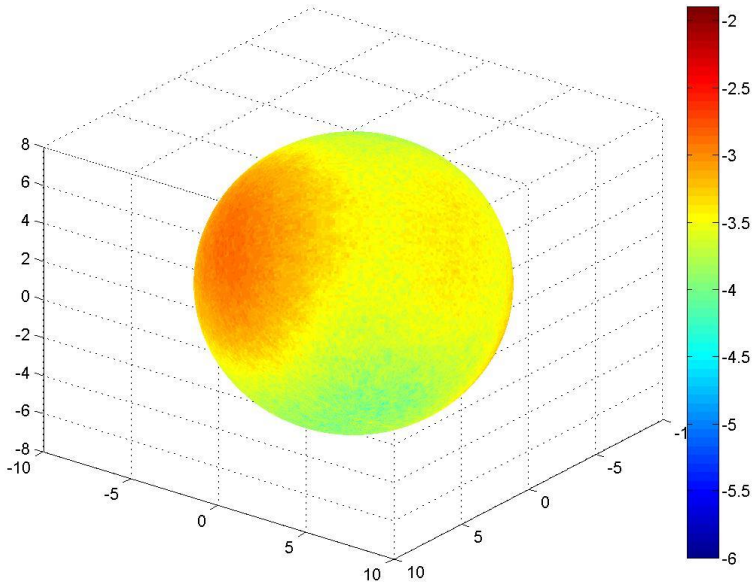

Figure B.38: Surface dose map for Design F, double beam irradiation, from 30 degrees below the equatorial plane, original scale.

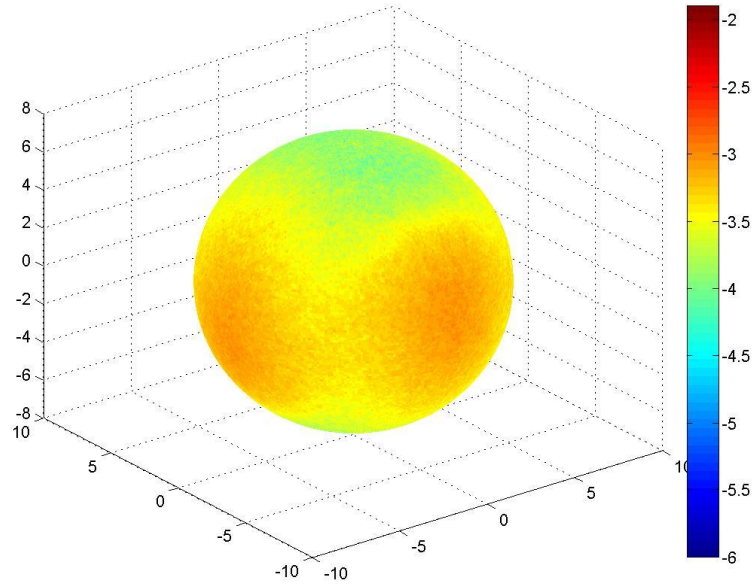

Figure B.39: Surface dose map for Design F, double beam irradiation with a 90° rotation about the vertical axis, from 30 degrees above the equatorial plane, original scale.

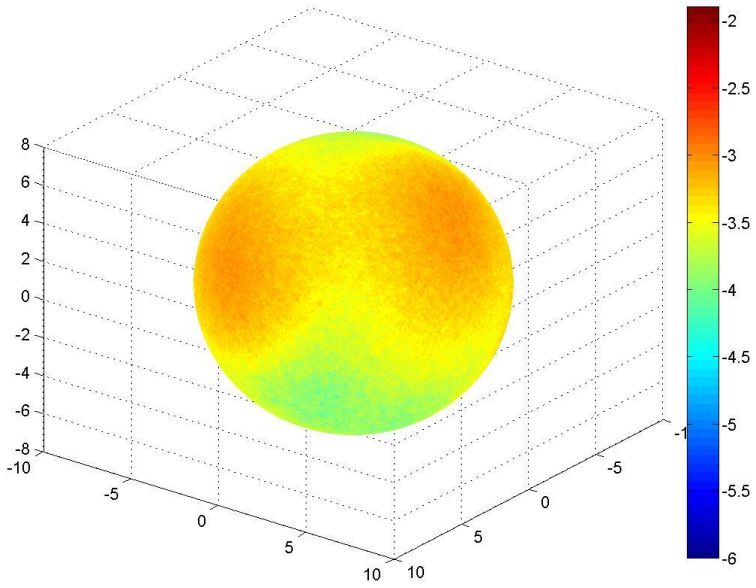

Figure B.40: Surface dose map for Design F, double beam irradiation with a 90° rotation about the vertical axis, from 30 degrees below the equatorial plane, original scale.

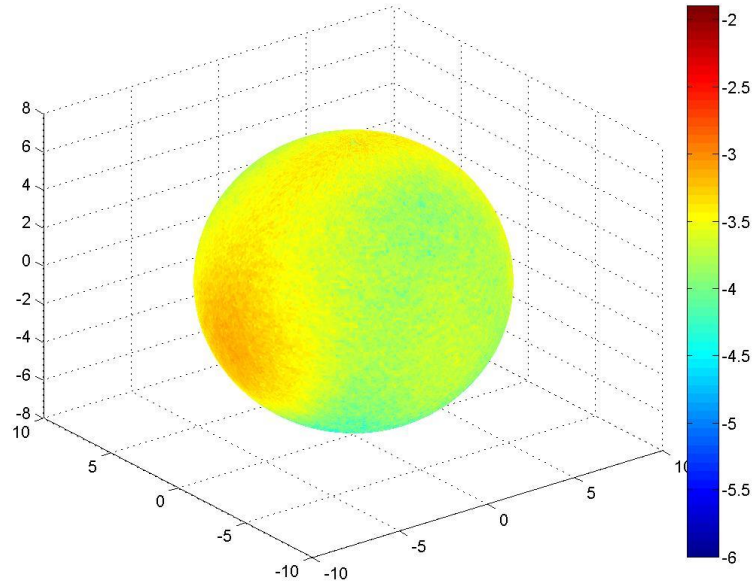

Figure B.41: Surface dose map for Design G, single beam irradiation, from 30 degrees above the equatorial plane, original scale.

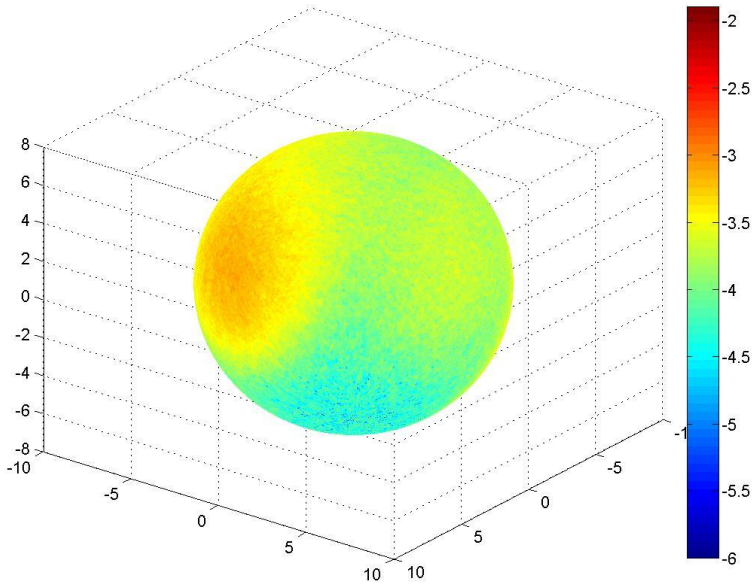

Figure B.42: Surface dose map for Design G, single beam irradiation, from 30 degrees below the equatorial plane, original scale.

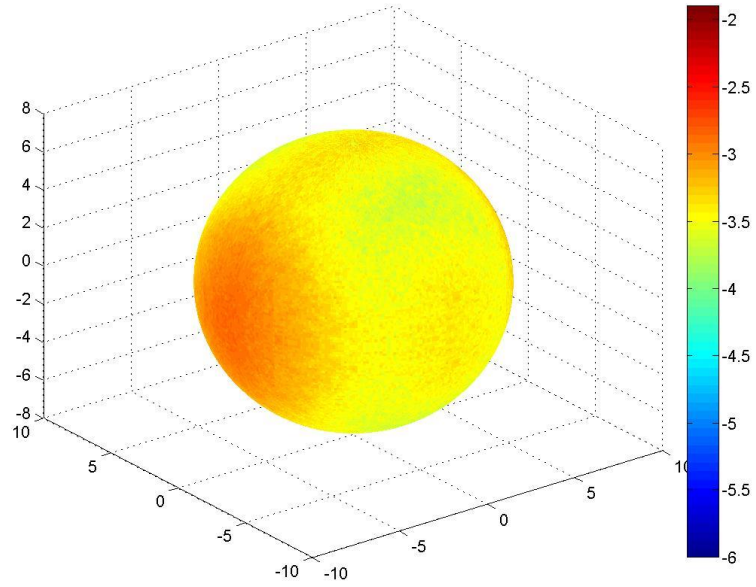

Figure B.43: Surface dose map for Design G, double beam irradiation, from 30 degrees above the equatorial plane, original scale.

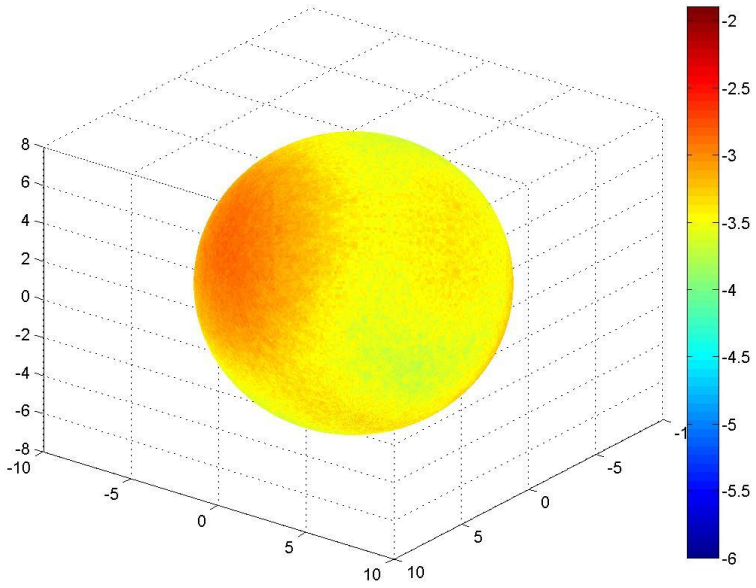

Figure B.44: Surface dose map for Design G, double beam irradiation, from 30 degrees below the equatorial plane, original scale.

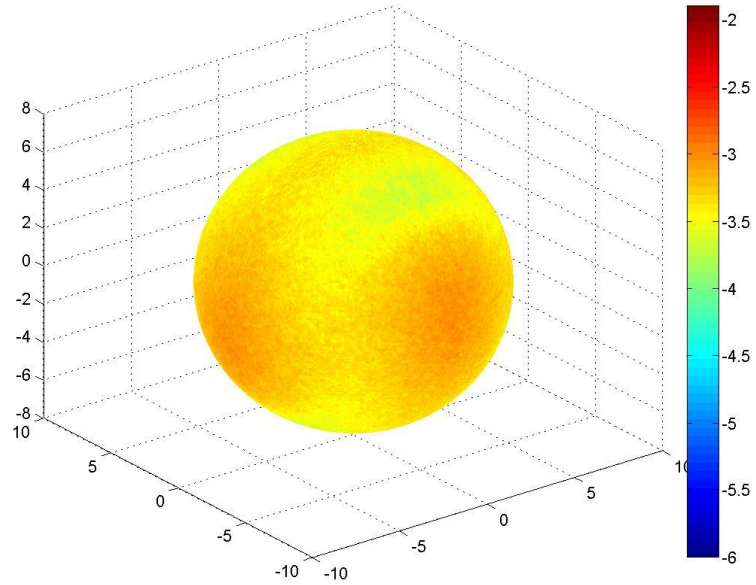

Figure B.45: Surface dose map for Design G, double beam irradiation with a 90° rotation about the vertical axis, from 30 degrees above the equatorial plane, original scale.

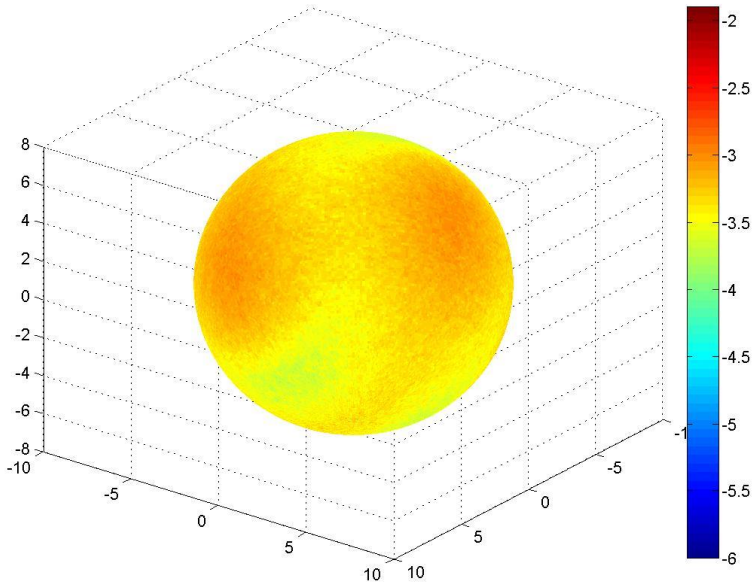

Figure B.46: Surface dose map for Design G, double beam irradiation with a 90° rotation about the vertical axis, from 30 degrees below the equatorial plane, original scale.

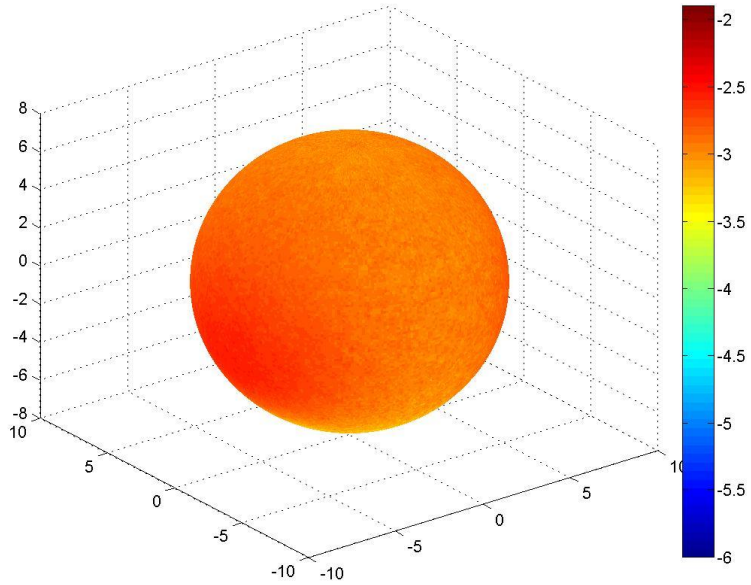

Figure B.47: Surface dose map for Design H, single beam irradiation, from 30 degrees above the equatorial plane, original scale.

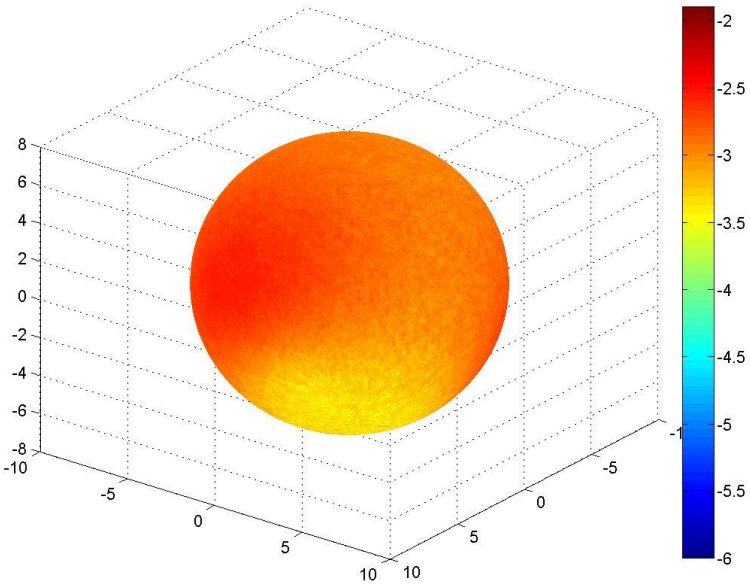

Figure B.48: Surface dose map for Design H, single beam irradiation, from 30 degrees below the equatorial plane, original scale.

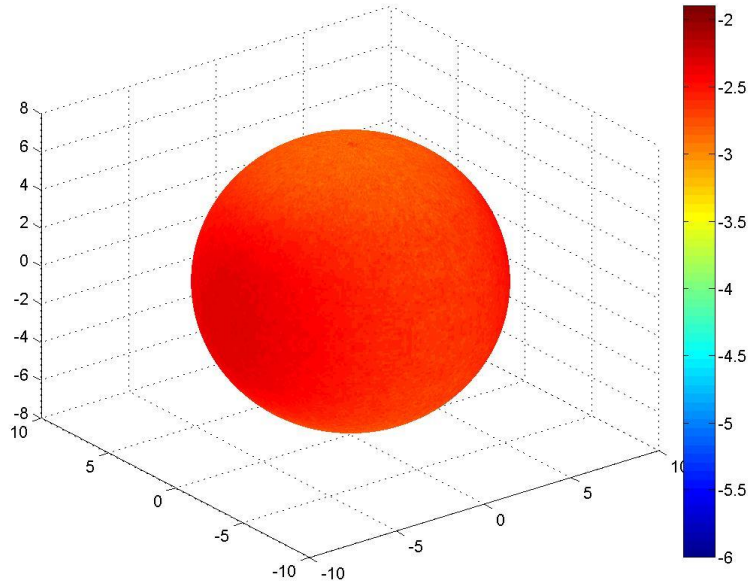

Figure B.49: Surface dose map for Design H, double beam irradiation, from 30 degrees above the equatorial plane, original scale.

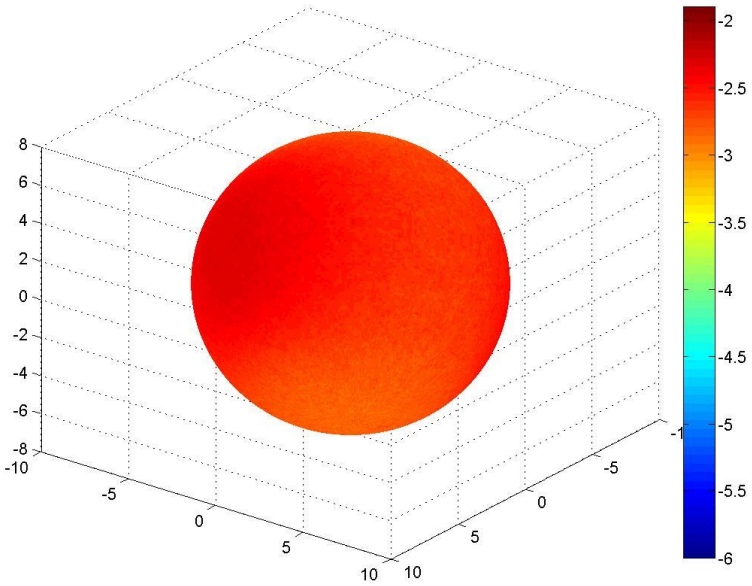

Figure B.50: Surface dose map for Design H, double beam irradiation, from 30 degrees below the equatorial plane, original scale.

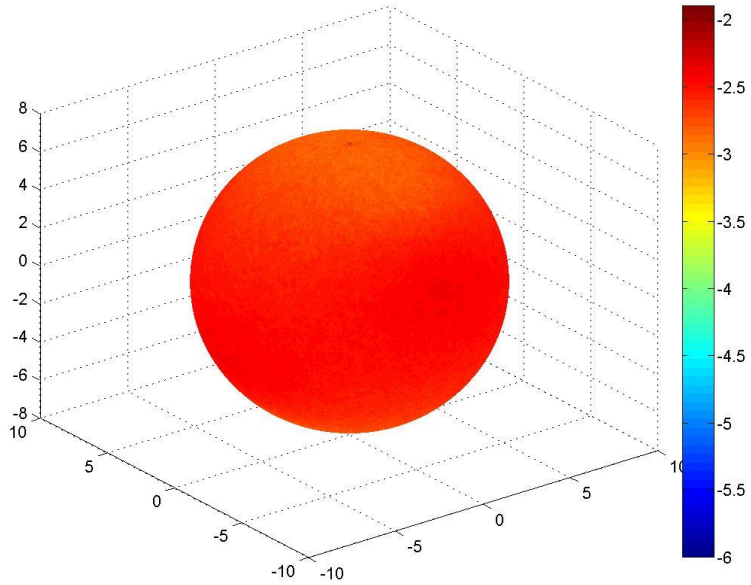

Figure B.51: Surface dose map for Design H, double beam irradiation with a 90° rotation about the vertical axis, from 30 degrees above the equatorial plane, original scale.

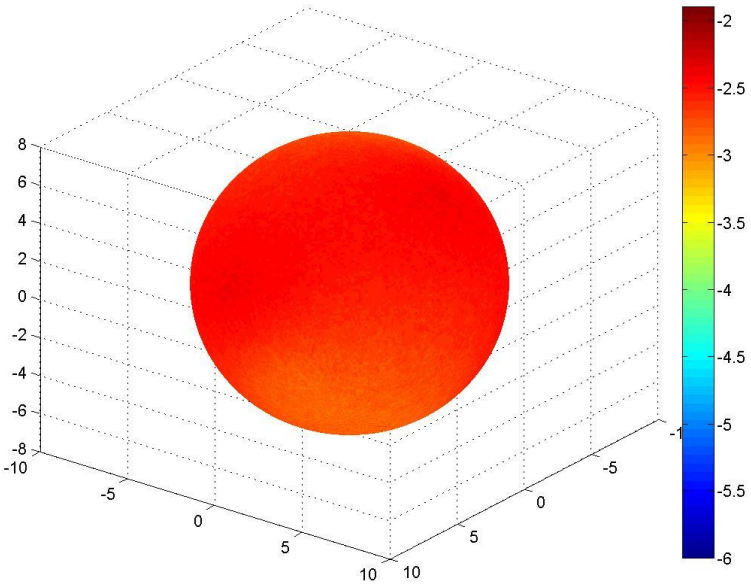

Figure B.52: Surface dose map for Design H, double beam irradiation with a 90° rotation about the vertical axis, from 30 degrees below the equatorial plane, original scale.

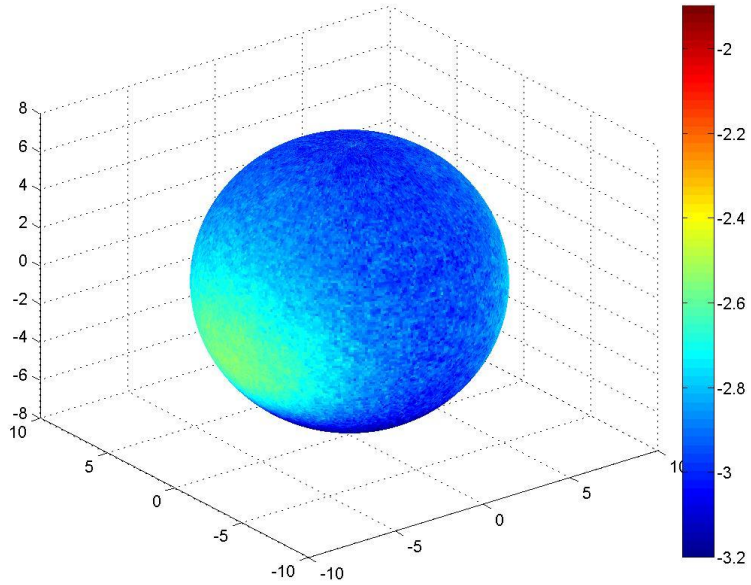

Figure B.53: Surface dose map for Design H, single beam irradiation, from 30 degrees above the equatorial plane, scale minimum raised to -3.2.

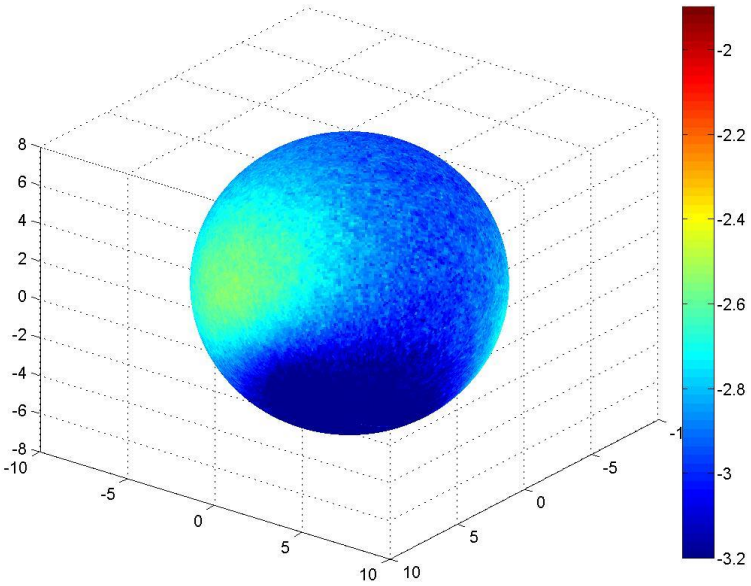

Figure B.54: Surface dose map for Design H, single beam irradiation, from 30 degrees below the equatorial plane, scale minimum raised to -3.2.

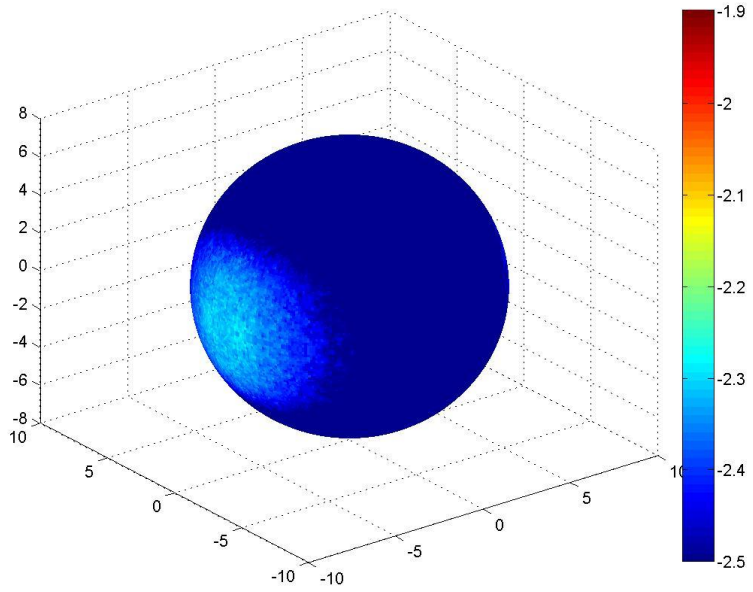

Figure B.55: Surface dose map for Design H, double beam irradiation, from 30 degrees above the equatorial plane, scale minimum raised to -2.5.

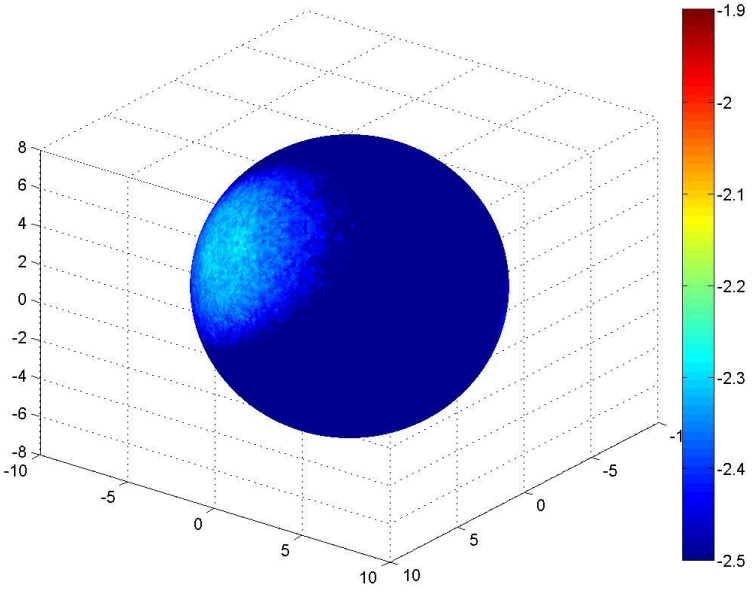

Figure B.56: Surface dose map for Design H, double beam irradiation, from 30 degrees below the equatorial plane, scale minimum raised to -2.5.

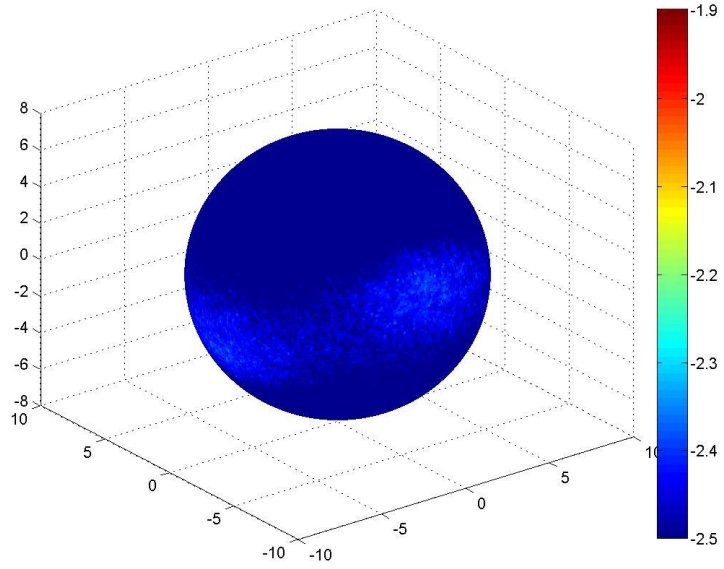

Figure B.57: Surface dose map for Design H, double beam irradiation with a 90° rotation about the vertical axis, from 30 degrees above the equatorial plane, scale minimum raised to -2.5.

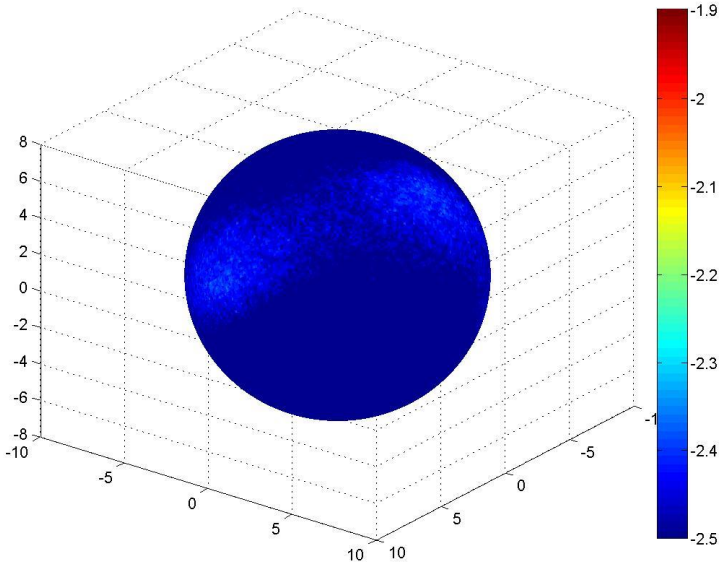

Figure B.58: Surface dose map for Design H, double beam irradiation with a 90° rotation about the vertical axis, from 30 degrees below the equatorial plane, scale minimum raised to -2.5.

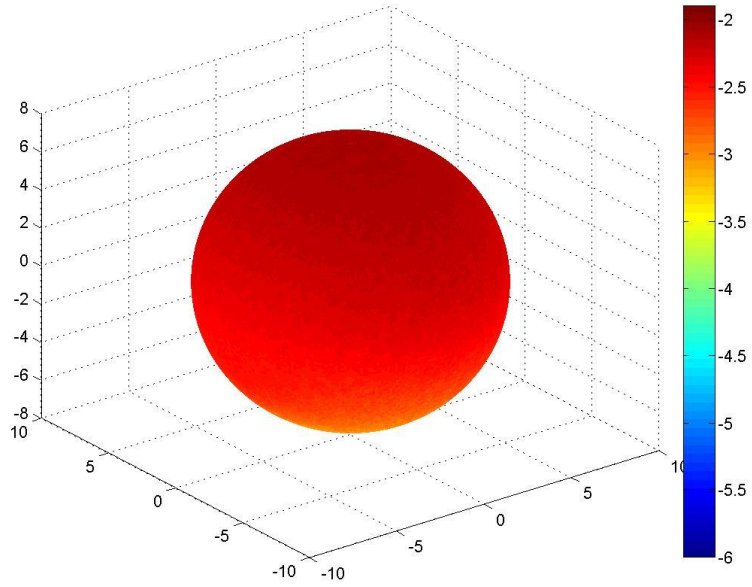

Figure B.59: Surface dose map for Design I, single beam irradiation, from 30 degrees above the equatorial plane, original scale.

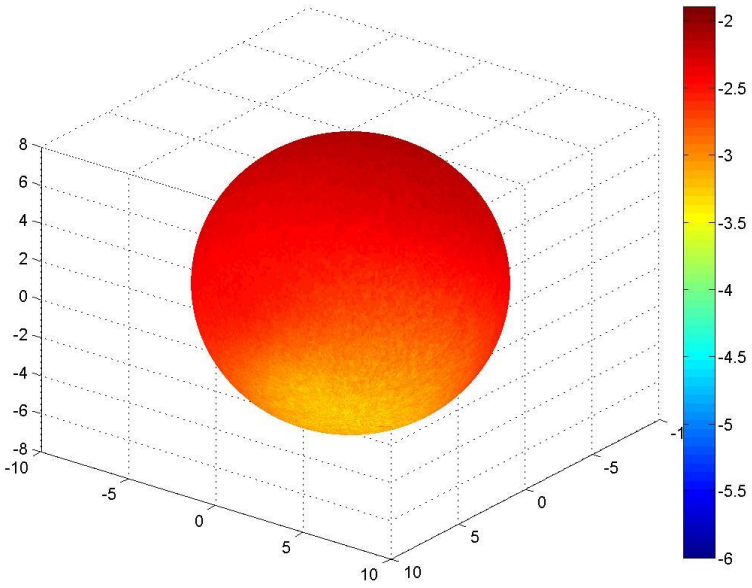

Figure B.60: Surface dose map for Design I, single beam irradiation, from 30 degrees below the equatorial plane, original scale.

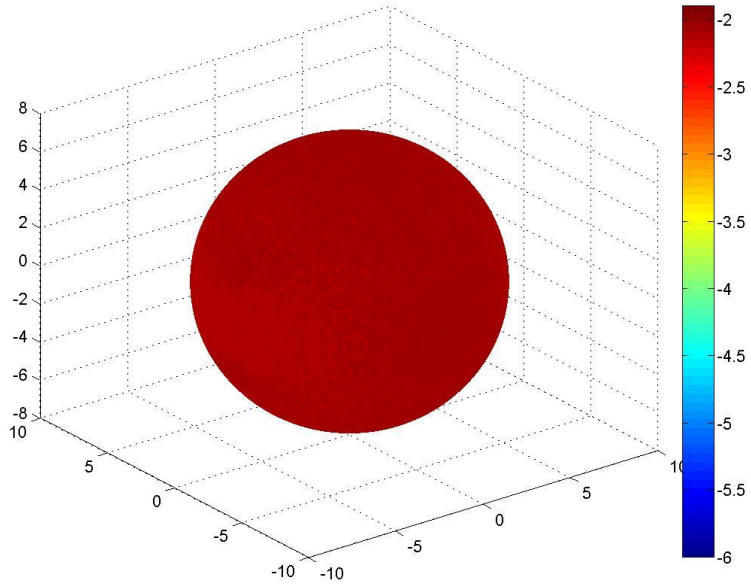

Figure B.61: Surface dose map for Design I, double beam irradiation, from 30 degrees above the equatorial plane, original scale.

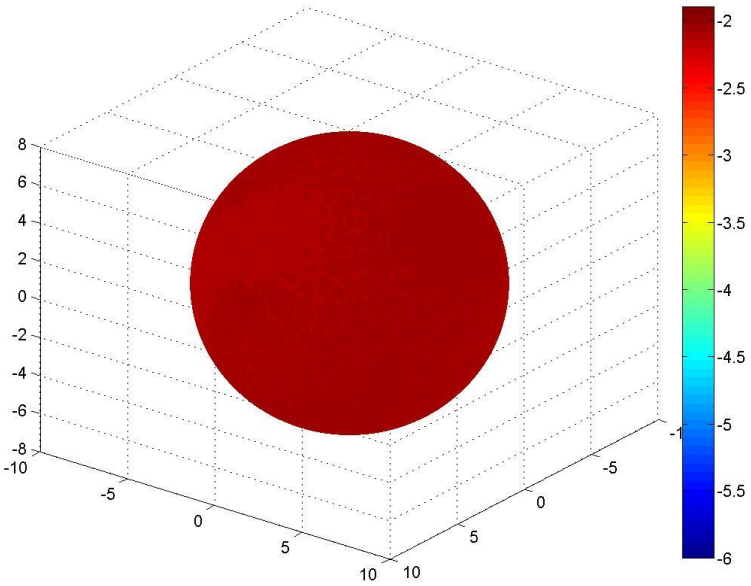

Figure B.62: Surface dose map for Design I, double beam irradiation, from 30 degrees below the equatorial plane, original scale.

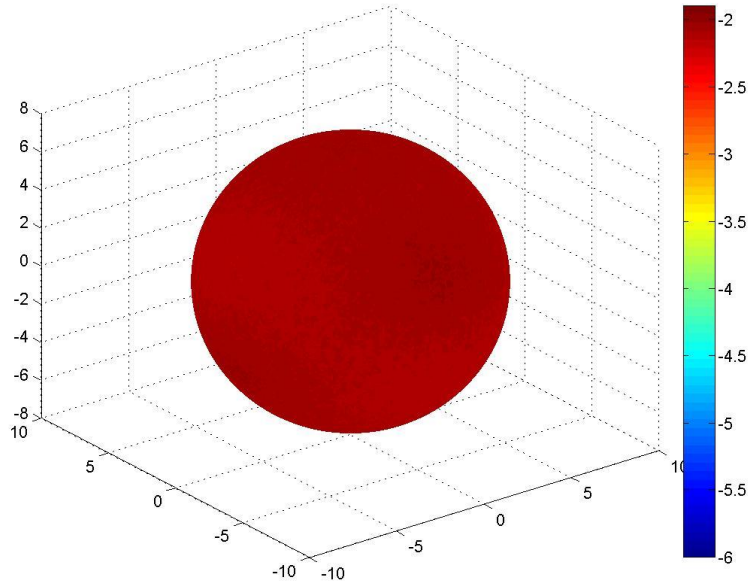

Figure B.63: Surface dose map for Design I, double beam irradiation with a 90° rotation about the vertical axis, from 30 degrees above the equatorial plane, original scale.

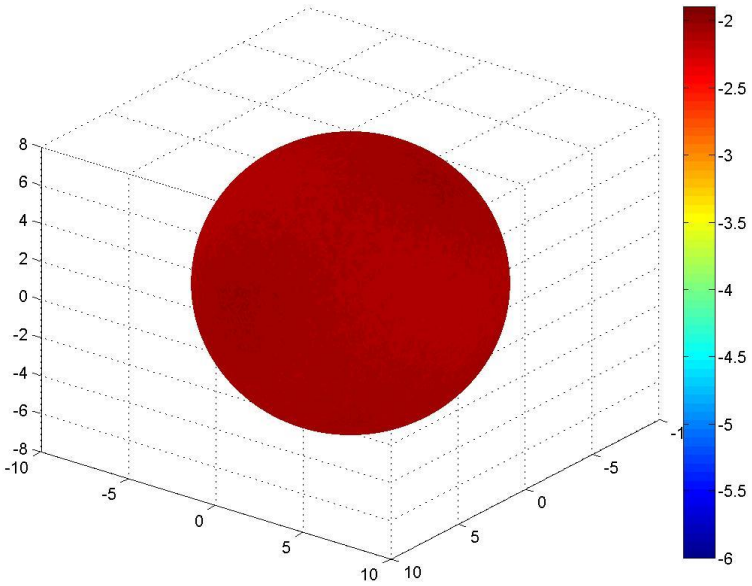

Figure B.64: Surface dose map for Design I, double beam irradiation with a 90° rotation about the vertical axis, from 30 degrees below the equatorial plane, original scale.

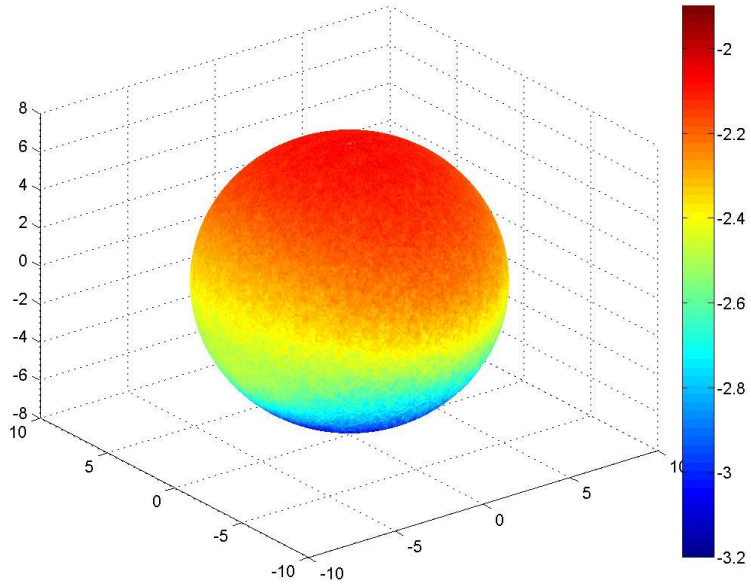

Figure B.65: Surface dose map for Design I, single beam irradiation, from 30 degrees above the equatorial plane, scale minimum raised to -3.2.

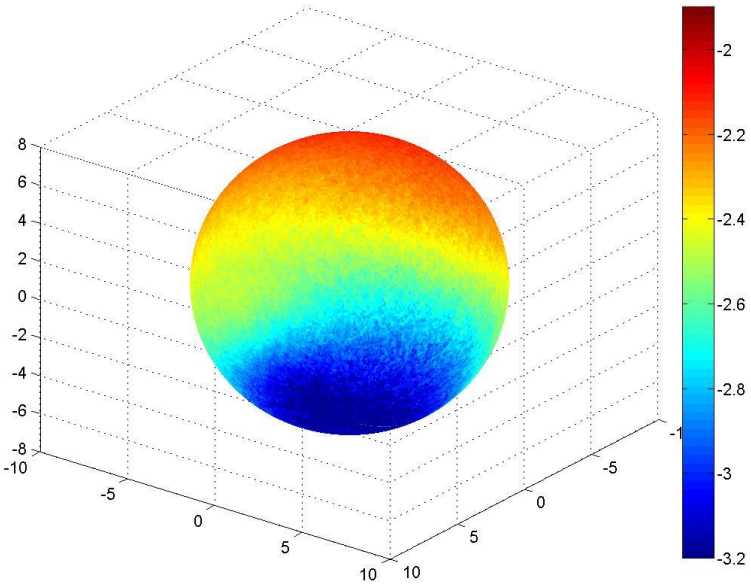

Figure B.66: Surface dose map for Design I, single beam irradiation, from 30 degrees below the equatorial plane, scale minimum raised to -3.2.

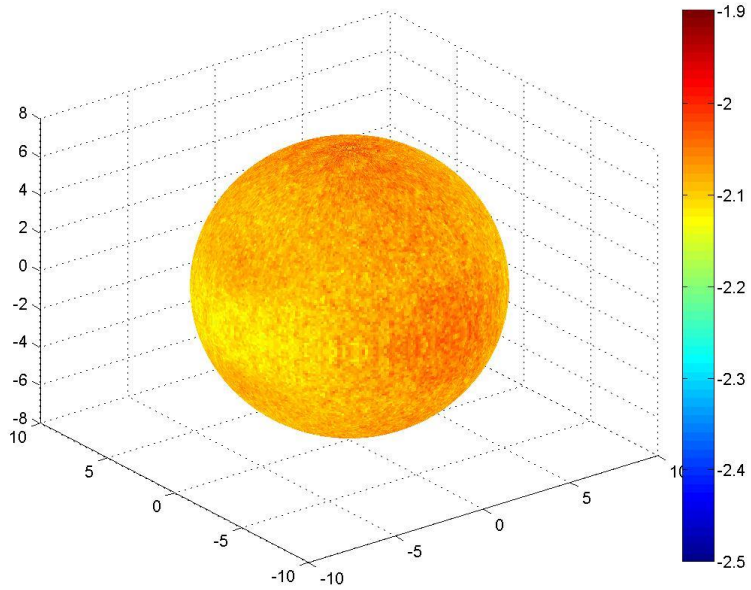

Figure B.67: Surface dose map for Design I, double beam irradiation, from 30 degrees above the equatorial plane, scale minimum raised to -2.5.

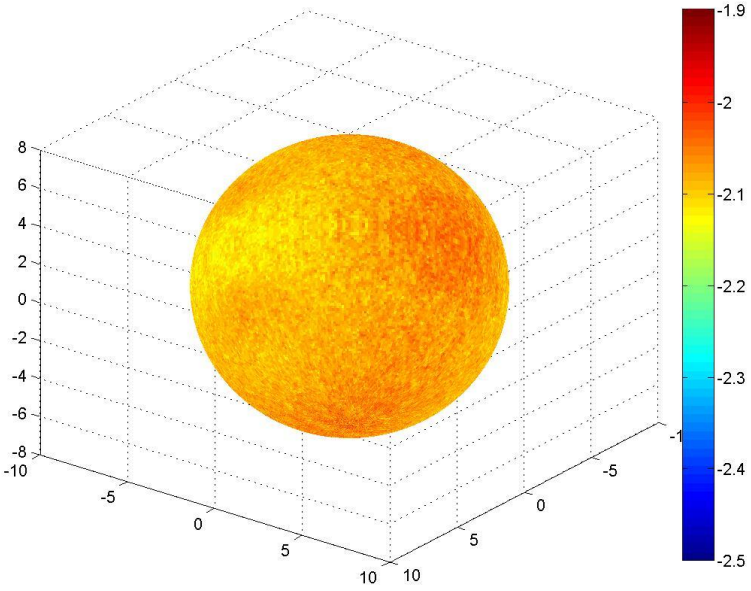

Figure B.68: Surface dose map for Design I, double beam irradiation, from 30 degrees below the equatorial plane, scale minimum raised to -2.5.

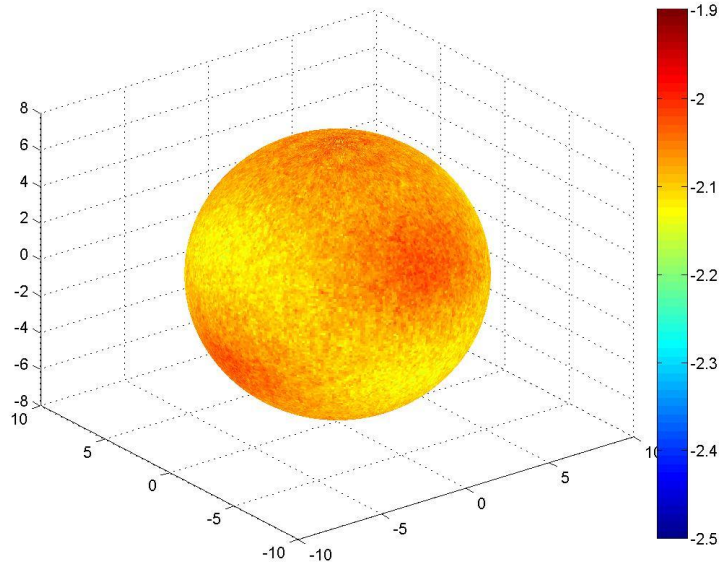

Figure B.69: Surface dose map for Design I, double beam irradiation with a 90° rotation about the vertical axis, from 30 degrees above the equatorial plane, scale minimum raised to -2.5.

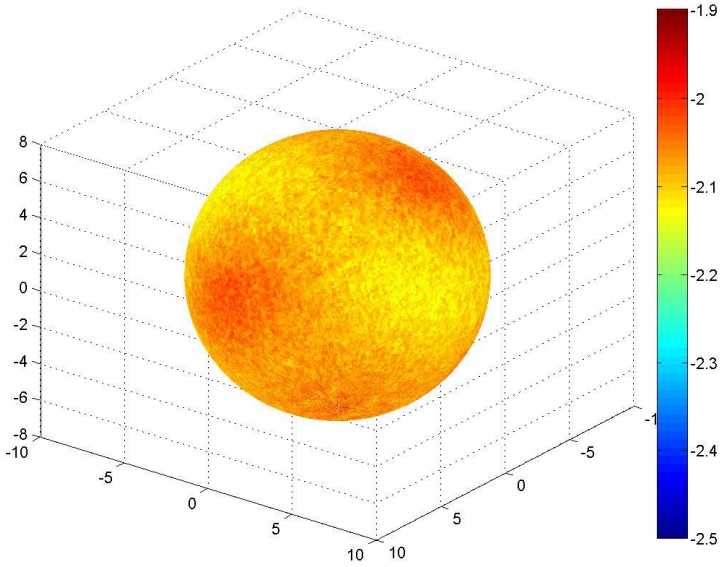

Figure B.70: Surface dose map for Design I, double beam irradiation with a 90° rotation about the vertical axis, from 30 degrees below the equatorial plane, scale minimum raised to -2.5.

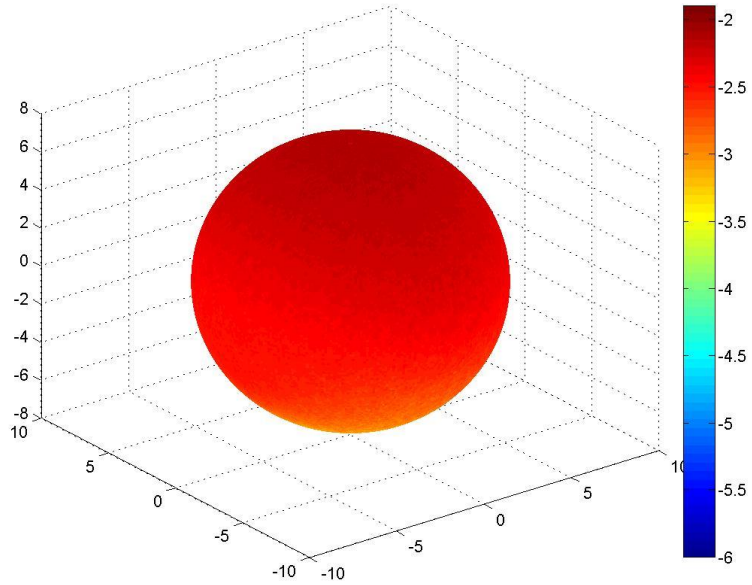

Figure B.71: Surface dose map for Design J, single beam irradiation, from 30 degrees above the equatorial plane, original scale.

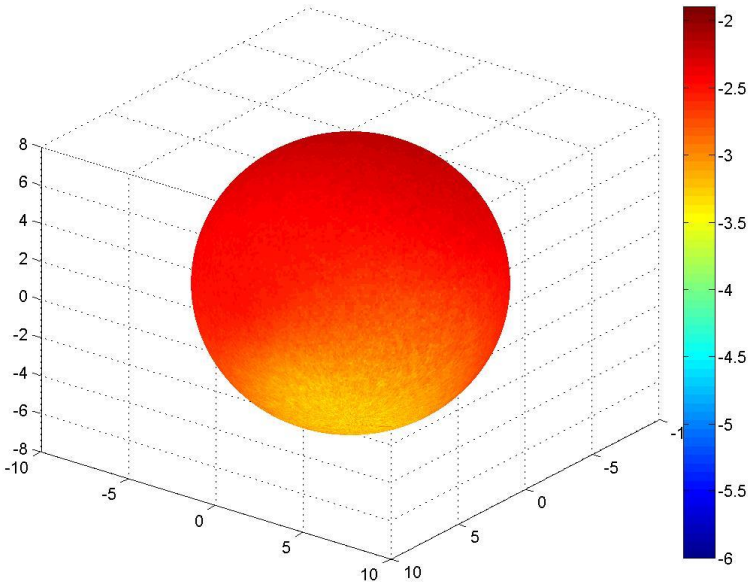

Figure B.72: Surface dose map for Design J, single beam irradiation, from 30 degrees below the equatorial plane, original scale.

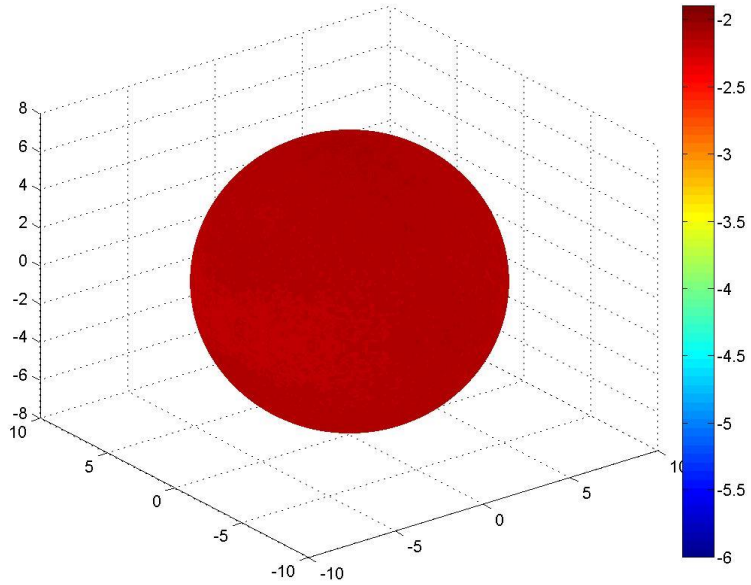

Figure B.73: Surface dose map for Design J, double beam irradiation, from 30 degrees above the equatorial plane, original scale.

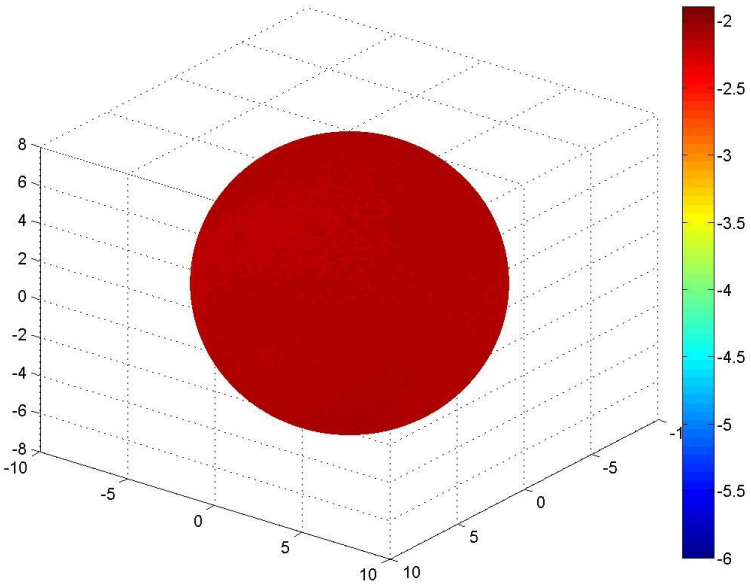

Figure B.74: Surface dose map for Design J, double beam irradiation, from 30 degrees below the equatorial plane, original scale.

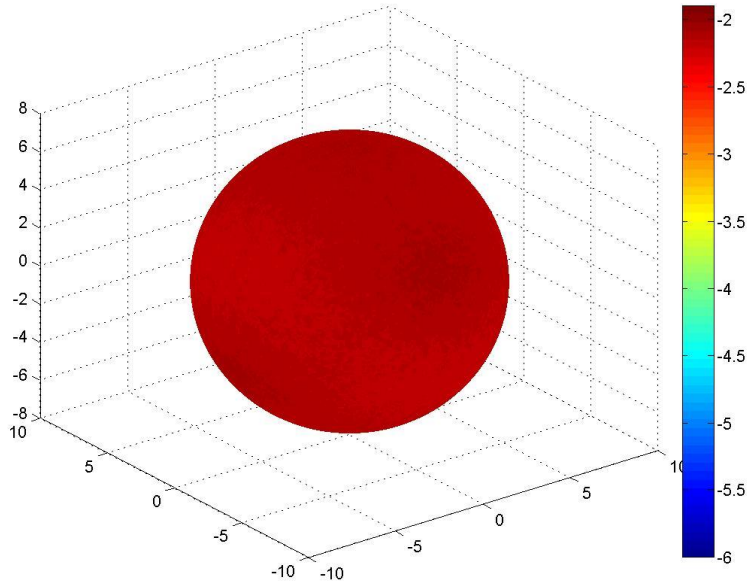

Figure B.75: Surface dose map for Design J, double beam irradiation with a 90° rotation about the vertical axis, from 30 degrees above the equatorial plane, original scale.

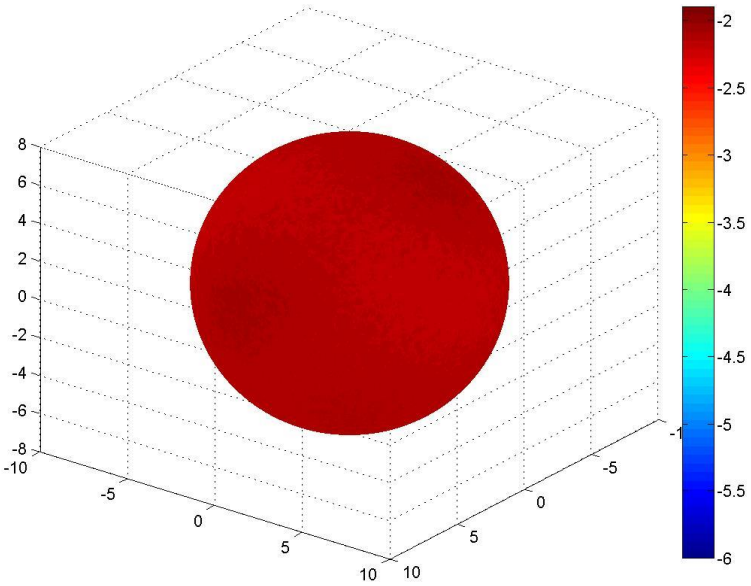

Figure B.76: Surface dose map for Design J, double beam irradiation with a 90° rotation about the vertical axis, from 30 degrees below the equatorial plane, original scale.

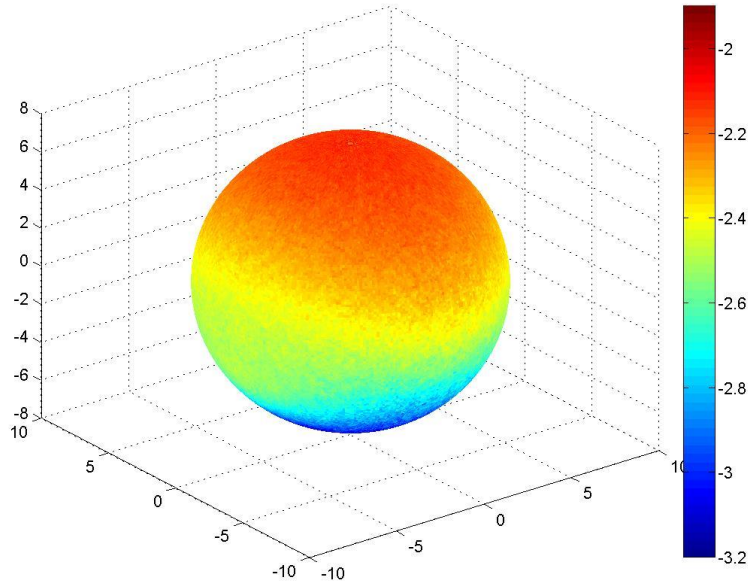

Figure B.77: Surface dose map for Design J, single beam irradiation, from 30 degrees above the equatorial plane, scale minimum raised to -3.2.

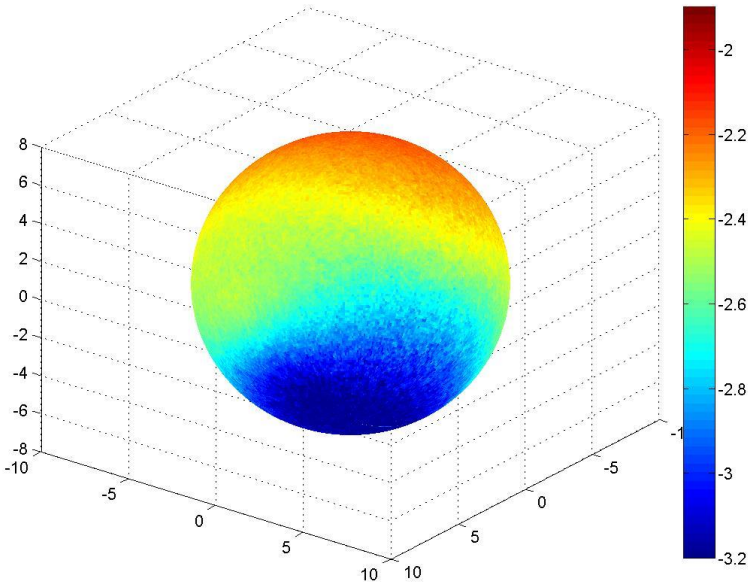

Figure B.78: Surface dose map for Design J, single beam irradiation, from 30 degrees below the equatorial plane, scale minimum raised to -3.2.

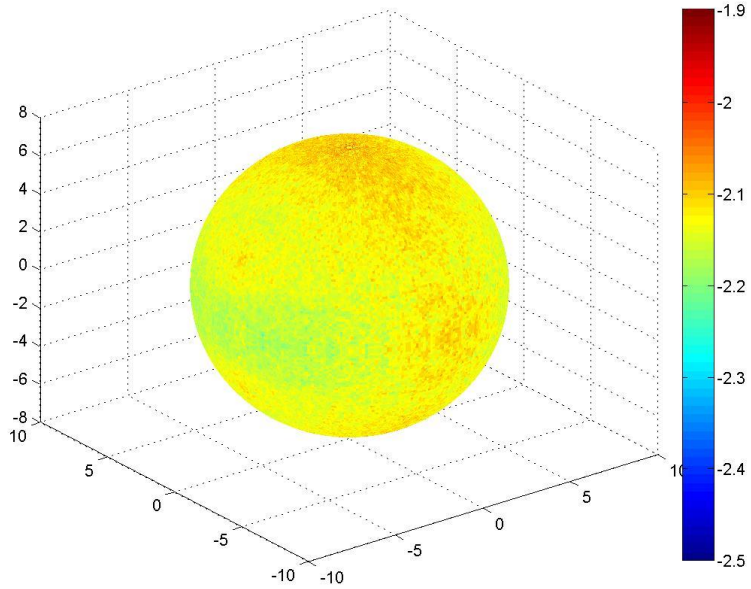

Figure B.79: Surface dose map for Design J, double beam irradiation, from 30 degrees above the equatorial plane, scale minimum raised to -2.5.

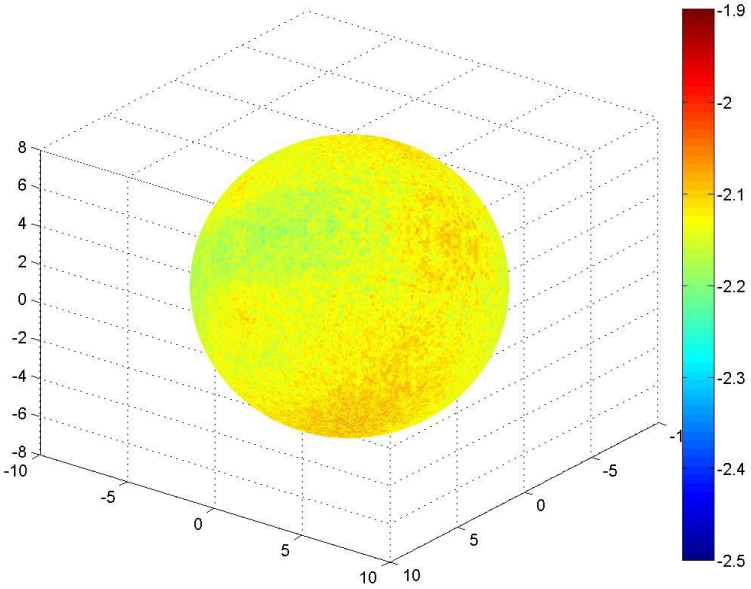

Figure B.80: Surface dose map for Design J, double beam irradiation, from 30 degrees below the equatorial plane, scale minimum raised to -2.5.

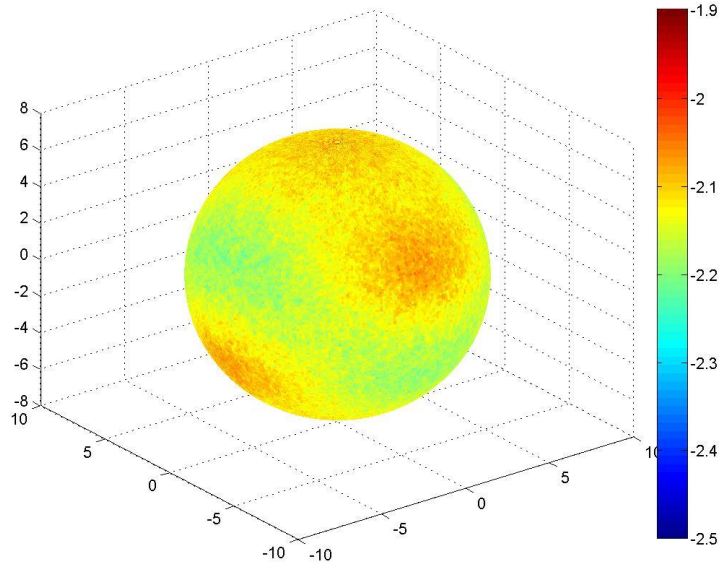

Figure B.81: Surface dose map for Design J, double beam irradiation with a 90° rotation about the vertical axis, from 30 degrees above the equatorial plane, scale minimum raised to -2.5.

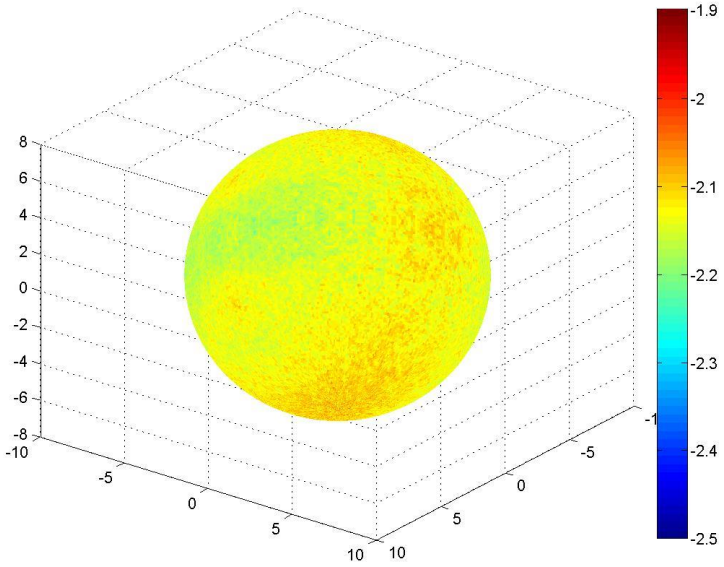

Figure B.82: Surface dose map for Design J, double beam irradiation with a 90° rotation about the vertical axis, from 30 degrees below the equatorial plane, scale minimum raised to -2.5.

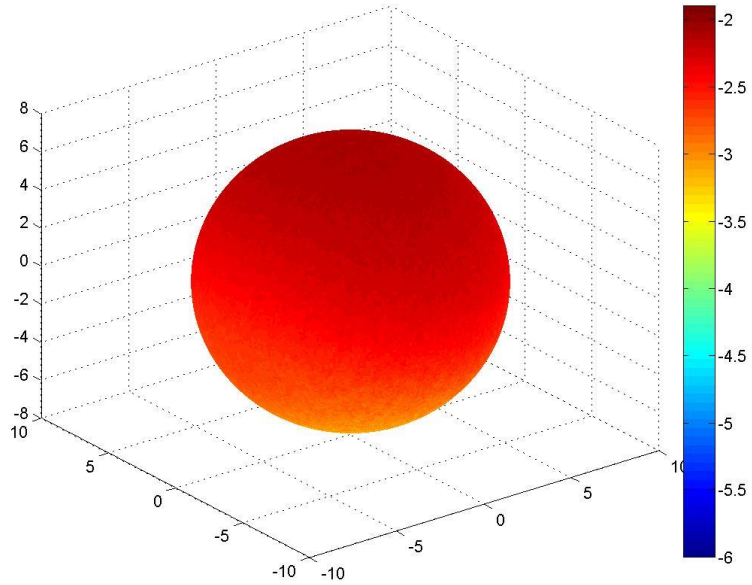

Figure B.83: Surface dose map for Design K, single beam irradiation, from 30 degrees above the equatorial plane, original scale.

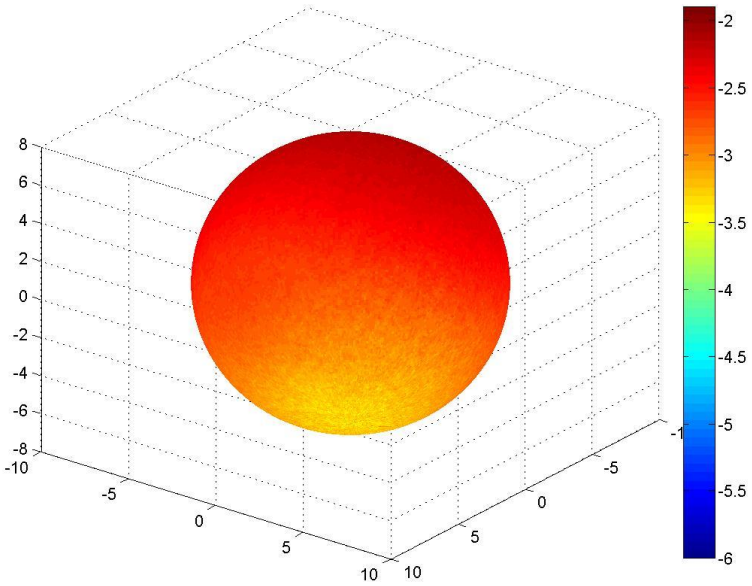

Figure B.84: Surface dose map for Design K, single beam irradiation, from 30 degrees below the equatorial plane, original scale.

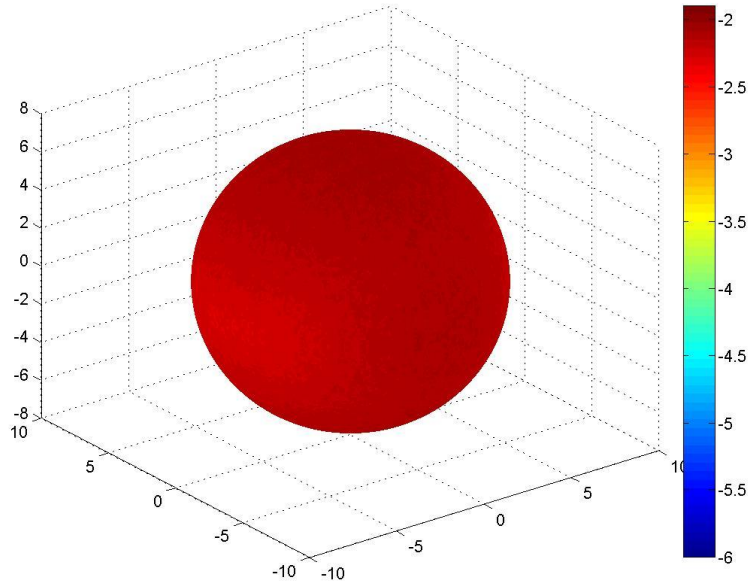

Figure B.85: Surface dose map for Design K, double beam irradiation, from 30 degrees above the equatorial plane, original scale.

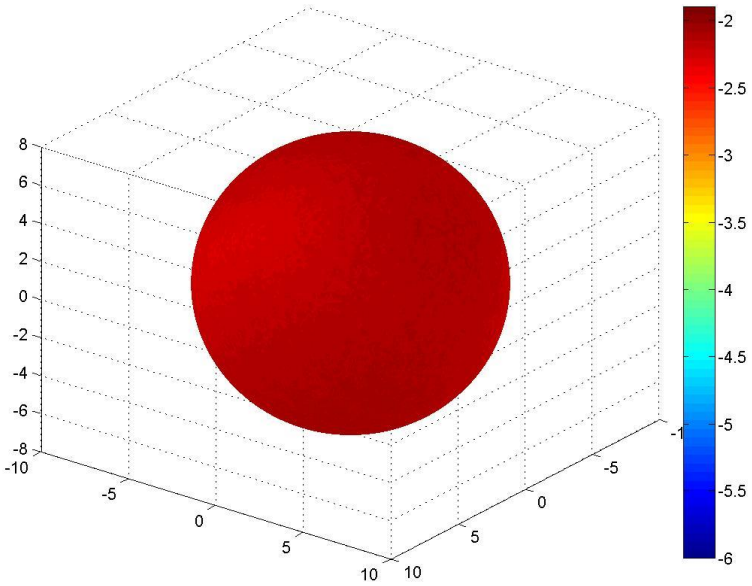

Figure B.86: Surface dose map for Design K, double beam irradiation, from 30 degrees below the equatorial plane, original scale.

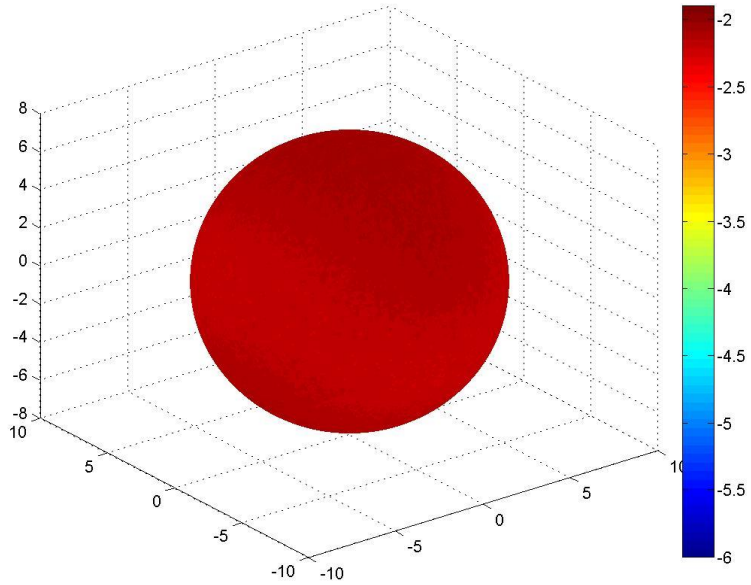

Figure B.87: Surface dose map for Design K, double beam irradiation with a 90° rotation about the vertical axis, from 30 degrees above the equatorial plane, original scale.

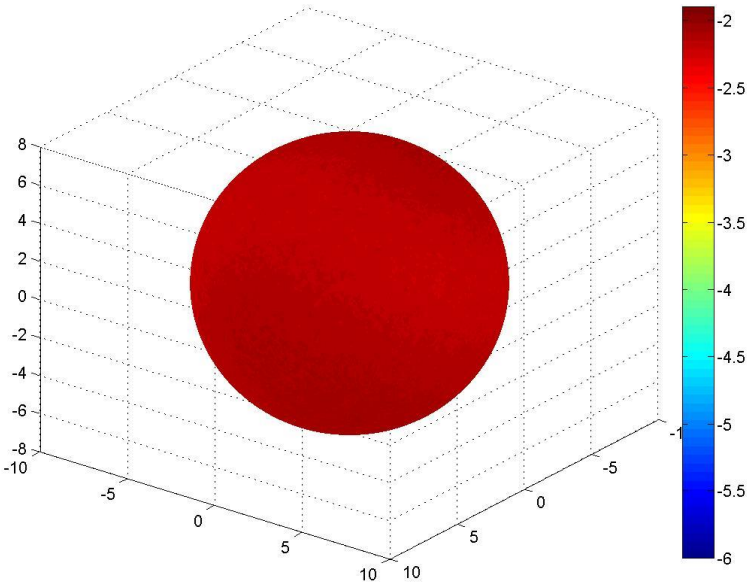

Figure B.88: Surface dose map for Design K, double beam irradiation with a 90° rotation about the vertical axis, from 30 degrees below the equatorial plane, original scale.

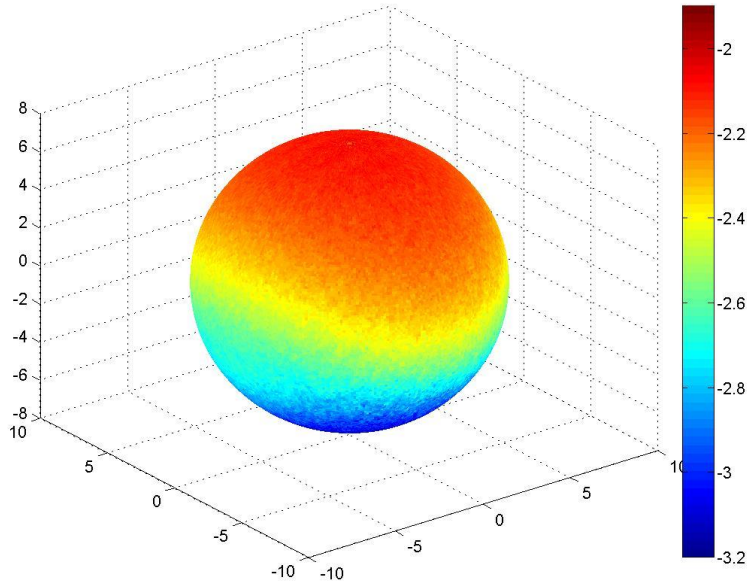

Figure B.89: Surface dose map for Design K, single beam irradiation, from 30 degrees above the equatorial plane, scale minimum raised to -3.2.

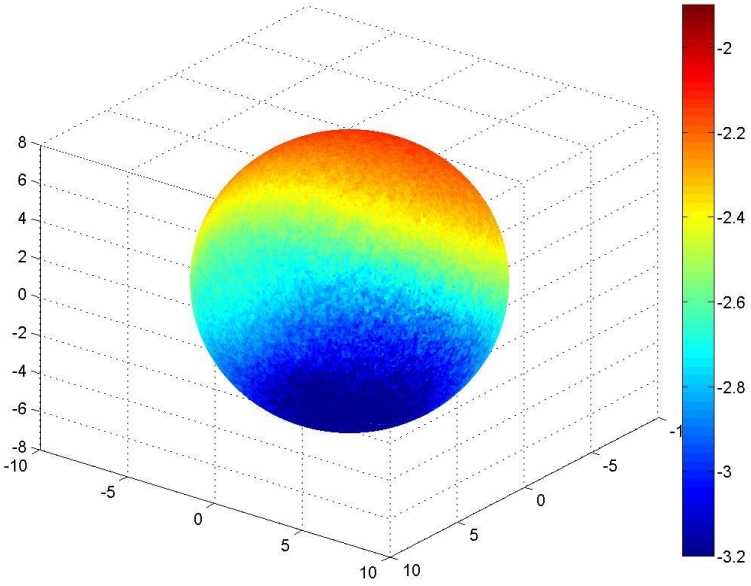

Figure B.90: Surface dose map for Design K, single beam irradiation, from 30 degrees below the equatorial plane, scale minimum raised to -3.2.

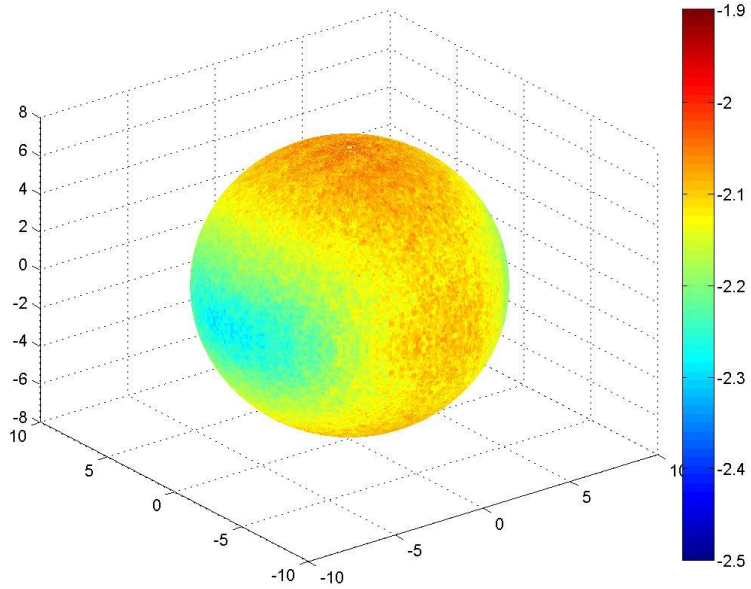

Figure B.91: Surface dose map for Design K, double beam irradiation, from 30 degrees above the equatorial plane, scale minimum raised to -2.5.

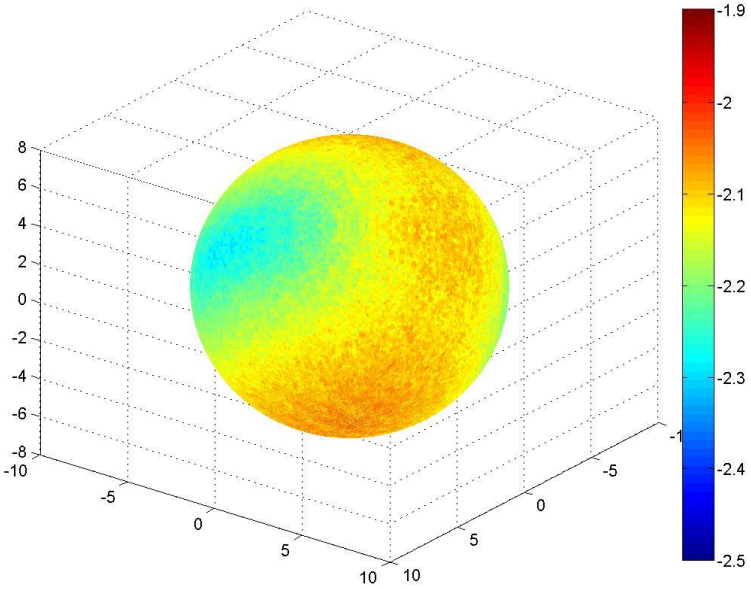

Figure B.92: Surface dose map for Design K, double beam irradiation, from 30 degrees below the equatorial plane, scale minimum raised to -2.5.

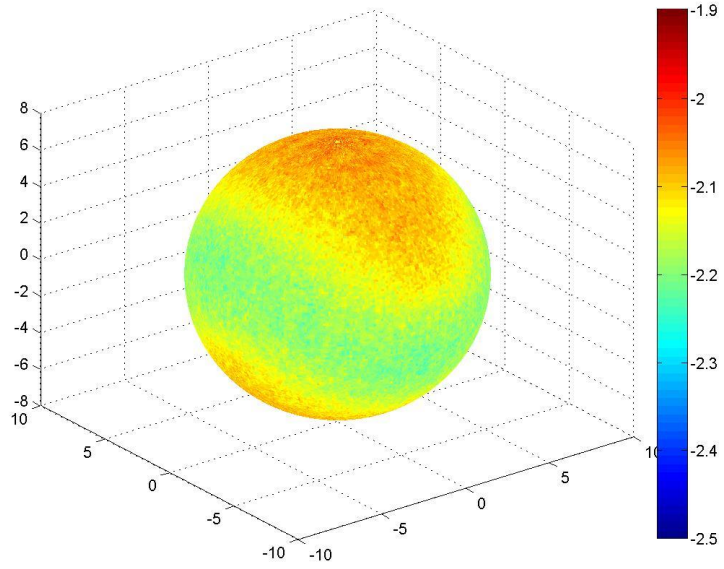

Figure B.93: Surface dose map for Design K, double beam irradiation with a 90° rotation about the vertical axis, from 30 degrees above the equatorial plane, scale minimum raised to -2.5.

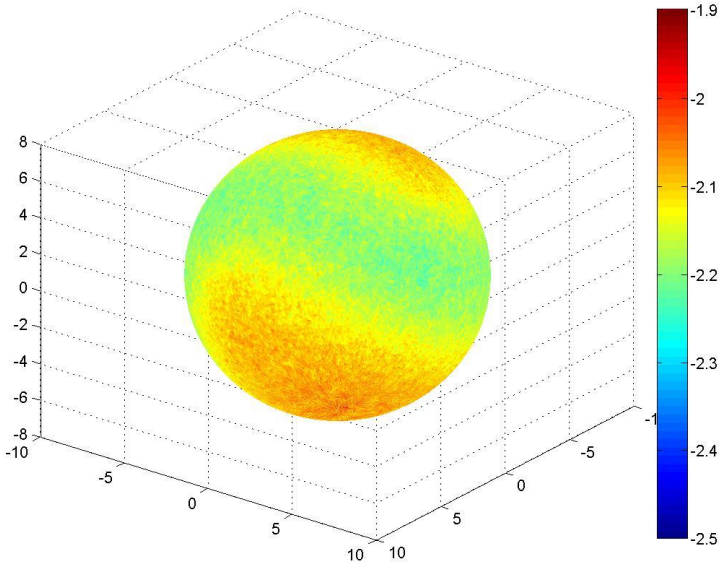

Figure B.94: Surface dose map for Design K, double beam irradiation with a 90° rotation about the vertical axis, from 30 degrees below the equatorial plane, scale minimum raised to -2.5.

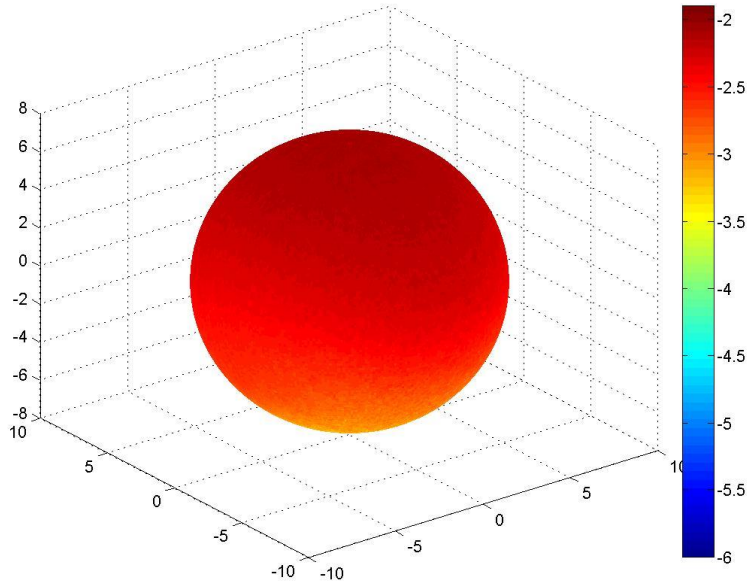

Figure B.95: Surface dose map for Design L, single beam irradiation, from 30 degrees above the equatorial plane, original scale.

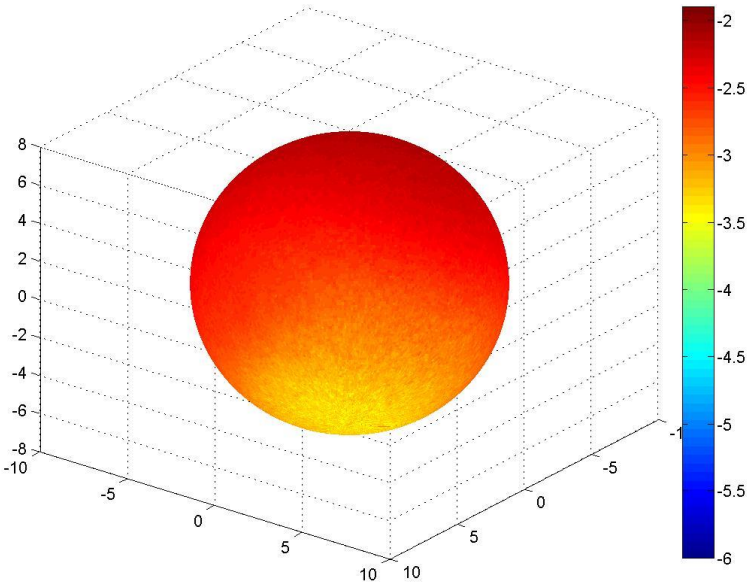

Figure B.96: Surface dose map for Design L, single beam irradiation, from 30 degrees below the equatorial plane, original scale.

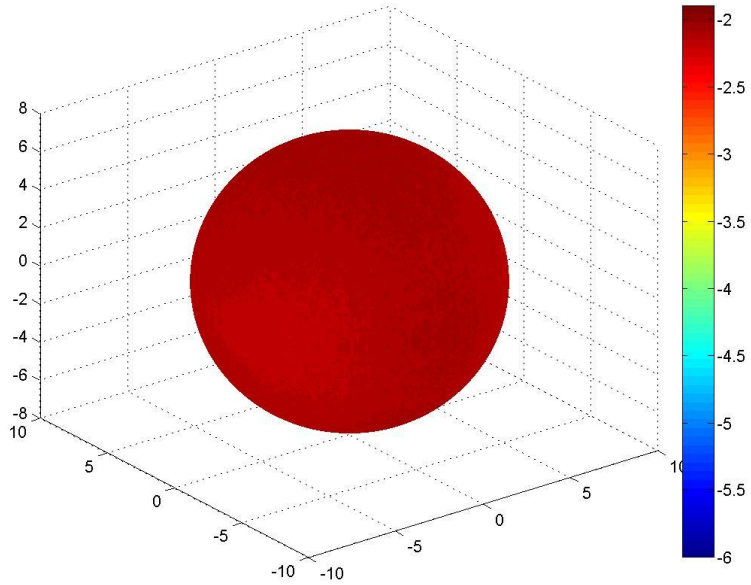

Figure B.97: Surface dose map for Design L, double beam irradiation, from 30 degrees above the equatorial plane, original scale.

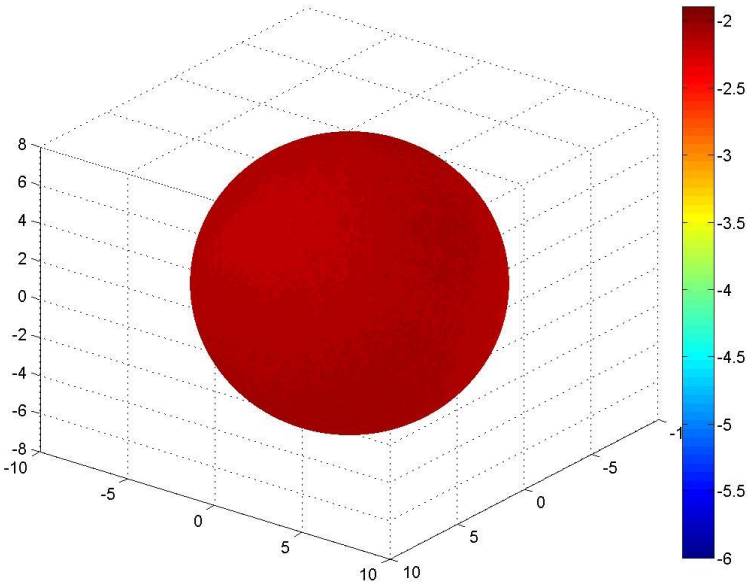

Figure B.98: Surface dose map for Design L, double beam irradiation, from 30 degrees below the equatorial plane, original scale.

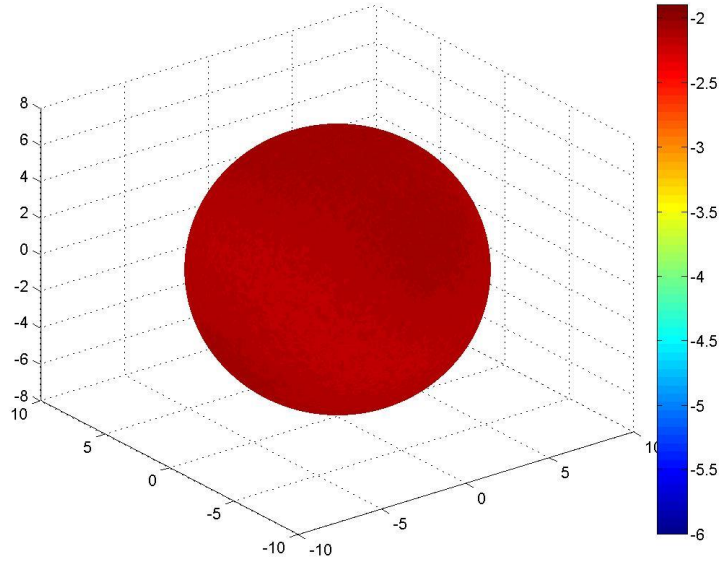

Figure B.99: Surface dose map for Design L, double beam irradiation with a 90° rotation about the vertical axis, from 30 degrees above the equatorial plane, original scale.

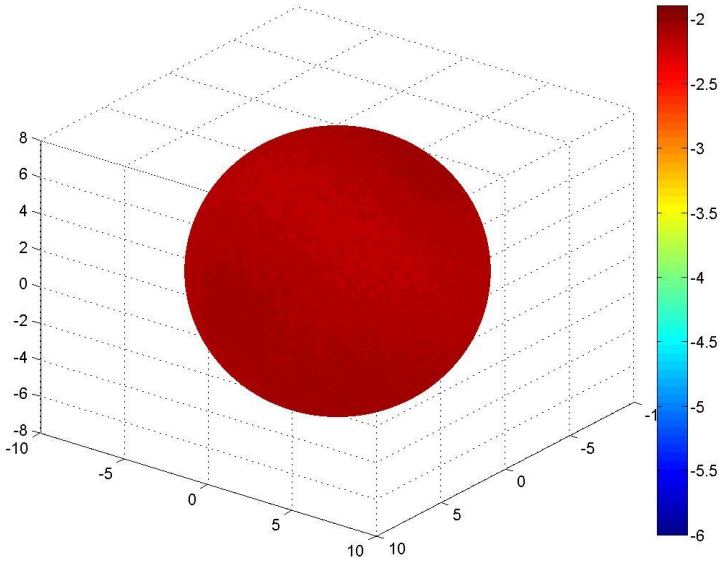

Figure B.100: Surface dose map for Design L, double beam irradiation with a 90° rotation about the vertical axis, from 30 degrees below the equatorial plane, original scale.

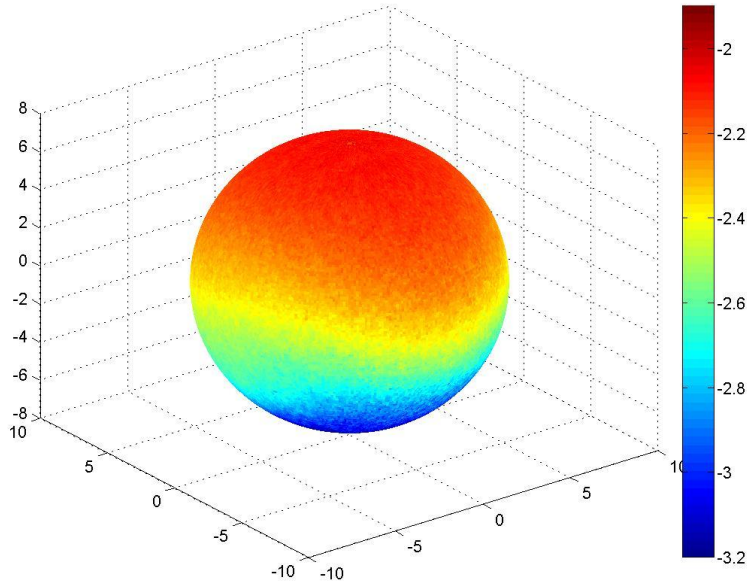

Figure B.101: Surface dose map for Design L, single beam irradiation, from 30 degrees above the equatorial plane, scale minimum raised to -3.2.

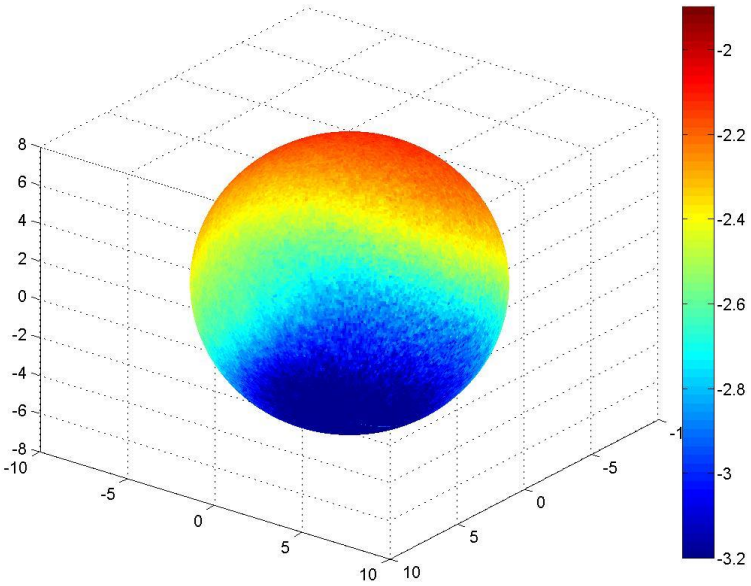

Figure B.102: Surface dose map for Design L, single beam irradiation, from 30 degrees below the equatorial plane, scale minimum raised to -3.2.

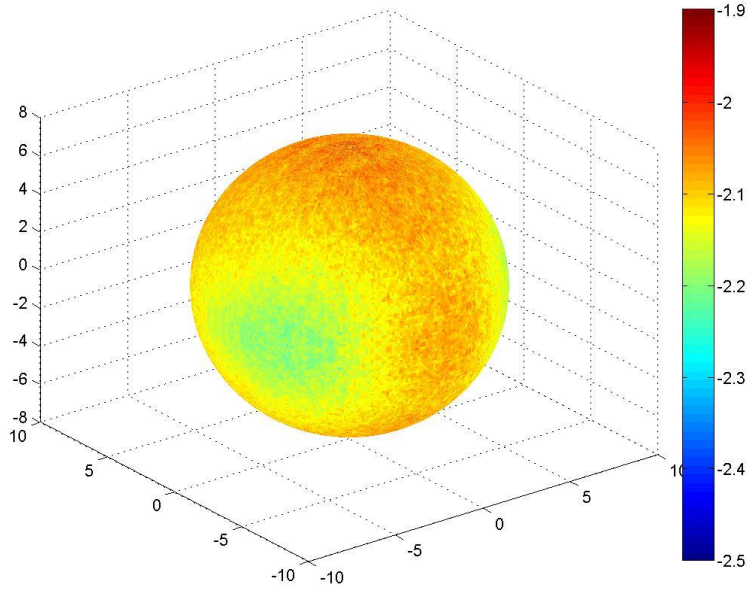

Figure B.103: Surface dose map for Design L, double beam irradiation, from 30 degrees above the equatorial plane, scale minimum raised to -2.5.

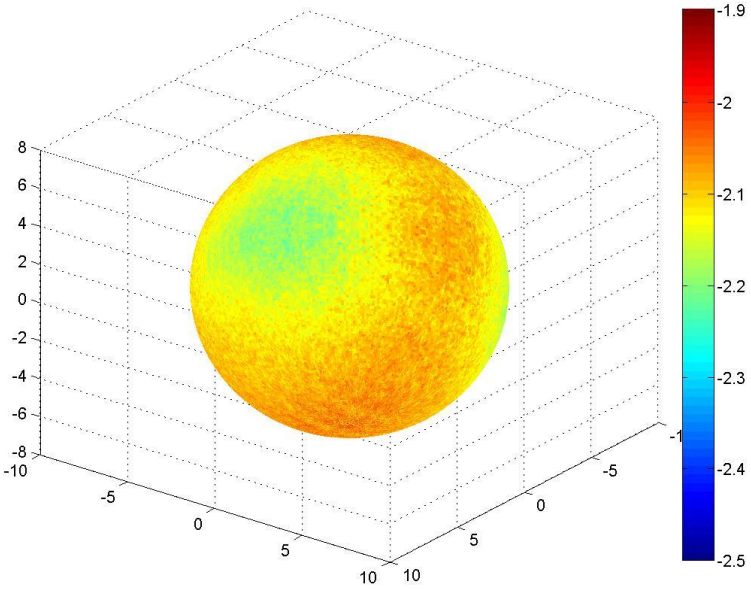

Figure B.104: Surface dose map for Design L, double beam irradiation, from 30 degrees below the equatorial plane, scale minimum raised to -2.5.

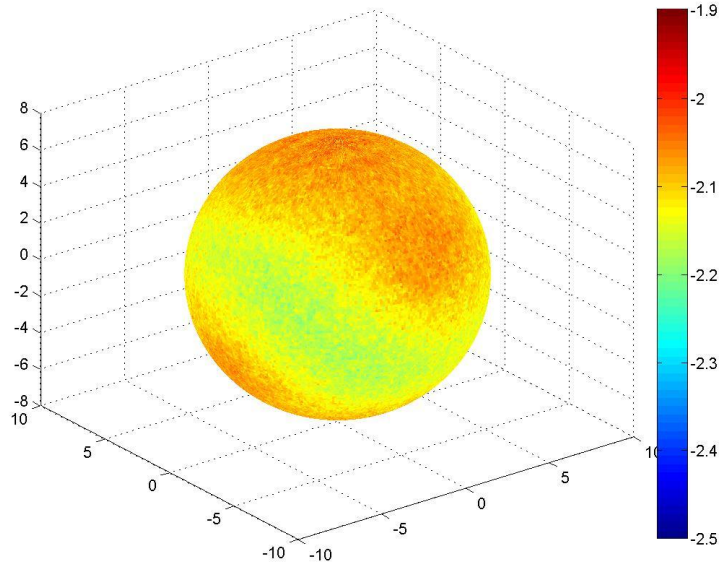

Figure B.105: Surface dose map for Design L, double beam irradiation with a 90° rotation about the vertical axis, from 30 degrees above the equatorial plane, scale minimum raised to -2.5.

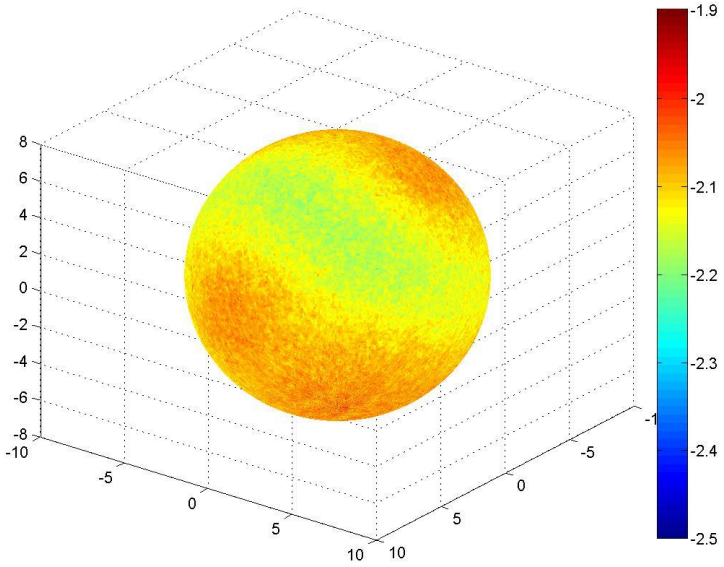

Figure B.106: Surface dose map for Design L, double beam irradiation with a 90° rotation about the vertical axis, from 30 degrees below the equatorial plane, scale minimum raised to -2.5.

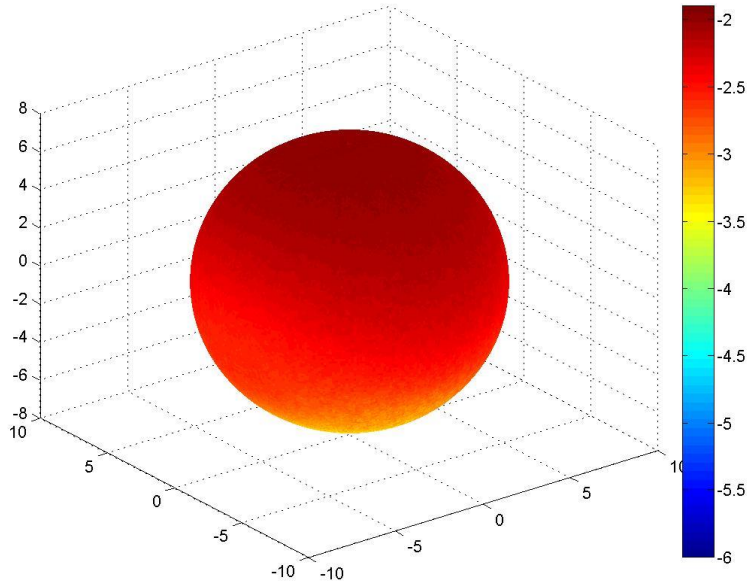

Figure B.107: Surface dose map for Design M, single beam irradiation, from 30 degrees above the equatorial plane, original scale.

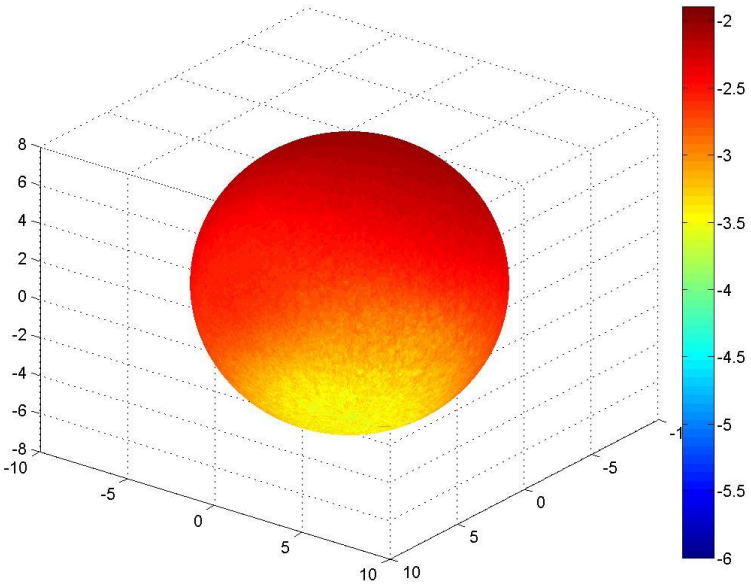

Figure B.108: Surface dose map for Design M, single beam irradiation, from 30 degrees below the equatorial plane, original scale.

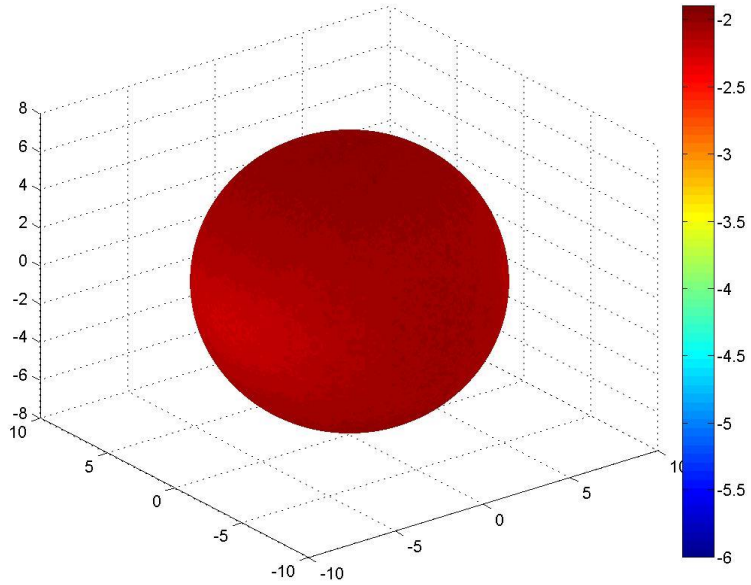

Figure B.109: Surface dose map for Design M, double beam irradiation, from 30 degrees above the equatorial plane, original scale.

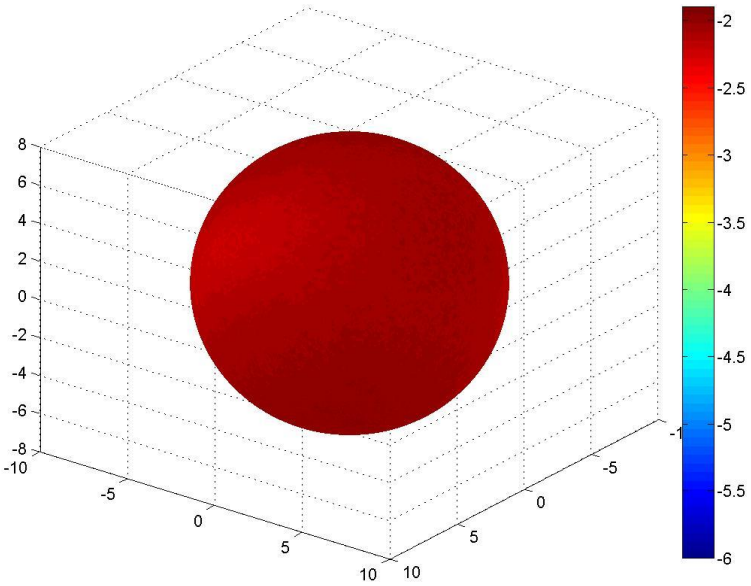

Figure B.110: Surface dose map for Design M, double beam irradiation, from 30 degrees below the equatorial plane, original scale.

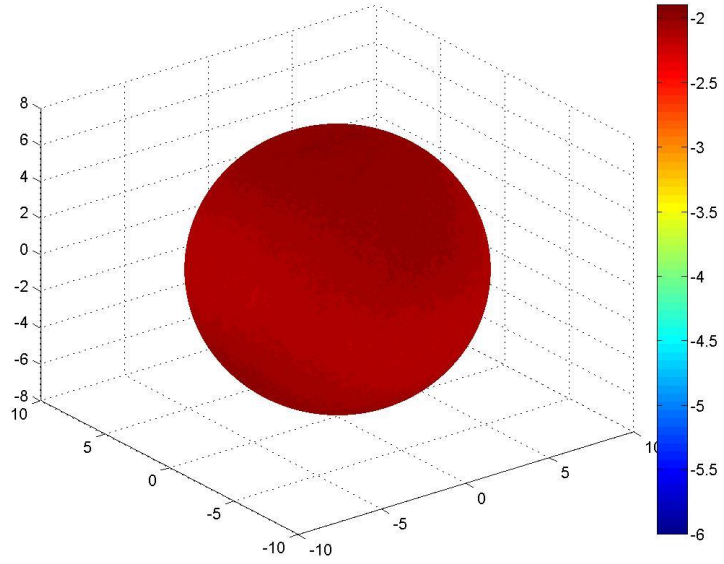

Figure B.111: Surface dose map for Design M, double beam irradiation with a 90° rotation about the vertical axis, from 30 degrees above the equatorial plane, original scale.

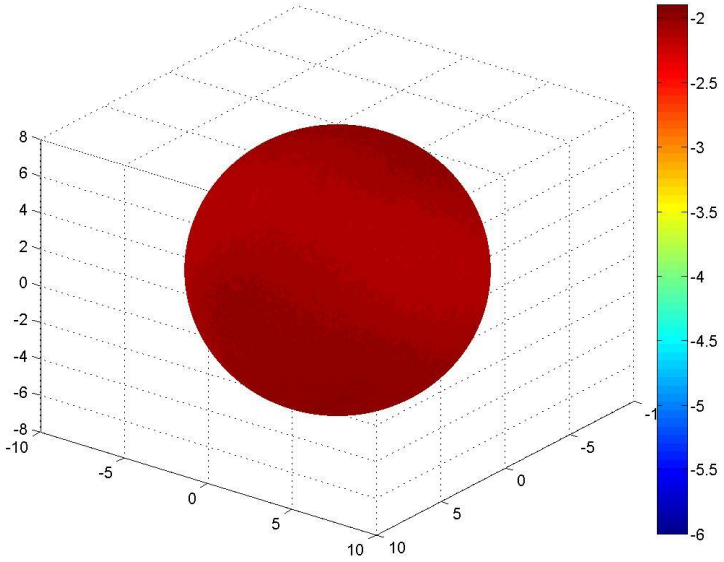

Figure B.112: Surface dose map for Design M, double beam irradiation with a 90° rotation about the vertical axis, from 30 degrees below the equatorial plane, original scale.

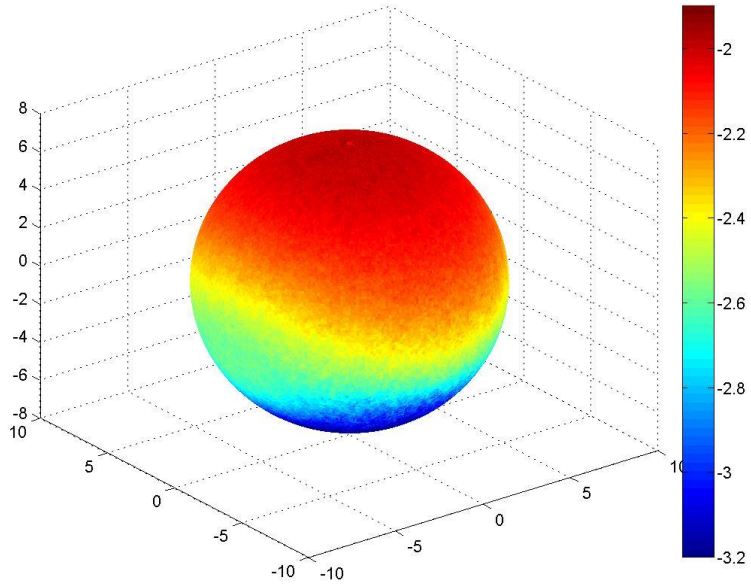

Figure B.113: Surface dose map for Design M, single beam irradiation, from 30 degrees above the equatorial plane, scale minimum raised to -3.2.

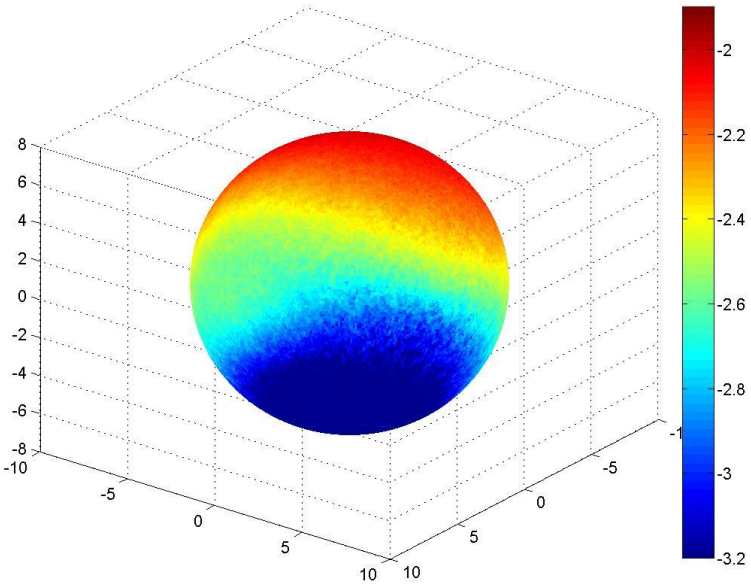

Figure B.114: Surface dose map for Design M, single beam irradiation, from 30 degrees below the equatorial plane, scale minimum raised to -3.2.

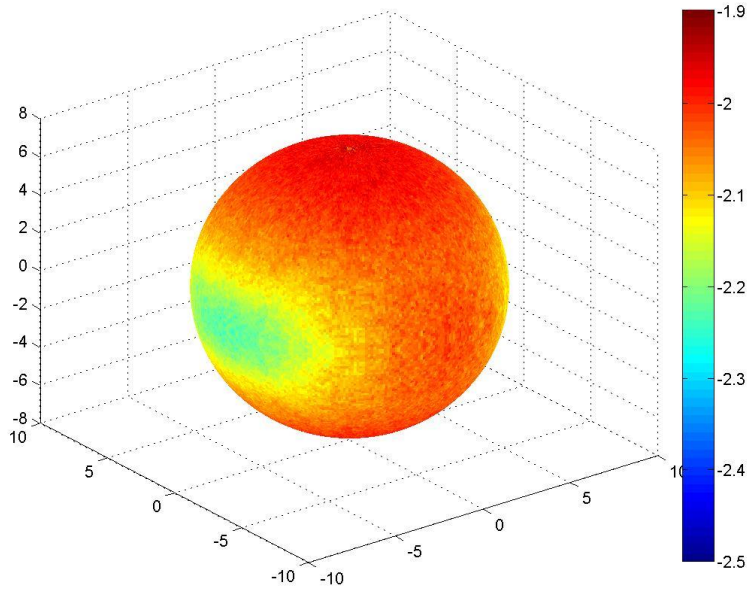

Figure B.115: Surface dose map for Design M, double beam irradiation, from 30 degrees above the equatorial plane, scale minimum raised to -2.5.

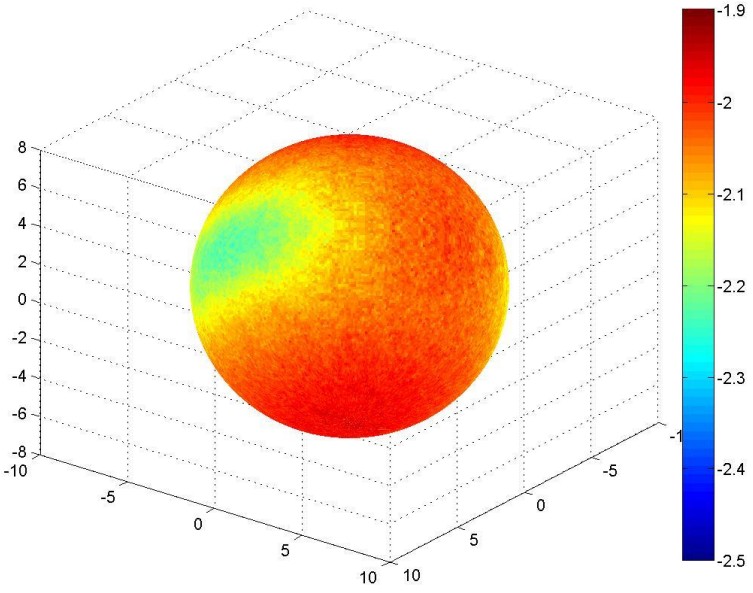

Figure B.116: Surface dose map for Design M, double beam irradiation, from 30 degrees below the equatorial plane, scale minimum raised to -2.5.

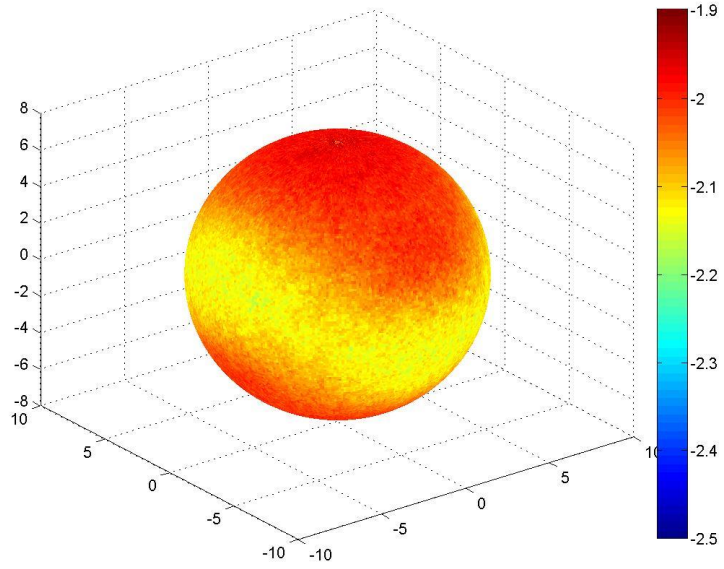

Figure B.117: Surface dose map for Design M, double beam irradiation with a 90° rotation about the vertical axis, from 30 degrees above the equatorial plane, scale minimum raised to -2.5.

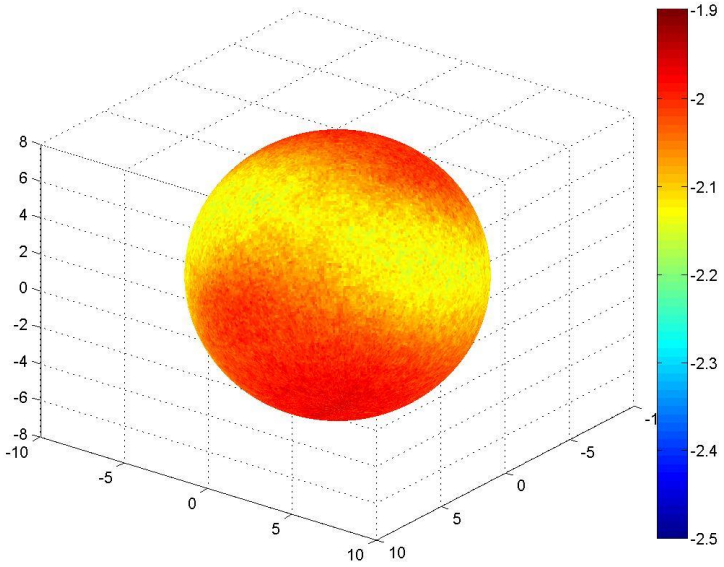

Figure B.118: Surface dose map for Design M, double beam irradiation with a 90° rotation about the vertical axis, from 30 degrees below the equatorial plane, scale minimum raised to -2.5.

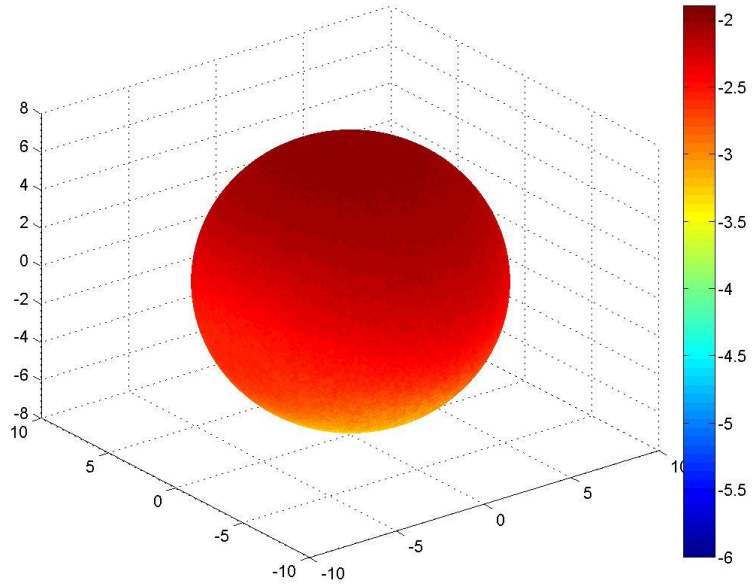

Figure B.119: Surface dose map for Design N, single beam irradiation, from 30 degrees above the equatorial plane, original scale.

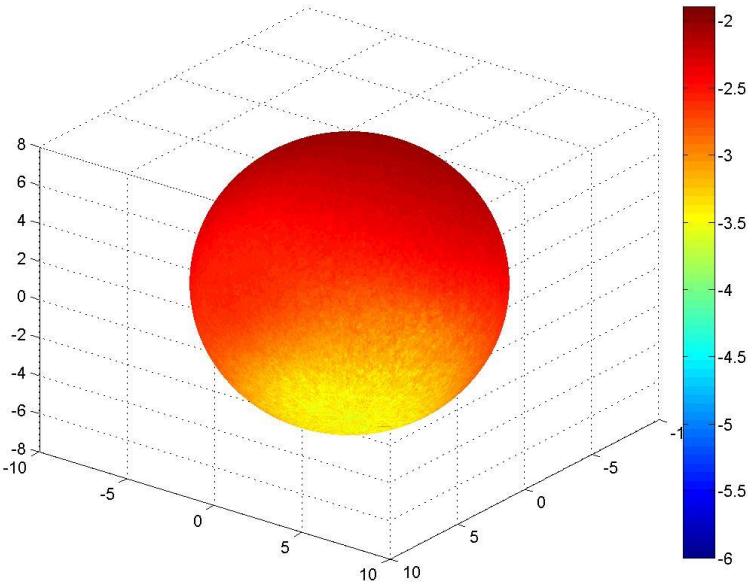

Figure B.120: Surface dose map for Design N, single beam irradiation, from 30 degrees below the equatorial plane, original scale.

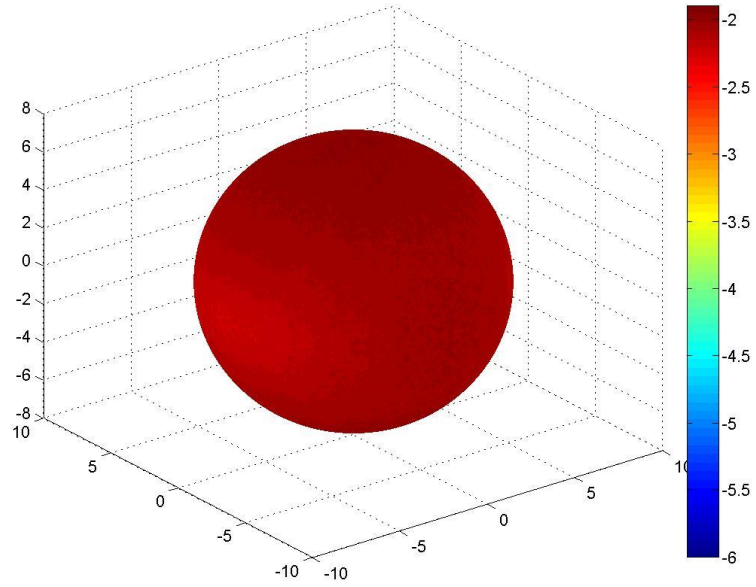

Figure B.121: Surface dose map for Design N, double beam irradiation, from 30 degrees above the equatorial plane, original scale.

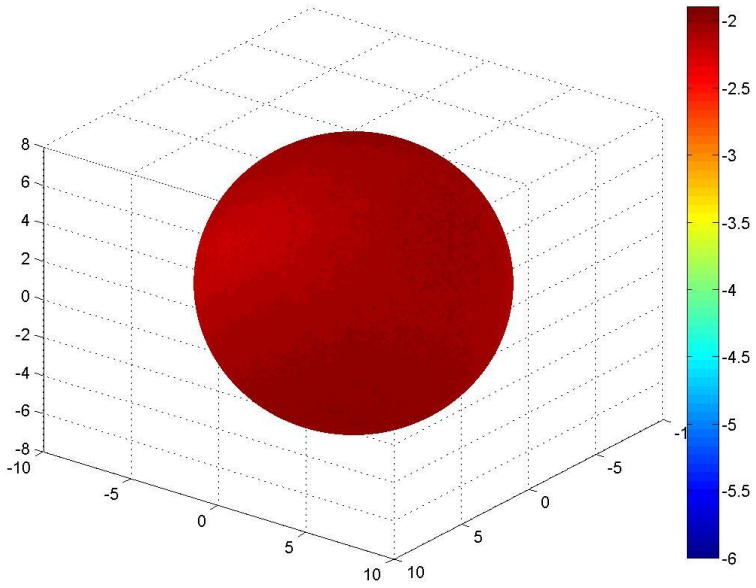

Figure B.122: Surface dose map for Design N, double beam irradiation, from 30 degrees below the equatorial plane, original scale.

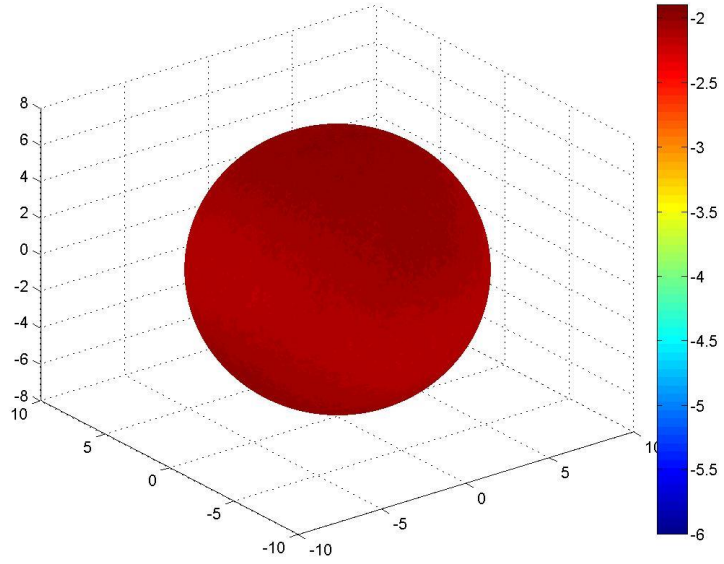

Figure B.123: Surface dose map for Design N, double beam irradiation with a 90° rotation about the vertical axis, from 30 degrees above the equatorial plane, original scale.

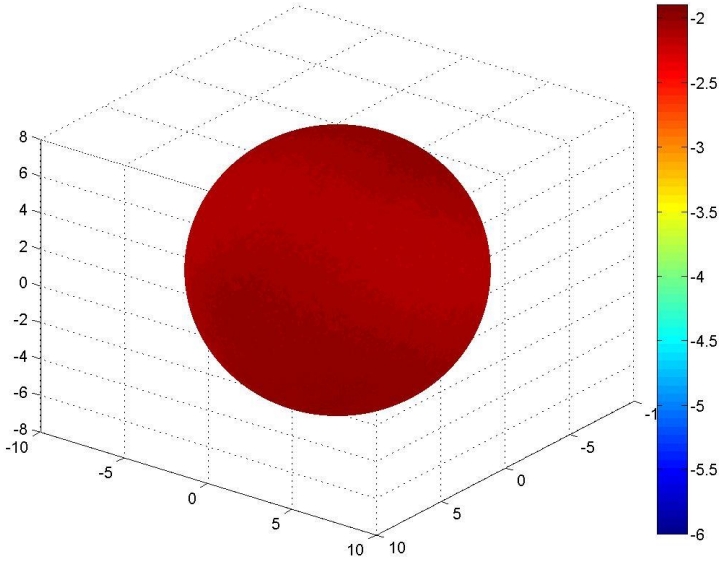

Figure B.124: Surface dose map for Design N, double beam irradiation with a 90° rotation about the vertical axis, from 30 degrees below the equatorial plane, original scale.

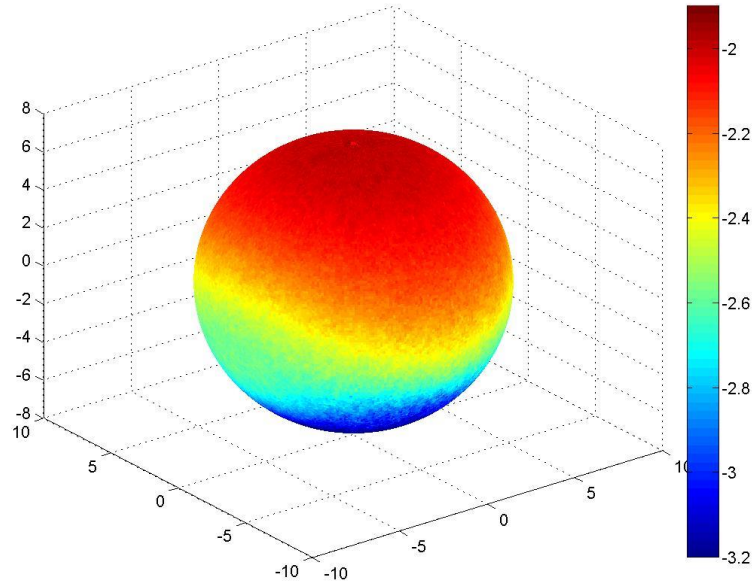

Figure B.125: Surface dose map for Design N, single beam irradiation, from 30 degrees above the equatorial plane, scale minimum raised to -3.2.

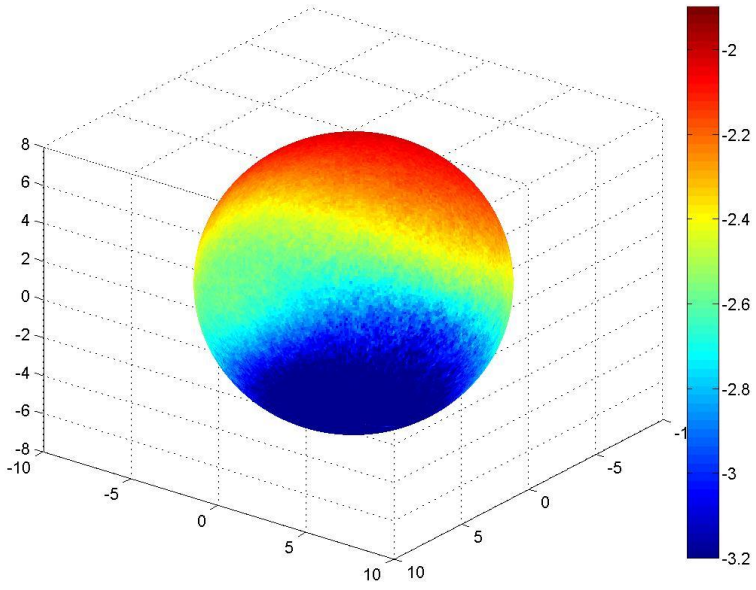

Figure B.126: Surface dose map for Design N, single beam irradiation, from 30 degrees below the equatorial plane, scale minimum raised to -3.2.

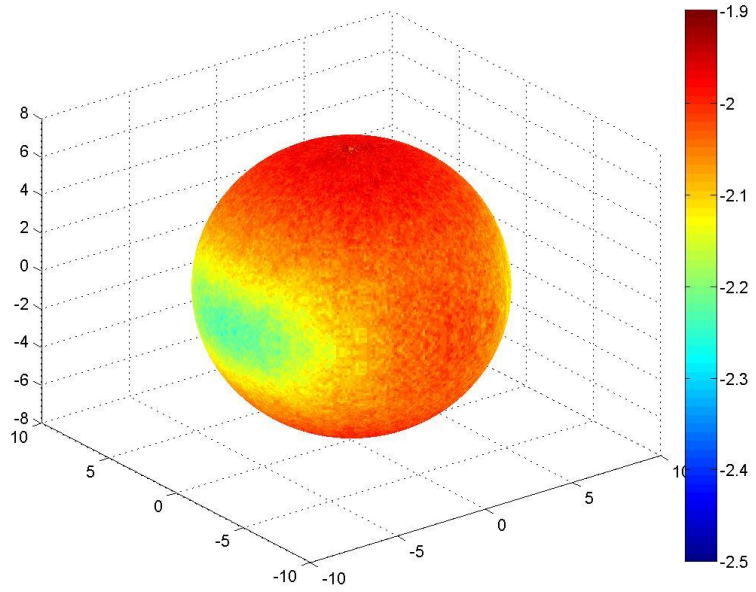

Figure B.127: Surface dose map for Design N, double beam irradiation, from 30 degrees above the equatorial plane, scale minimum raised to -2.5.

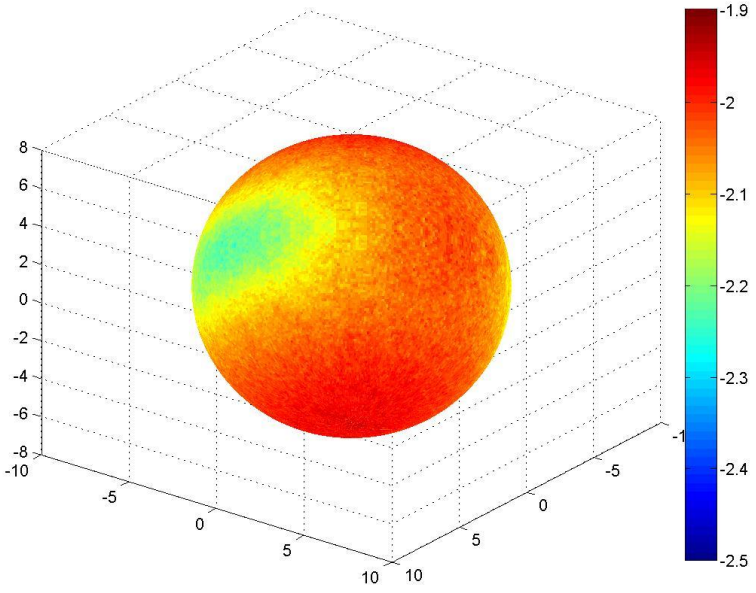

Figure B.128: Surface dose map for Design N, double beam irradiation, from 30 degrees below the equatorial plane, scale minimum raised to -2.5.

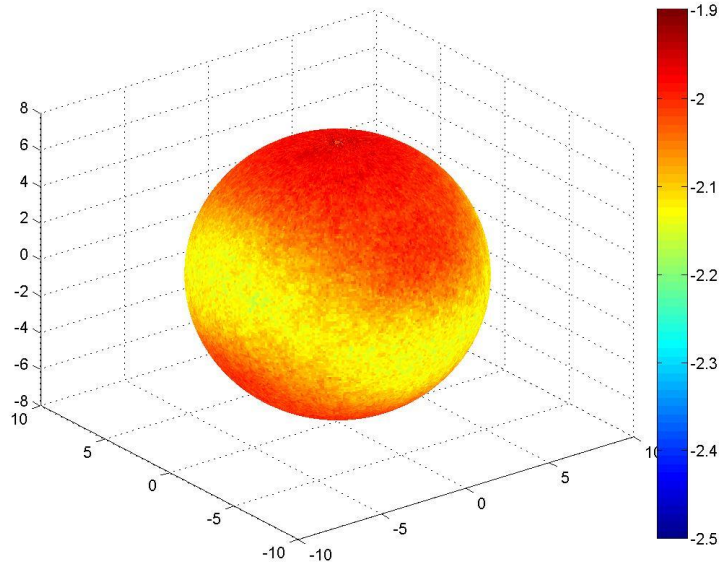

Figure B.129: Surface dose map for Design N, double beam irradiation with a 90° rotation about the vertical axis, from 30 degrees above the equatorial plane, scale minimum raised to -2.5.

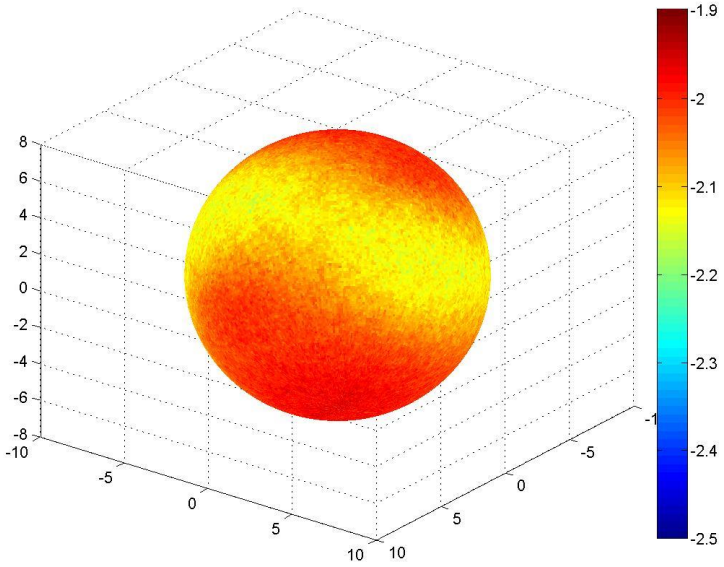

Figure B.130: Surface dose map for Design N, double beam irradiation with a 90° rotation about the vertical axis, from 30 degrees below the equatorial plane, scale minimum raised to -2.5.

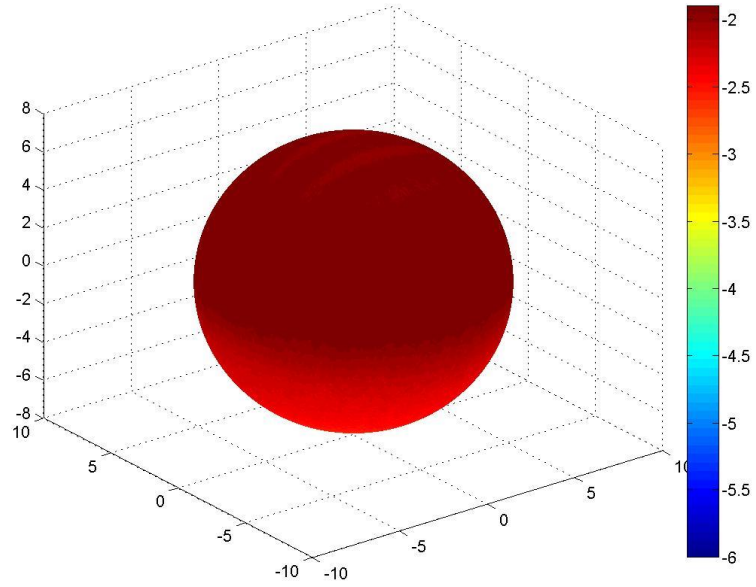

Figure B.131: Surface dose map for Design O, single beam irradiation, from 30 degrees above the equatorial plane, original scale.

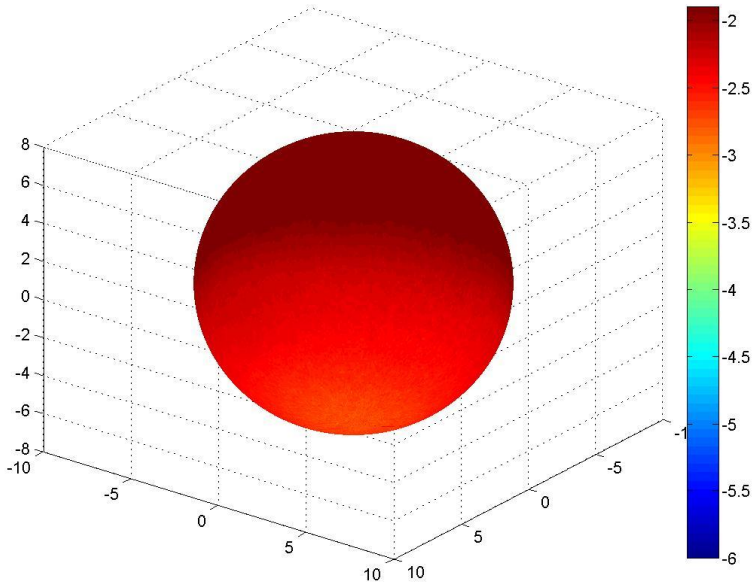

Figure B.132: Surface dose map for Design O, single beam irradiation, from 30 degrees below the equatorial plane, original scale.

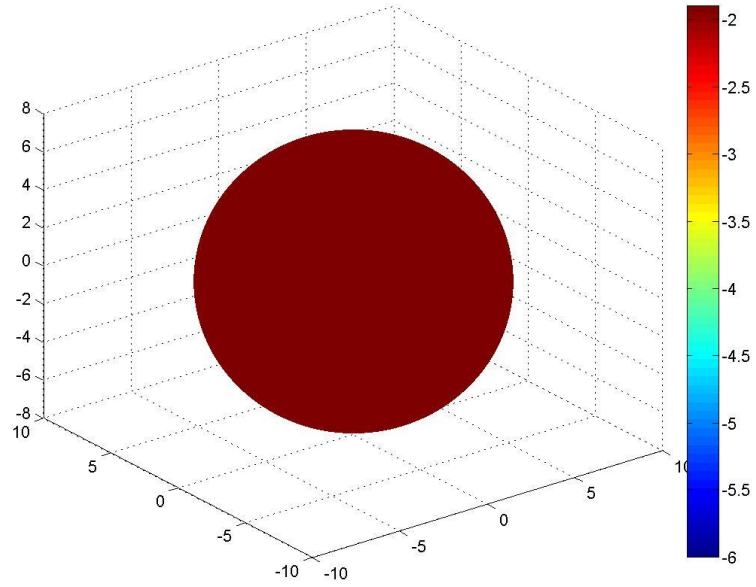

Figure B.133: Surface dose map for Design O, double beam irradiation, from 30 degrees above the equatorial plane, original scale.

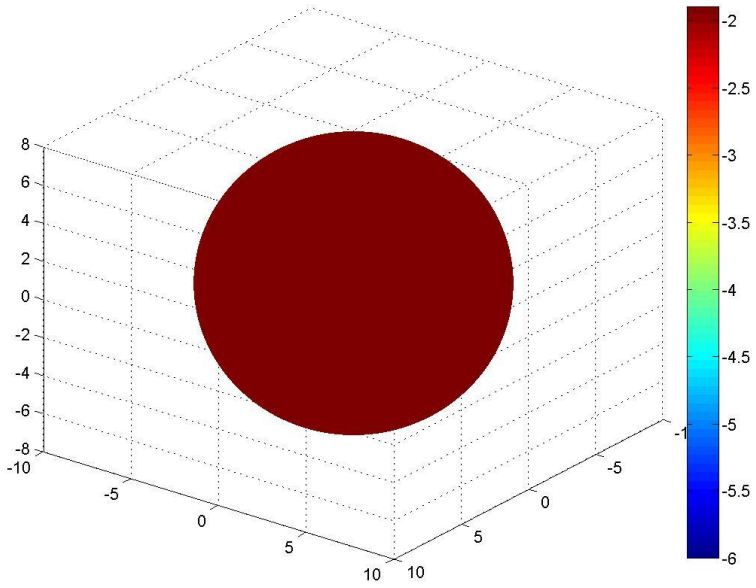

Figure B.134: Surface dose map for Design O, double beam irradiation, from 30 degrees below the equatorial plane, original scale.

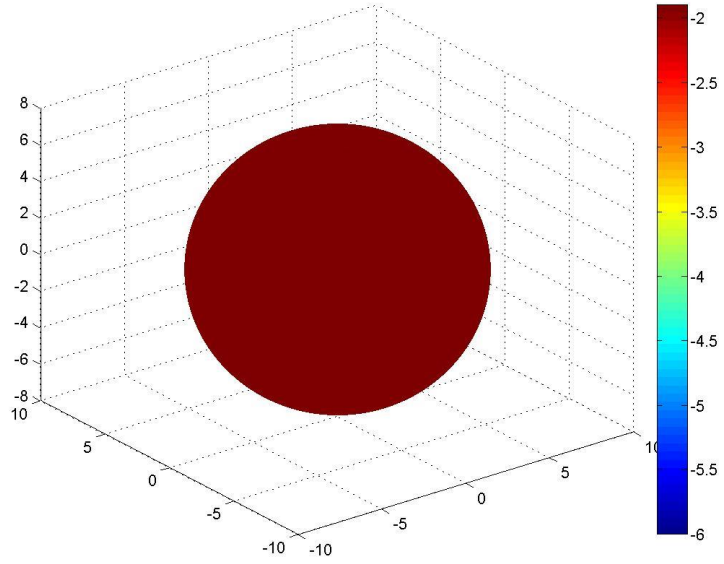

Figure B.135: Surface dose map for Design O, double beam irradiation with a 90° rotation about the vertical axis, from 30 degrees above the equatorial plane, original scale.

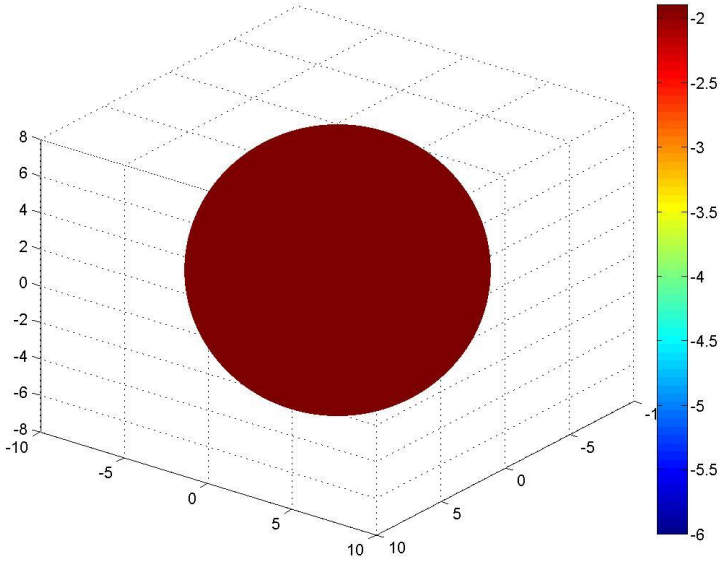

Figure B.136: Surface dose map for Design O, double beam irradiation with a 90° rotation about the vertical axis, from 30 degrees below the equatorial plane, original scale.

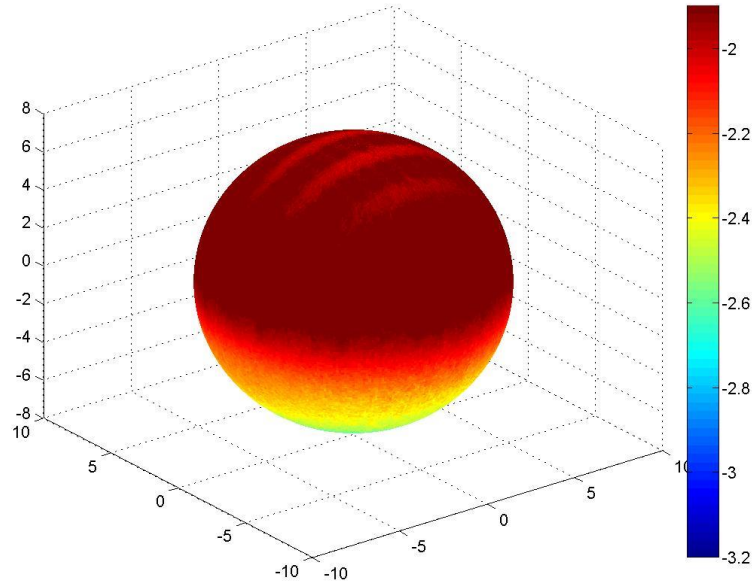

Figure B.137: Surface dose map for Design O, single beam irradiation, from 30 degrees above the equatorial plane, scale minimum raised to -3.2.

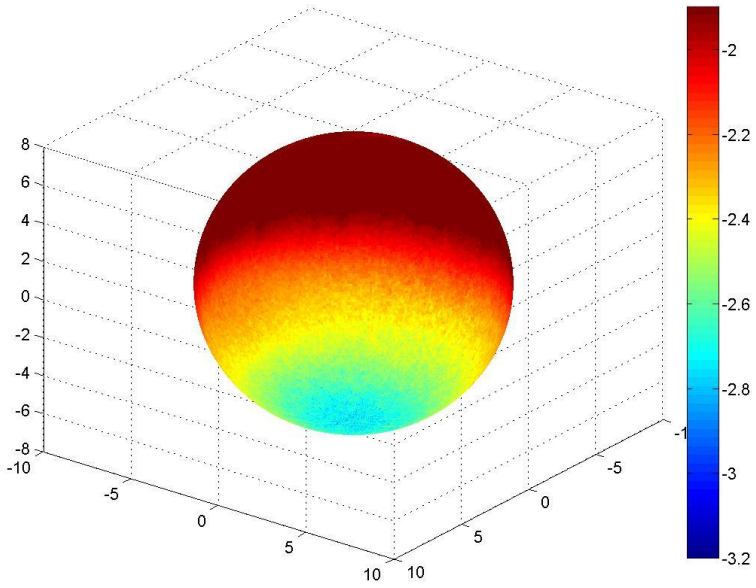

Figure B.138: Surface dose map for Design O, single beam irradiation, from 30 degrees below the equatorial plane, scale minimum raised to -3.2.

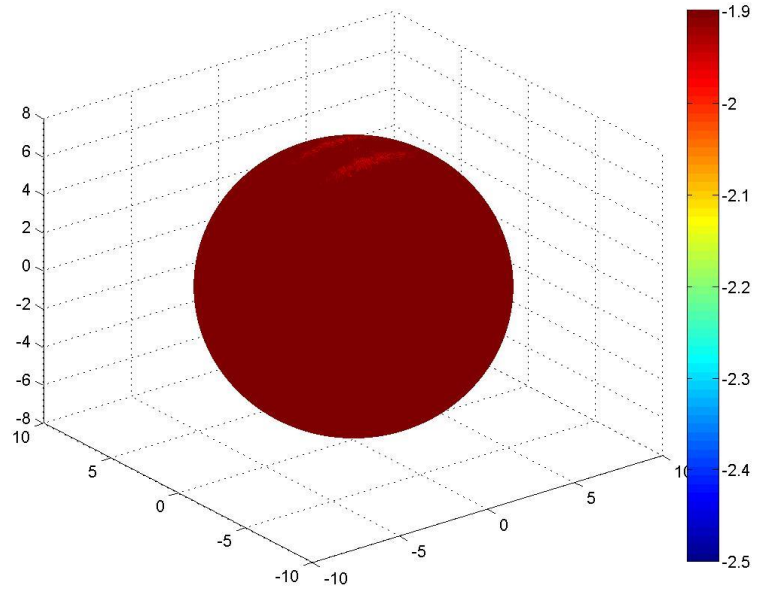

Figure B.139: Surface dose map for Design O, double beam irradiation, from 30 degrees above the equatorial plane, scale minimum raised to -2.5.

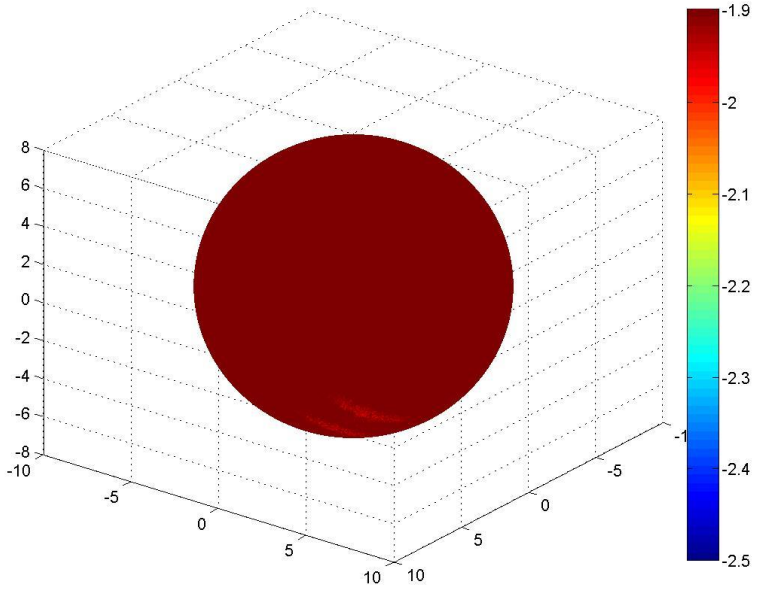

Figure B.140: Surface dose map for Design O, double beam irradiation, from 30 degrees below the equatorial plane, scale minimum raised to -2.5.

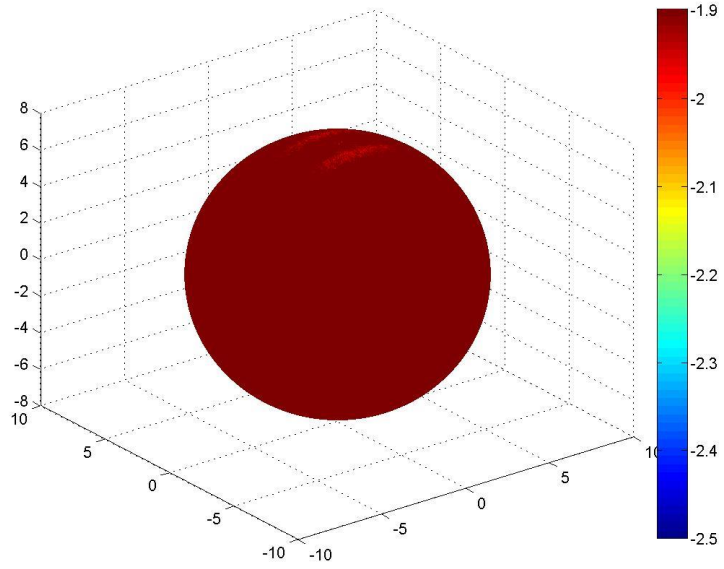

Figure B.141: Surface dose map for Design O, double beam irradiation with a 90° rotation about the vertical axis, from 30 degrees above the equatorial plane, scale minimum raised to -2.5.

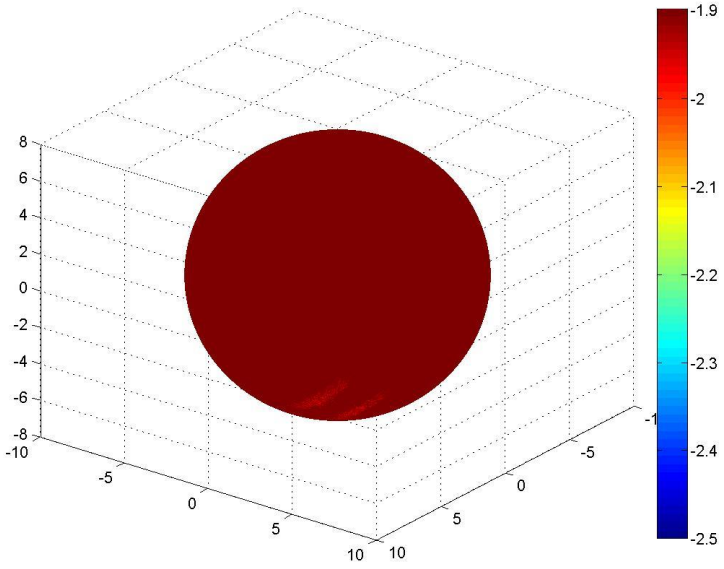

Figure B.142: Surface dose map for Design O, double beam irradiation with a 90° rotation about the vertical axis, from 30 degrees below the equatorial plane, scale minimum raised to -2.5.

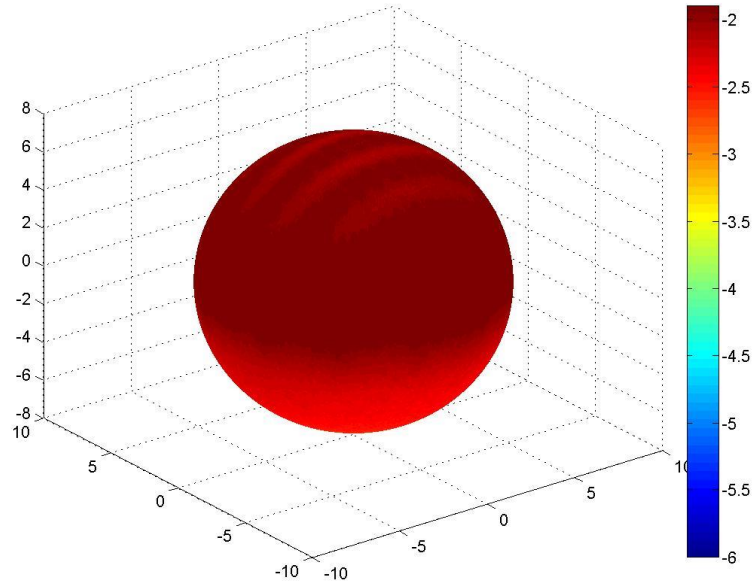

Figure B.143: Surface dose map for Design P, single beam irradiation, from 30 degrees above the equatorial plane, original scale.

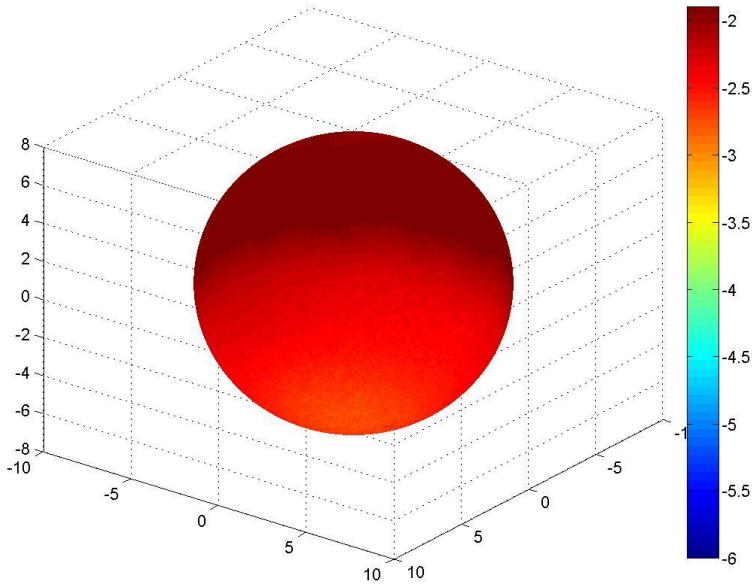

Figure B.144: Surface dose map for Design P, single beam irradiation, from 30 degrees below the equatorial plane, original scale.

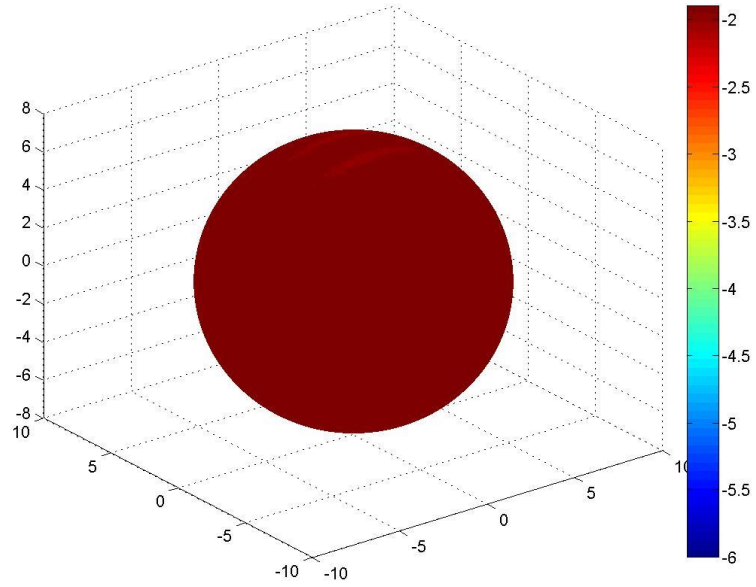

Figure B.145: Surface dose map for Design P, double beam irradiation, from 30 degrees above the equatorial plane, original scale.

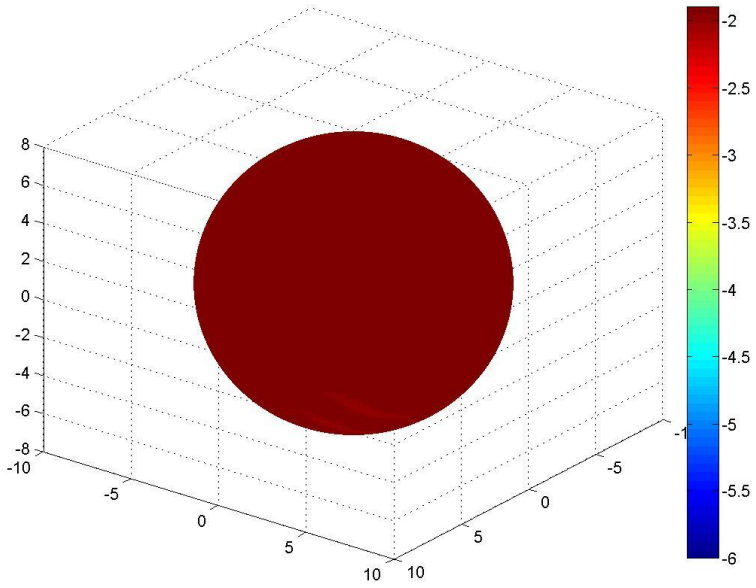

Figure B.146: Surface dose map for Design P, double beam irradiation, from 30 degrees below the equatorial plane, original scale.

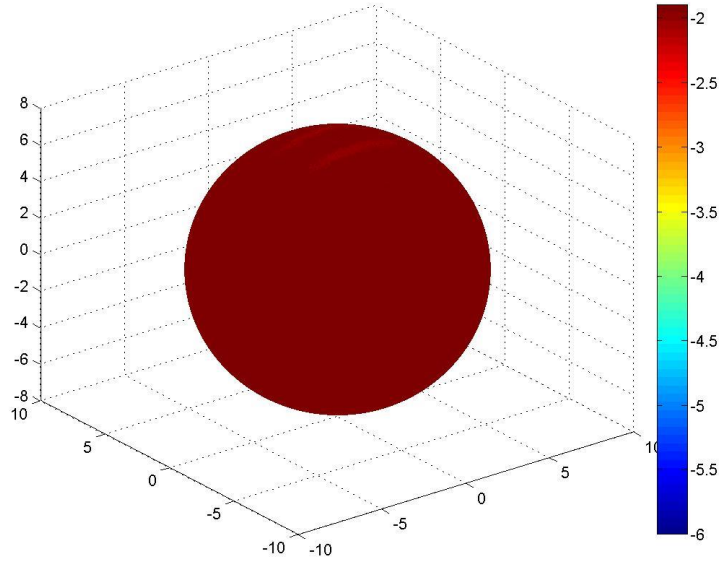

Figure B.147: Surface dose map for Design P, double beam irradiation with a 90° rotation about the vertical axis, from 30 degrees above the equatorial plane, original scale.

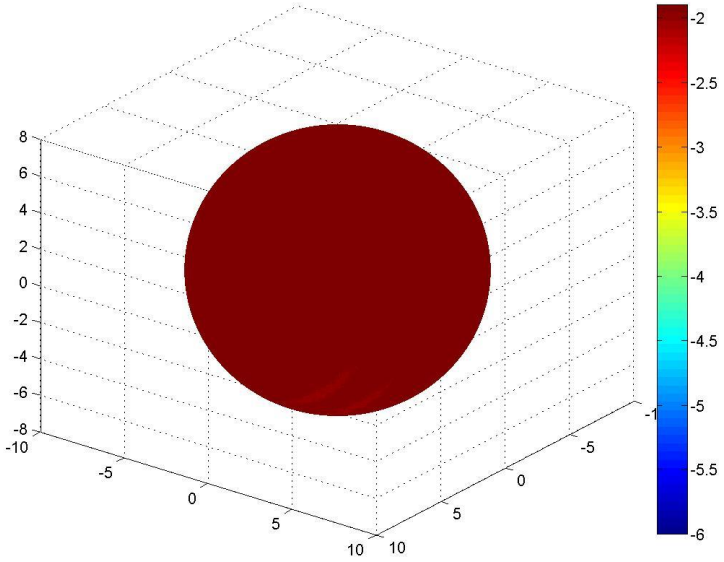

Figure B.148: Surface dose map for Design P, double beam irradiation with a 90° rotation about the vertical axis, from 30 degrees below the equatorial plane, original scale.

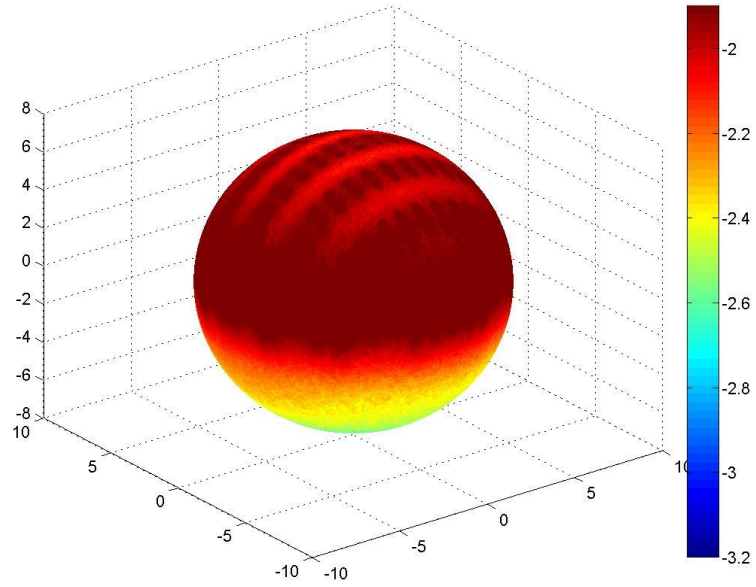

Figure B.149: Surface dose map for Design P, single beam irradiation, from 30 degrees above the equatorial plane, scale minimum raised to -3.2.

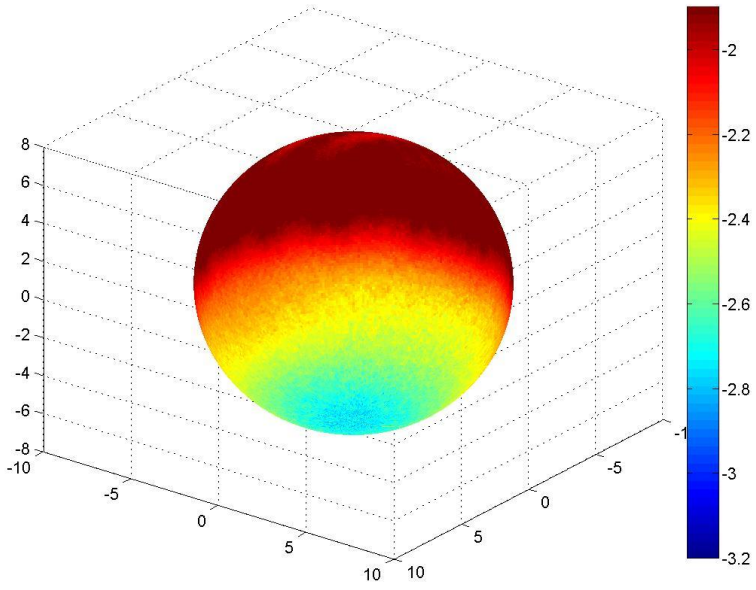

Figure B.150: Surface dose map for Design P, single beam irradiation, from 30 degrees below the equatorial plane, scale minimum raised to -3.2.

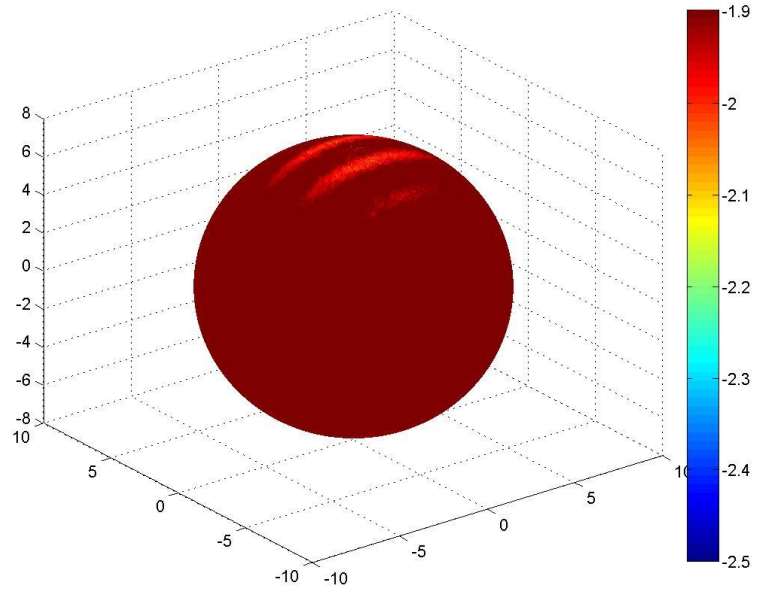

Figure B.151: Surface dose map for Design P, double beam irradiation, from 30 degrees above the equatorial plane, scale minimum raised to -2.5.

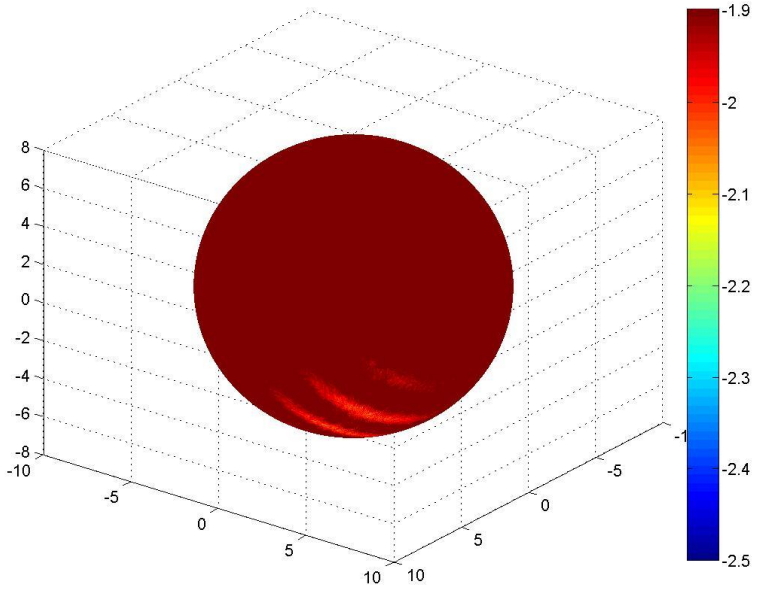

Figure B.152: Surface dose map for Design P, double beam irradiation, from 30 degrees below the equatorial plane, scale minimum raised to -2.5.

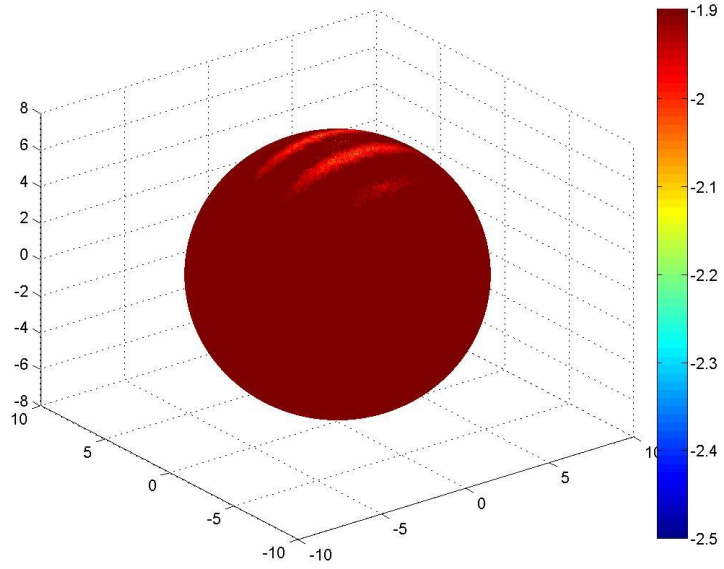

Figure B.153: Surface dose map for Design P, double beam irradiation with a 90° rotation about the vertical axis, from 30 degrees above the equatorial plane, scale minimum raised to -2.5.

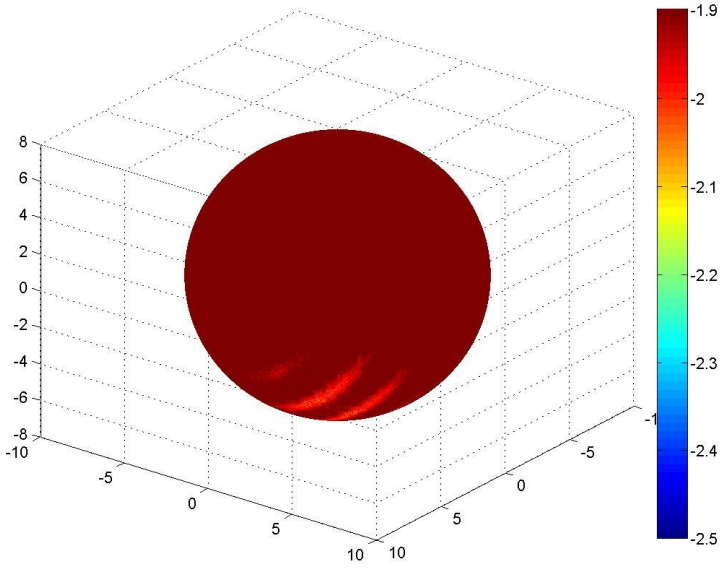

Figure B.154: Surface dose map for Design P, double beam irradiation with a 90° rotation about the vertical axis, from 30 degrees below the equatorial plane, scale minimum raised to -2.5.

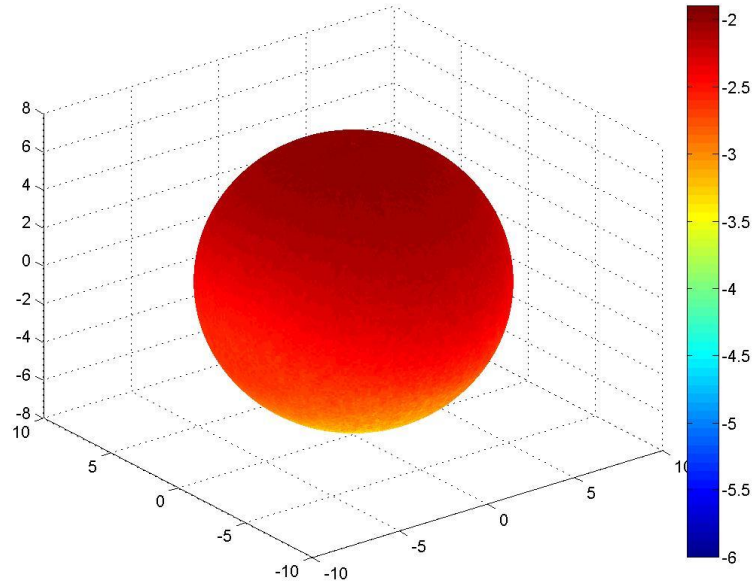

Figure B.155: Surface dose map for Design Q, single beam irradiation, from 30 degrees above the equatorial plane, original scale.

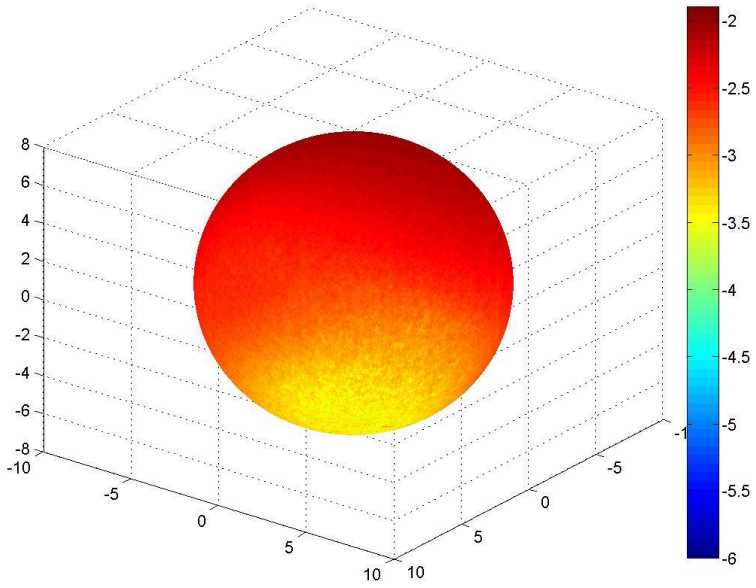

Figure B.156: Surface dose map for Design Q, single beam irradiation, from 30 degrees below the equatorial plane, original scale.

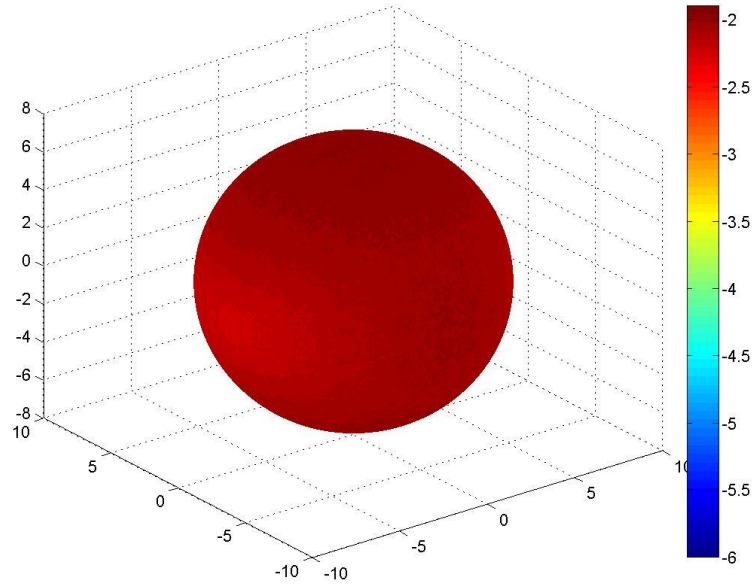

Figure B.157: Surface dose map for Design Q, double beam irradiation, from 30 degrees above the equatorial plane, original scale.

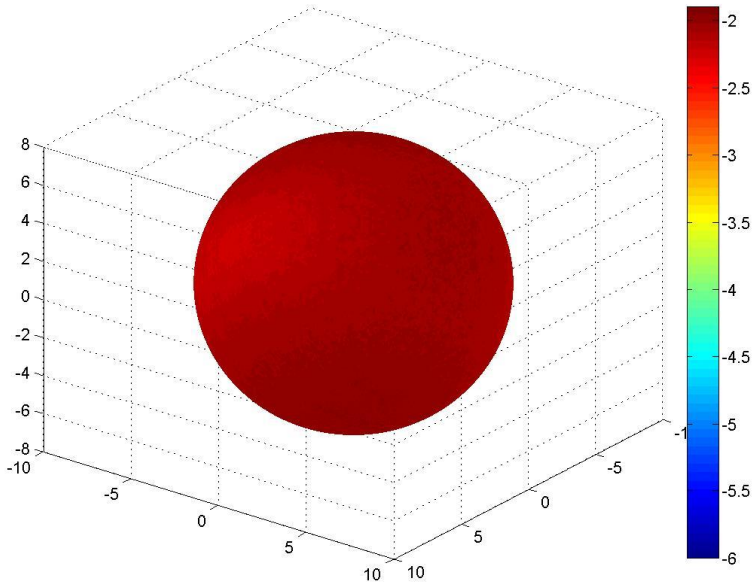

Figure B.158: Surface dose map for Design Q, double beam irradiation, from 30 degrees below the equatorial plane, original scale.

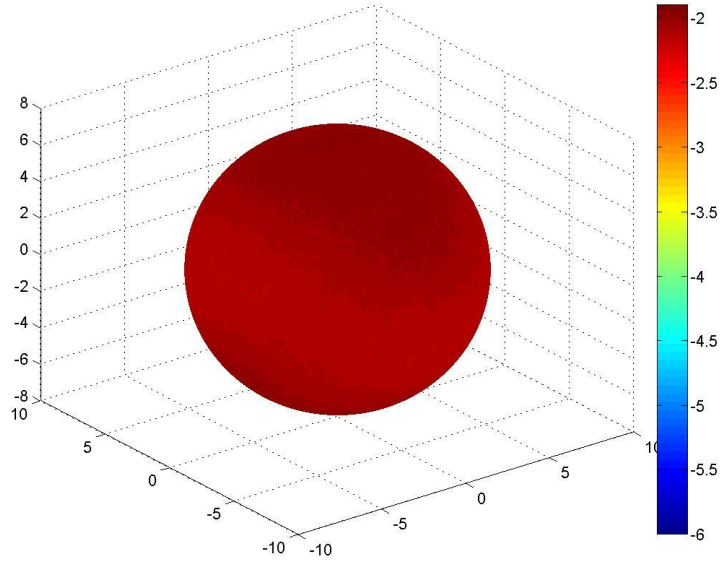

Figure B.159: Surface dose map for Design Q, double beam irradiation with a 90° rotation about the vertical axis, from 30 degrees above the equatorial plane, original scale.

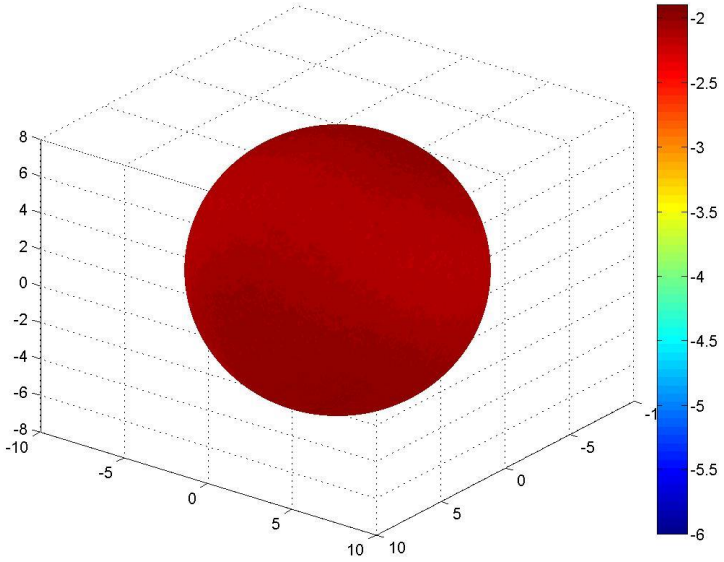

Figure B.160: Surface dose map for Design Q, double beam irradiation with a 90° rotation about the vertical axis, from 30 degrees below the equatorial plane, original scale.

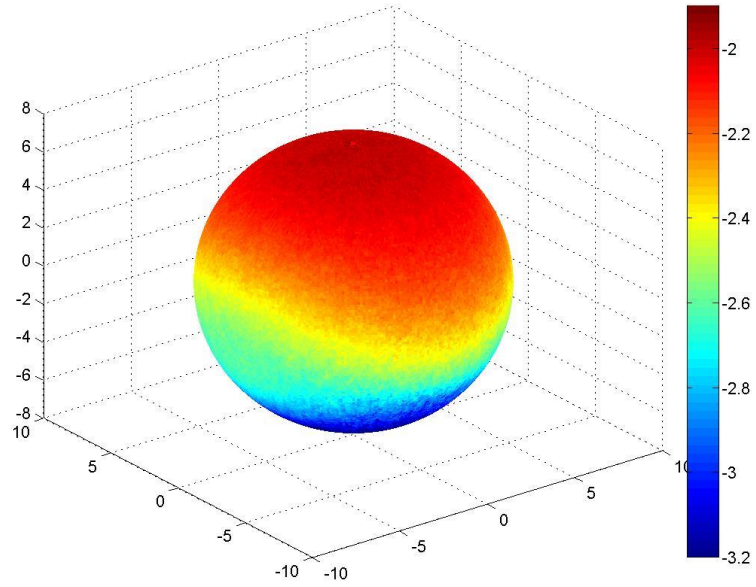

Figure B.161: Surface dose map for Design Q, single beam irradiation, from 30 degrees above the equatorial plane, scale minimum raised to -3.2.

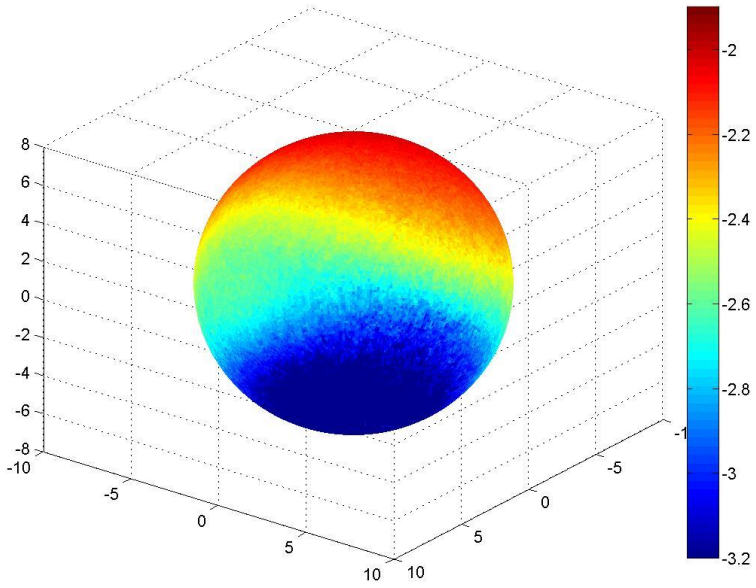

Figure B.162: Surface dose map for Design Q, single beam irradiation, from 30 degrees below the equatorial plane, scale minimum raised to -3.2.

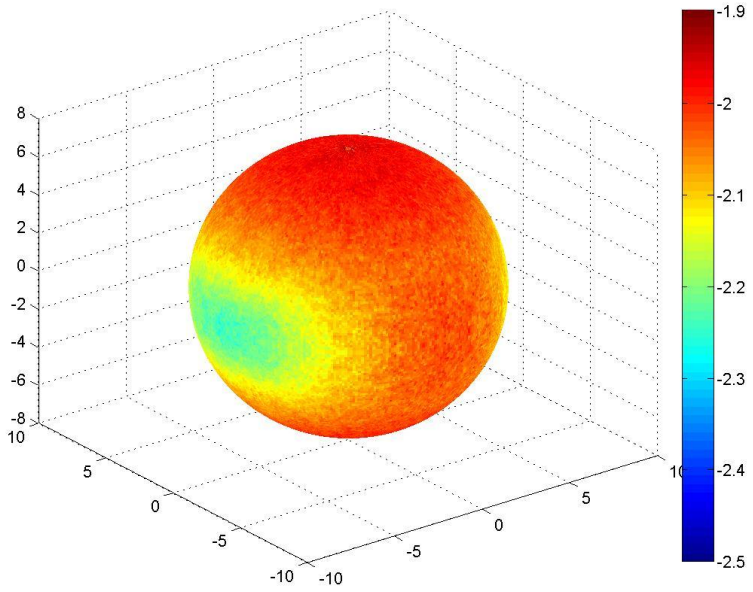

Figure B.163: Surface dose map for Design Q, double beam irradiation, from 30 degrees above the equatorial plane, scale minimum raised to -2.5.

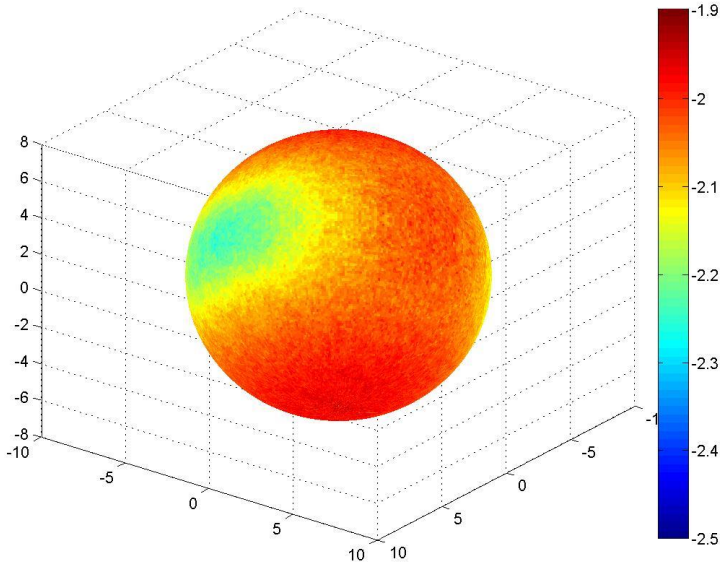

Figure B.164: Surface dose map for Design Q, double beam irradiation, from 30 degrees below the equatorial plane, scale minimum raised to -2.5.

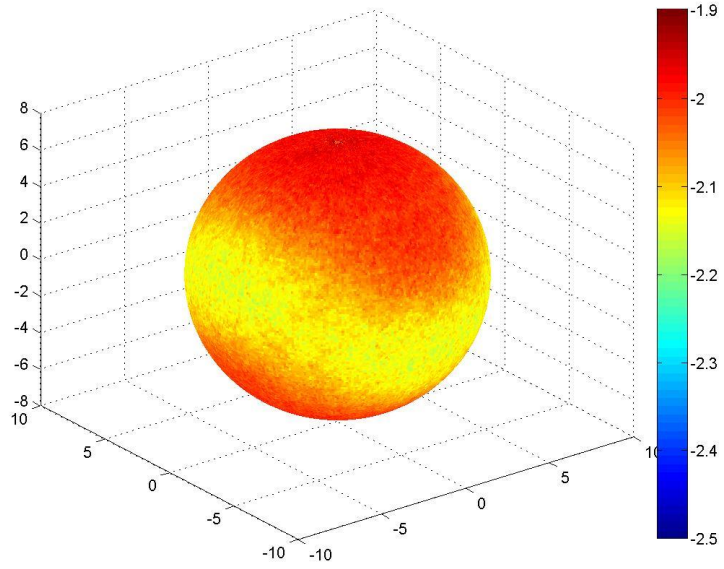

Figure B.165: Surface dose map for Design Q, double beam irradiation with a 90° rotation about the vertical axis, from 30 degrees above the equatorial plane, scale minimum raised to -2.5.

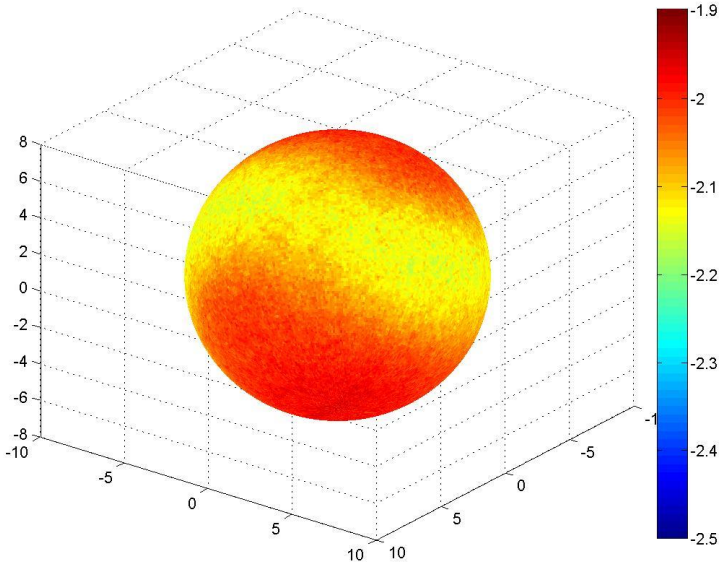

Figure B.166: Surface dose map for Design Q, double beam irradiation with a 90° rotation about the vertical axis, from 30 degrees below the equatorial plane, scale minimum raised to -2.5.

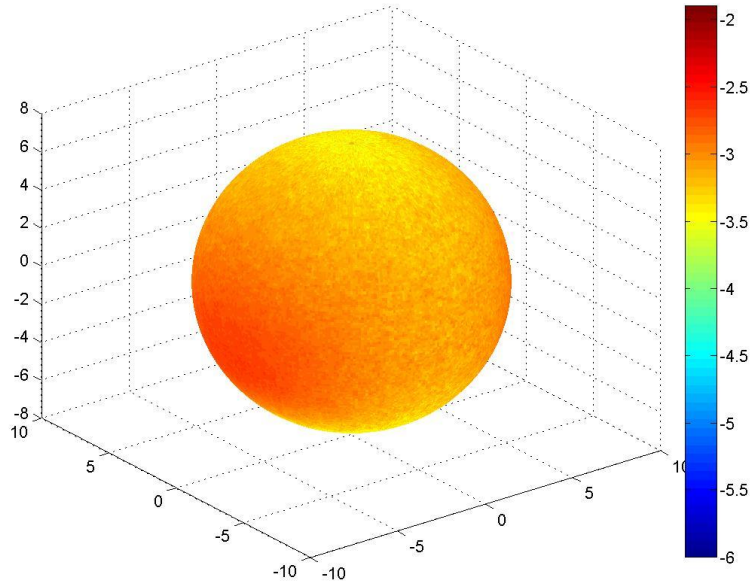

Figure B.167: Surface dose map for Design R, single beam irradiation, from 30 degrees above the equatorial plane, original scale.

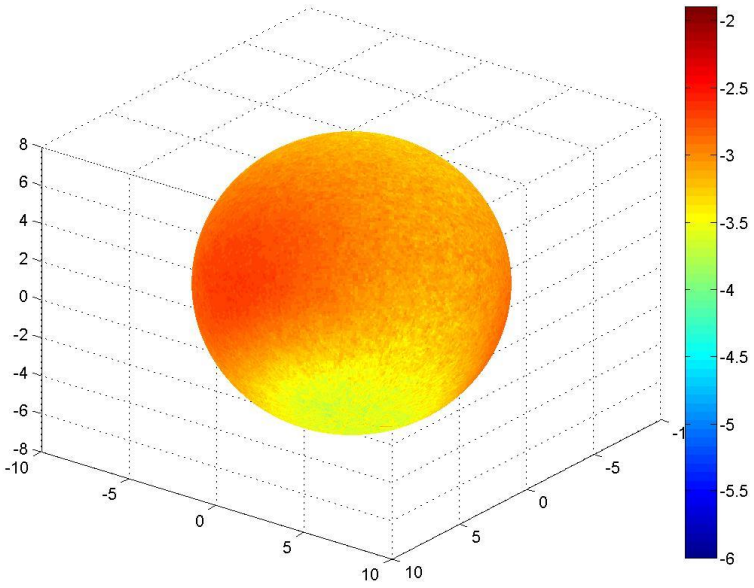

Figure B.168: Surface dose map for Design R, single beam irradiation, from 30 degrees below the equatorial plane, original scale.

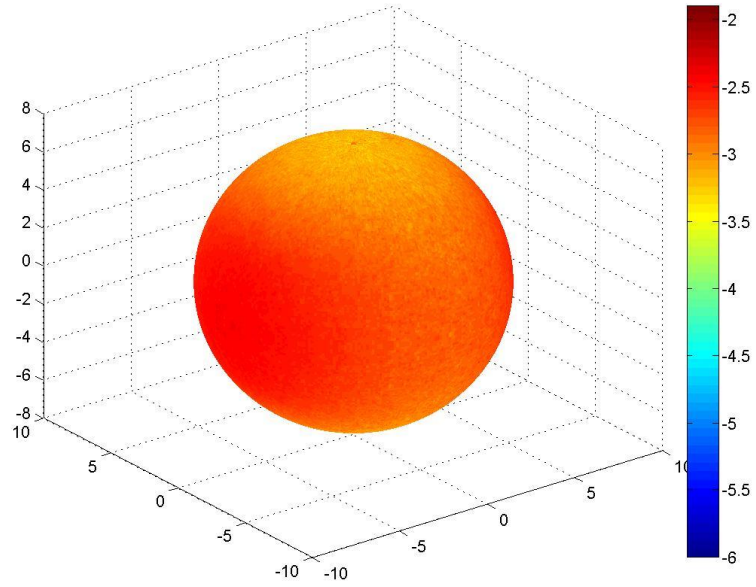

Figure B.169: Surface dose map for Design R, double beam irradiation, from 30 degrees above the equatorial plane, original scale.

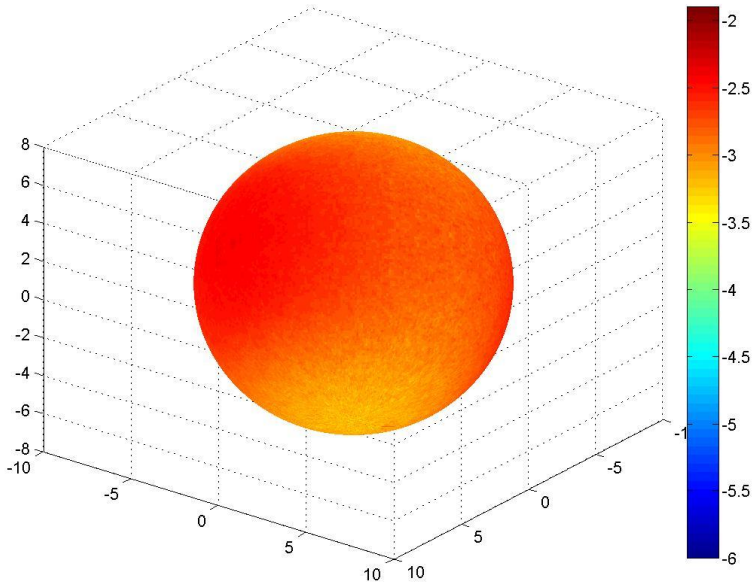

Figure B.170: Surface dose map for Design R, double beam irradiation, from 30 degrees below the equatorial plane, original scale.

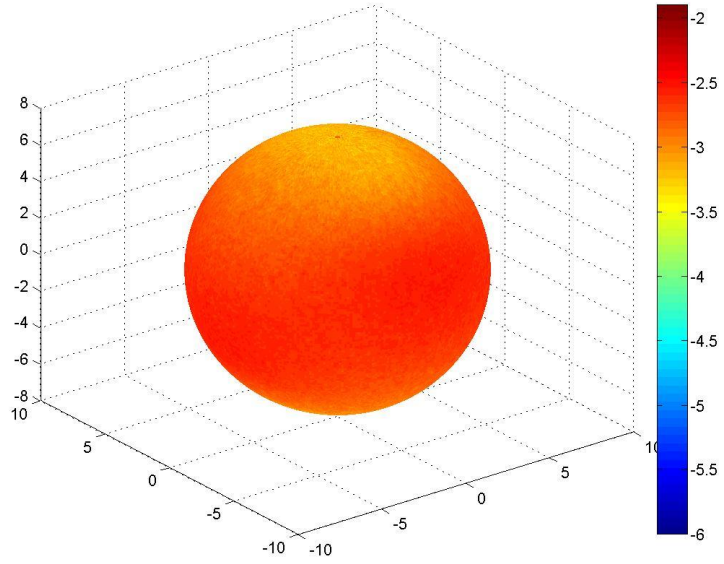

Figure B.171: Surface dose map for Design R, double beam irradiation with a 90° rotation about the vertical axis, from 30 degrees above the equatorial plane, original scale.

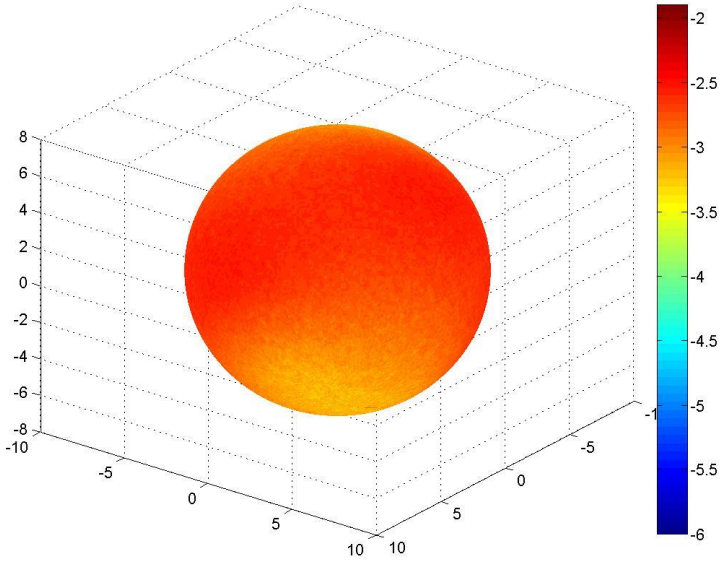

Figure B.172: Surface dose map for Design R, double beam irradiation with a 90° rotation about the vertical axis, from 30 degrees below the equatorial plane, original scale.

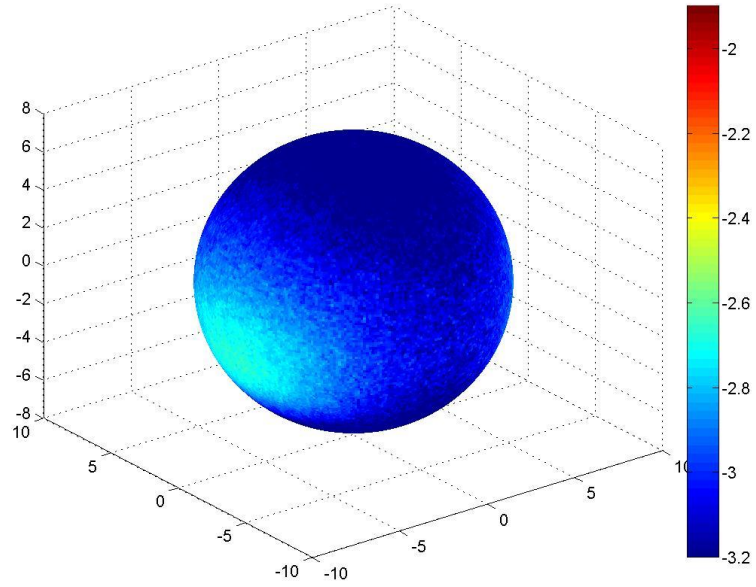

Figure B.173: Surface dose map for Design R, single beam irradiation, from 30 degrees above the equatorial plane, scale minimum raised to -3.2.

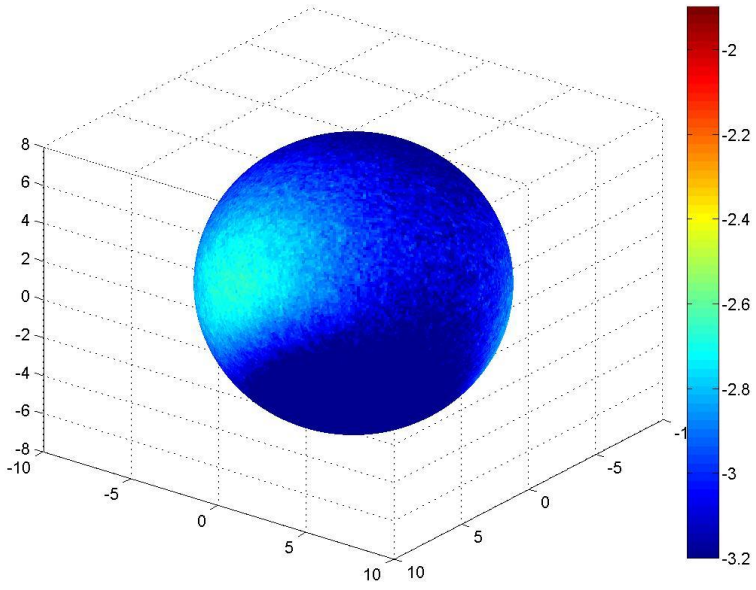

Figure B.174: Surface dose map for Design R, single beam irradiation, from 30 degrees below the equatorial plane, scale minimum raised to -3.2.

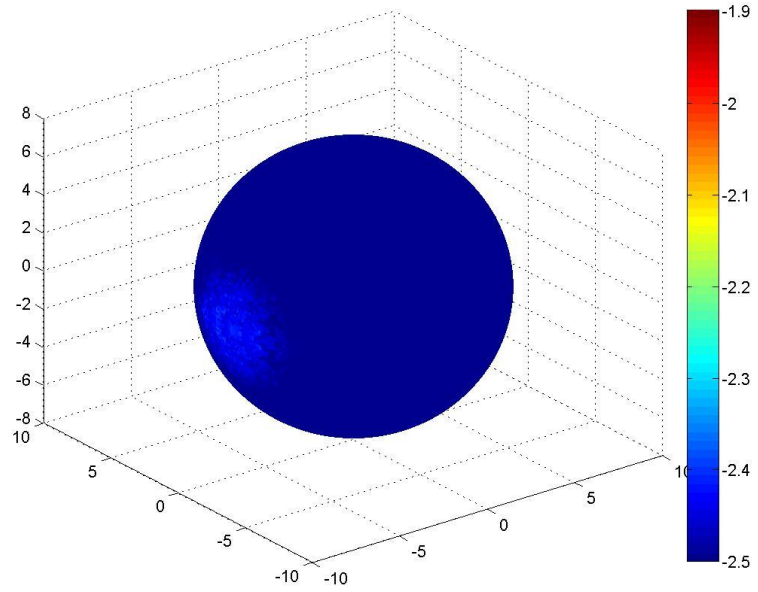

Figure B.175: Surface dose map for Design R, double beam irradiation, from 30 degrees above the equatorial plane, scale minimum raised to -2.5.

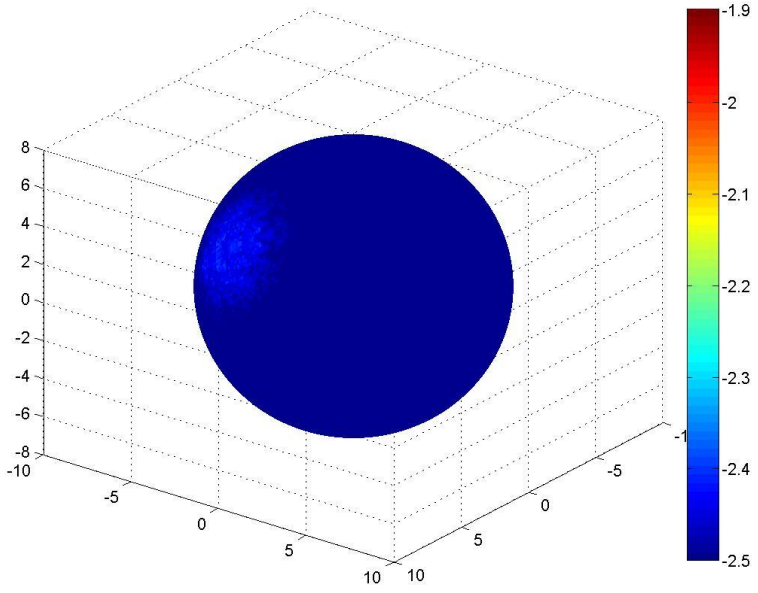

Figure B.176: Surface dose map for Design R, double beam irradiation, from 30 degrees below the equatorial plane, scale minimum raised to -2.5.

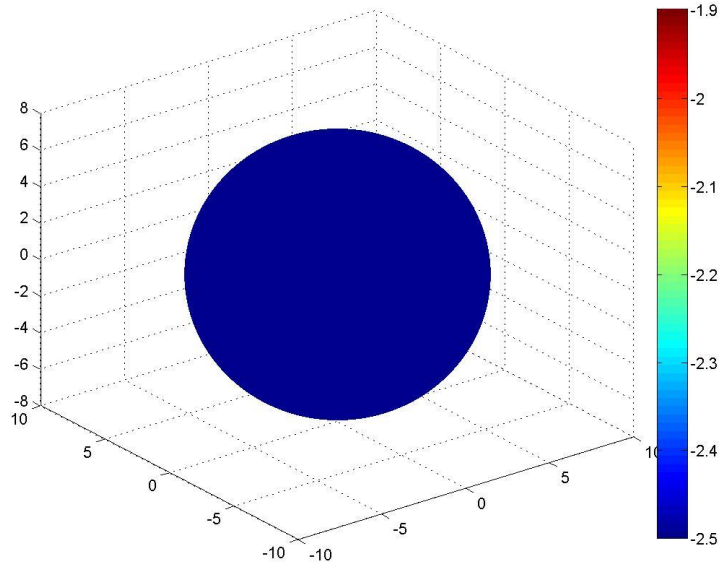

Figure B.177: Surface dose map for Design R, double beam irradiation with a 90° rotation about the vertical axis, from 30 degrees above the equatorial plane, scale minimum raised to -2.5.

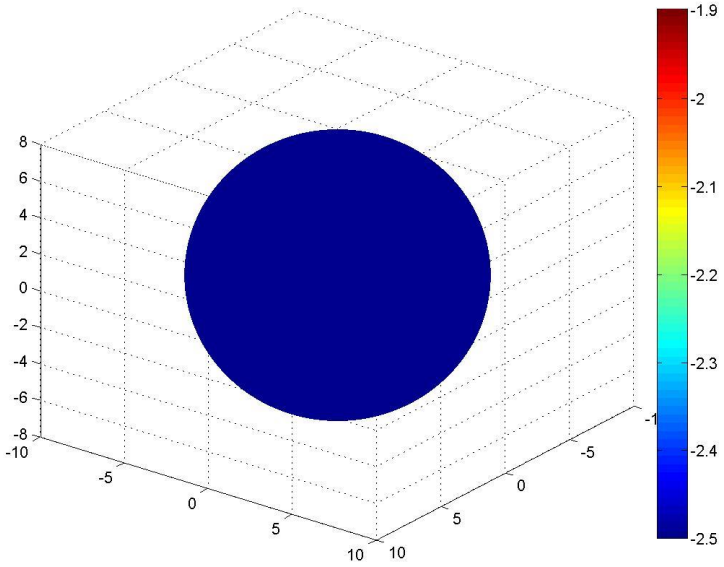

Figure B.178: Surface dose map for Design R, double beam irradiation with a 90° rotation about the vertical axis, from 30 degrees below the equatorial plane, scale minimum raised to -2.5.

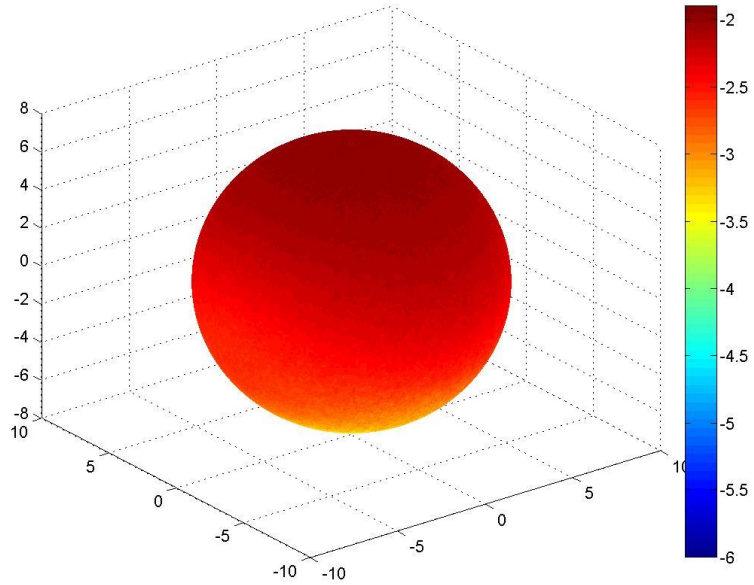

Figure B.179: Surface dose map for Design S, single beam irradiation, from 30 degrees above the equatorial plane, original scale.

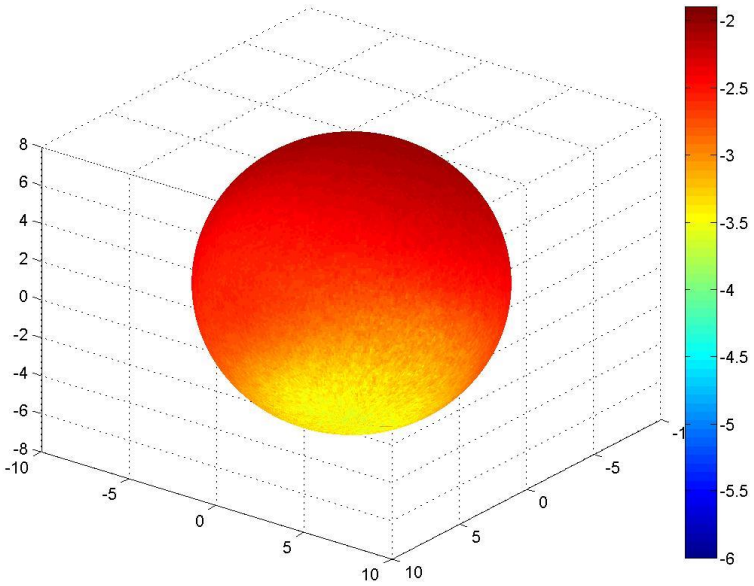

Figure B.180: Surface dose map for Design S, single beam irradiation, from 30 degrees below the equatorial plane, original scale.

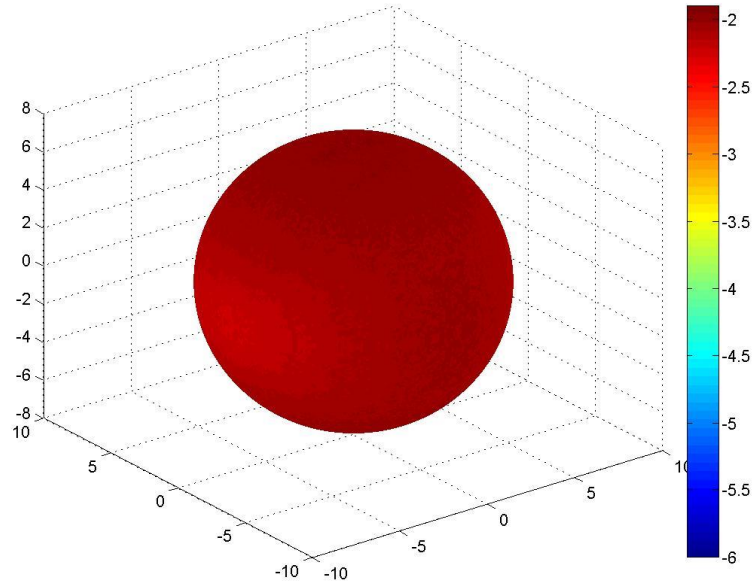

Figure B.181: Surface dose map for Design S, double beam irradiation, from 30 degrees above the equatorial plane, original scale.

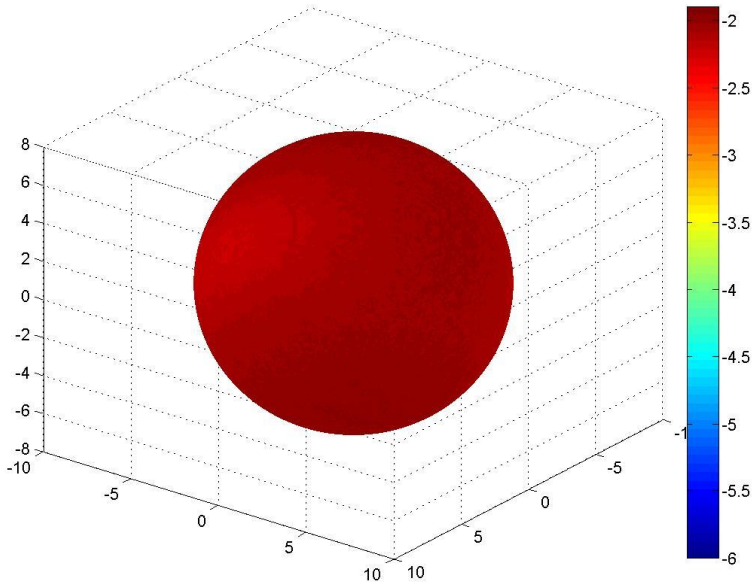

Figure B.182: Surface dose map for Design S, double beam irradiation, from 30 degrees below the equatorial plane, original scale.

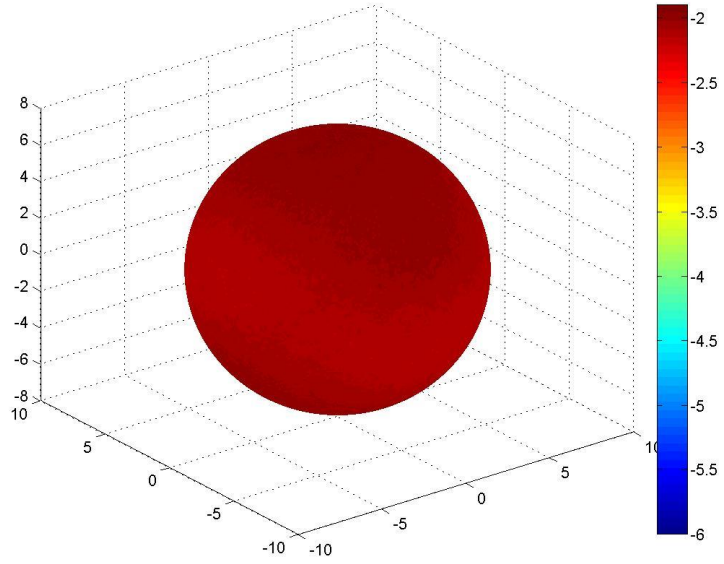

Figure B.183: Surface dose map for Design S, double beam irradiation with a 90° rotation about the vertical axis, from 30 degrees above the equatorial plane, original scale.

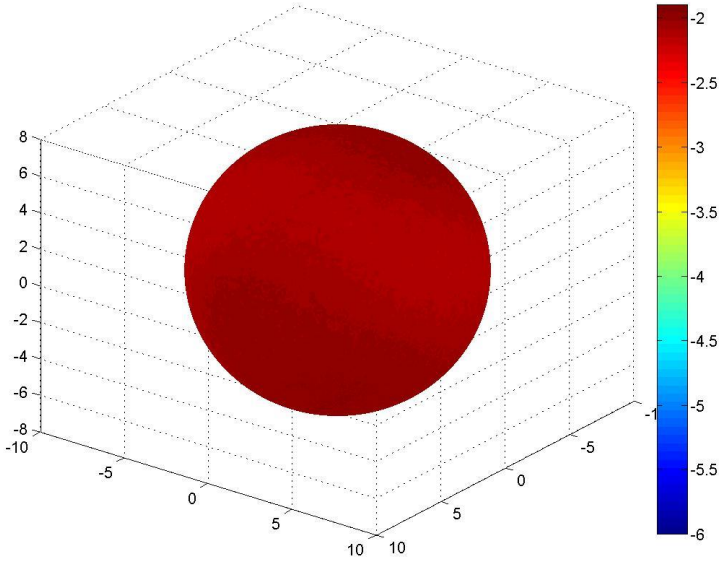

Figure B.184: Surface dose map for Design S, double beam irradiation with a 90° rotation about the vertical axis, from 30 degrees below the equatorial plane, original scale.

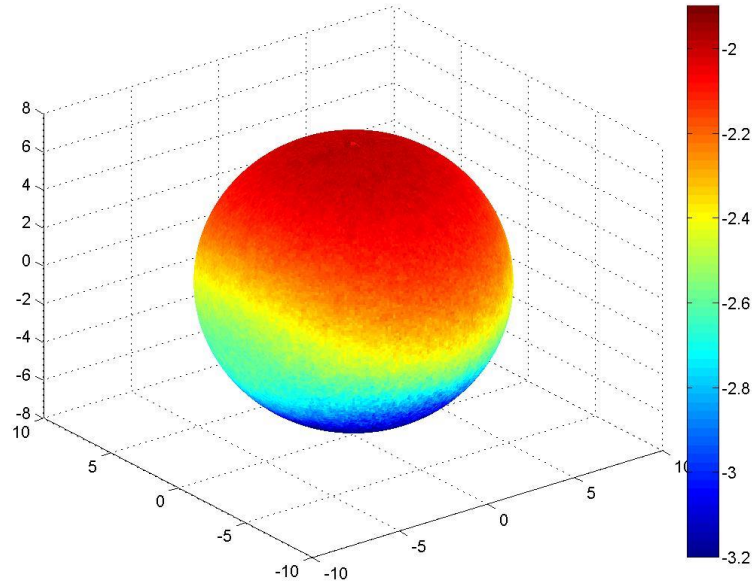

Figure B.185: Surface dose map for Design S, single beam irradiation, from 30 degrees above the equatorial plane, scale minimum raised to -3.2.

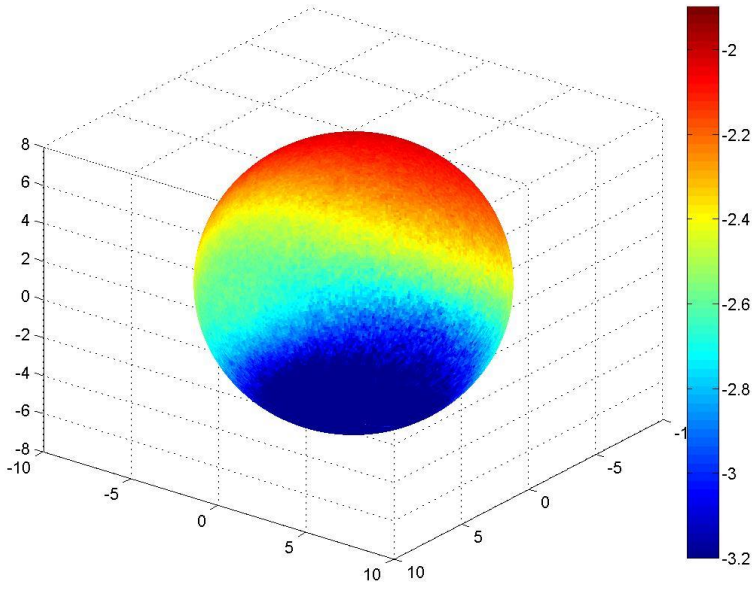

Figure B.186: Surface dose map for Design S, single beam irradiation, from 30 degrees below the equatorial plane, scale minimum raised to -3.2.

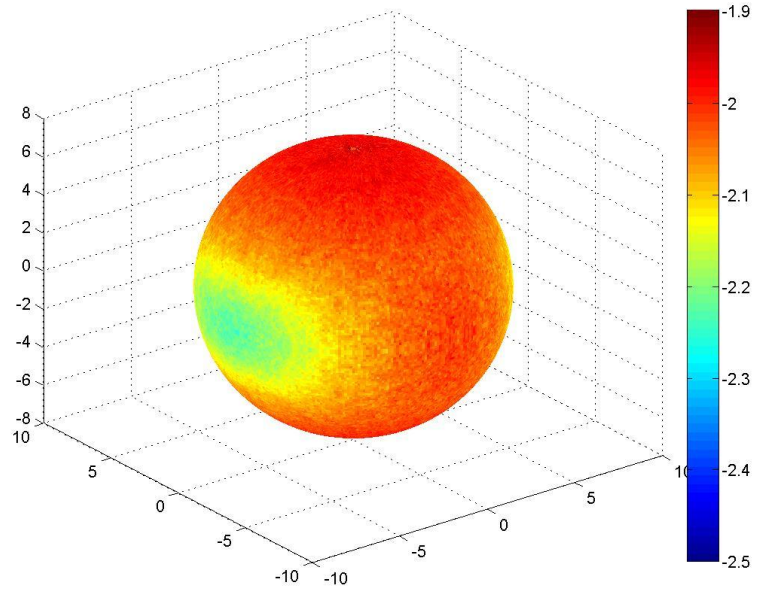

Figure B.187: Surface dose map for Design S, double beam irradiation, from 30 degrees above the equatorial plane, scale minimum raised to -2.5.

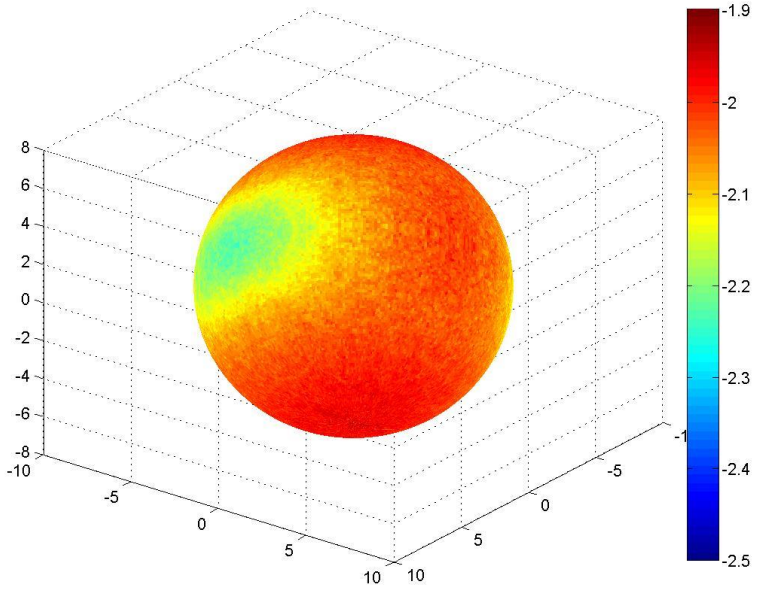

Figure B.188: Surface dose map for Design S, double beam irradiation, from 30 degrees below the equatorial plane, scale minimum raised to -2.5.

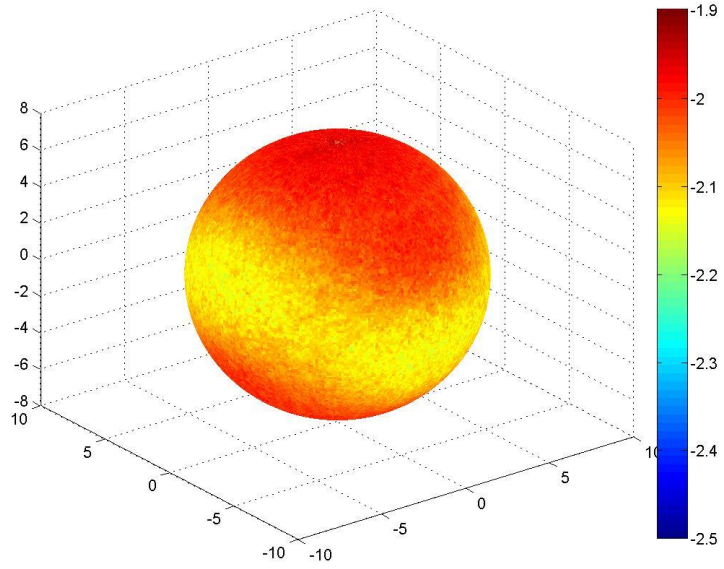

Figure B.189: Surface dose map for Design S, double beam irradiation with a 90° rotation about the vertical axis, from 30 degrees above the equatorial plane, scale minimum raised to -2.5.

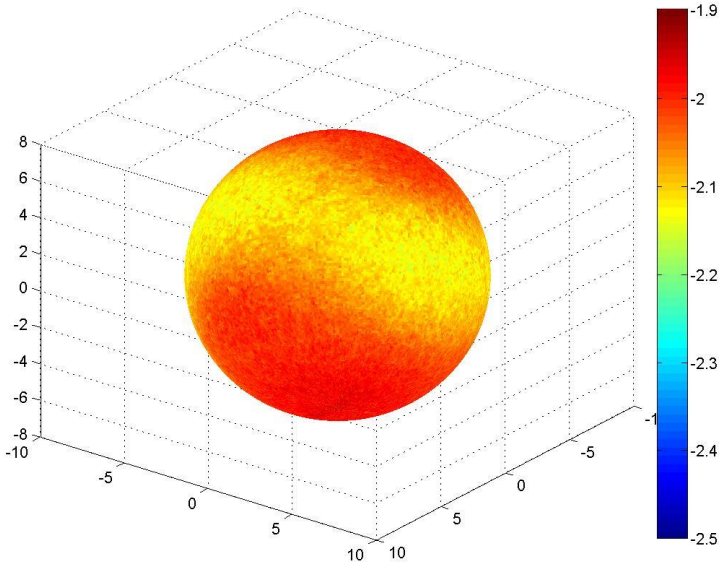

Figure B.190: Surface dose map for Design S, double beam irradiation with a 90° rotation about the vertical axis, from 30 degrees below the equatorial plane, scale minimum raised to -2.5.

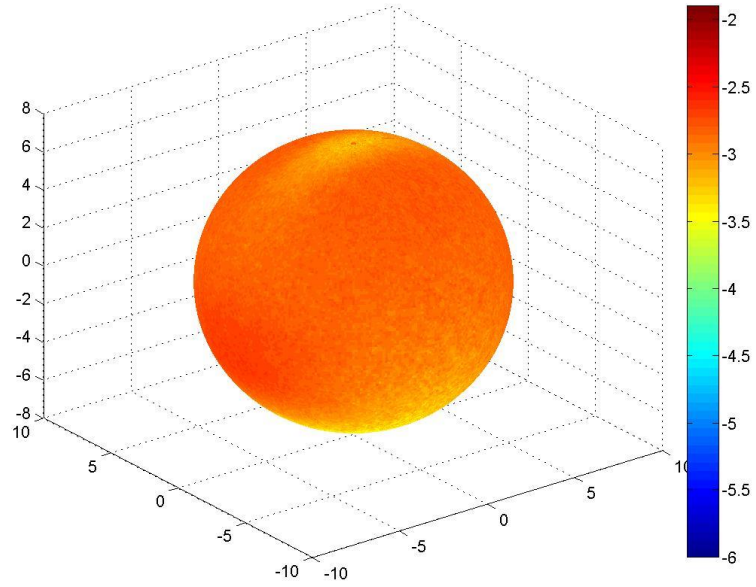

Figure B.191: Surface dose map for Design T, single beam irradiation, from 30 degrees above the equatorial plane, original scale.

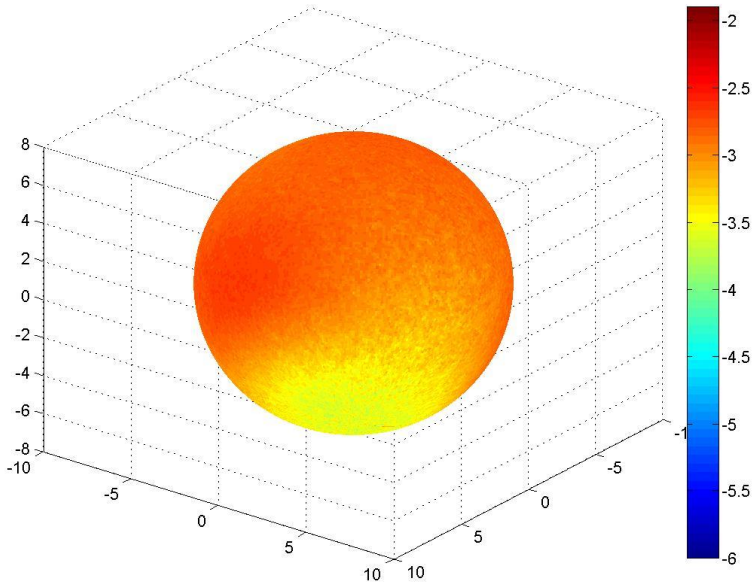

Figure B.192: Surface dose map for Design T, single beam irradiation, from 30 degrees below the equatorial plane, original scale.

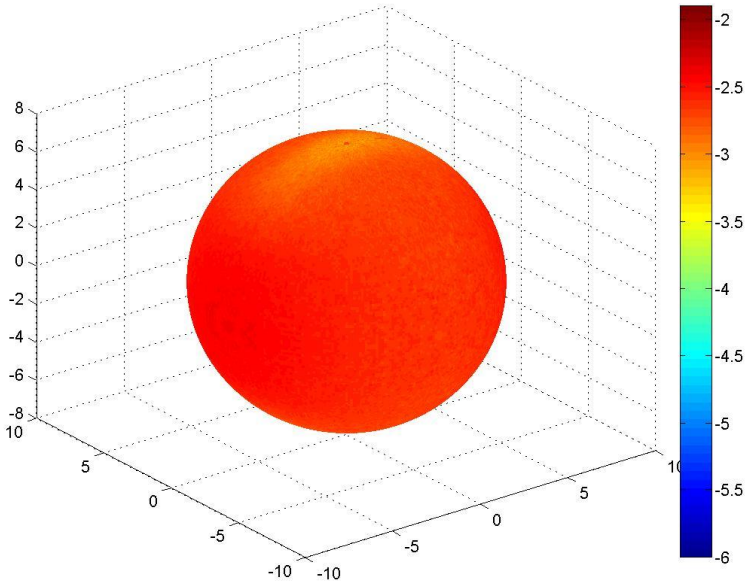

Figure B.193: Surface dose map for Design T, double beam irradiation, from 30 degrees above the equatorial plane, original scale.

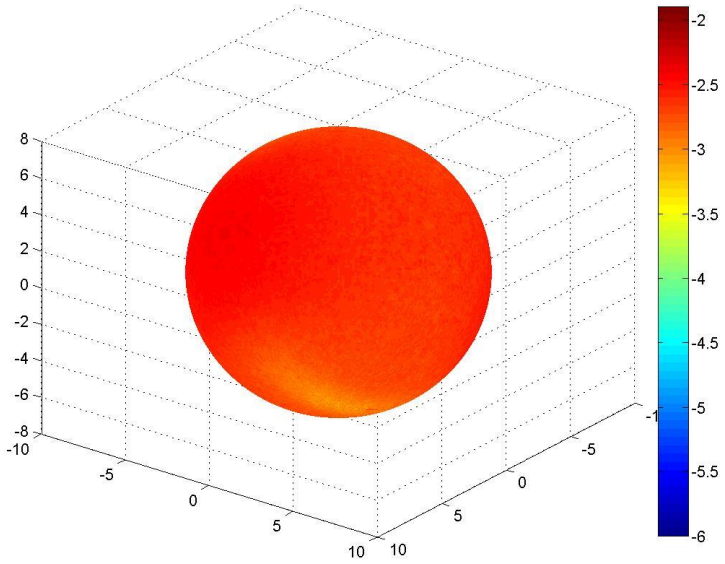

Figure B.194: Surface dose map for Design T, double beam irradiation, from 30 degrees below the equatorial plane, original scale.

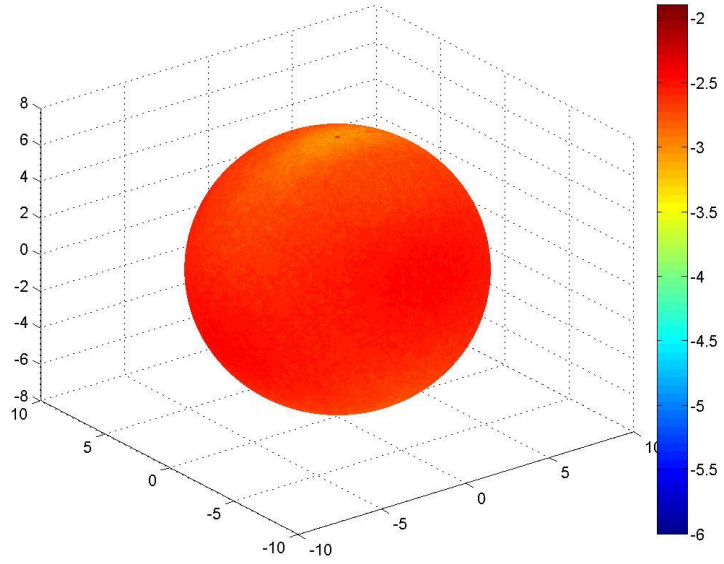

Figure B.195: Surface dose map for Design T, double beam irradiation with a 90° rotation about the vertical axis, from 30 degrees above the equatorial plane, original scale.

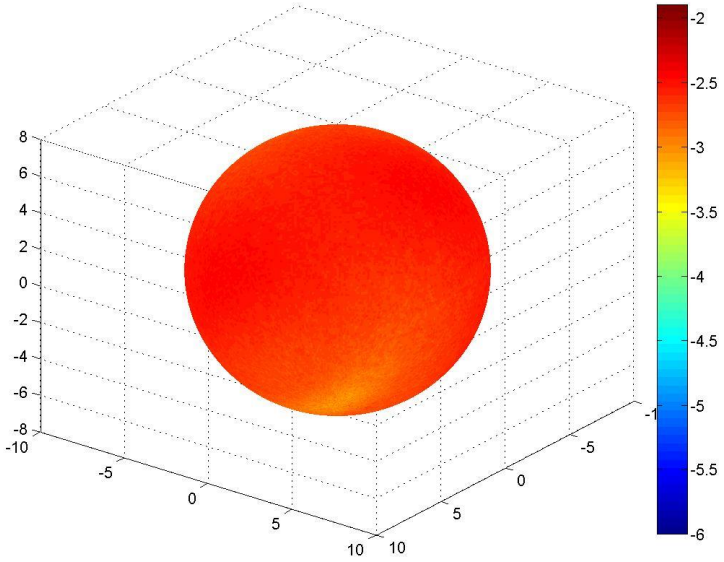

Figure B.196: Surface dose map for Design T, double beam irradiation with a 90° rotation about the vertical axis, from 30 degrees below the equatorial plane, original scale.

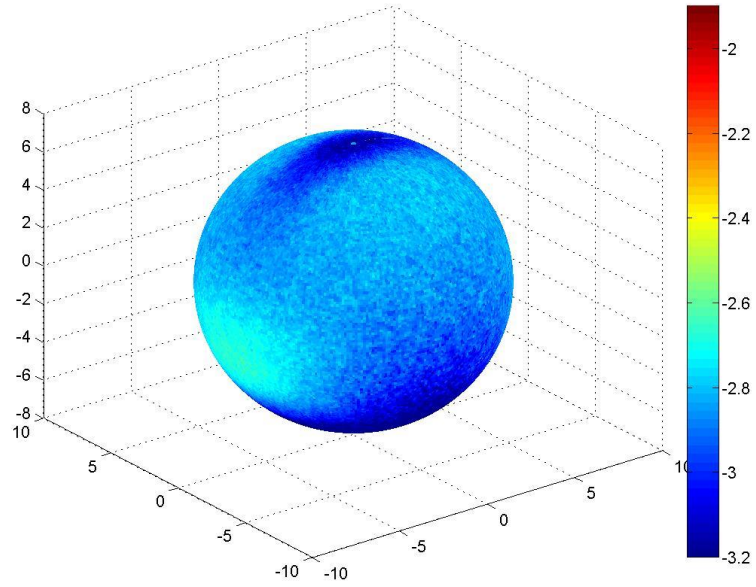

Figure B.197: Surface dose map for Design T, single beam irradiation, from 30 degrees above the equatorial plane, scale minimum raised to -3.2.

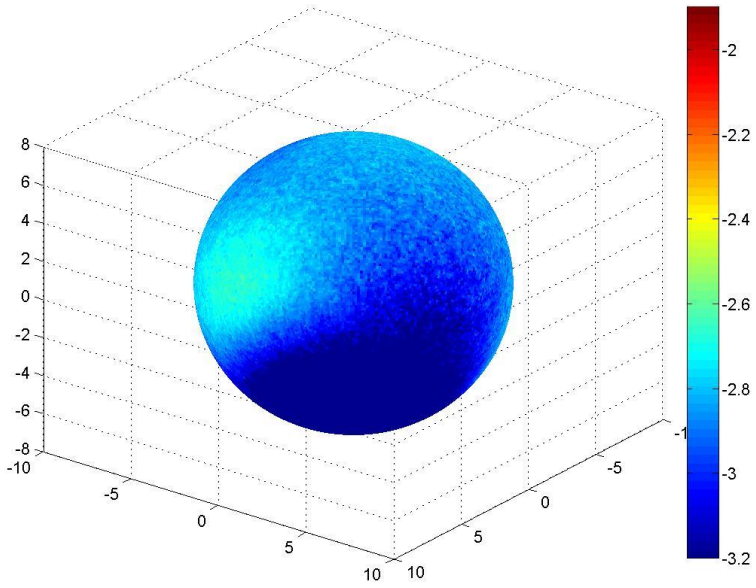

Figure B.198: Surface dose map for Design T, single beam irradiation, from 30 degrees below the equatorial plane, scale minimum raised to -3.2.

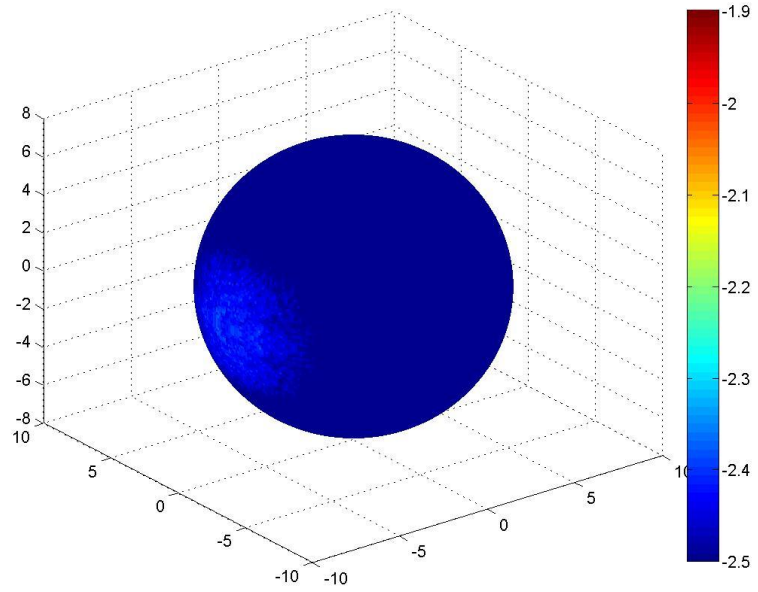

Figure B.199: Surface dose map for Design T, double beam irradiation, from 30 degrees above the equatorial plane, scale minimum raised to -2.5.

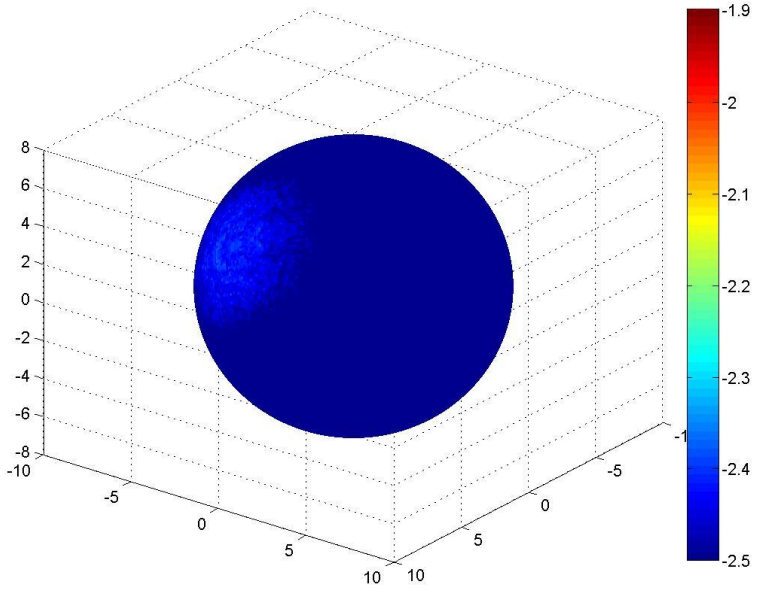

Figure B.200: Surface dose map for Design T, double beam irradiation, from 30 degrees below the equatorial plane, scale minimum raised to -2.5.

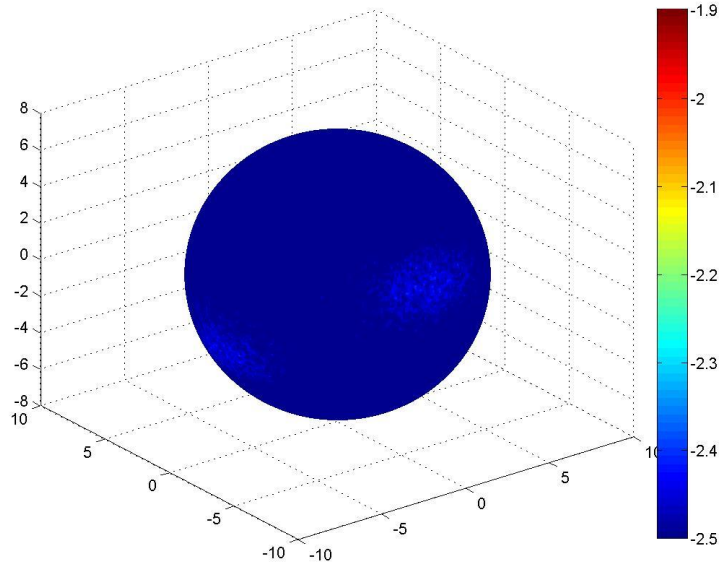

Figure B.201: Surface dose map for Design T, double beam irradiation with a 90° rotation about the vertical axis, from 30 degrees above the equatorial plane, scale minimum raised to -2.5.

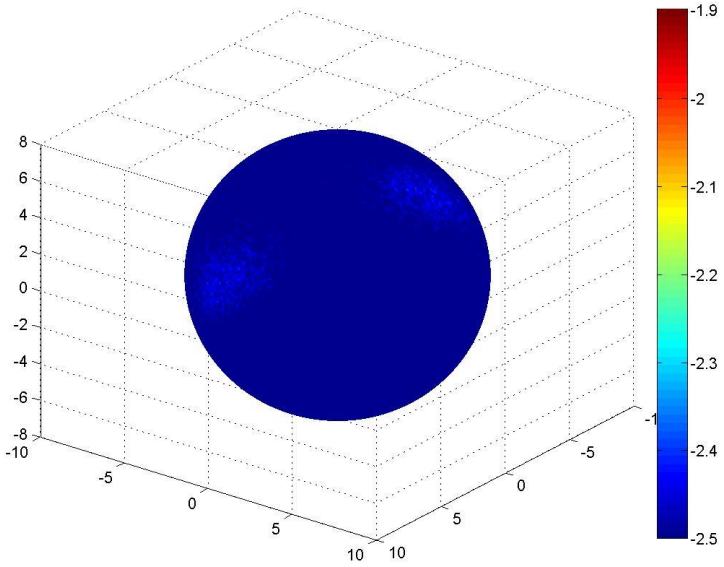

Figure B.202: Surface dose map for Design T, double beam irradiation with a 90° rotation about the vertical axis, from 30 degrees below the equatorial plane, scale minimum raised to -2.5.

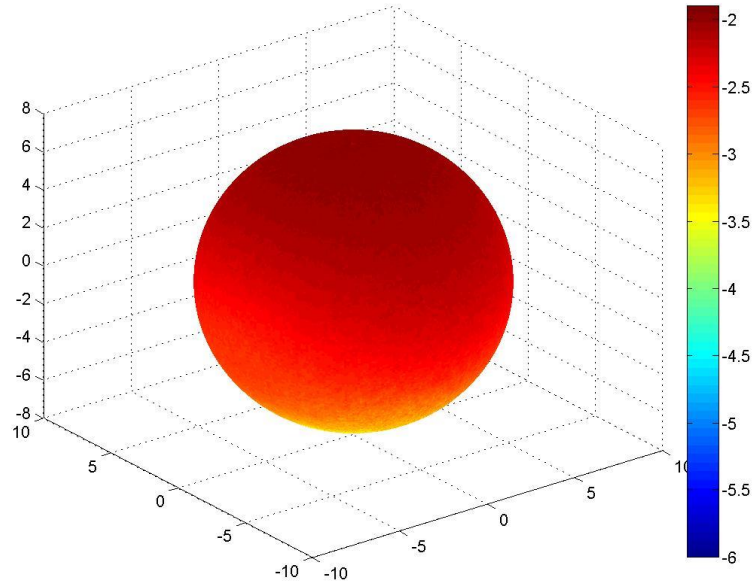

Figure B.203: Surface dose map for Design U, single beam irradiation, from 30 degrees above the equatorial plane, original scale.

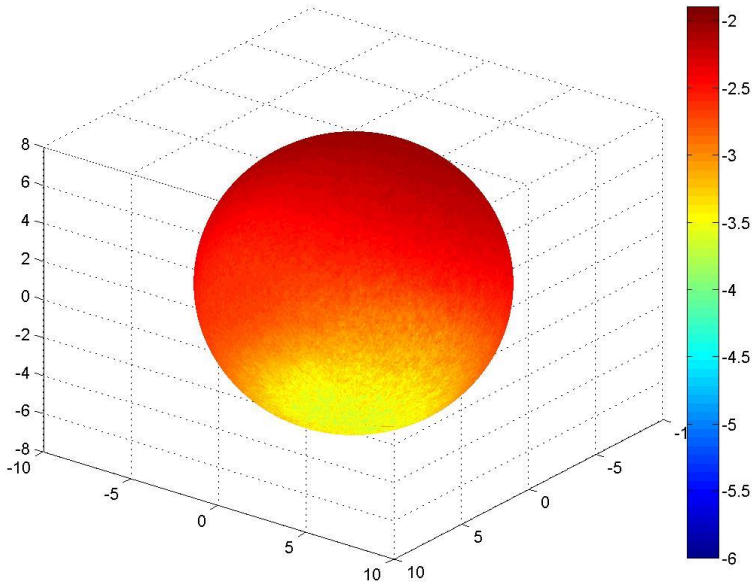

Figure B.204: Surface dose map for Design U, single beam irradiation, from 30 degrees below the equatorial plane, original scale.

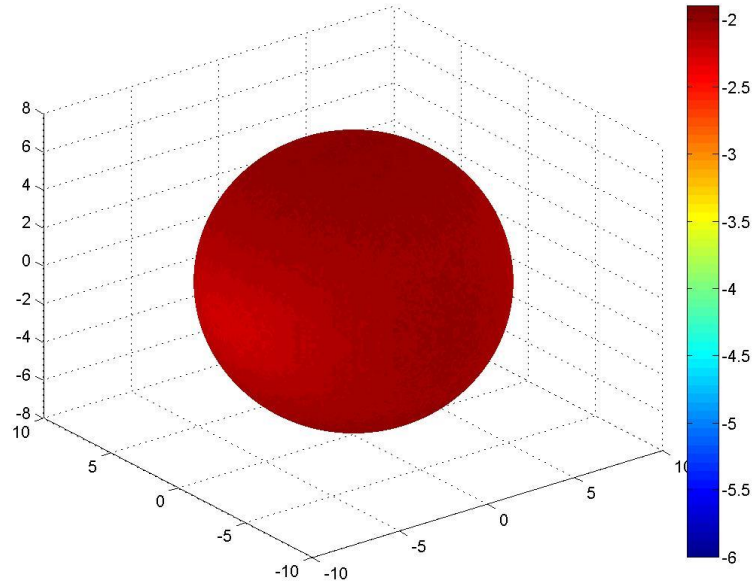

Figure B.205: Surface dose map for Design U, double beam irradiation, from 30 degrees above the equatorial plane, original scale.

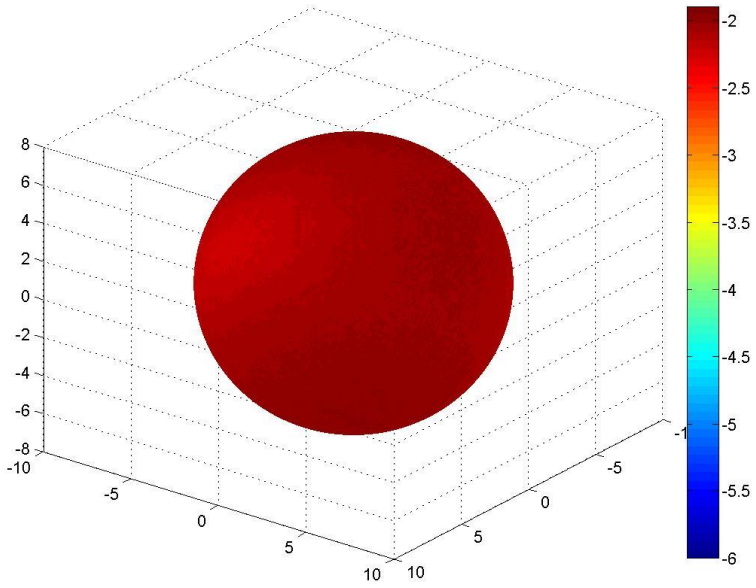

Figure B.206: Surface dose map for Design U, double beam irradiation, from 30 degrees below the equatorial plane, original scale.

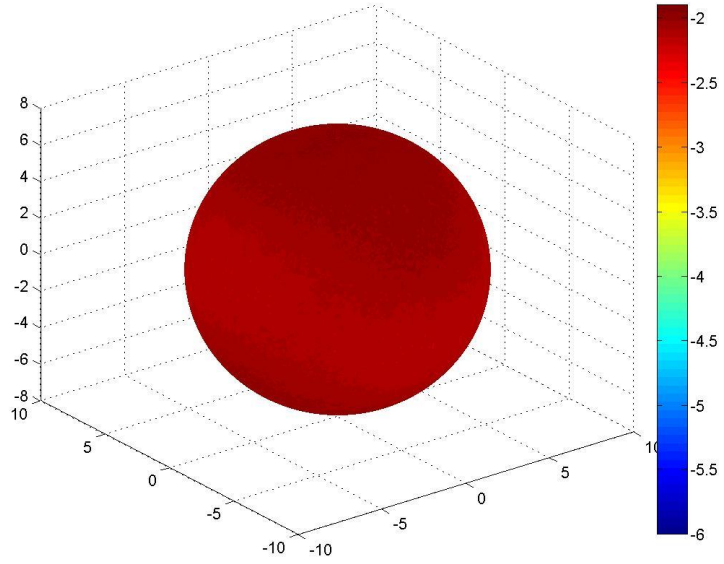

Figure B.207: Surface dose map for Design U, double beam irradiation with a 90° rotation about the vertical axis, from 30 degrees above the equatorial plane, original scale.

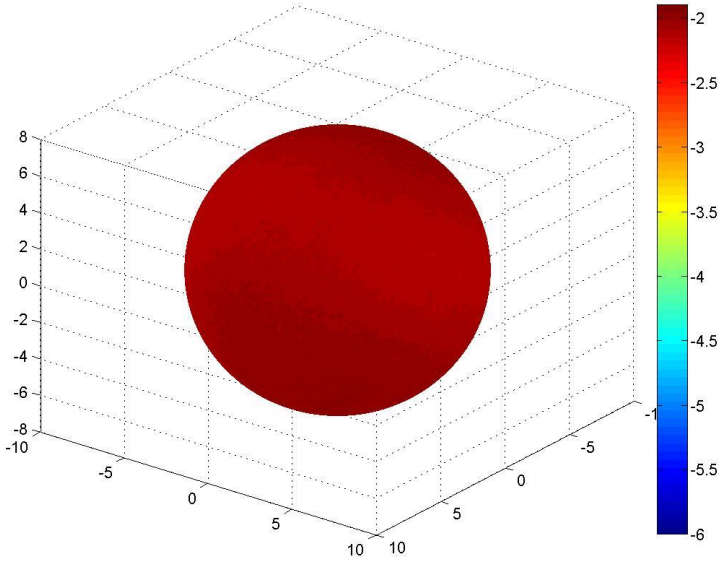

Figure B.208: Surface dose map for Design U, double beam irradiation with a 90° rotation about the vertical axis, from 30 degrees below the equatorial plane, original scale.

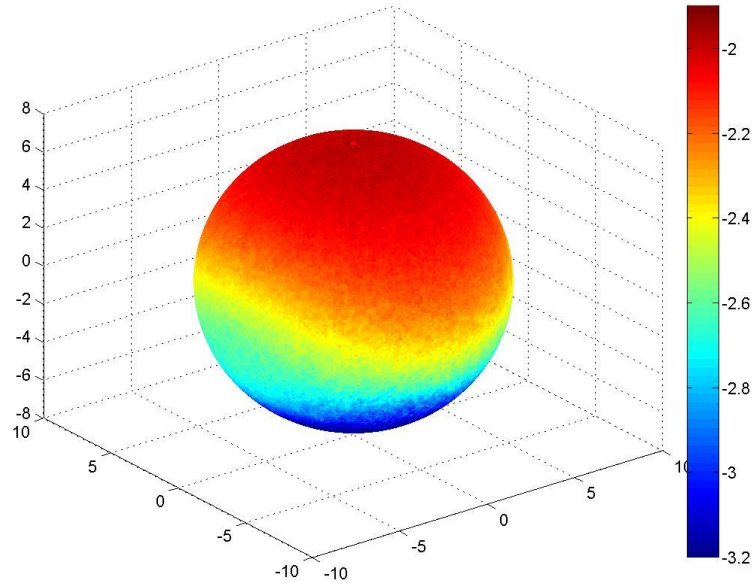

Figure B.209: Surface dose map for Design U, single beam irradiation, from 30 degrees above the equatorial plane, scale minimum raised to -3.2.

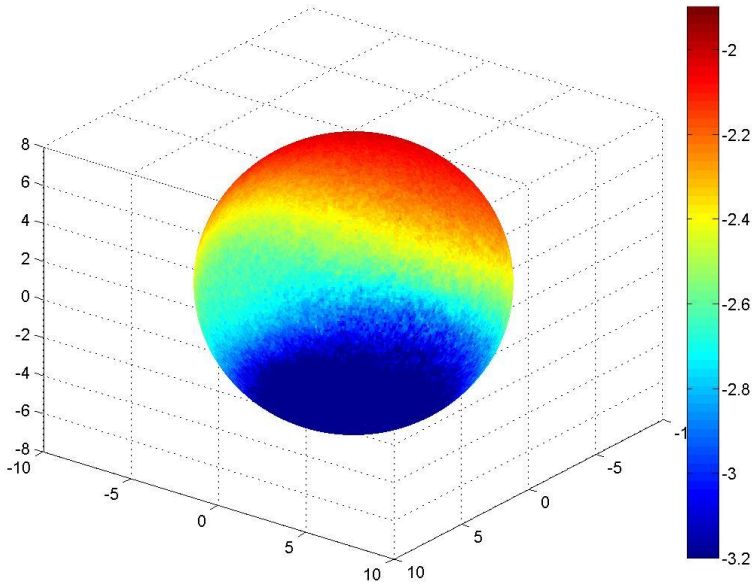

Figure B.210: Surface dose map for Design U, single beam irradiation, from 30 degrees below the equatorial plane, scale minimum raised to -3.2.

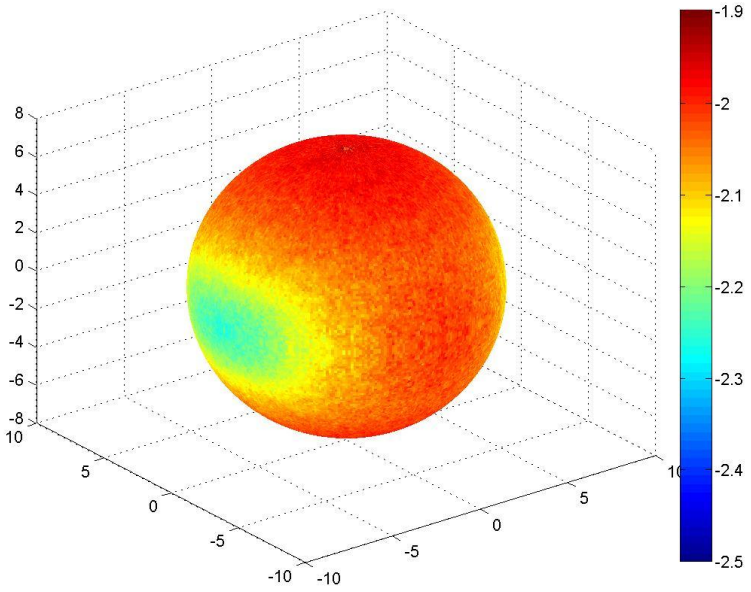

Figure B.211: Surface dose map for Design U, double beam irradiation, from 30 degrees above the equatorial plane, scale minimum raised to -2.5.

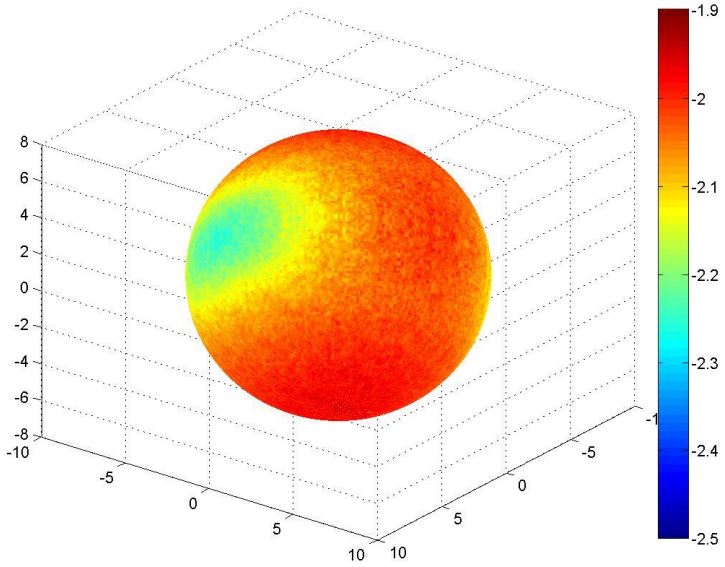

Figure B.212: Surface dose map for Design U, double beam irradiation, from 30 degrees below the equatorial plane, scale minimum raised to -2.5.

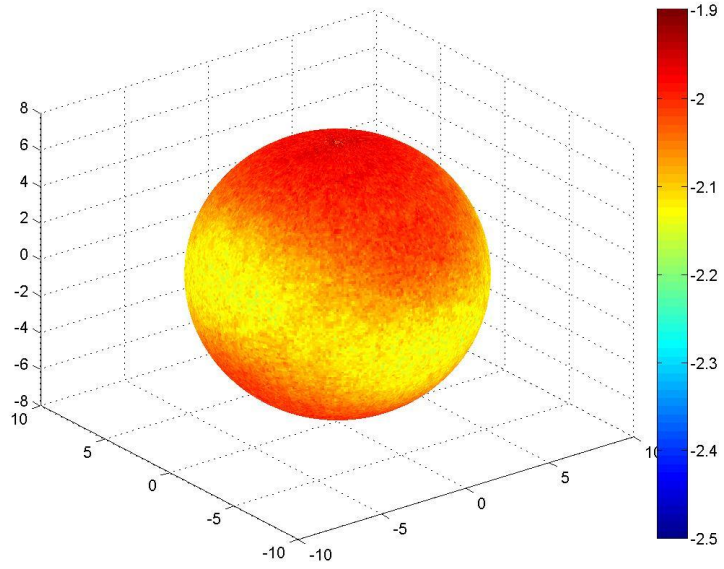

Figure B.213: Surface dose map for Design U, double beam irradiation with a 90° rotation about the vertical axis, from 30 degrees above the equatorial plane, scale minimum raised to -2.5.

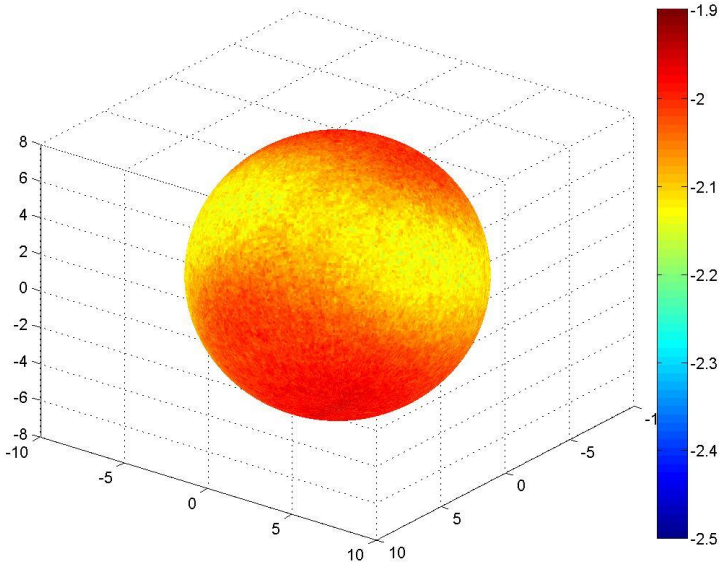

Figure B.214: Surface dose map for Design U, double beam irradiation with a 90° rotation about the vertical axis, from 30 degrees below the equatorial plane, scale minimum raised to -2.5.

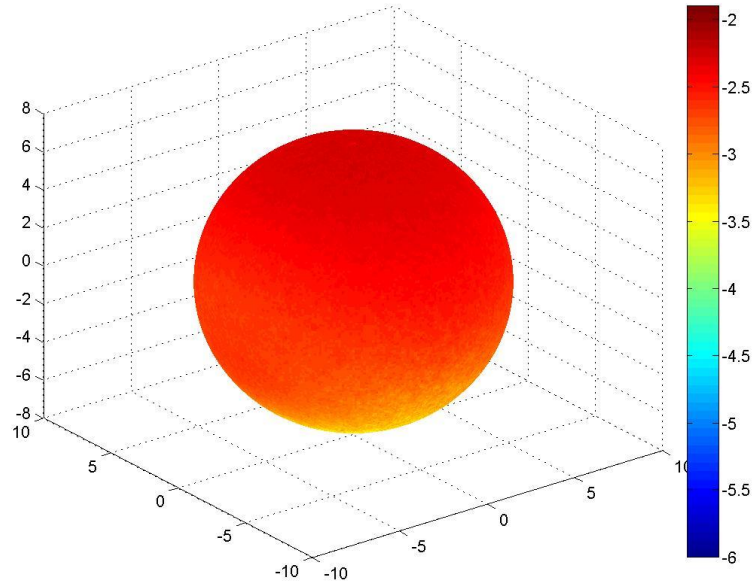

Figure B.215: Surface dose map for Design V, single beam irradiation, from 30 degrees above the equatorial plane, original scale.

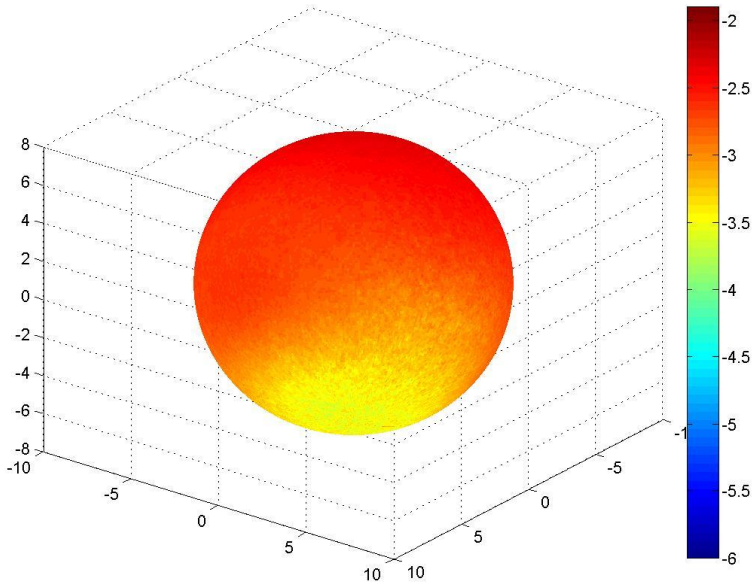

Figure B.216: Surface dose map for Design V, single beam irradiation, from 30 degrees below the equatorial plane, original scale.

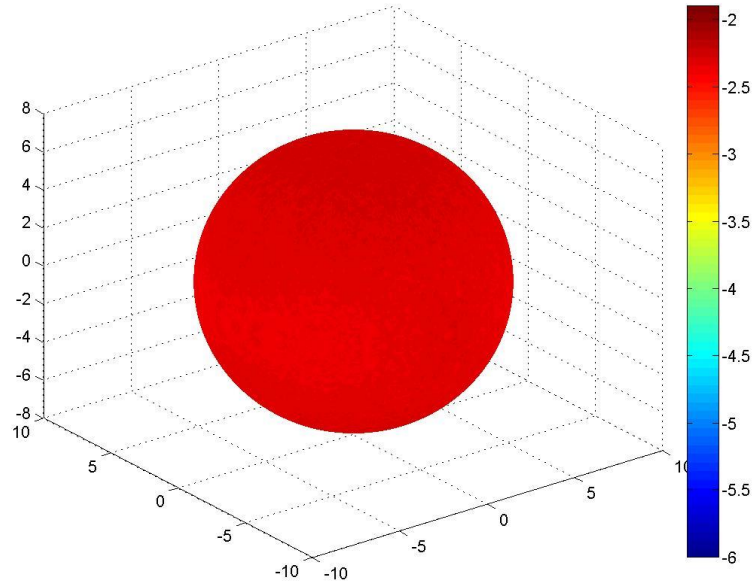

Figure B.217: Surface dose map for Design V, double beam irradiation, from 30 degrees above the equatorial plane, original scale.

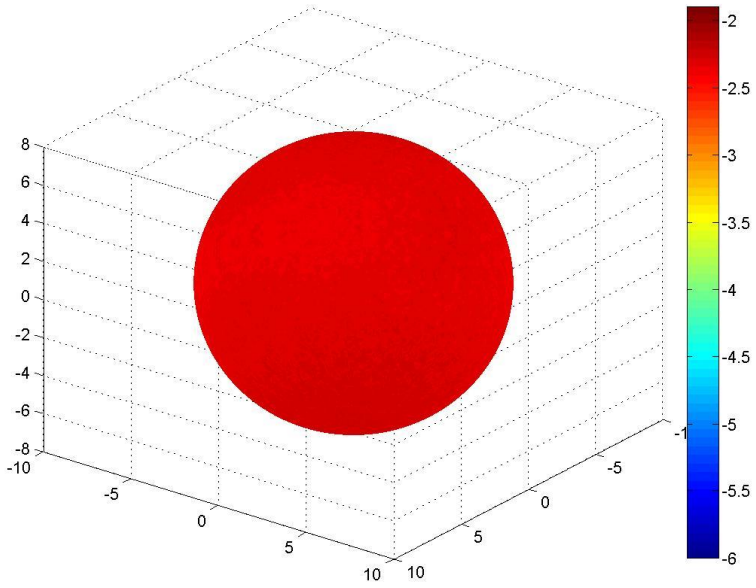

Figure B.218: Surface dose map for Design V, double beam irradiation, from 30 degrees below the equatorial plane, original scale.

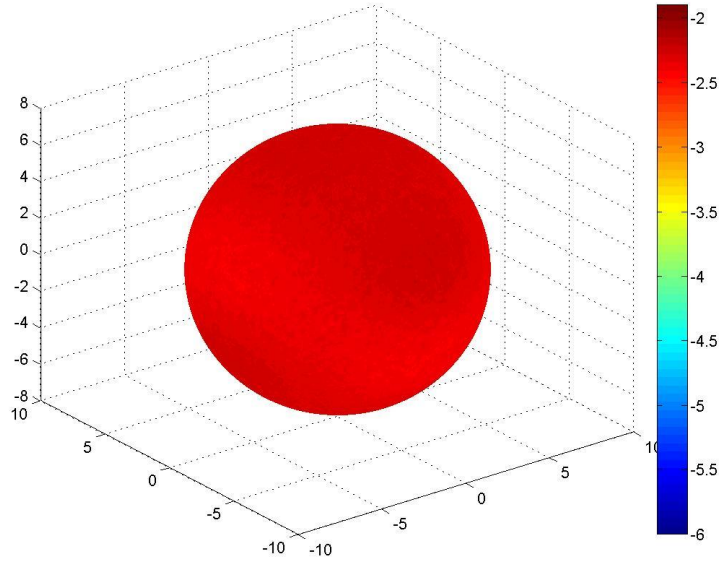

Figure B.219: Surface dose map for Design V, double beam irradiation with a 90° rotation about the vertical axis, from 30 degrees above the equatorial plane, original scale.

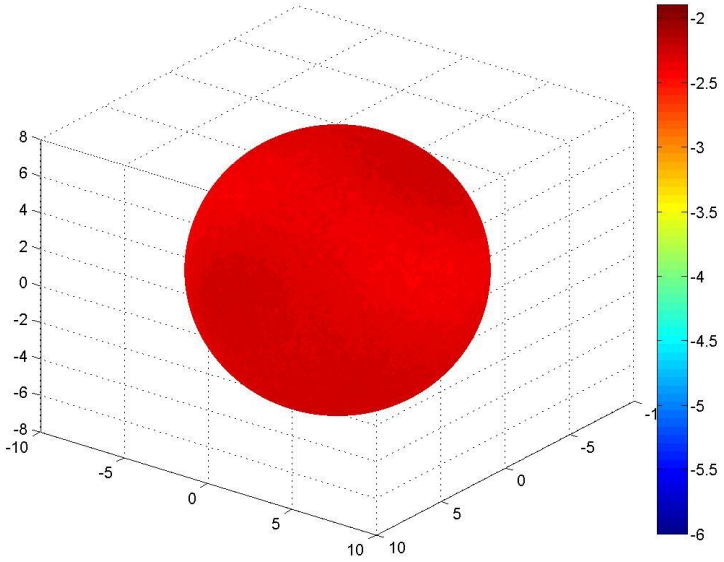

Figure B.220: Surface dose map for Design V, double beam irradiation with a 90° rotation about the vertical axis, from 30 degrees below the equatorial plane, original scale.

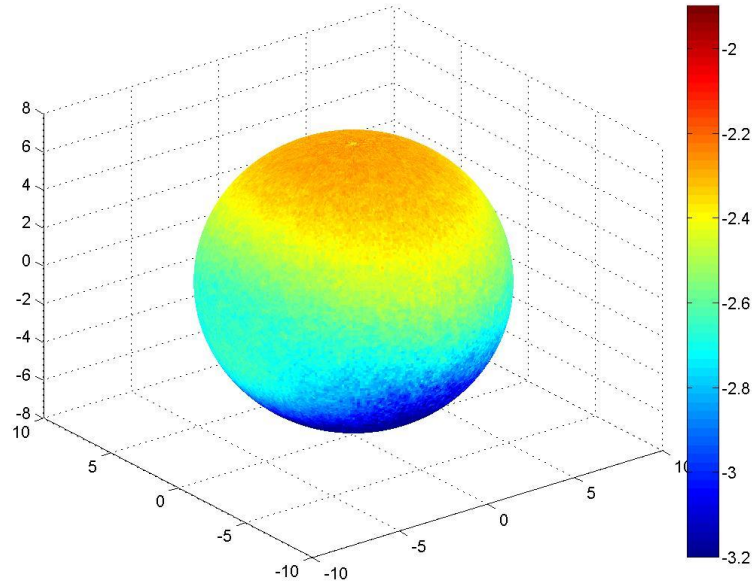

Figure B.221: Surface dose map for Design V, single beam irradiation, from 30 degrees above the equatorial plane, scale minimum raised to -3.2.

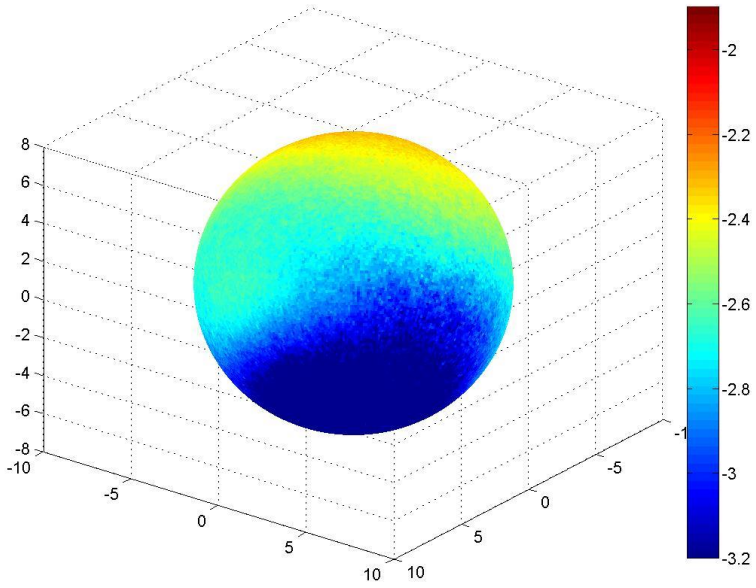

Figure B.222: Surface dose map for Design V, single beam irradiation, from 30 degrees below the equatorial plane, scale minimum raised to -3.2.

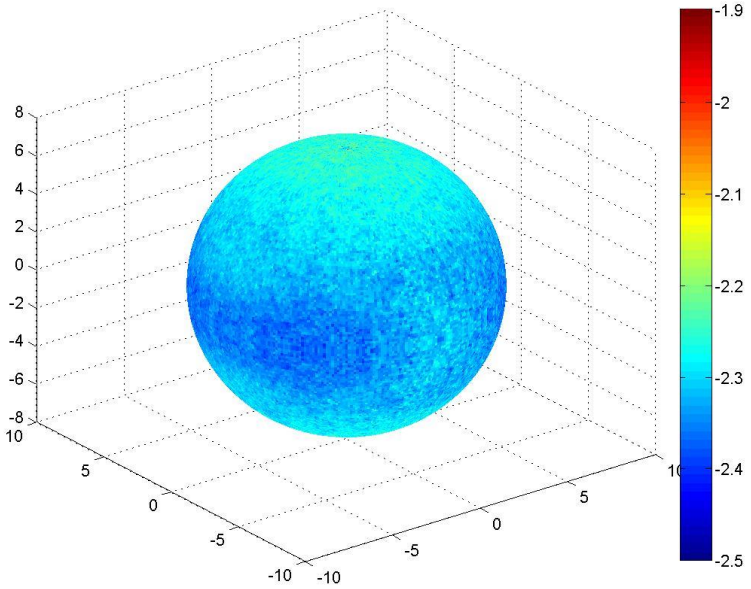

Figure B.223: Surface dose map for Design V, double beam irradiation, from 30 degrees above the equatorial plane, scale minimum raised to -2.5.

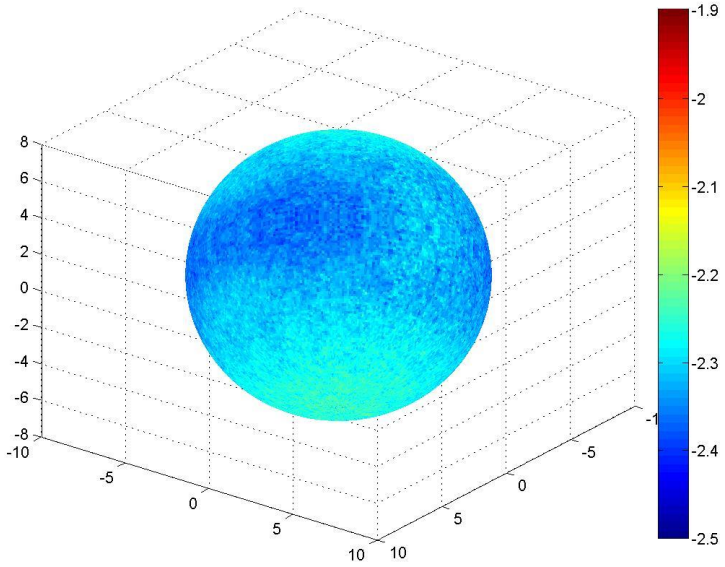

Figure B.224: Surface dose map for Design V, double beam irradiation, from 30 degrees below the equatorial plane, scale minimum raised to -2.5.

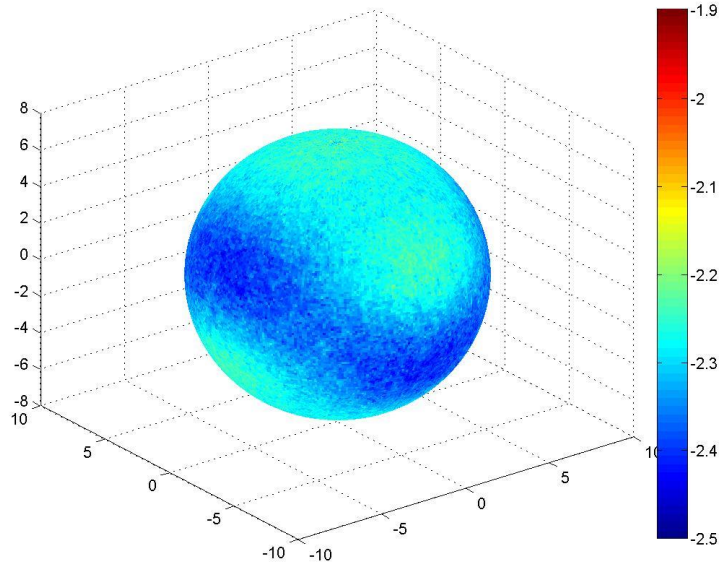

Figure B.225: Surface dose map for Design V, double beam irradiation with a 90° rotation about the vertical axis, from 30 degrees above the equatorial plane, scale minimum raised to -2.5.

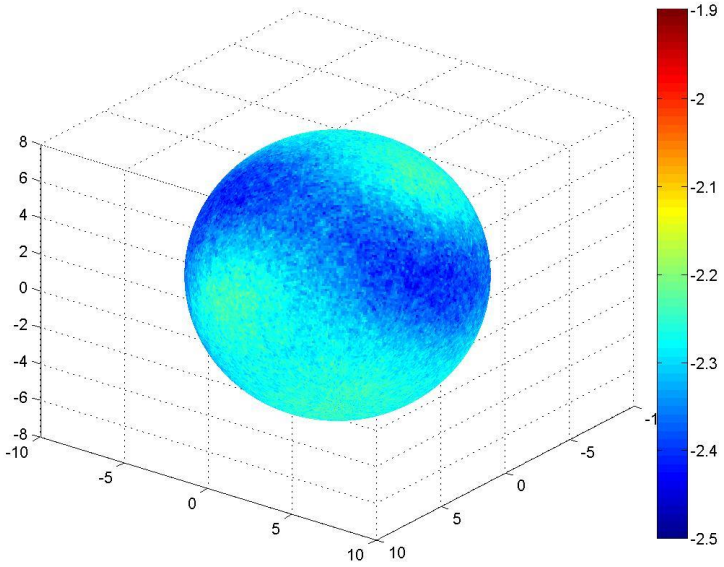

Figure B.226: Surface dose map for Design V, double beam irradiation with a 90° rotation about the vertical axis, from 30 degrees below the equatorial plane, scale minimum raised to -2.5.

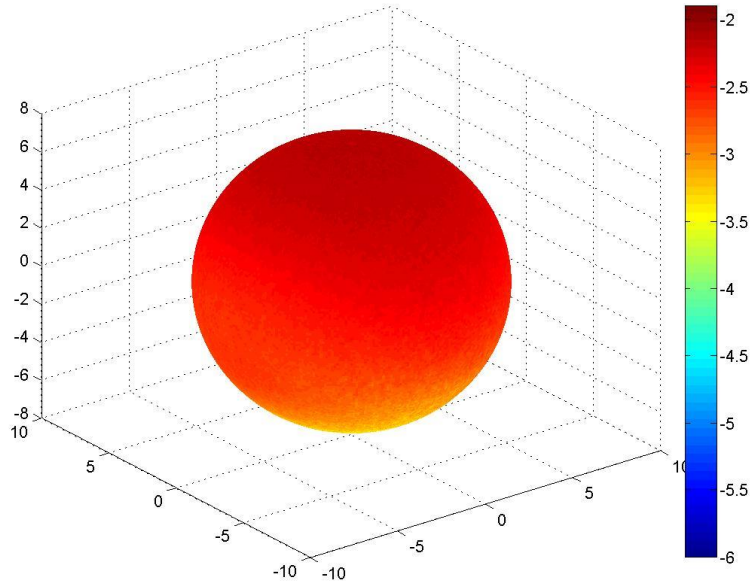

Figure B.227: Surface dose map for Design W, single beam irradiation, from 30 degrees above the equatorial plane, original scale.

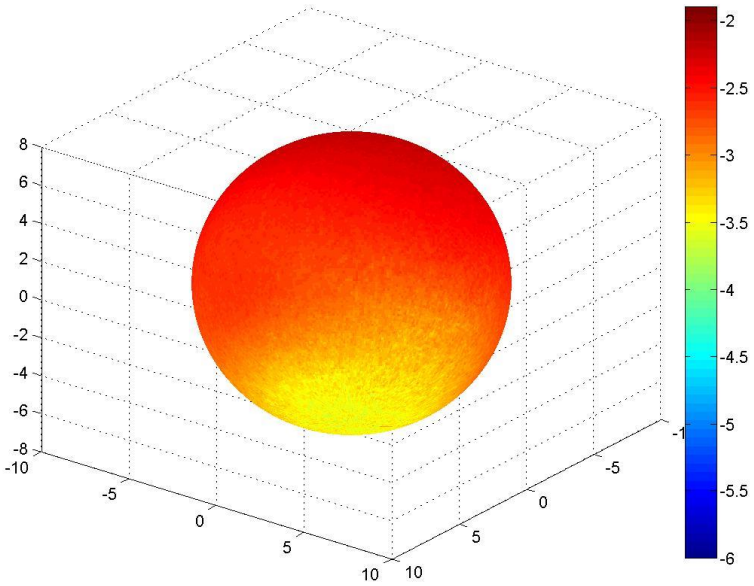

Figure B.228: Surface dose map for Design W, single beam irradiation, from 30 degrees below the equatorial plane, original scale.

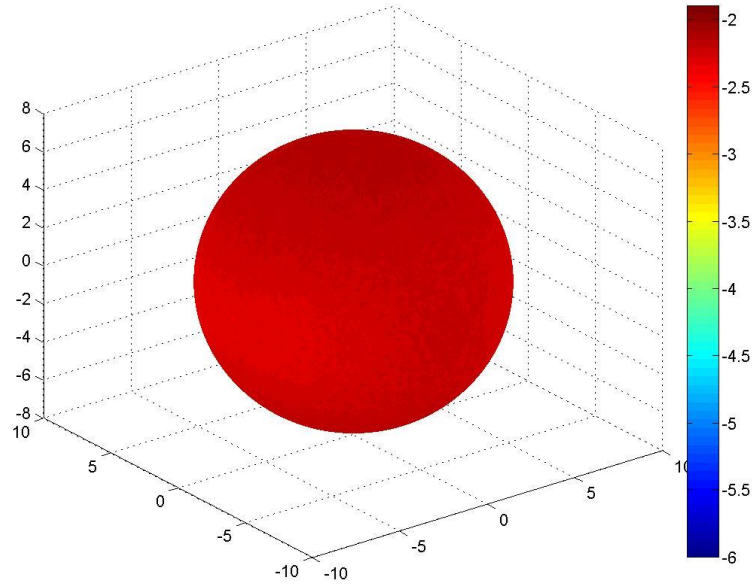

Figure B.229: Surface dose map for Design W, double beam irradiation, from 30 degrees above the equatorial plane, original scale.

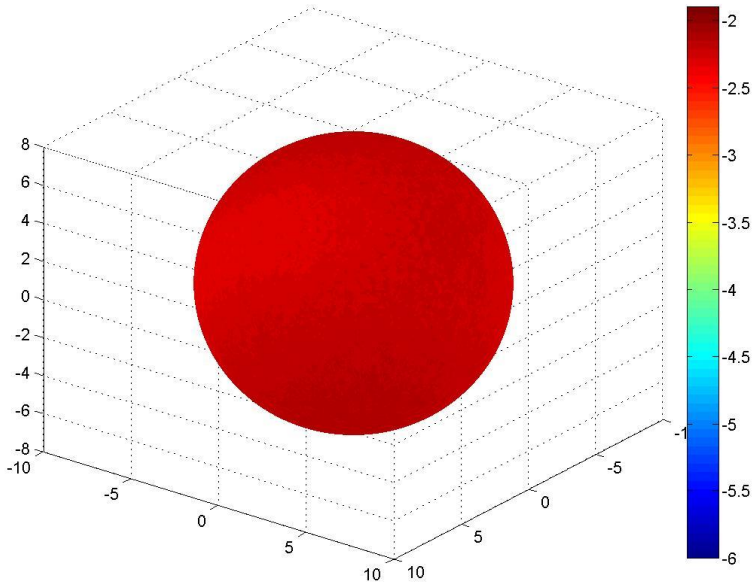

Figure B.230: Surface dose map for Design W, double beam irradiation, from 30 degrees below the equatorial plane, original scale.

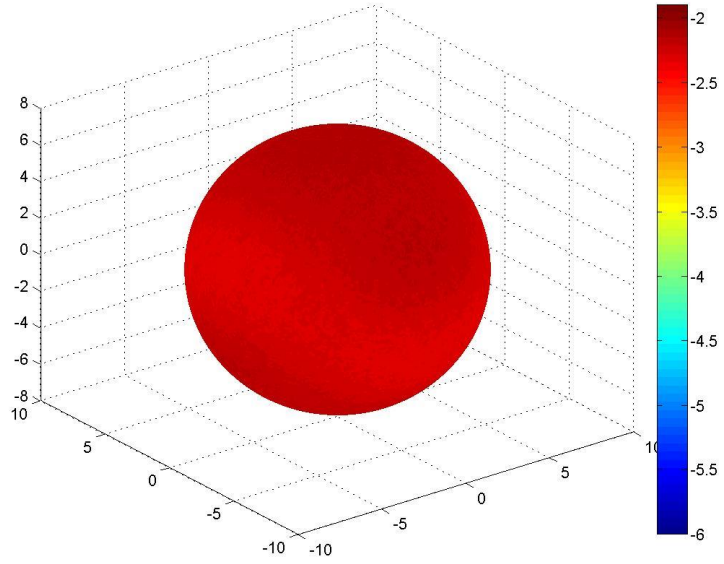

Figure B.231: Surface dose map for Design W, double beam irradiation with a 90° rotation about the vertical axis, from 30 degrees above the equatorial plane, original scale.

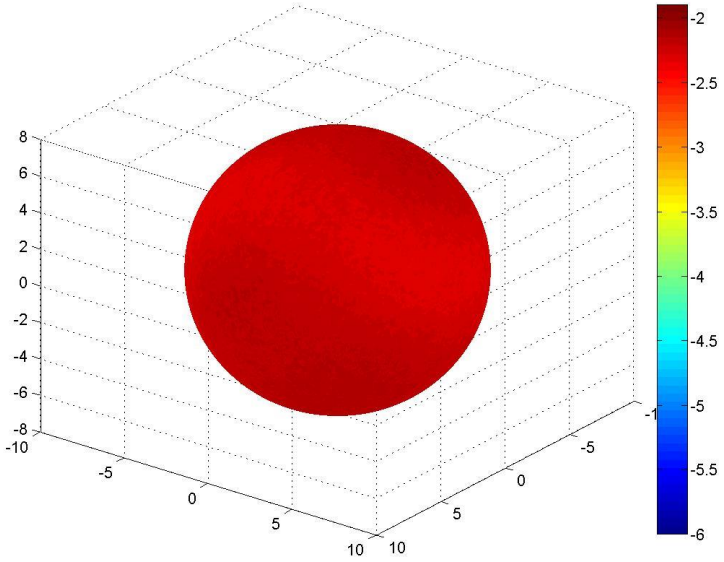

Figure B.232: Surface dose map for Design W, double beam irradiation with a 90° rotation about the vertical axis, from 30 degrees below the equatorial plane, original scale.

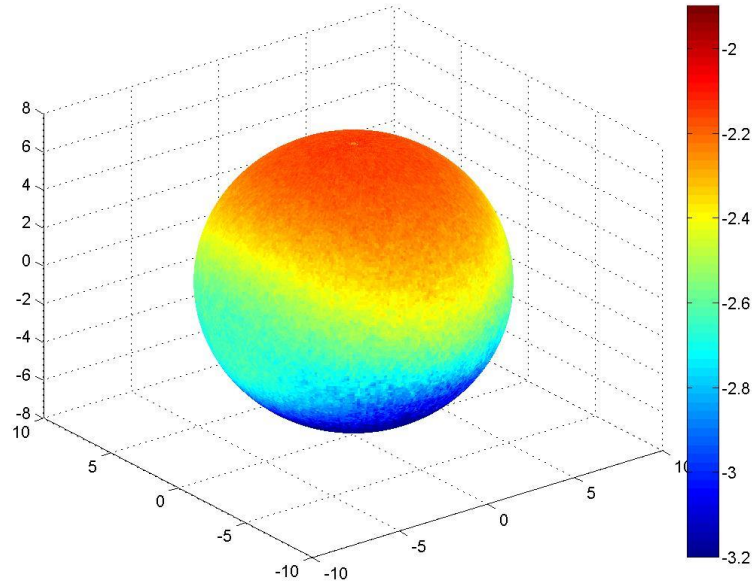

Figure B.233: Surface dose map for Design W, single beam irradiation, from 30 degrees above the equatorial plane, scale minimum raised to -3.2.

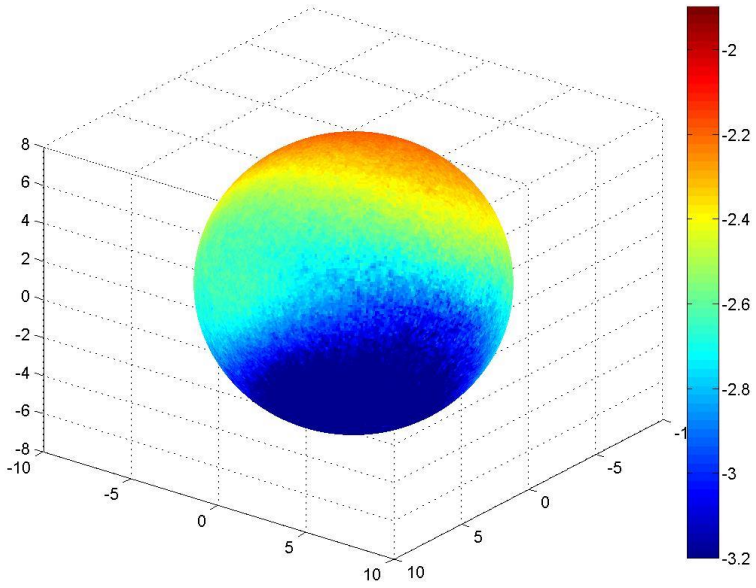

Figure B.234: Surface dose map for Design W, single beam irradiation, from 30 degrees below the equatorial plane, scale minimum raised to -3.2.

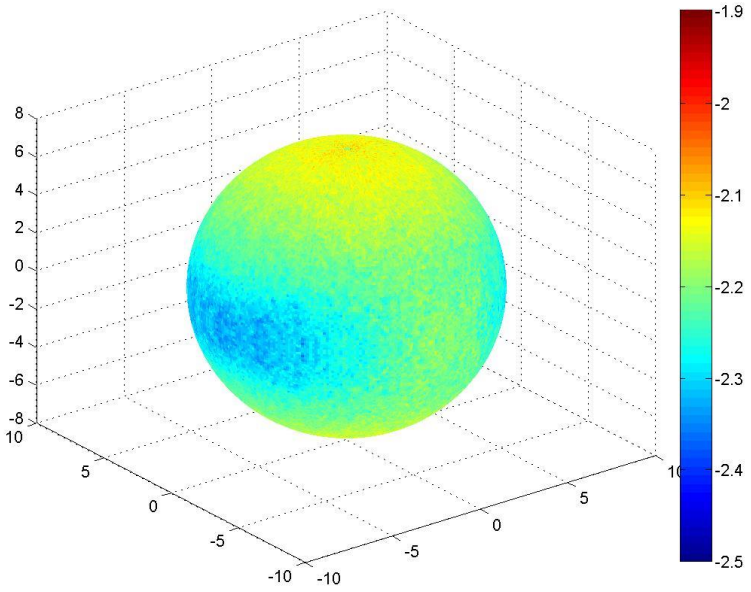

Figure B.235: Surface dose map for Design W, double beam irradiation, from 30 degrees above the equatorial plane, scale minimum raised to -2.5.

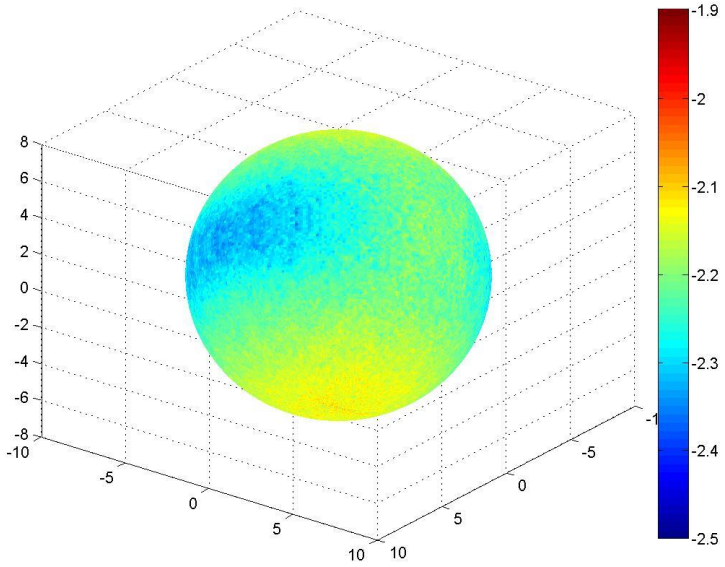

Figure B.236: Surface dose map for Design W, double beam irradiation, from 30 degrees below the equatorial plane, scale minimum raised to -2.5.

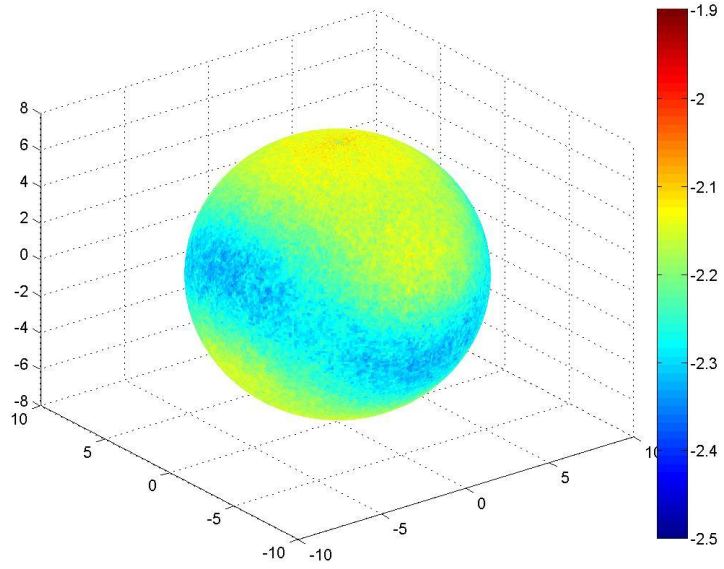

Figure B.237: Surface dose map for Design W, double beam irradiation with a 90° rotation about the vertical axis, from 30 degrees above the equatorial plane, scale minimum raised to -2.5.

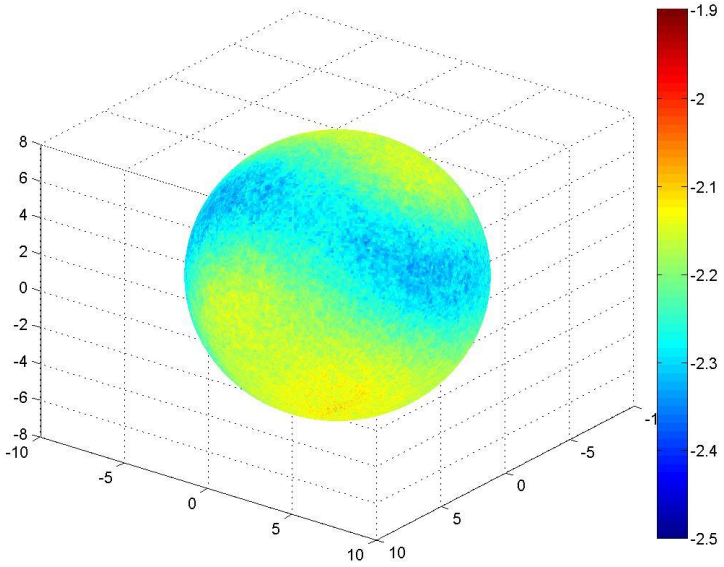

Figure B.238: Surface dose map for Design W, double beam irradiation with a 90° rotation about the vertical axis, from 30 degrees below the equatorial plane, scale minimum raised to -2.5.

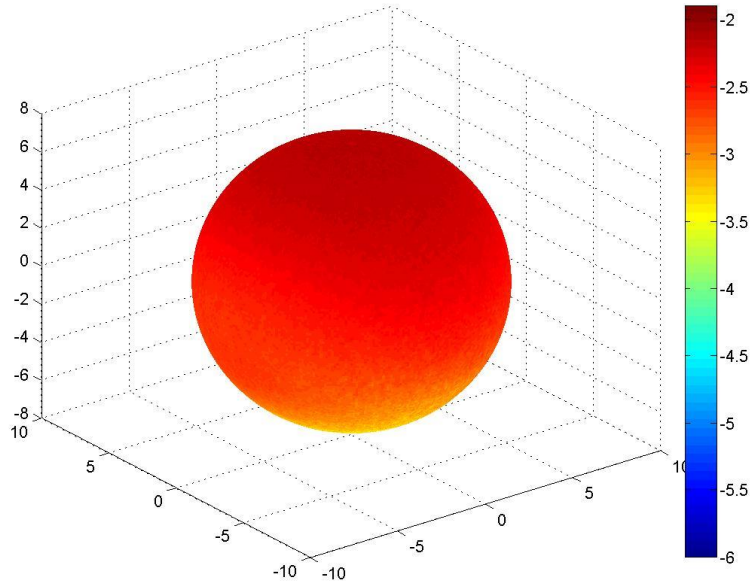

Figure B.239: Surface dose map for Design X, single beam irradiation, from 30 degrees above the equatorial plane, original scale.

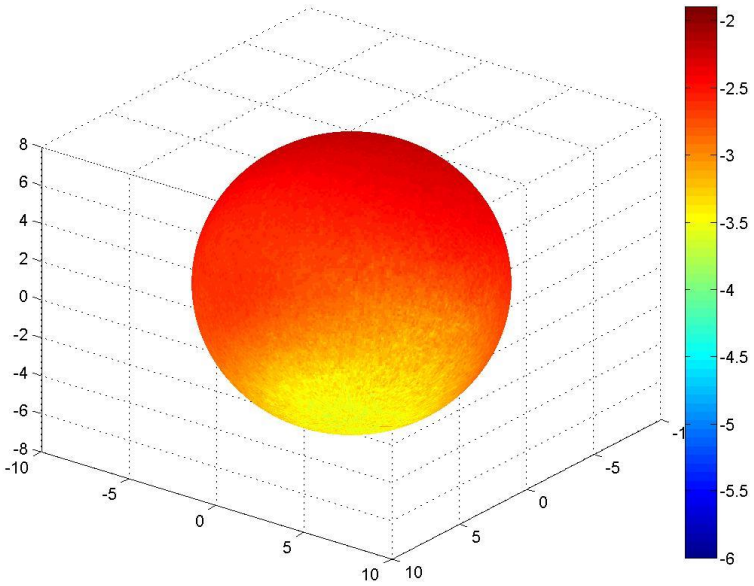

Figure B.240: Surface dose map for Design X, single beam irradiation, from 30 degrees below the equatorial plane, original scale.

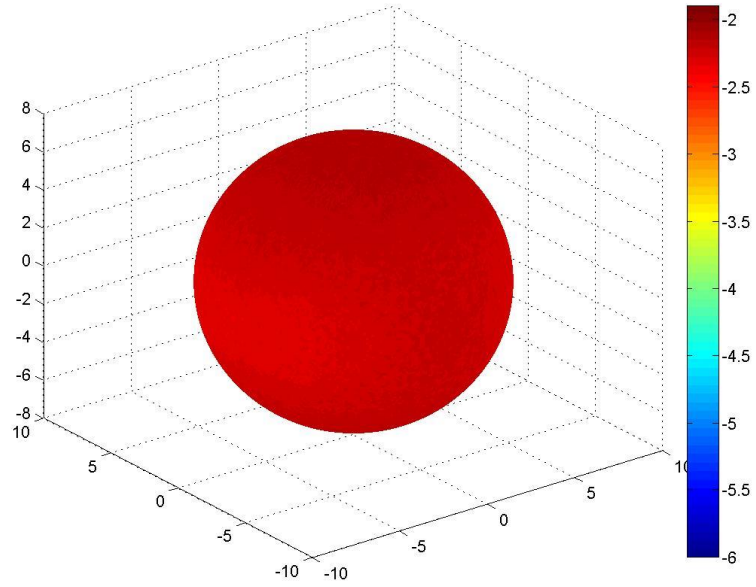

Figure B.241: Surface dose map for Design X, double beam irradiation, from 30 degrees above the equatorial plane, original scale.

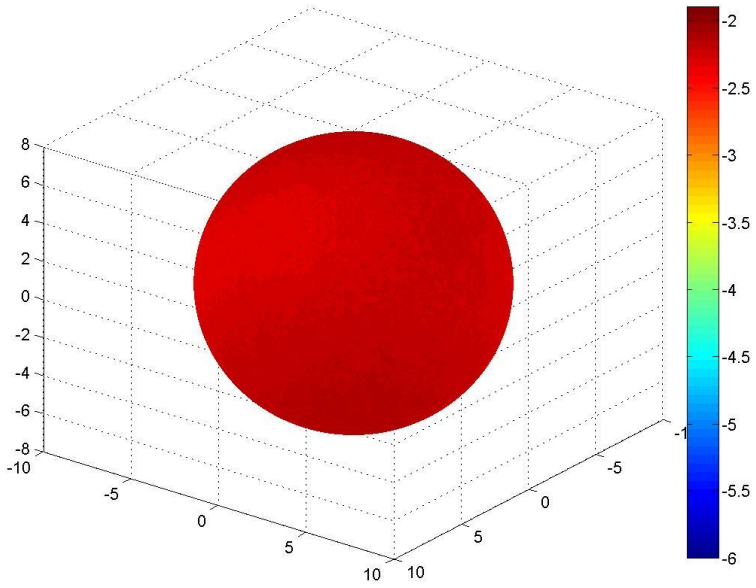

Figure B.242: Surface dose map for Design X, double beam irradiation, from 30 degrees below the equatorial plane, original scale.

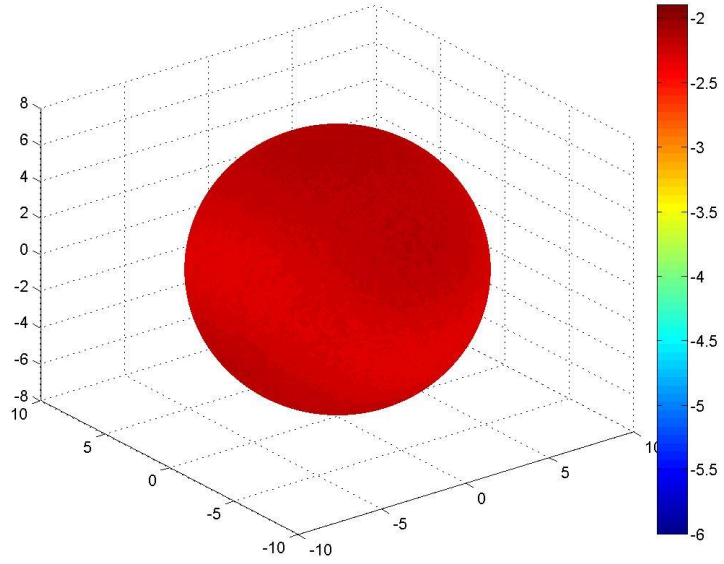

Figure B.243: Surface dose map for Design X, double beam irradiation with a 90° rotation about the vertical axis, from 30 degrees above the equatorial plane, original scale.

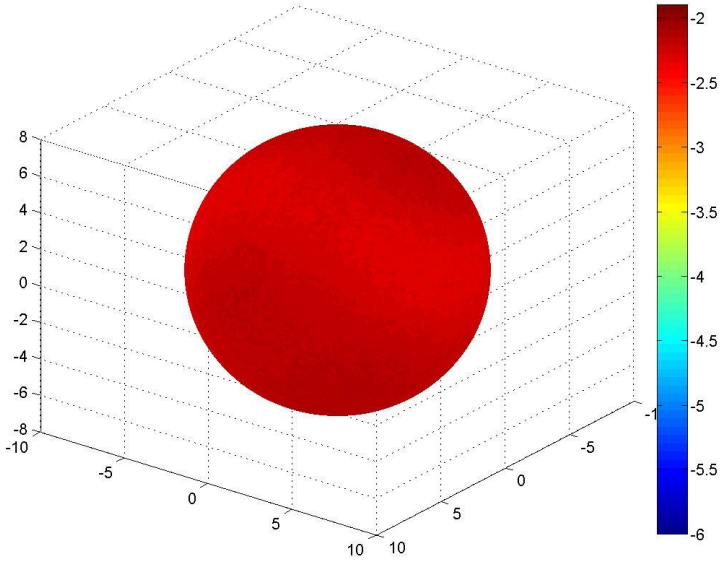

Figure B.244: Surface dose map for Design X, double beam irradiation with a 90° rotation about the vertical axis, from 30 degrees below the equatorial plane, original scale.

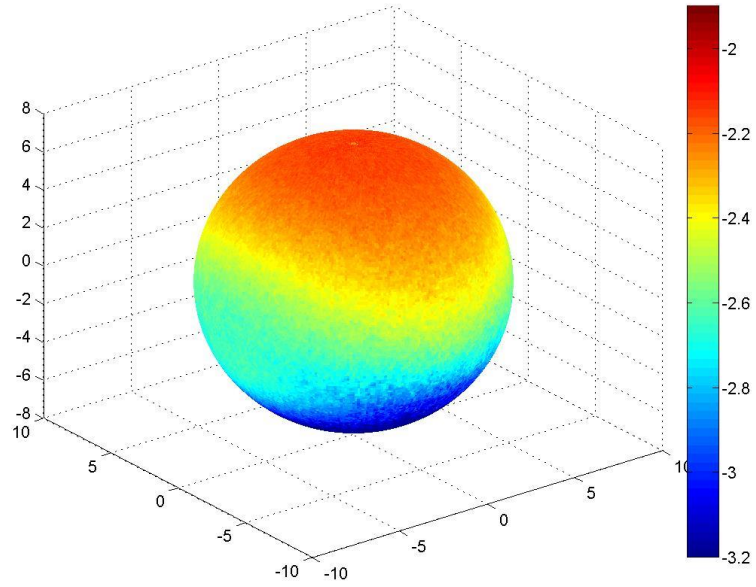

Figure B.245: Surface dose map for Design X, single beam irradiation, from 30 degrees above the equatorial plane, scale minimum raised to -3.2.

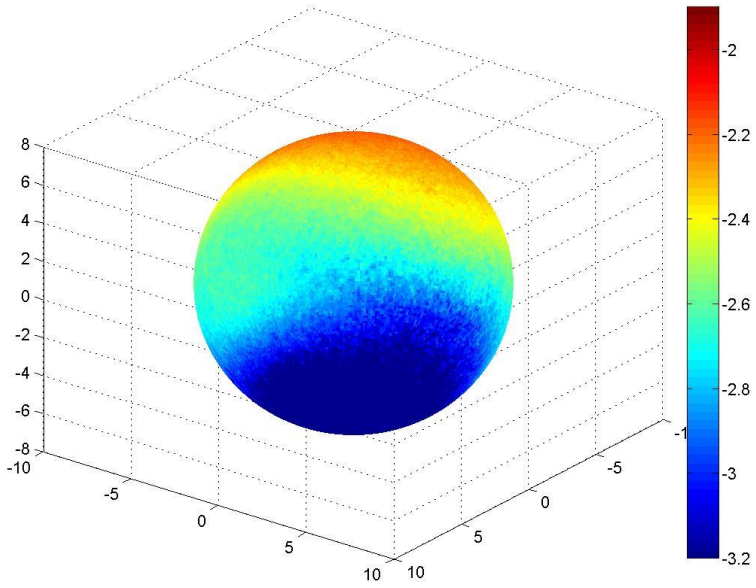

Figure B.246: Surface dose map for Design X, single beam irradiation, from 30 degrees below the equatorial plane, scale minimum raised to -3.2.

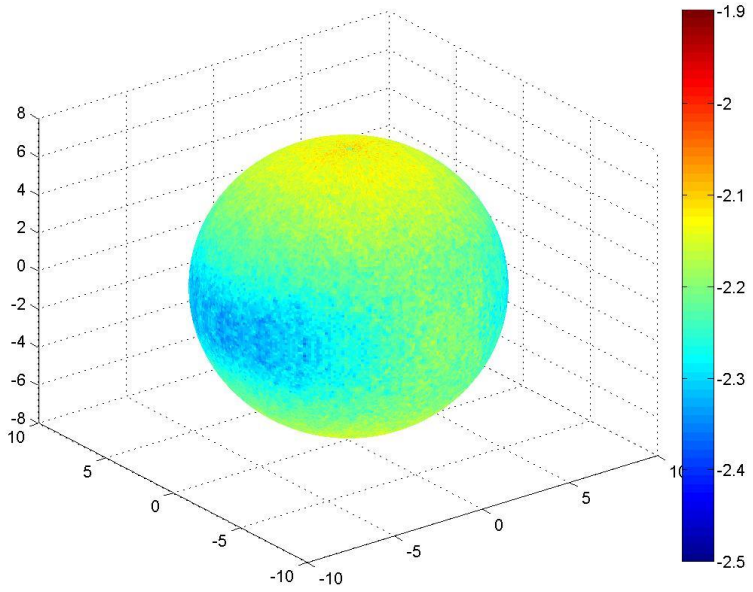

Figure B.247: Surface dose map for Design X, double beam irradiation, from 30 degrees above the equatorial plane, scale minimum raised to -2.5.

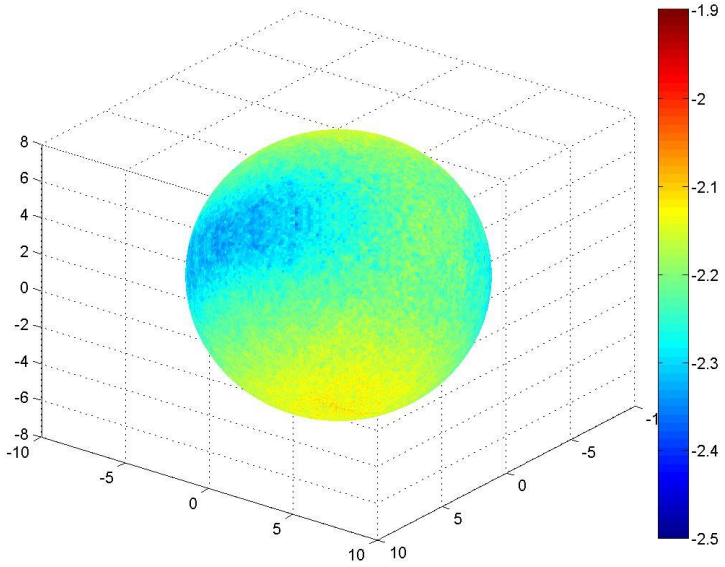

Figure B.248: Surface dose map for Design X, double beam irradiation, from 30 degrees below the equatorial plane, scale minimum raised to -2.5.

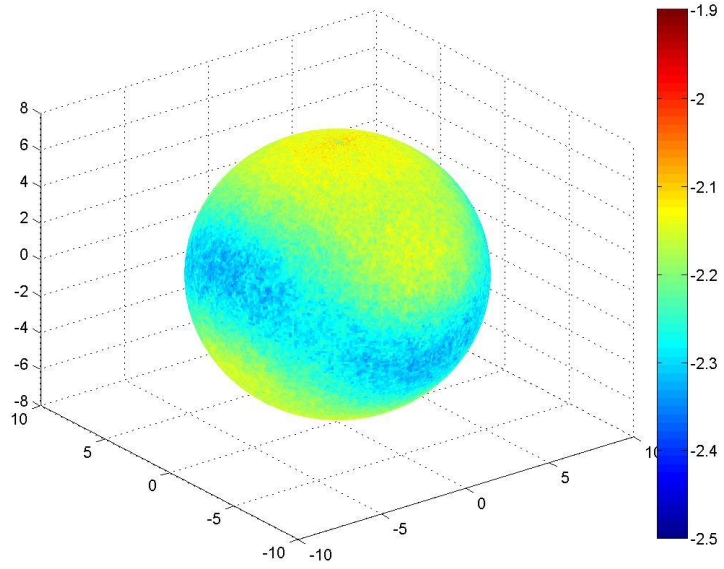

Figure B.249: Surface dose map for Design X, double beam irradiation with a 90° rotation about the vertical axis, from 30 degrees above the equatorial plane, scale minimum raised to -2.5.

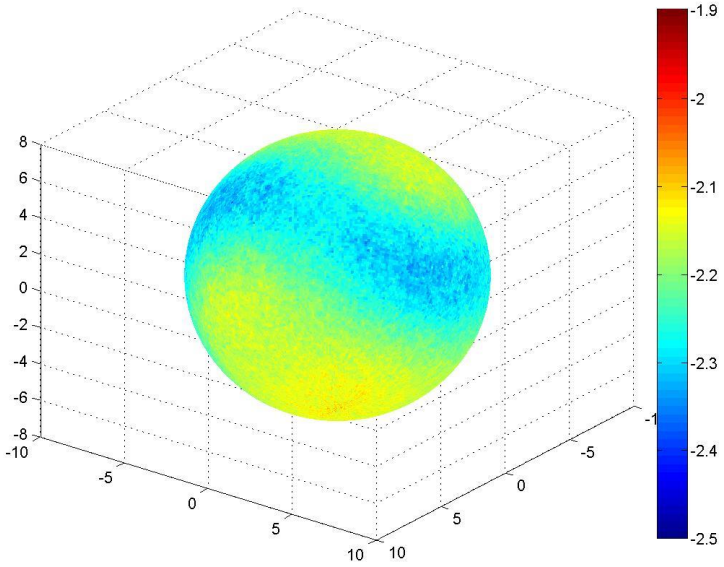

Figure B.250: Surface dose map for Design X, double beam irradiation with a 90° rotation about the vertical axis, from 30 degrees below the equatorial plane, scale minimum raised to -2.5.

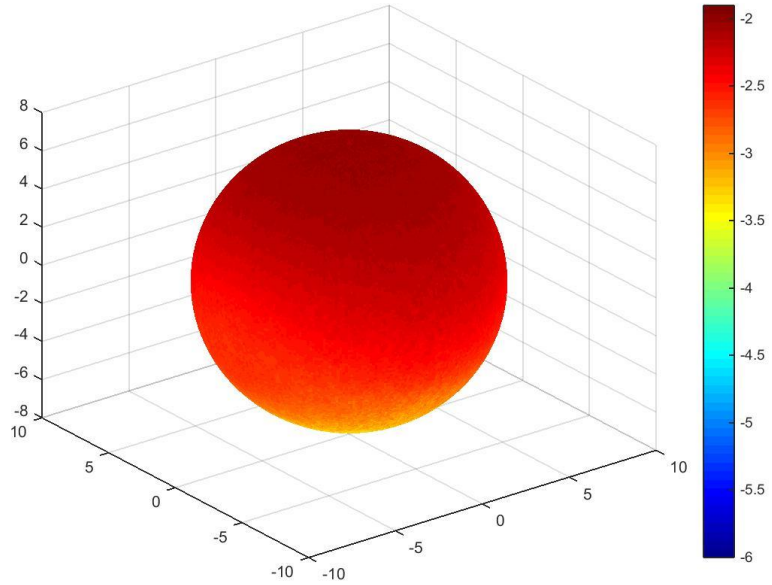

Figure B.251: Surface dose map for Design Y, single beam irradiation, from 30 degrees above the equatorial plane, original scale.

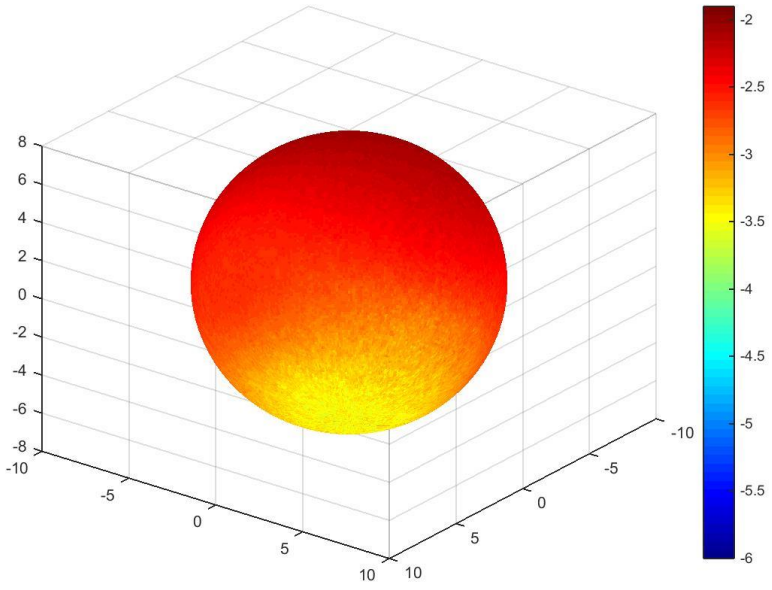

Figure B.252: Surface dose map for Design Y, single beam irradiation, from 30 degrees below the equatorial plane, original scale.

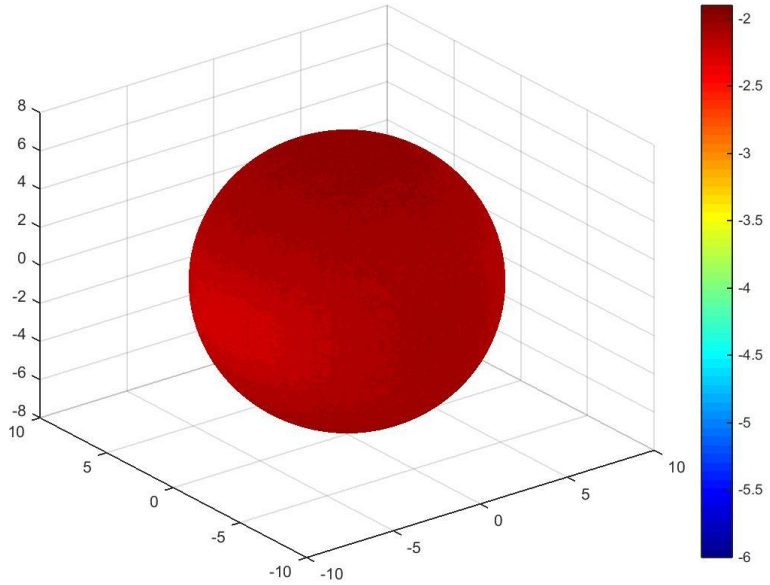

Figure B.253: Surface dose map for Design Y, double beam irradiation, from 30 degrees above the equatorial plane, original scale.

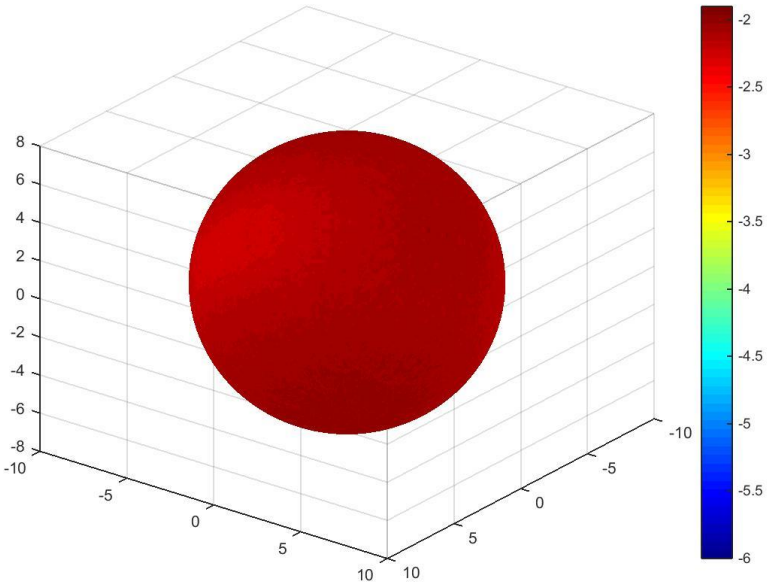

Figure B.254: Surface dose map for Design Y, double beam irradiation, from 30 degrees below the equatorial plane, original scale.

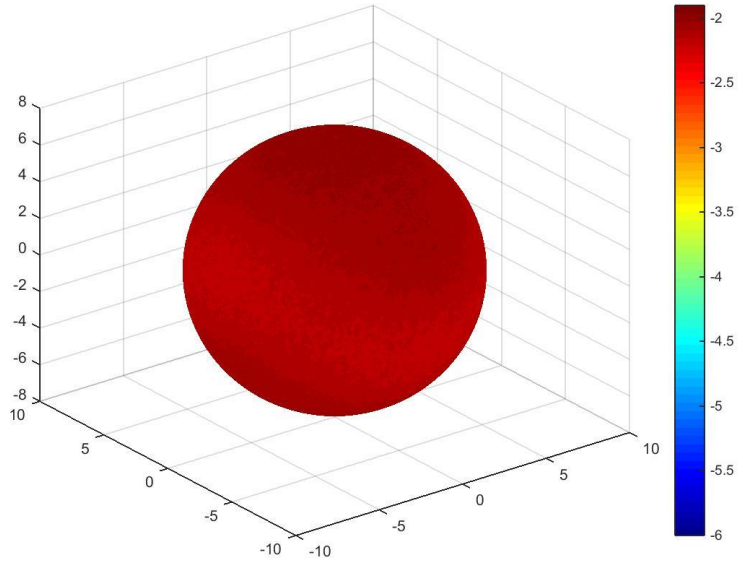

Figure B.255: Surface dose map for Design Y, double beam irradiation with a 90° rotation about the vertical axis, from 30 degrees above the equatorial plane, original scale.

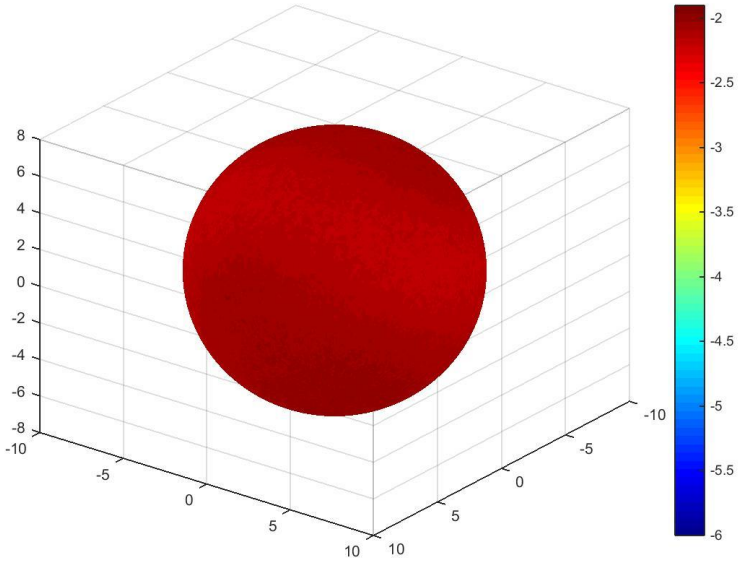

Figure B.256: Surface dose map for Design Y, double beam irradiation with a 90° rotation about the vertical axis, from 30 degrees below the equatorial plane, original scale.

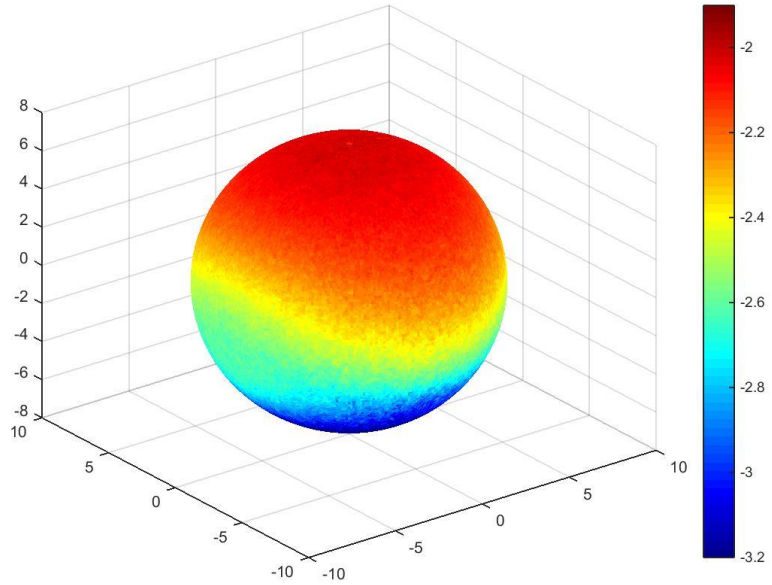

Figure B.257: Surface dose map for Design Y, single beam irradiation, from 30 degrees above the equatorial plane, scale minimum raised to -3.2.

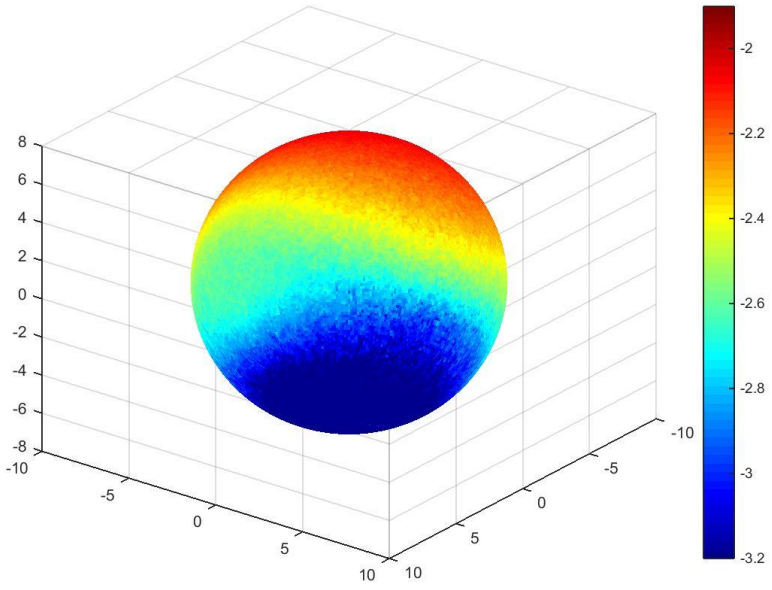

Figure B.258: Surface dose map for Design Y, single beam irradiation, from 30 degrees below the equatorial plane, scale minimum raised to -3.2.

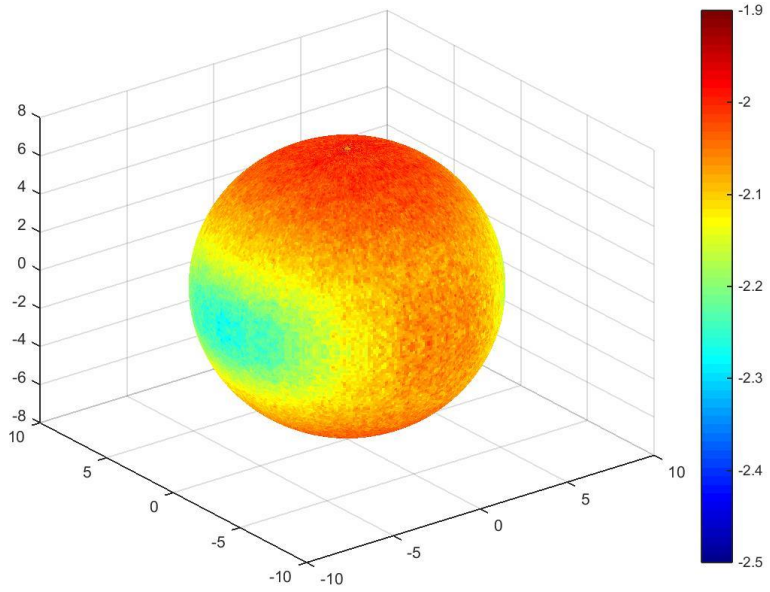

Figure B.259: Surface dose map for Design Y, double beam irradiation, from 30 degrees above the equatorial plane, scale minimum raised to -2.5.

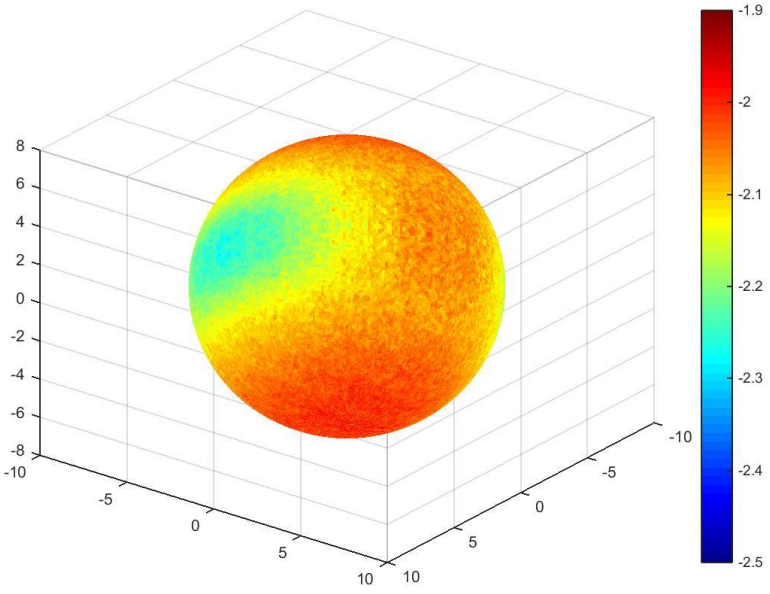

Figure B.260: Surface dose map for Design Y, double beam irradiation, from 30 degrees below the equatorial plane, scale minimum raised to -2.5.

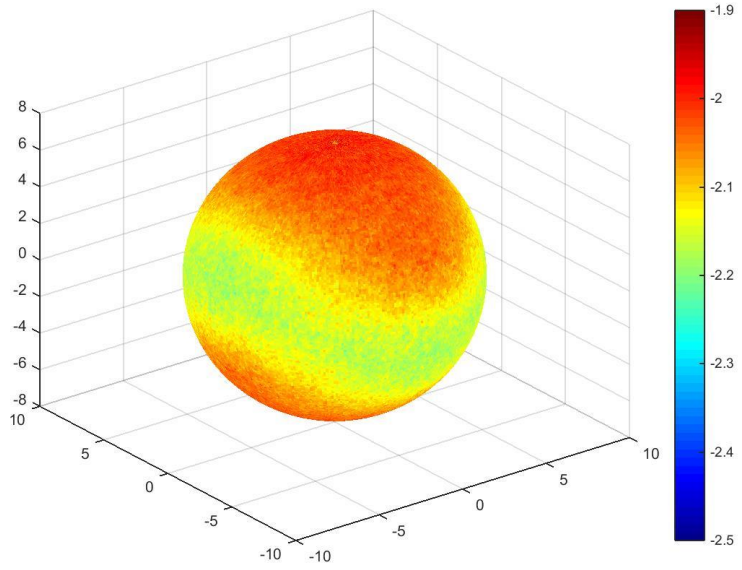

Figure B.261: Surface dose map for Design Y, double beam irradiation with a 90° rotation about the vertical axis, from 30 degrees above the equatorial plane, scale minimum raised to -2.5.

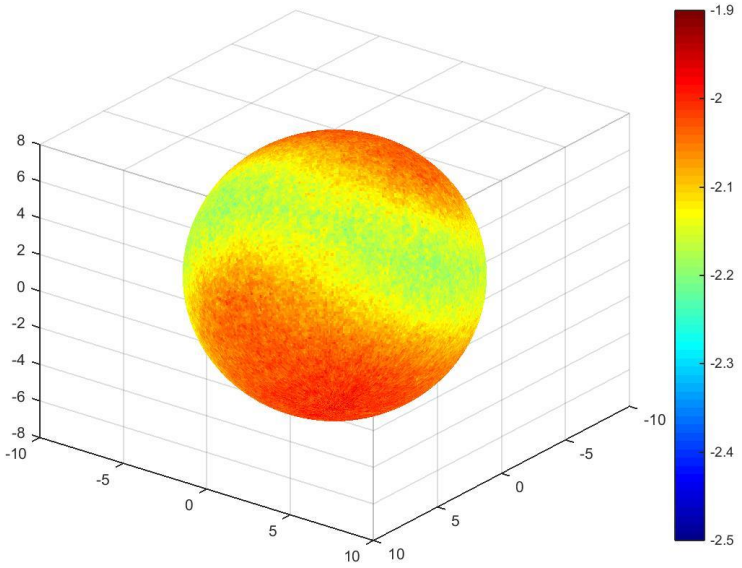

Figure B.262: Surface dose map for Design Y, double beam irradiation with a 90° rotation about the vertical axis, from 30 degrees below the equatorial plane, scale minimum raised to -2.5.

APPENDIX C

DOSE DEPTH CURVES

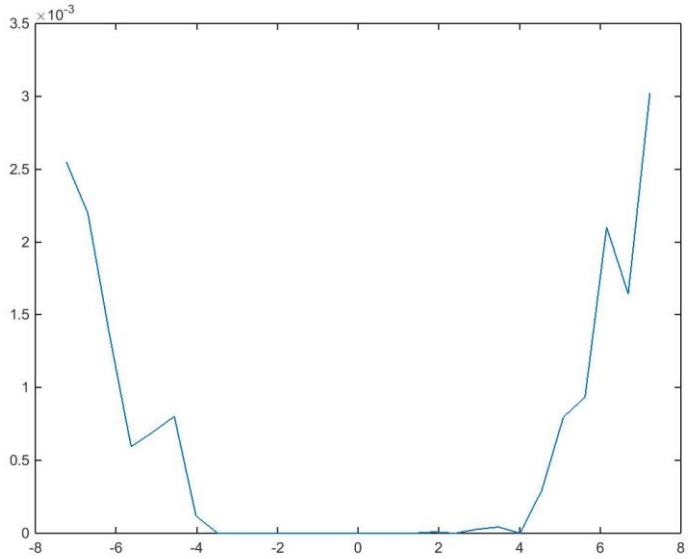

Figure C.1: Dose depth curve for (r,90,0), control model, double beam irradiation.

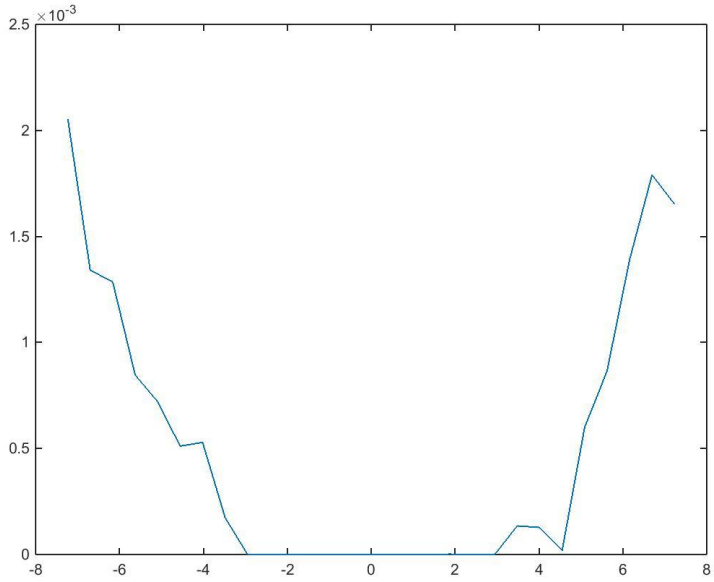

Figure C.2: Dose depth curve for (r,90,90), control model, double beam irradiation.

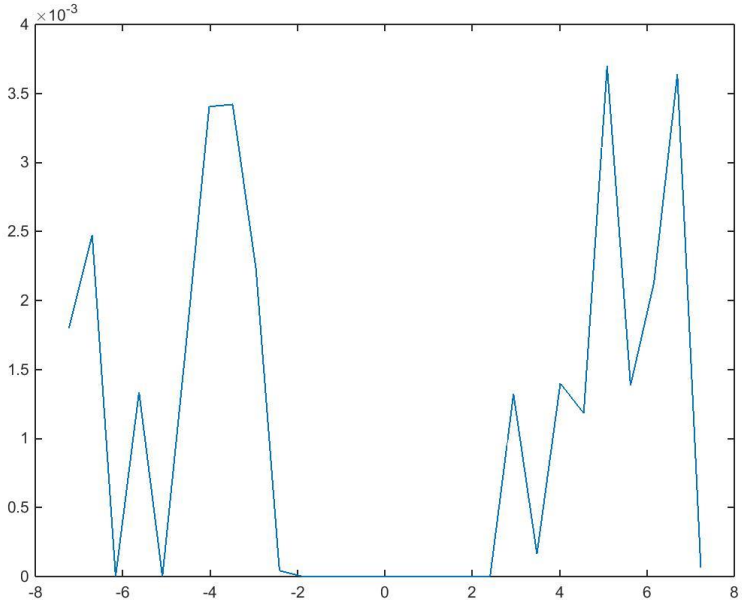

Figure C.3: Dose depth curve for (r, 0,0), control model, double beam irradiation.

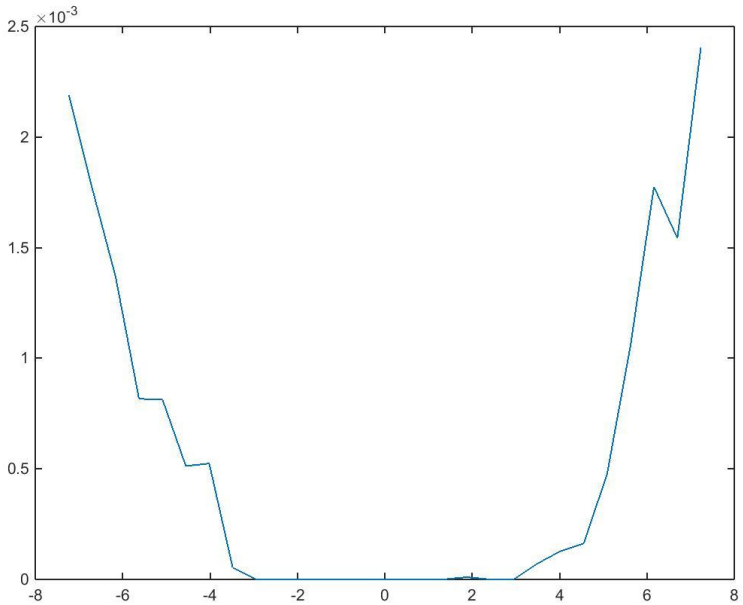

Figure C.4: Dose depth curve for (r,90,0), control model, double beam irradiation with a 90° rotation about the vertical axis.

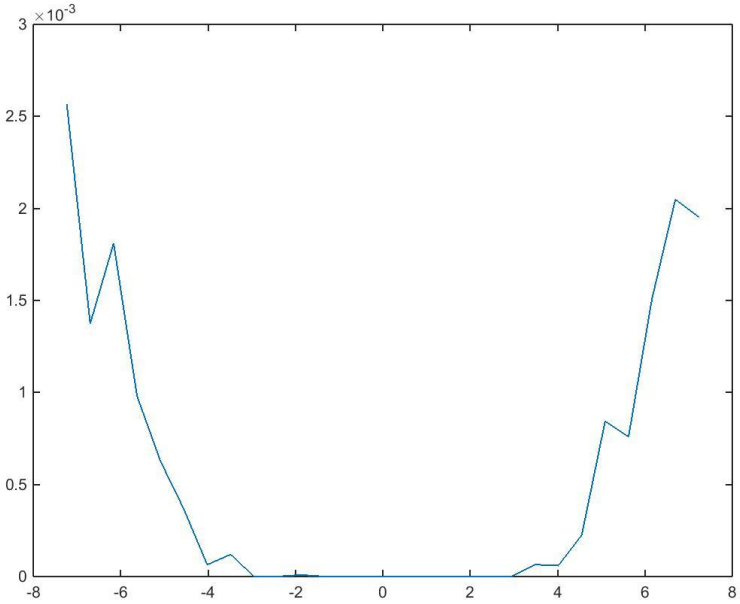

Figure C.5: Dose depth curve for (r,90,90), control model, double beam irradiation with a 90° rotation about the vertical axis.

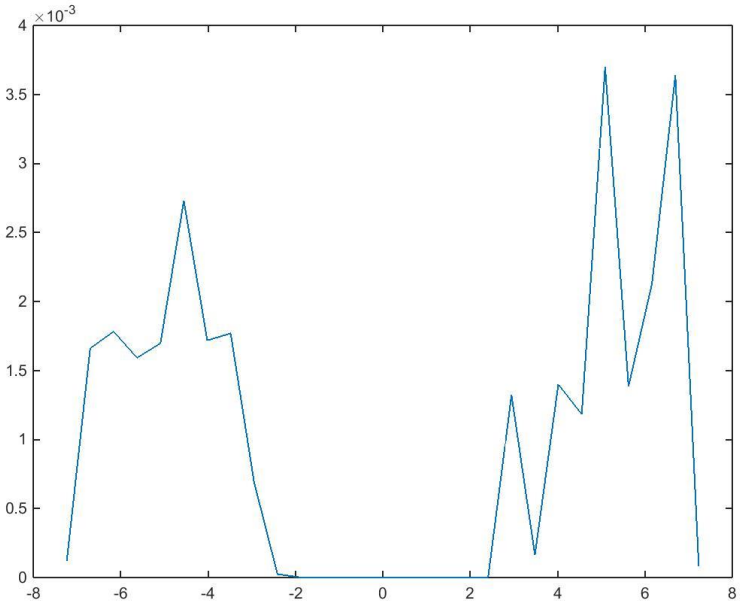

Figure C.6: Dose depth curve for (r, 0,0), control model, double beam irradiation with a 90° rotation about the vertical axis.

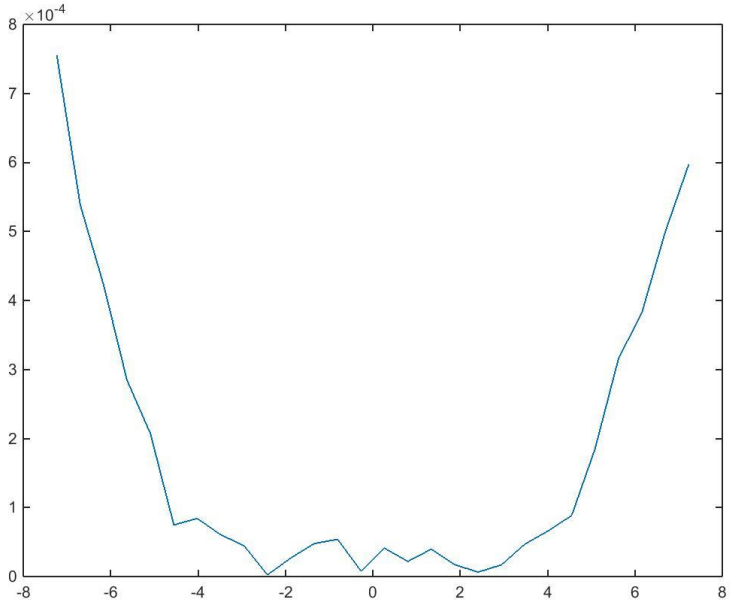

Figure C.7: Dose depth curve for (r,90,0), Design A, single beam irradiation.

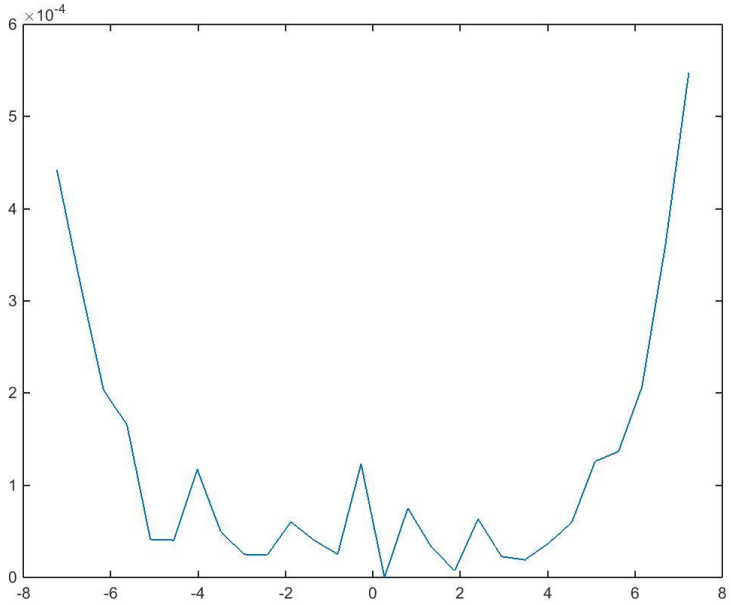

Figure C.8: Dose depth curve for (r,90,90), Design A, single beam irradiation.

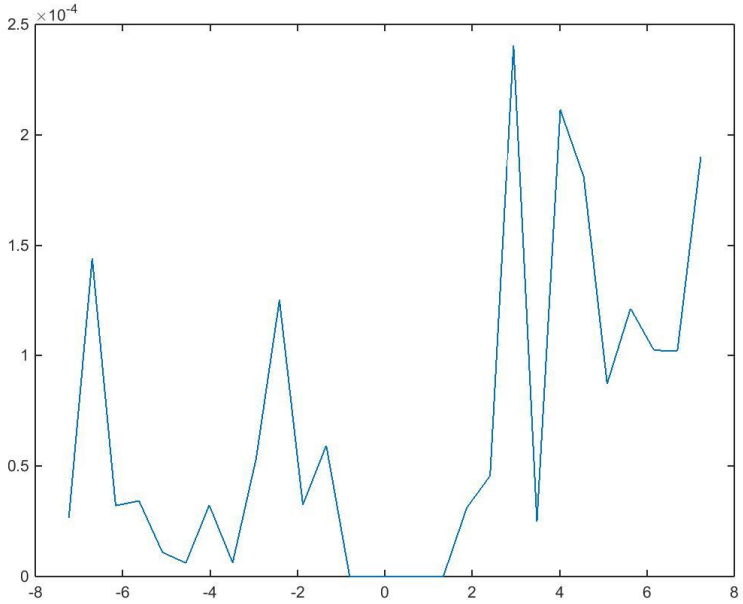

Figure C.9: Dose depth curve for (r, 0,0), Design A, single beam irradiation.

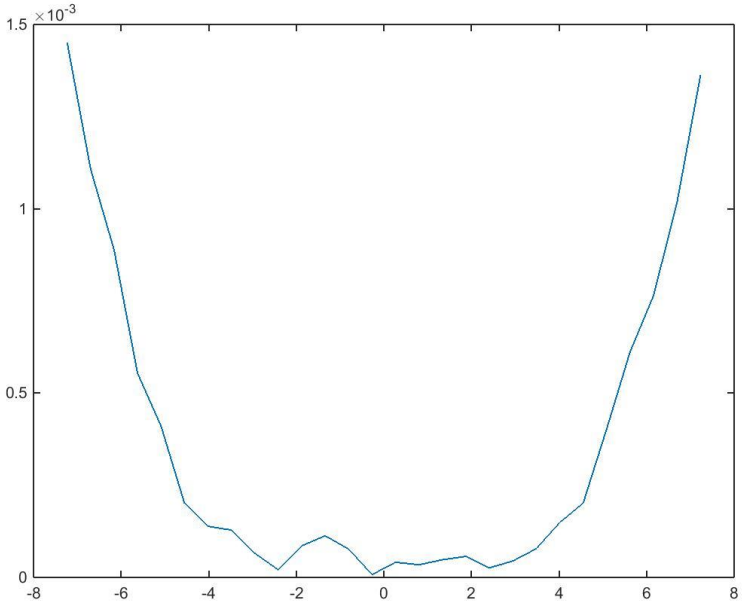

Figure C.10: Dose depth curve for (r,90,0), Design A, double beam irradiation.

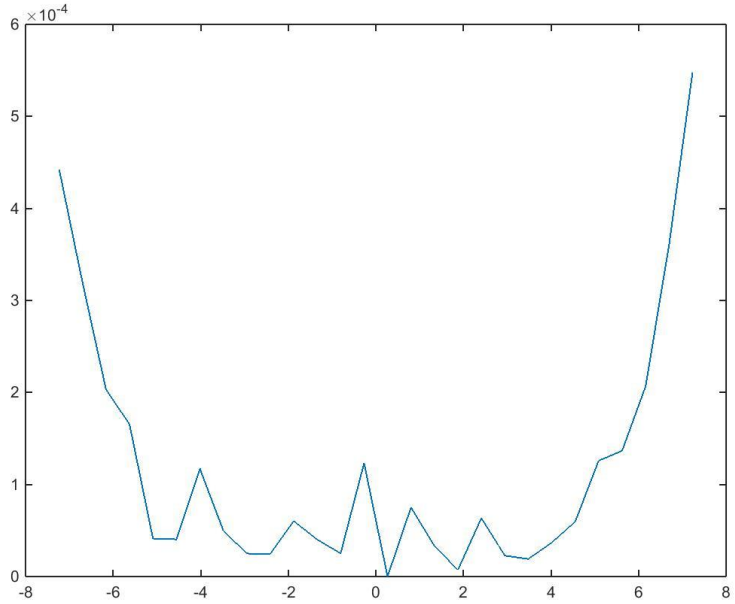

Figure C.11: Dose depth curve for (r,90,90), Design A, double beam irradiation.

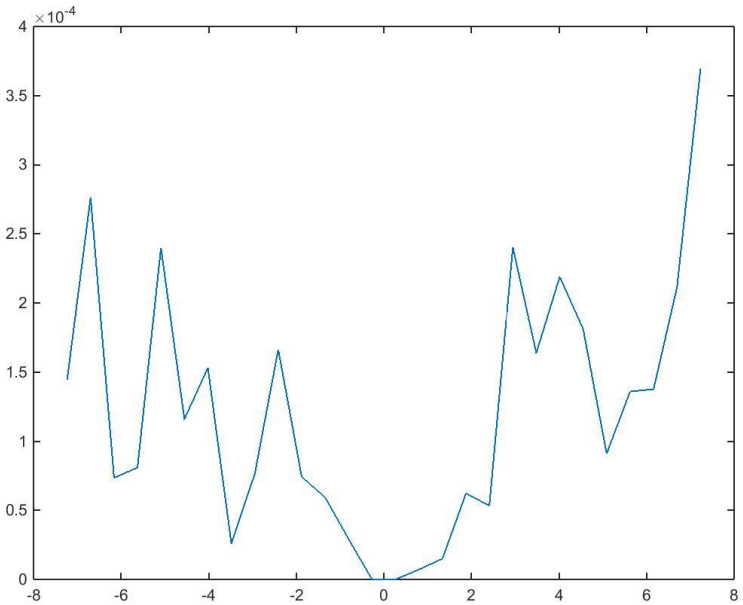

Figure C.12: Dose depth curve for (r, 0,0), Design A, double beam irradiation.

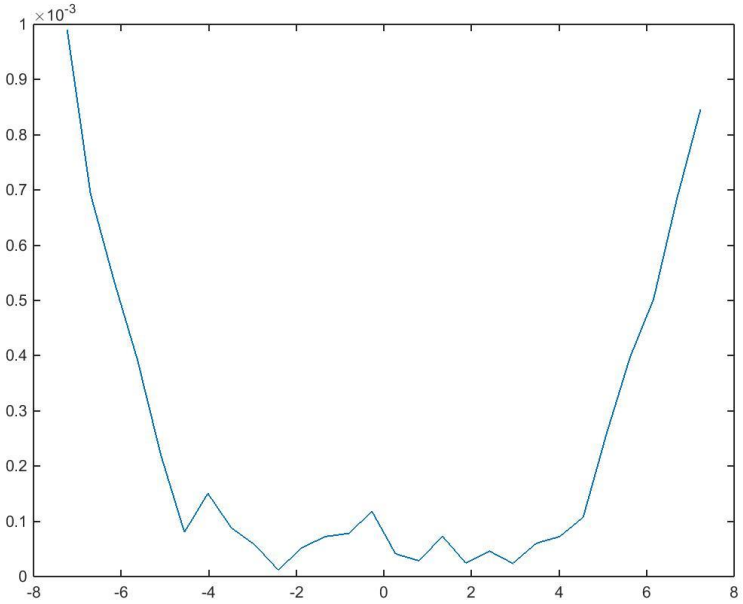

Figure C.13: Dose depth curve for (r,90,0), Design A, double beam irradiation with a 90° rotation about the vertical axis.

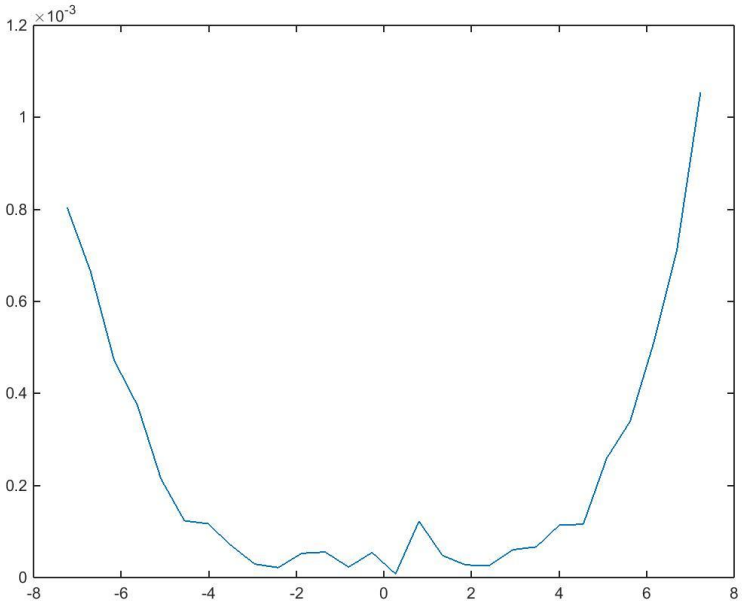

Figure C.14: Dose depth curve for (r,90,90), Design A, double beam irradiation with a 90° rotation about the vertical axis.

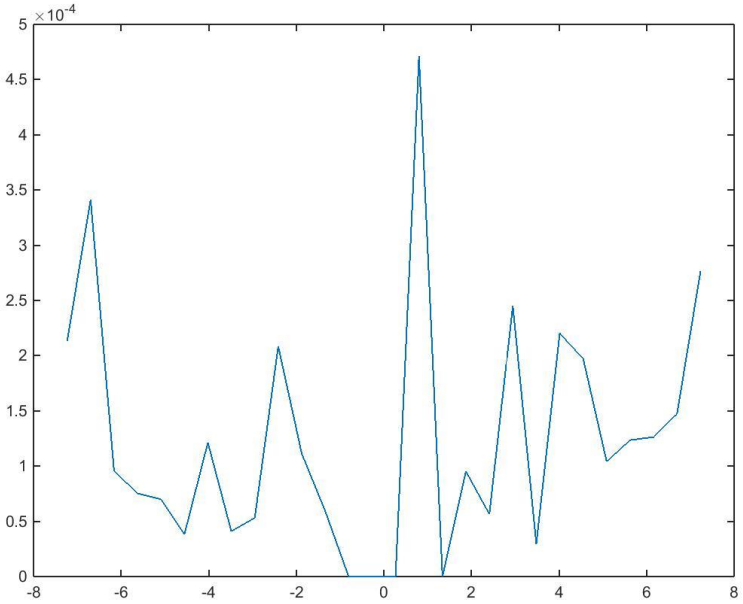

Figure C.15: Dose depth curve for (r, 0,0), Design A, double beam irradiation with a 90° rotation about the vertical axis.

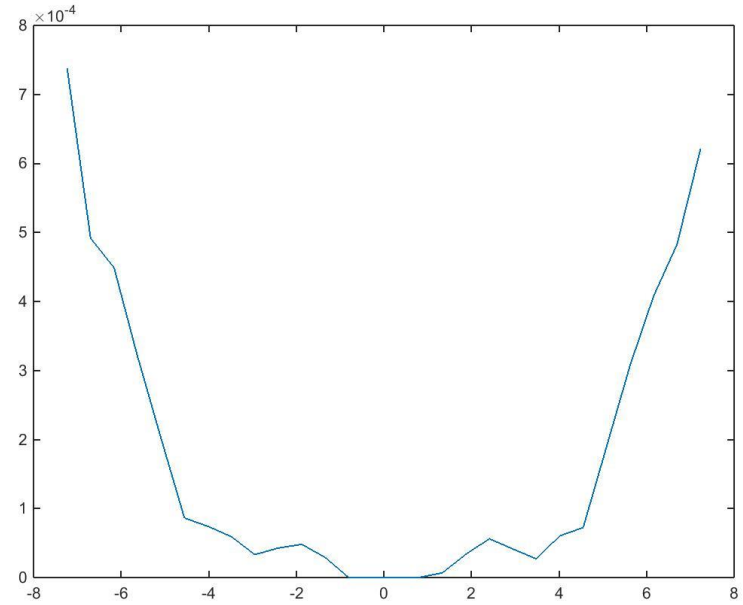

Figure C.16: Dose depth curve for (r,90,0), Design B, single beam irradiation.

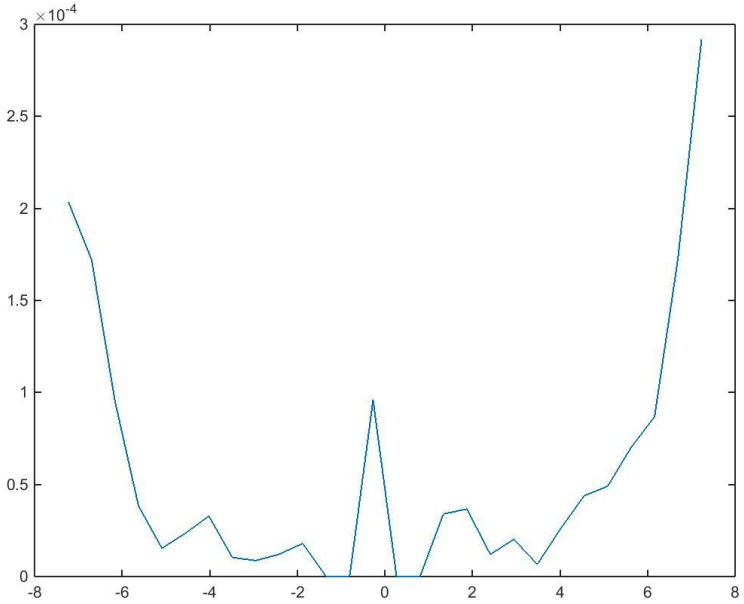

Figure C.17: Dose depth curve for (r,90,90), Design B, single beam irradiation.

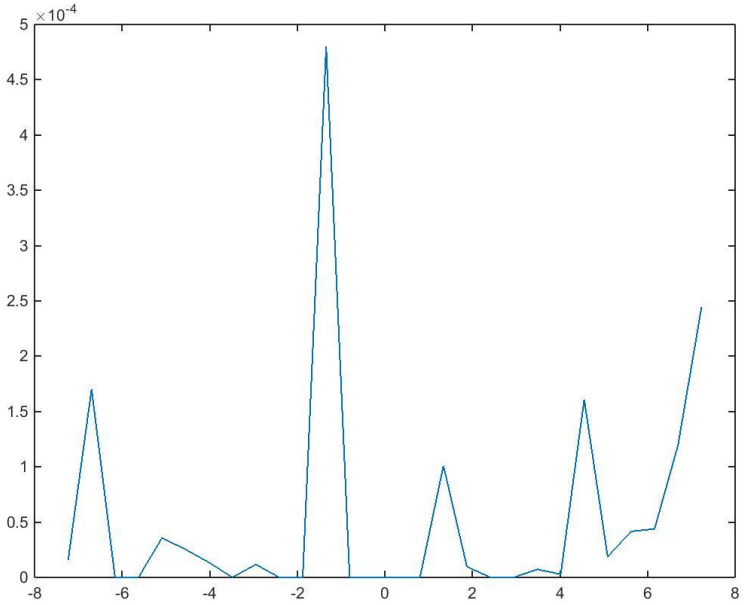

Figure C.18: Dose depth curve for (r, 0,0), Design B, single beam irradiation.

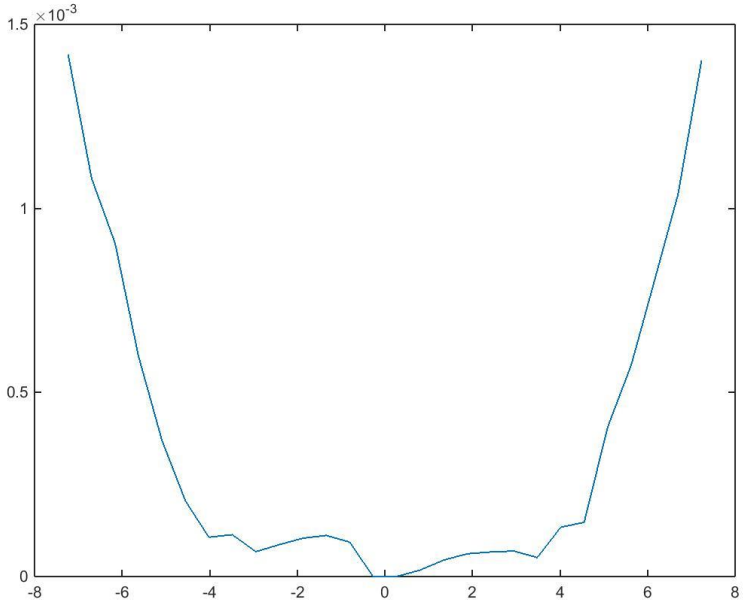

Figure C.19: Dose depth curve for (r,90,0), Design B, double beam irradiation.

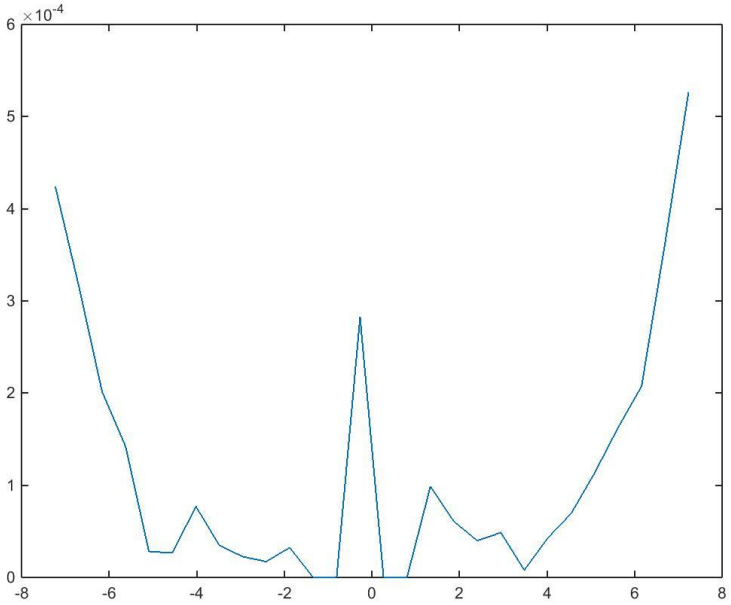

Figure C.20: Dose depth curve for (r,90,90), Design B, double beam irradiation.

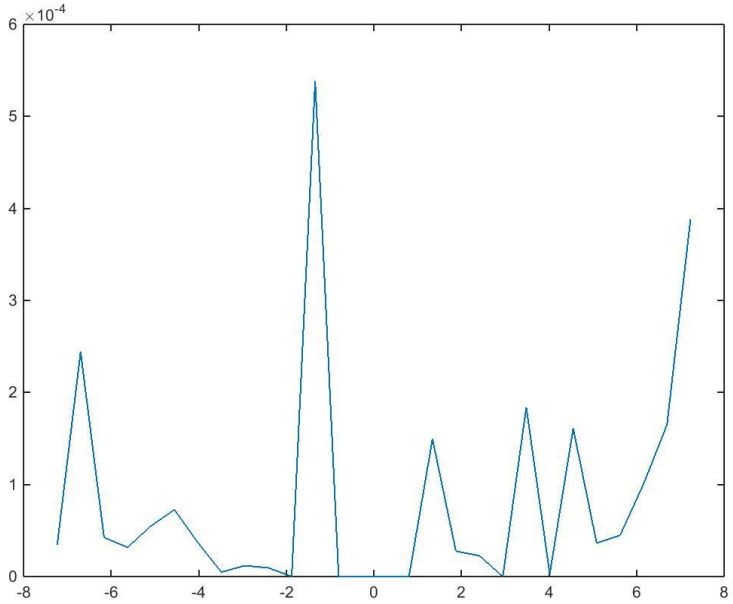

Figure C.21: Dose depth curve for (r, 0,0), Design B, double beam irradiation.

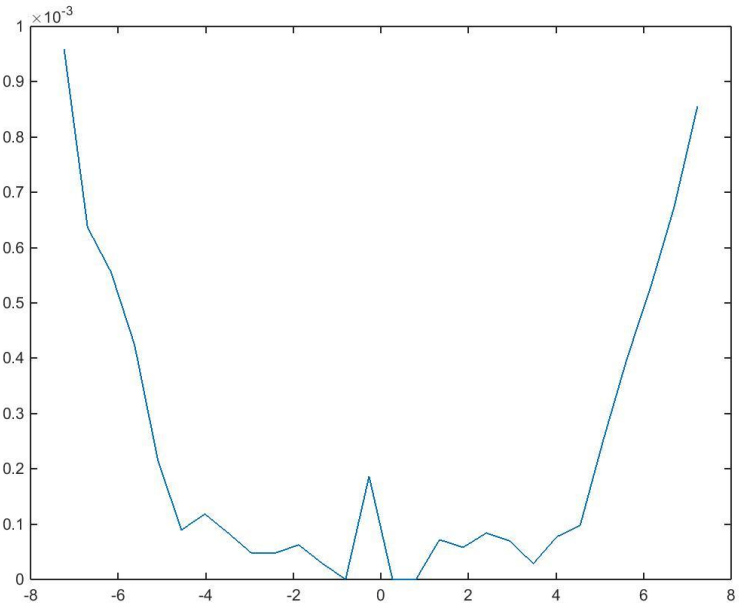

Figure C.22: Dose depth curve for (r,90,0), Design B, double beam irradiation with a 90° rotation about the vertical axis.

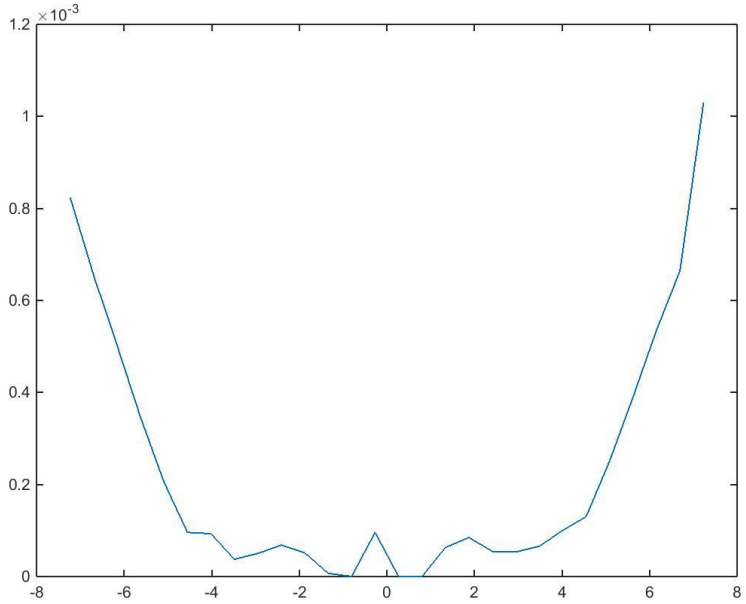

Figure C.23: Dose depth curve for (r,90,90), Design B, double beam irradiation with a 90° rotation about the vertical axis..

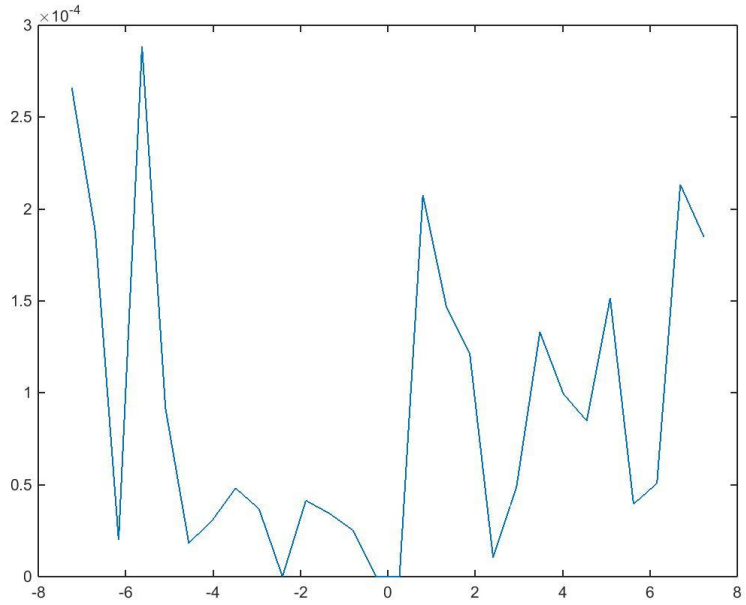

Figure C.24: Dose depth curve for (r, 0,0), Design B, double beam irradiation with a 90° rotation about the vertical axis.

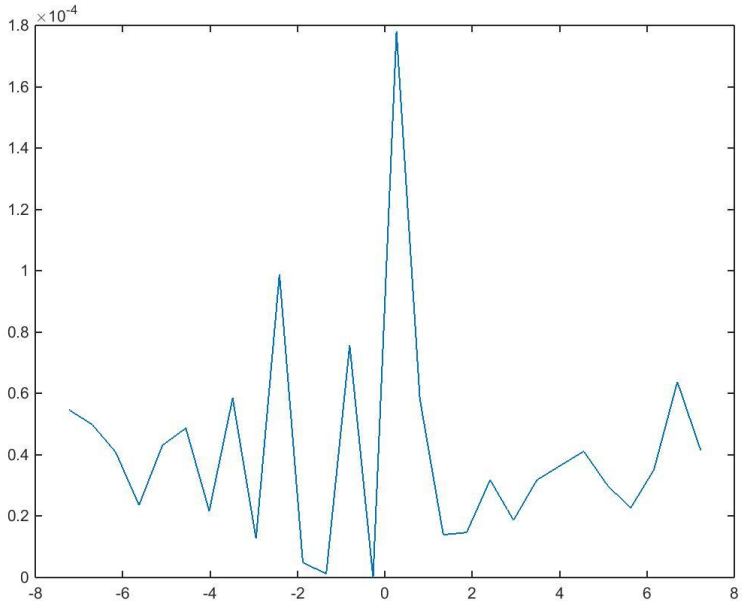

Figure C.25: Dose depth curve for (r,90,0), Design C, single beam irradiation.

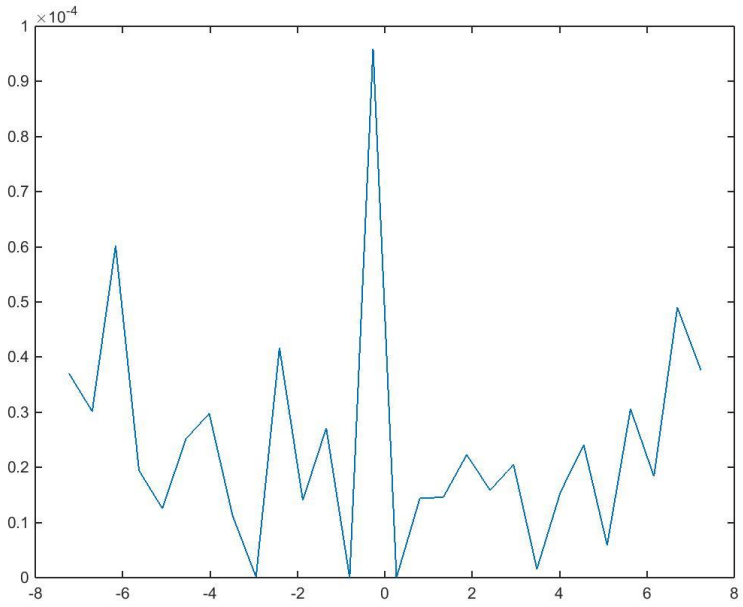

Figure C.26: Dose depth curve for (r,90,90), Design C, single beam irradiation.

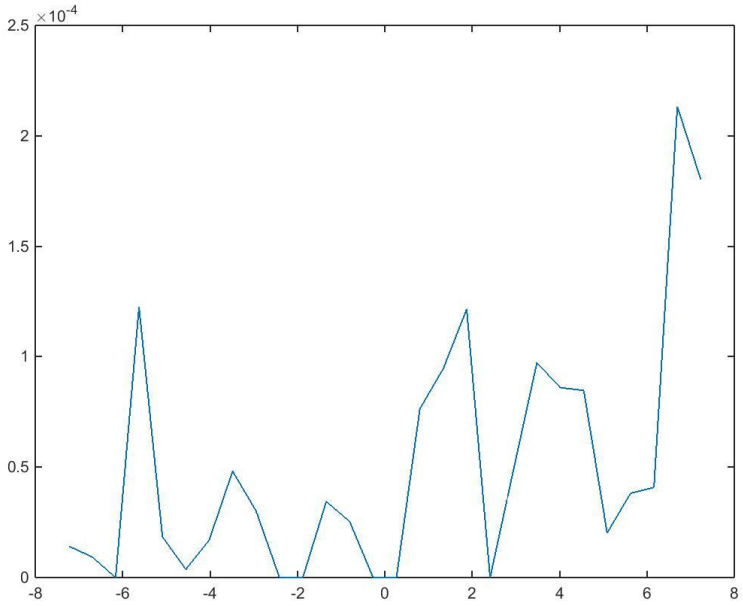

Figure C.27: Dose depth curve for (r, 0,0), Design C, single beam irradiation.

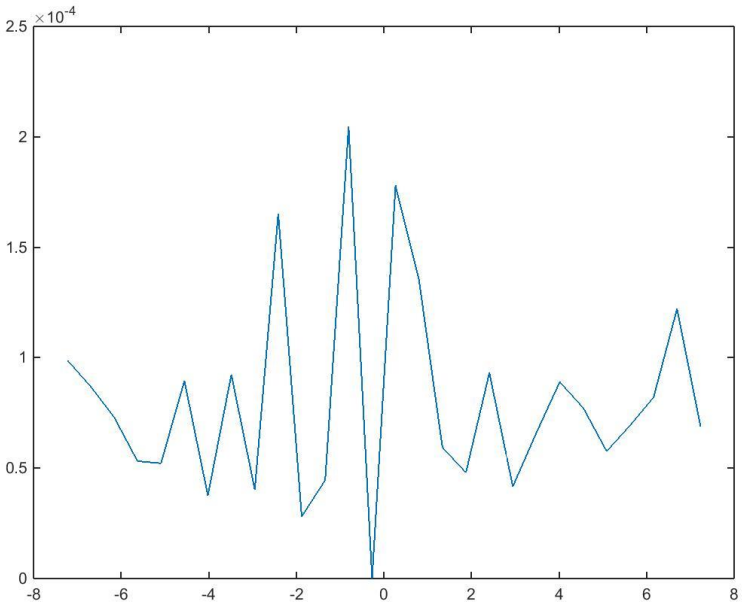

Figure C.28: Dose depth curve for (r,90,0), Design C, double beam irradiation.

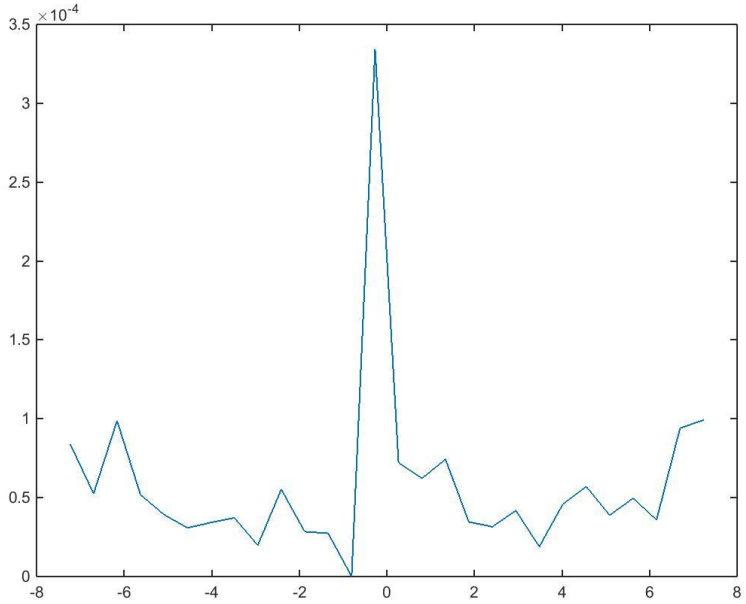

Figure C.29: Dose depth curve for (r,90,90), Design C, double beam irradiation.

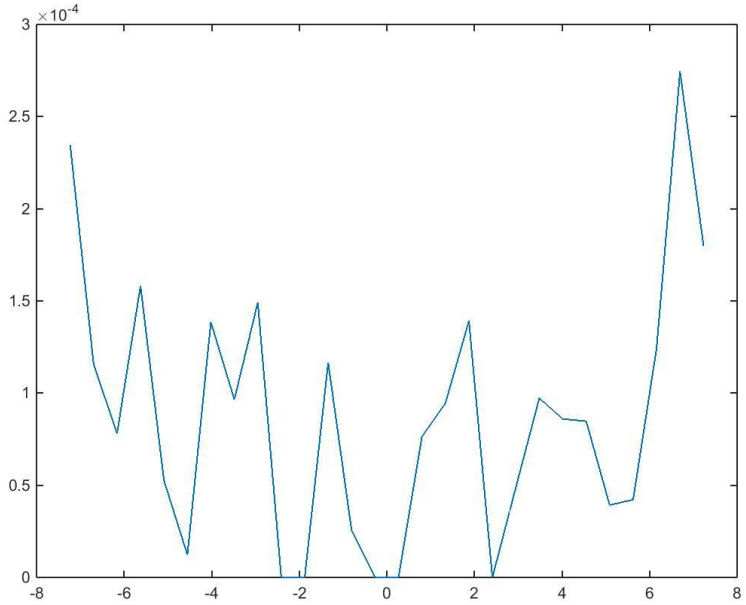

Figure C.30: Dose depth curve for (r, 0,0), Design C, double beam irradiation.

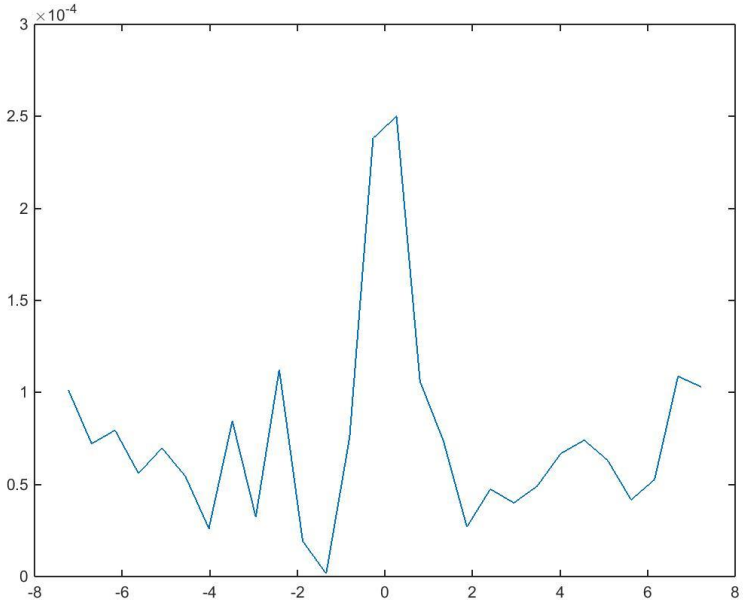

Figure C.31: Dose depth curve for (r,90,0), Design C, double beam irradiation with a 90° rotation about the vertical axis.

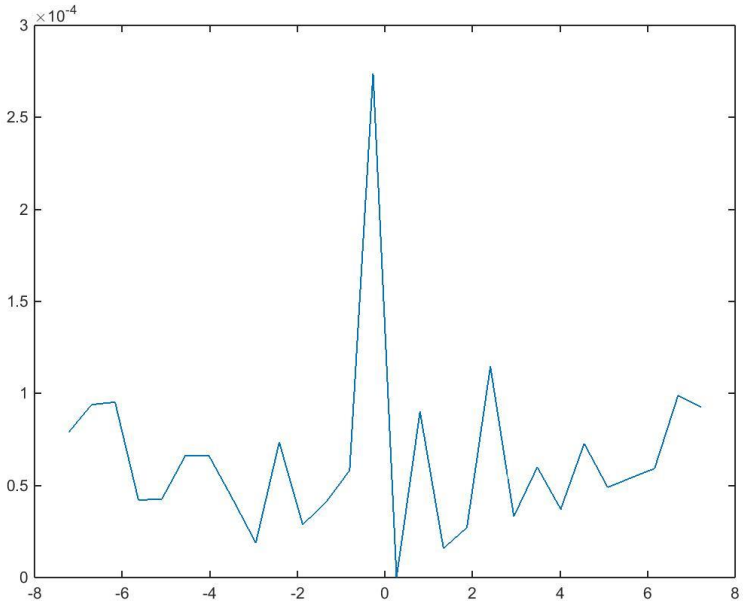

Figure C.32: Dose depth curve for (r,90,90), Design C, double beam irradiation with a 90° rotation about the vertical axis.

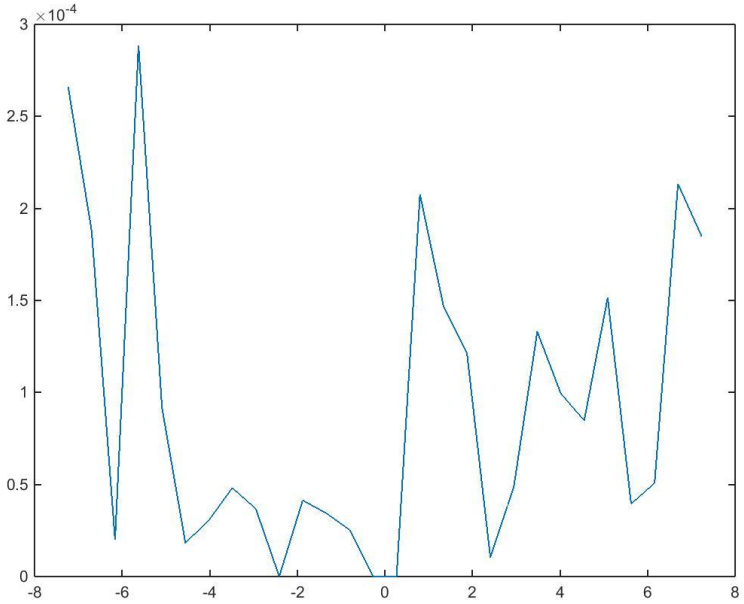

Figure C.33: Dose depth curve for (r, 0,0), Design C, double beam irradiation with a 90° rotation about the vertical axis.

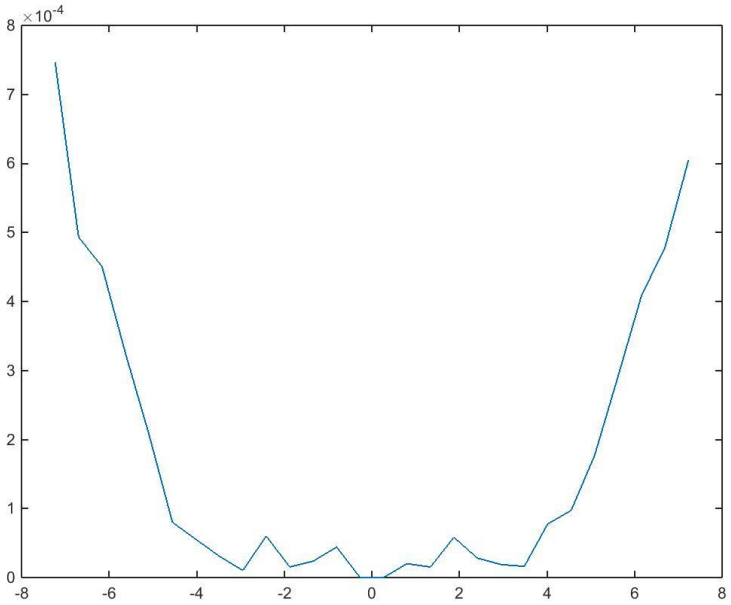

Figure C.34: Dose depth curve for (r,90,0), Design D, single beam irradiation.

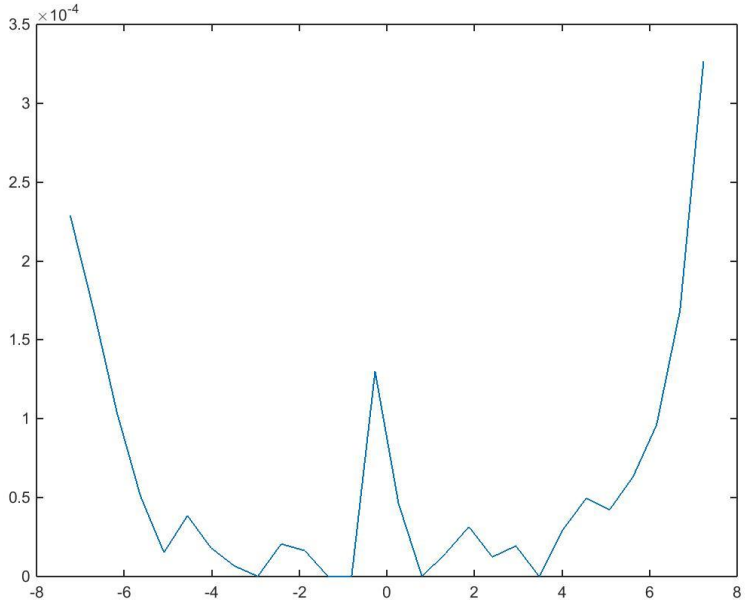

Figure C.35: Dose depth curve for (r,90,90), Design D, single beam irradiation.

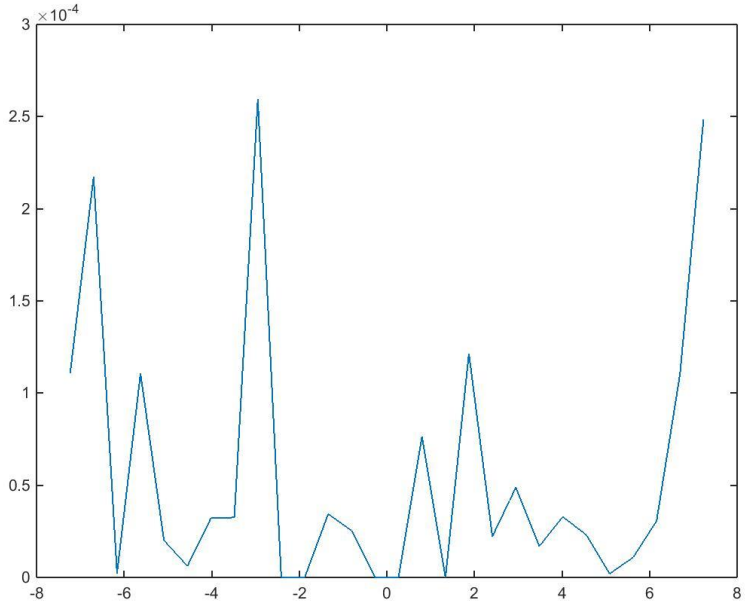

Figure C.36: Dose depth curve for (r, 0,0), Design D, single beam irradiation.

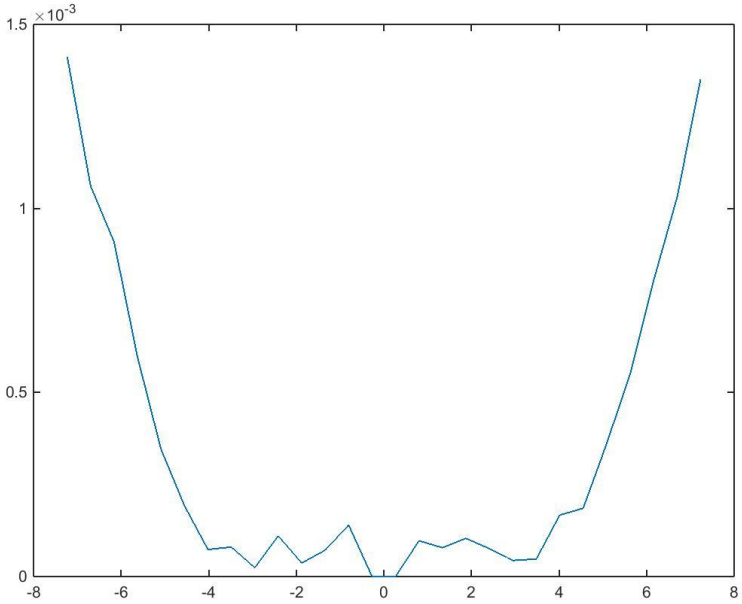

Figure C.37: Dose depth curve for (r,90,0), Design D, double beam irradiation.

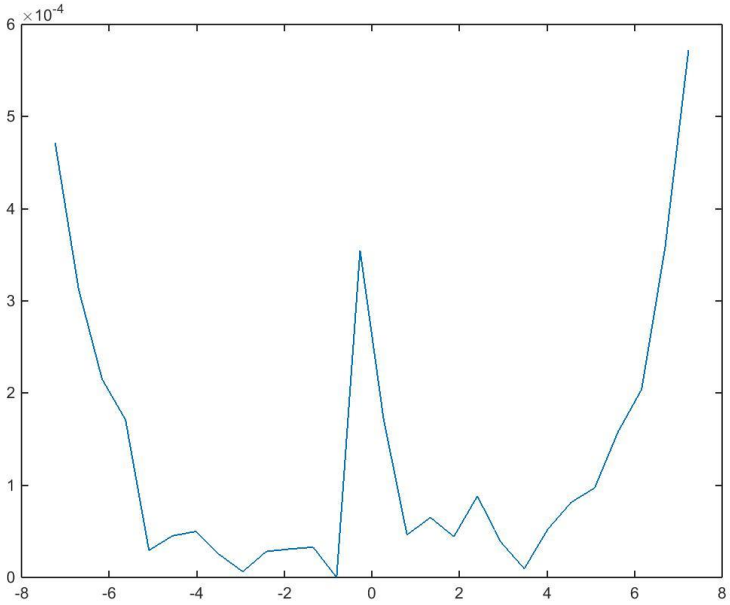

Figure C.38: Dose depth curve for (r,90,90), Design D, double beam irradiation.

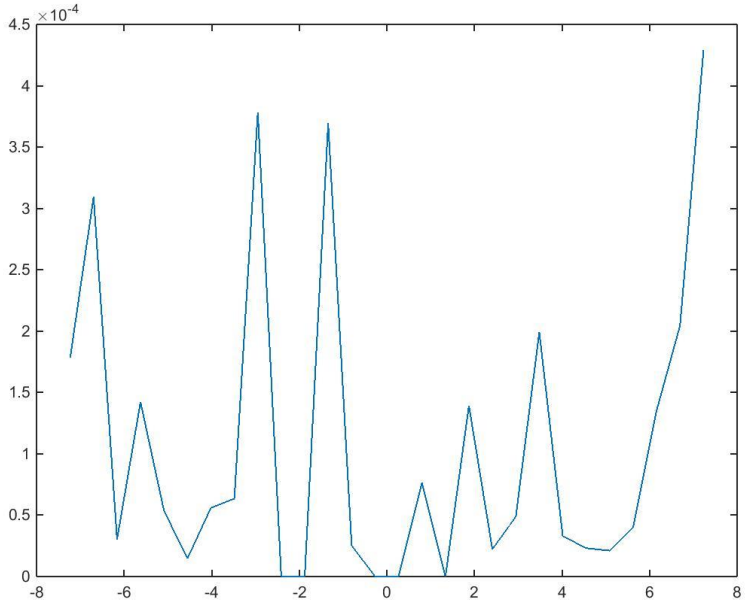

Figure C.39: Dose depth curve for (r, 0,0), Design D, double beam irradiation.

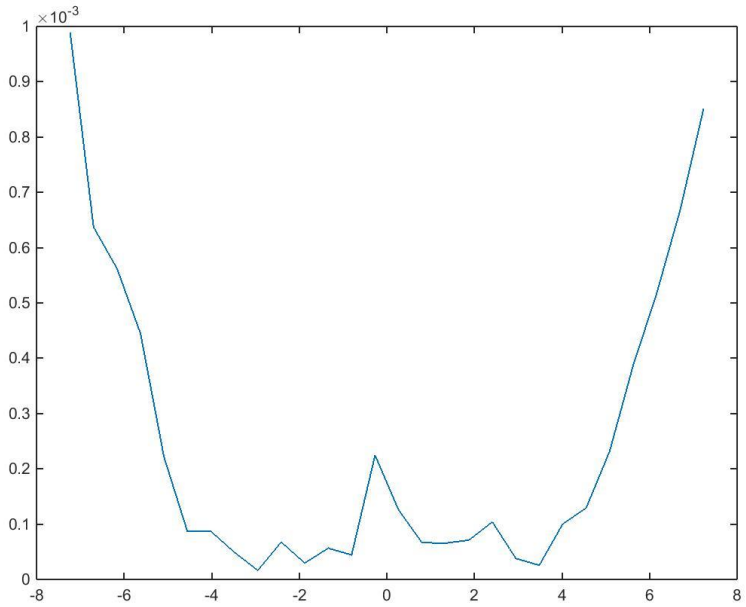

Figure C.40: Dose depth curve for (r,90,0), Design D, double beam irradiation with a 90° rotation about the vertical axis.

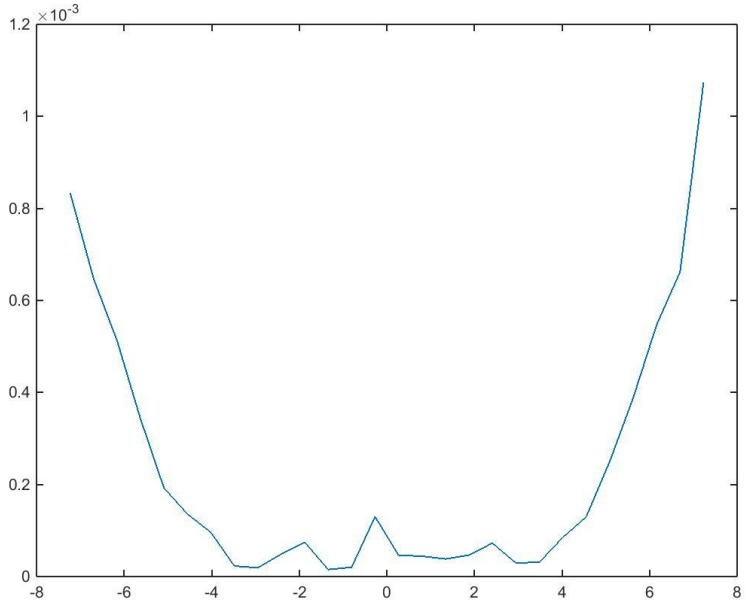

Figure C.41: Dose depth curve for (r,90,90), Design D, double beam irradiation with a 90° rotation about the vertical axis..

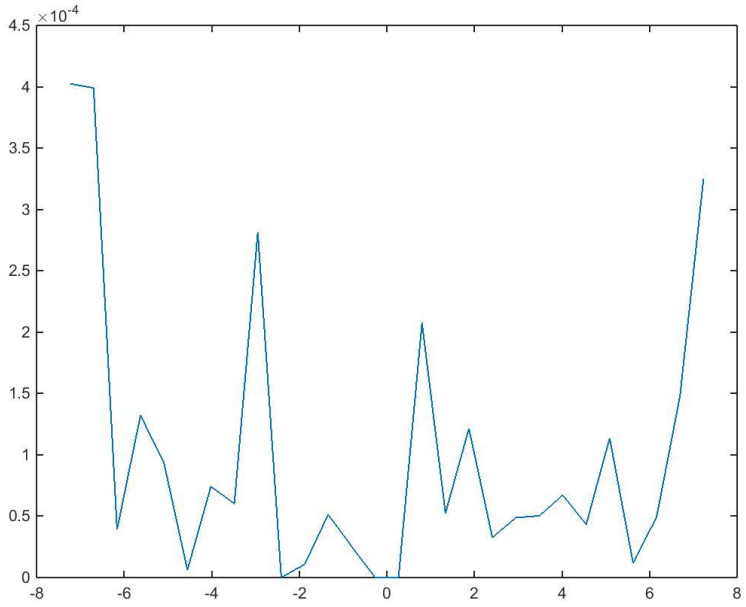

Figure C.42: Dose depth curve for (r, 0,0), Design D, double beam irradiation with a 90° rotation about the vertical axis.

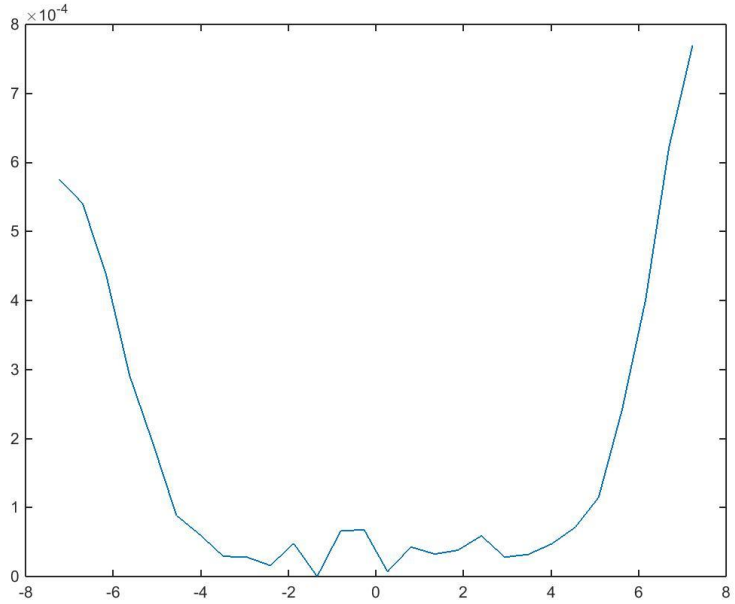

Figure C.43: Dose depth curve for (r,90,0), Design E, single beam irradiation.

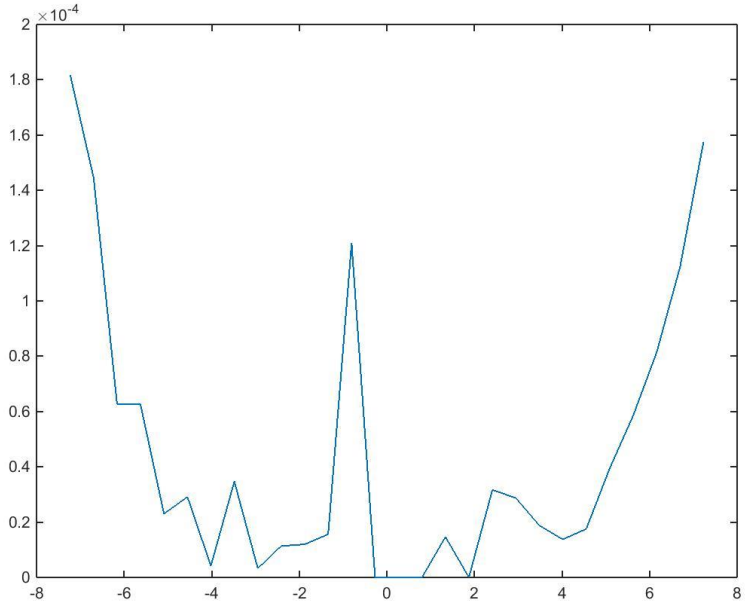

Figure C.44: Dose depth curve for (r,90,90), Design E, single beam irradiation.

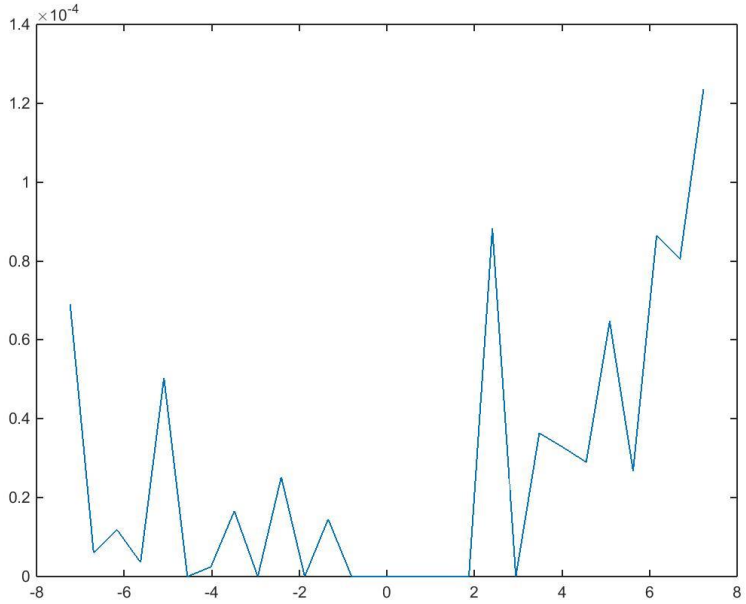

Figure C.45: Dose depth curve for (r, 0,0), Design E, single beam irradiation.

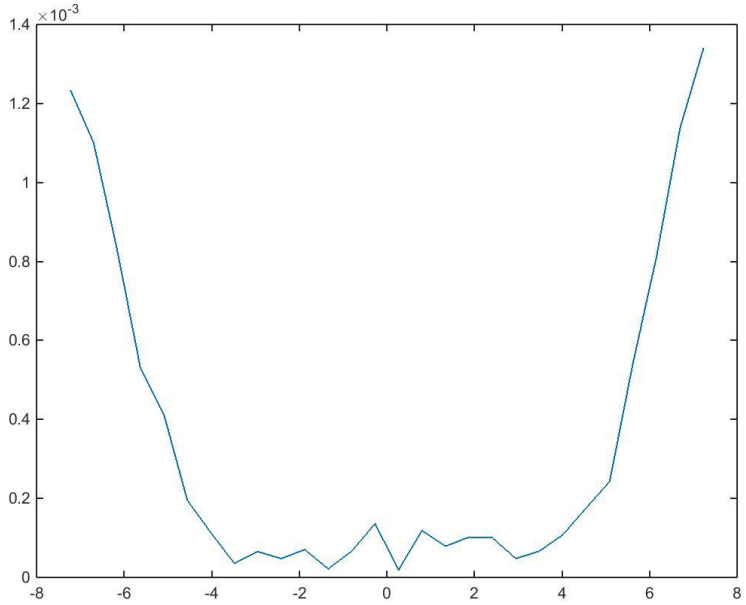

Figure C.46: Dose depth curve for (r,90,0), Design E, double beam irradiation.

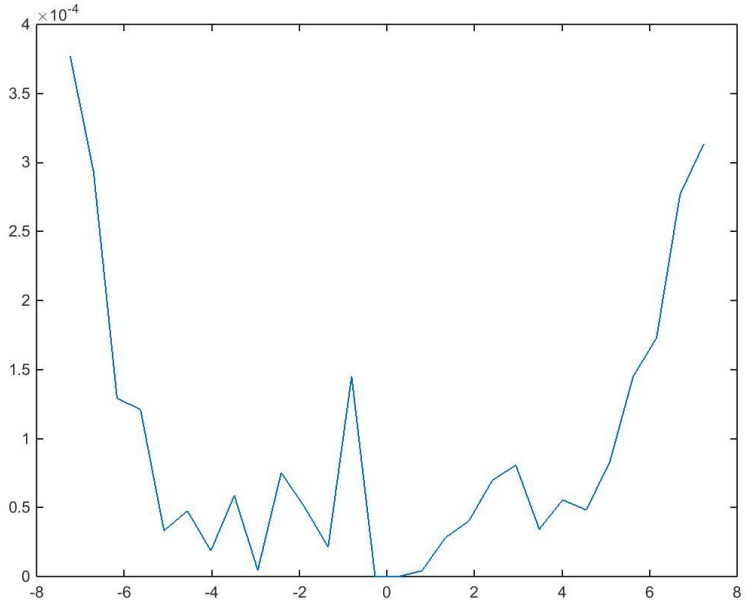

Figure C.47: Dose depth curve for (r,90,90), Design E, double beam irradiation.

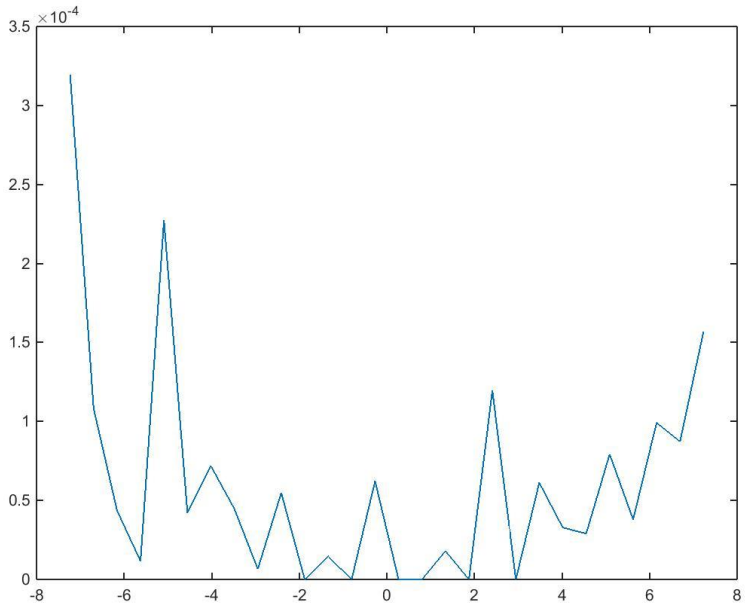

Figure C.48: Dose depth curve for (r, 0,0), Design E, double beam irradiation.

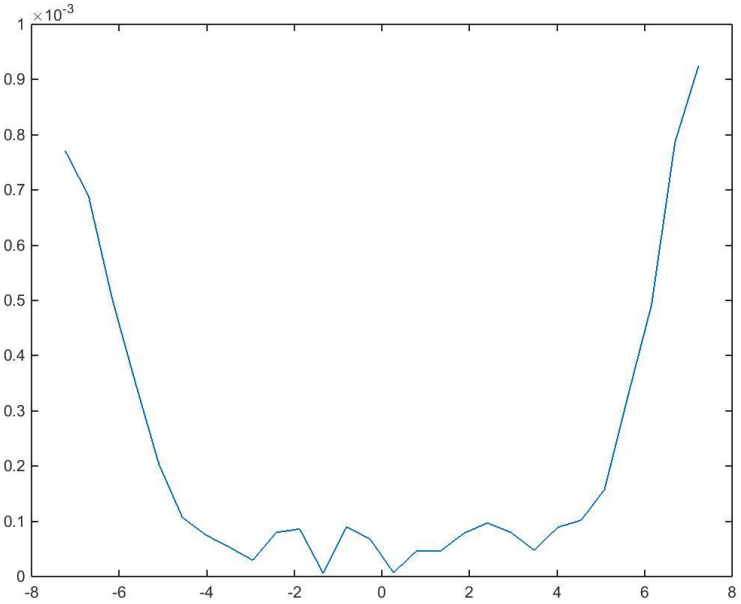

Figure C.49: Dose depth curve for (r,90,0), Design E, double beam irradiation with a 90° rotation about the vertical axis.

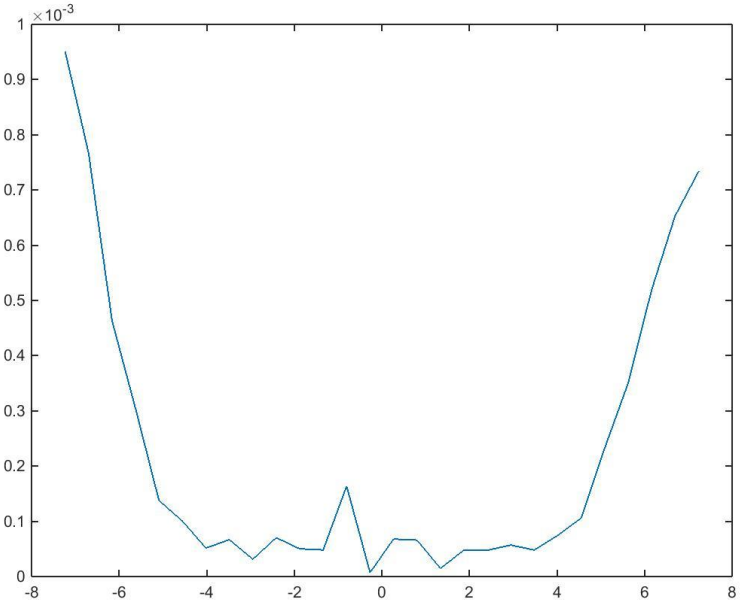

Figure C.50: Dose depth curve for (r,90,90), Design E, double beam irradiation with a 90° rotation about the vertical axis.

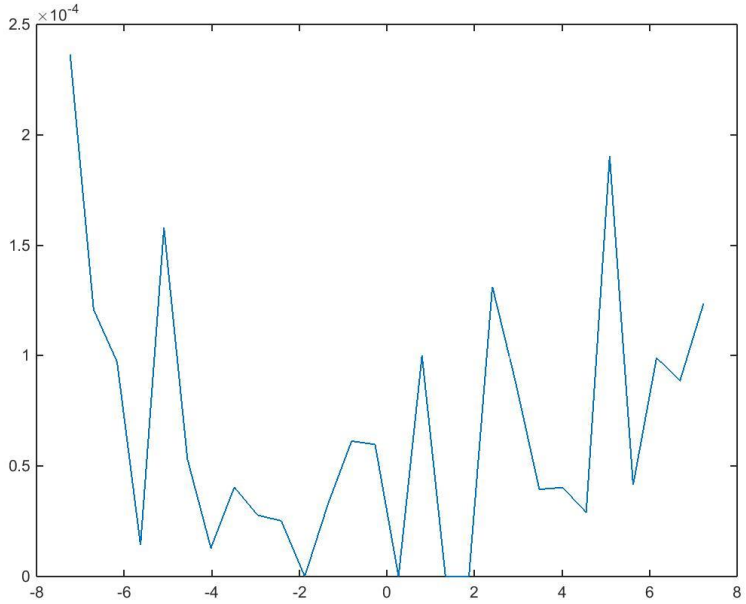

Figure C.51: Dose depth curve for (r, 0,0), Design E, double beam irradiation with a 90° rotation about the vertical axis.

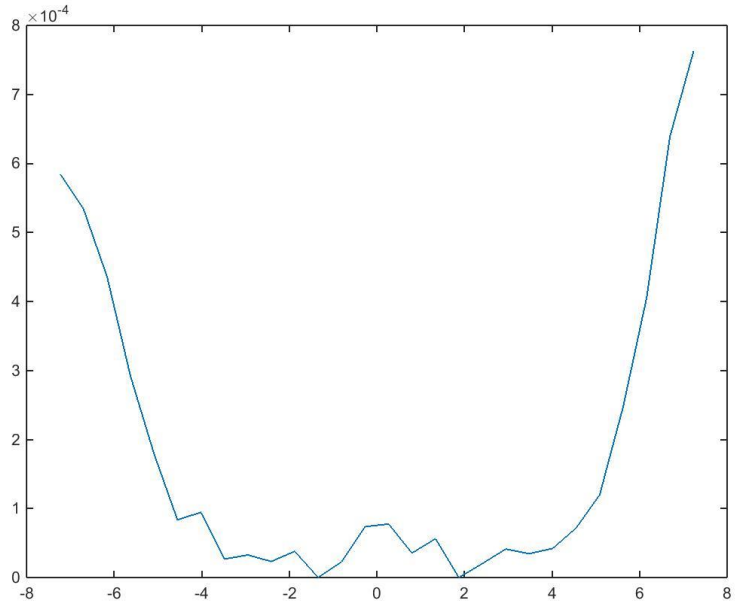

Figure C.52: Dose depth curve for (r,90,0), Design F, single beam irradiation.

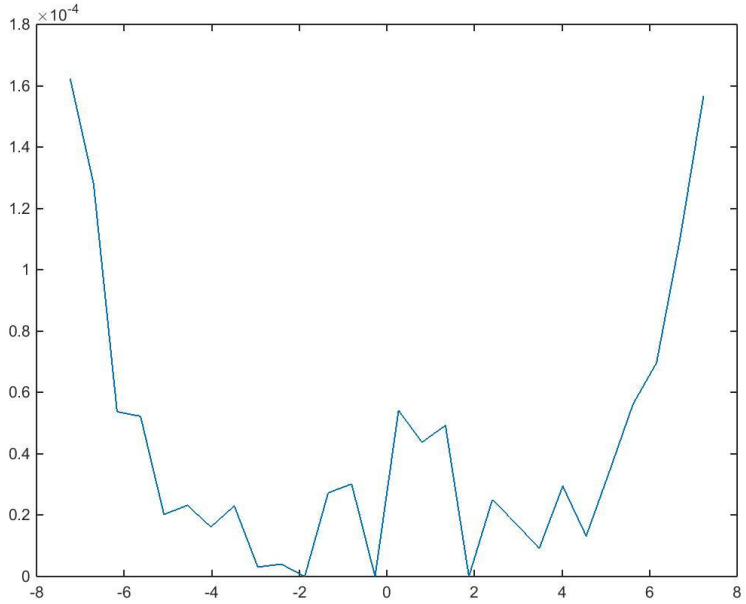

Figure C.53: Dose depth curve for (r,90,90), Design F, single beam irradiation.

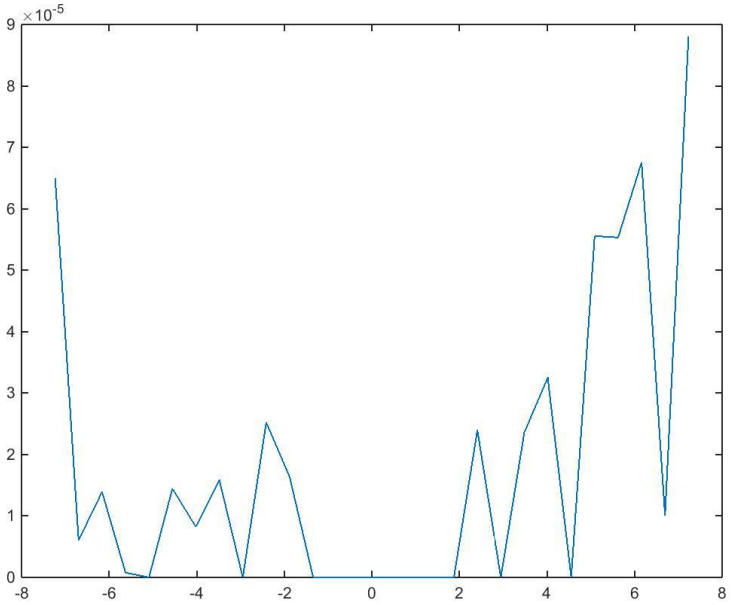

Figure C.54: Dose depth curve for (r, 0,0), Design F, single beam irradiation.

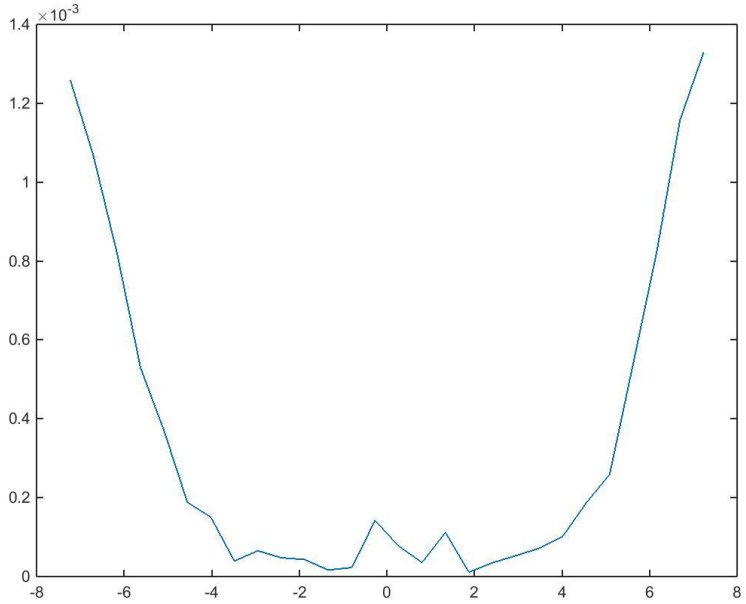

Figure C.55: Dose depth curve for (r,90,0), Design F, double beam irradiation.

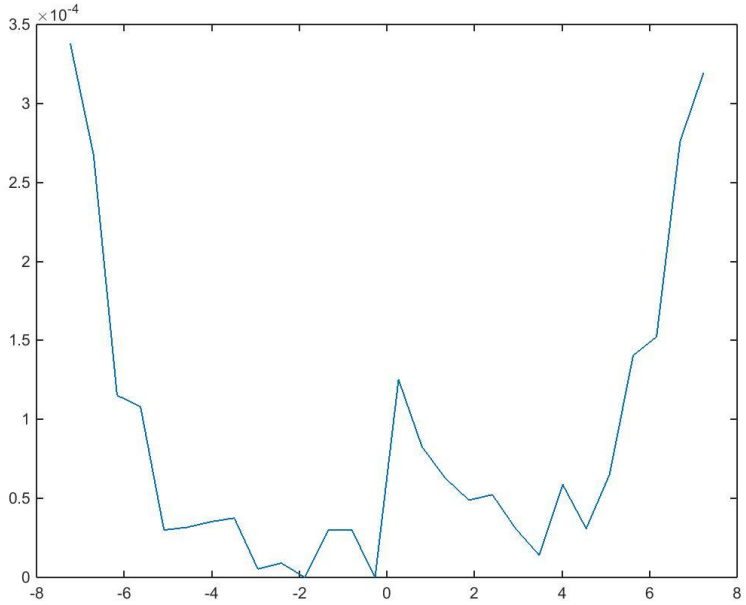

Figure C.56: Dose depth curve for (r,90,90), Design F, double beam irradiation.

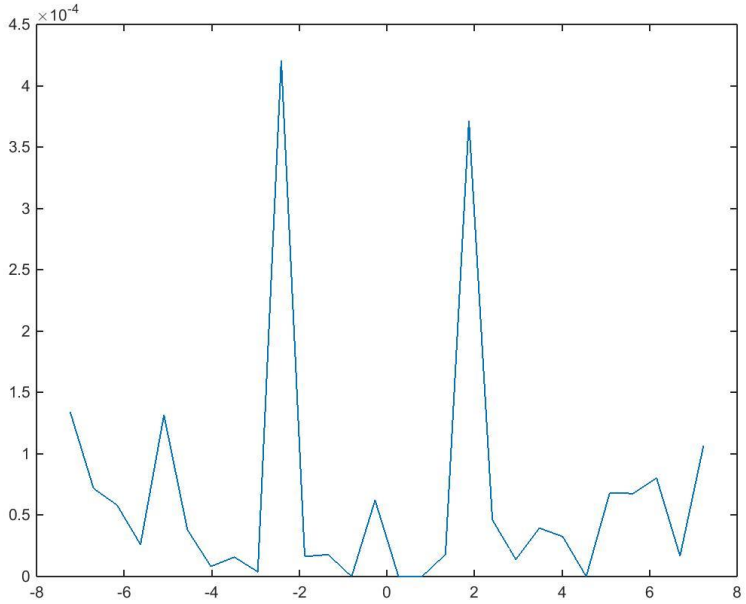

Figure C.57: Dose depth curve for (r, 0,0), Design F, double beam irradiation.

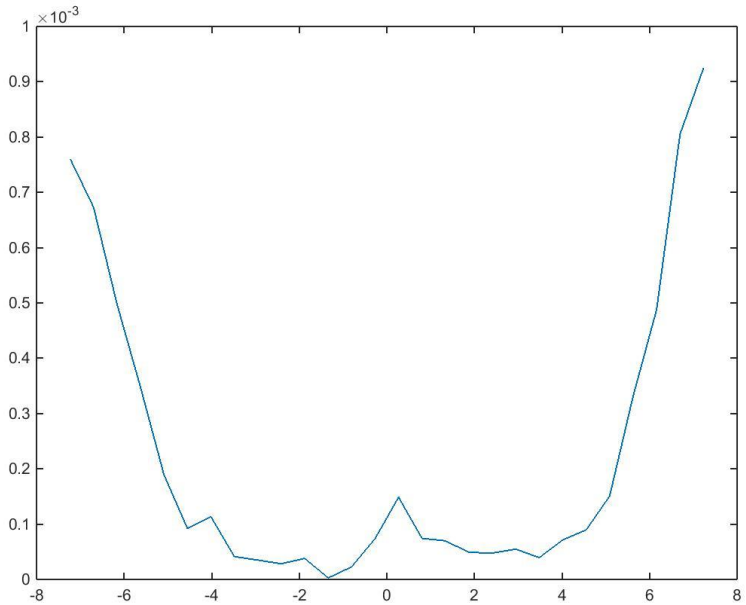

Figure C.58: Dose depth curve for (r,90,0), Design F, double beam irradiation with a 90° rotation about the vertical axis.

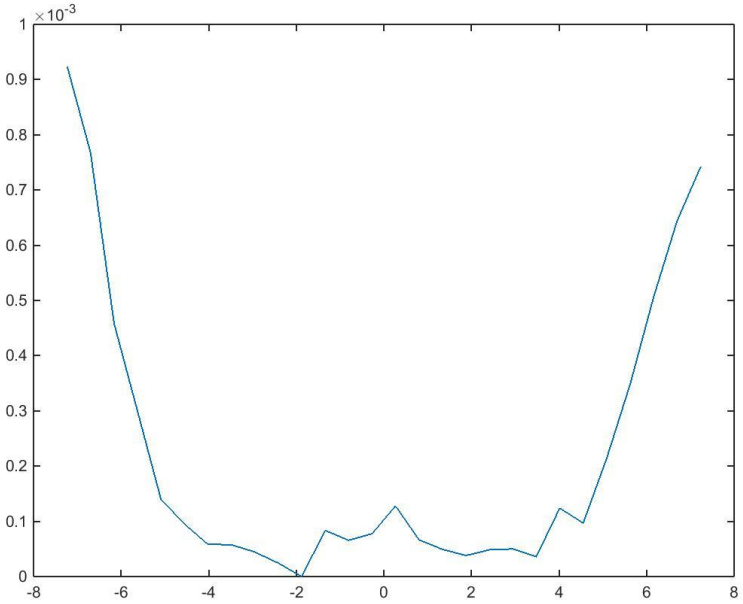

Figure C.59: Dose depth curve for (r,90,90), Design F, double beam irradiation with a 90° rotation about the vertical axis..

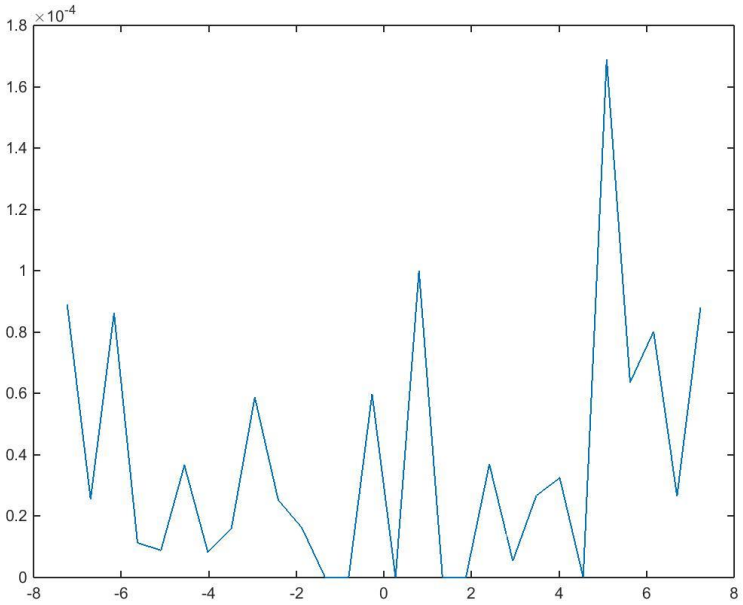

Figure C.60: Dose depth curve for (r, 0,0), Design F, double beam irradiation with a 90° rotation about the vertical axis.

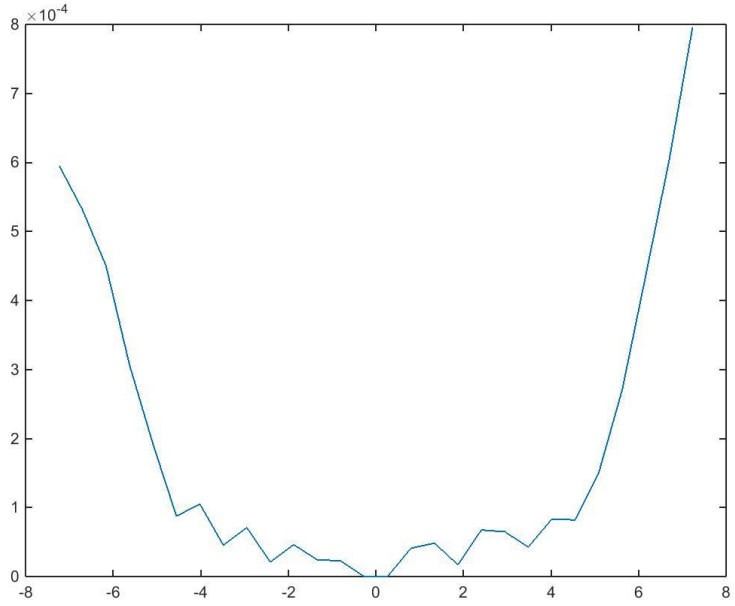

Figure C.61: Dose depth curve for (r,90,0), Design G, single beam irradiation.

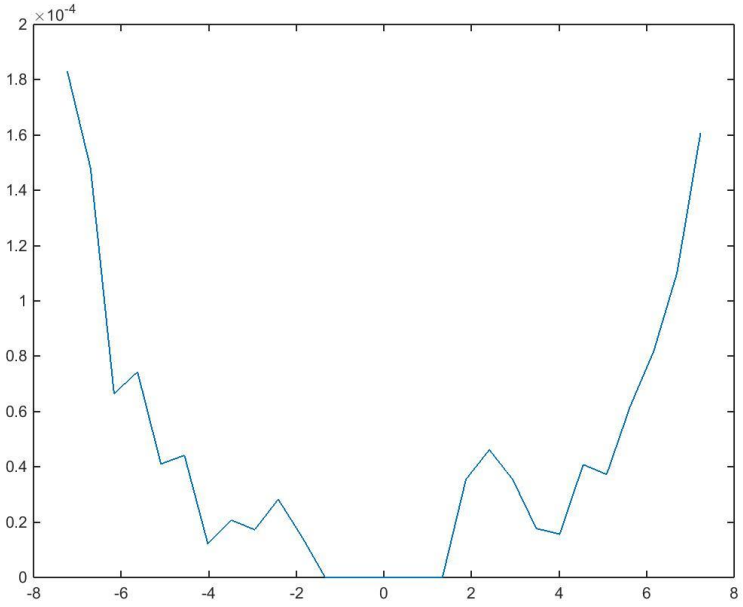

Figure C.62: Dose depth curve for (r,90,90), Design G, single beam irradiation.

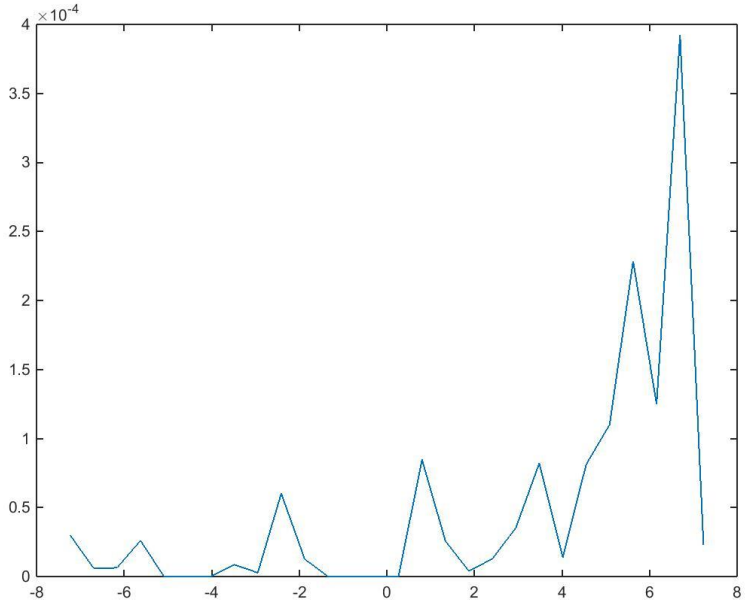

Figure C.63: Dose depth curve for (r, 0,0), Design G, single beam irradiation.

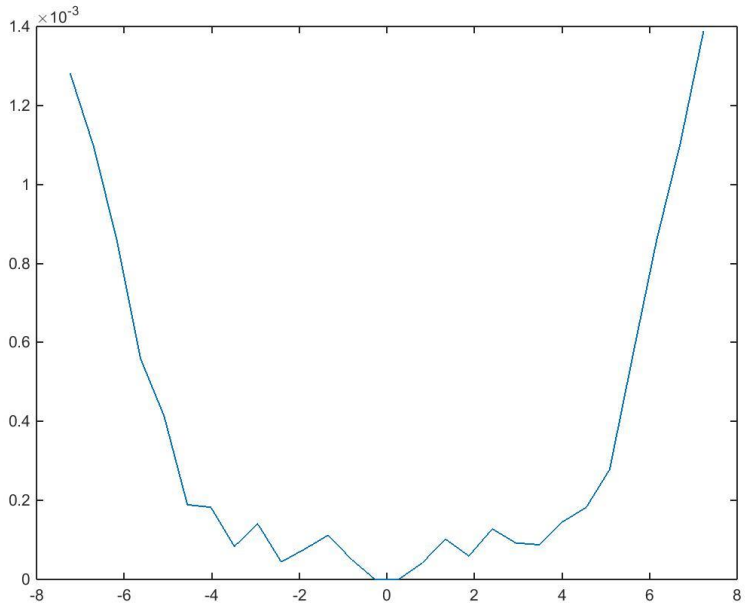

Figure C.64: Dose depth curve for (r,90,0), Design G, double beam irradiation.

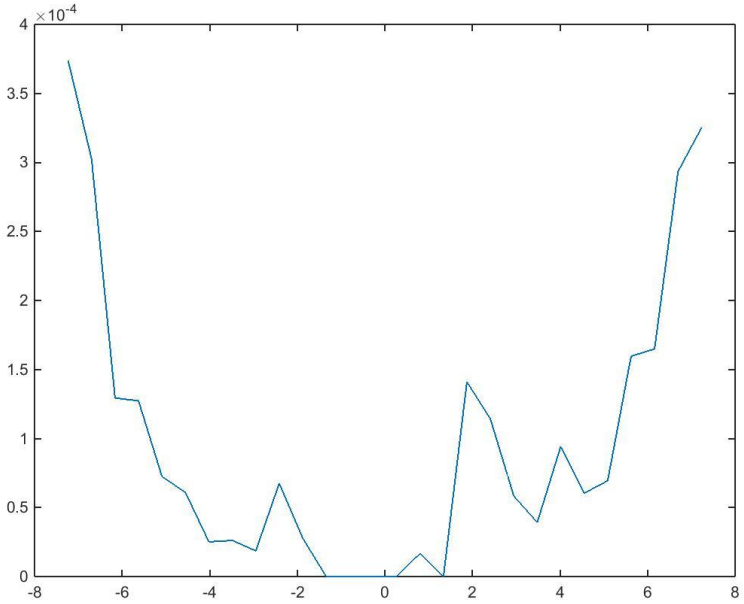

Figure C.65: Dose depth curve for (r,90,90), Design G, double beam irradiation.

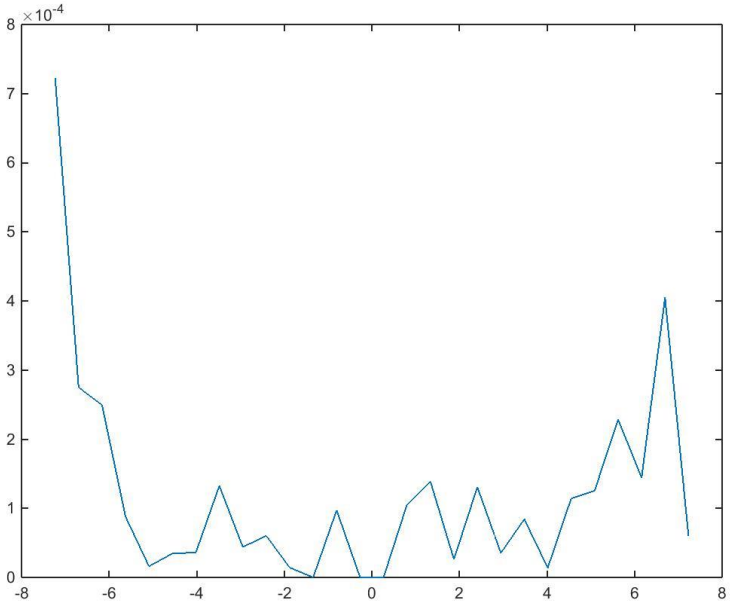

Figure C.66: Dose depth curve for (r, 0,0), Design G, double beam irradiation.

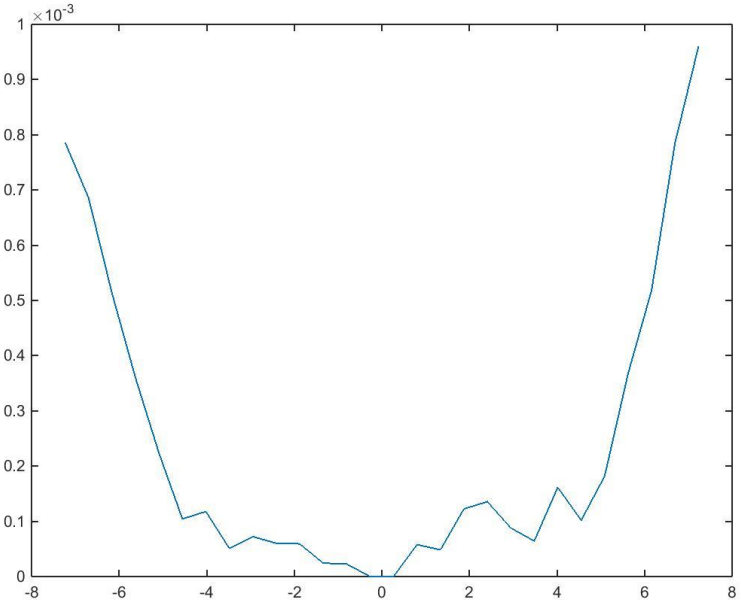

Figure C.67: Dose depth curve for (r,90,0), Design G, double beam irradiation with a 90° rotation about the vertical axis.

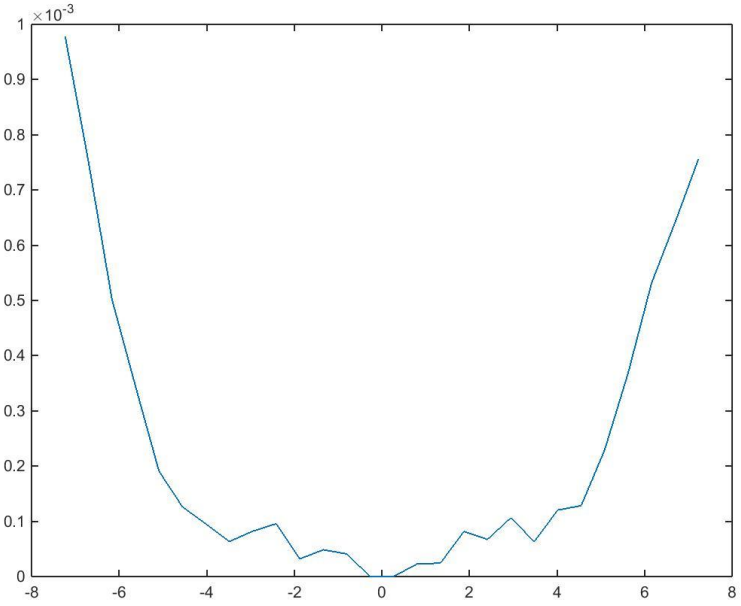

Figure C.68: Dose depth curve for (r,90,90), Design G, double beam irradiation with a 90° rotation about the vertical axis.

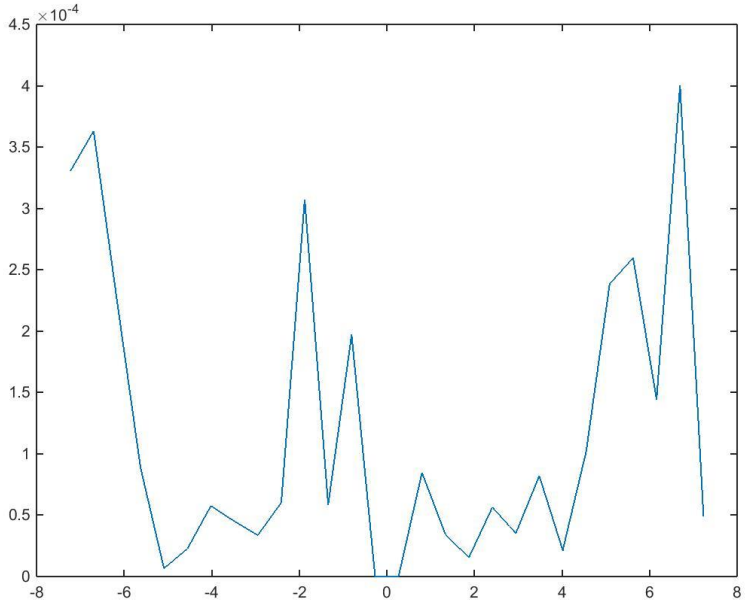

Figure C.69: Dose depth curve for (r, 0,0), Design G, double beam irradiation with a 90° rotation about the vertical axis.

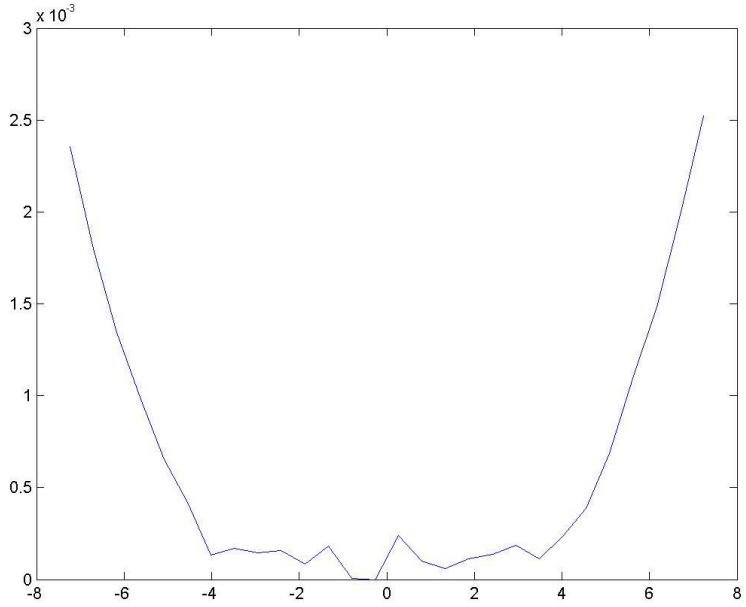

Figure C.70: Dose depth curve for (r,90,0), Design H, single beam irradiation.

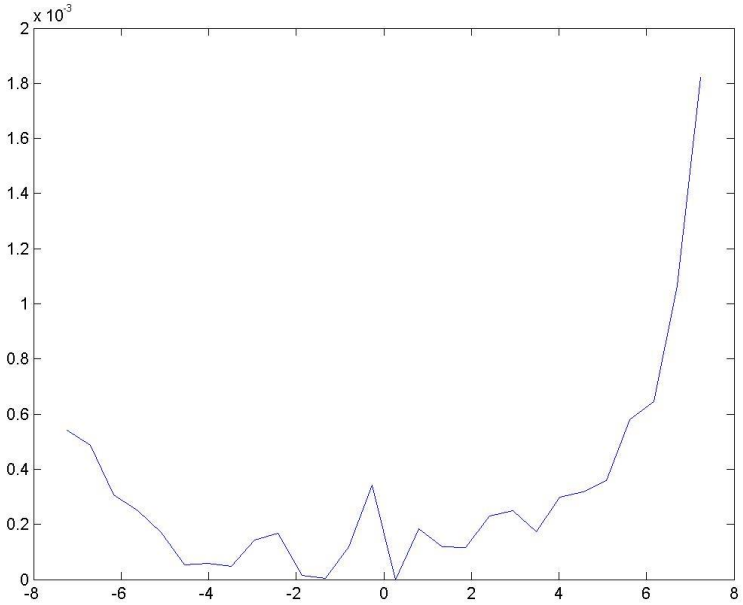

Figure C.71: Dose depth curve for (r,90,90), Design H, single beam irradiation.

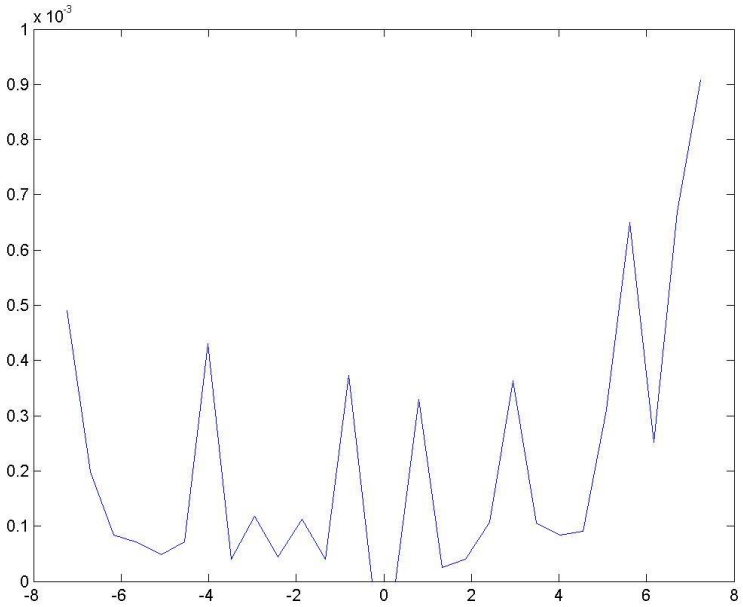

Figure C.72: Dose depth curve for (r, 0,0), Design H, single beam irradiation.

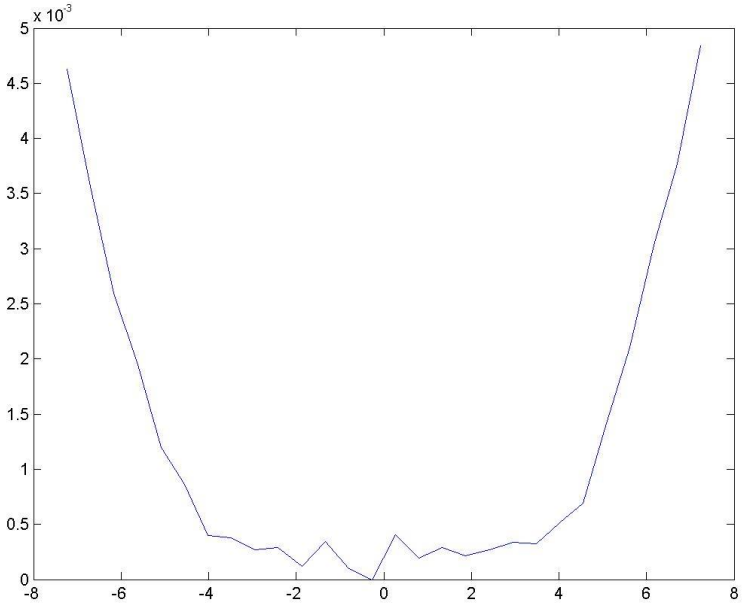

Figure C.73: Dose depth curve for (r,90,0), Design H, double beam irradiation.

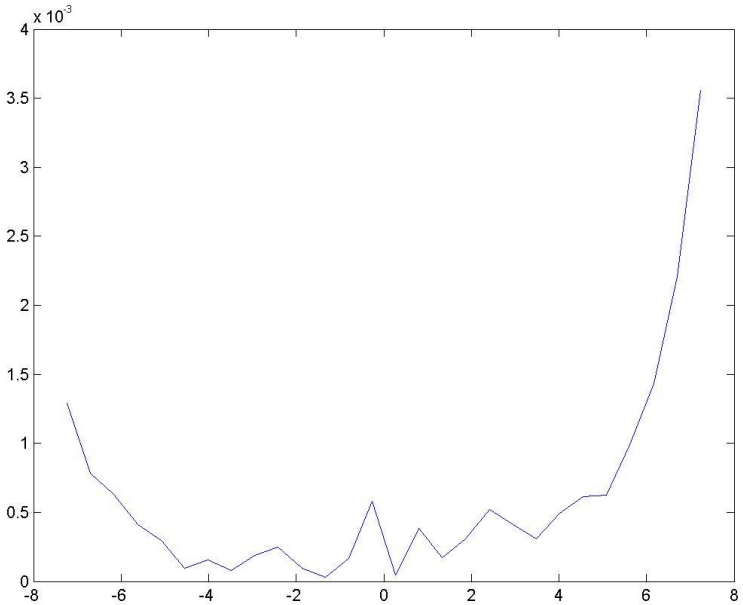

Figure C.74: Dose depth curve for (r,90,90), Design H, double beam irradiation.

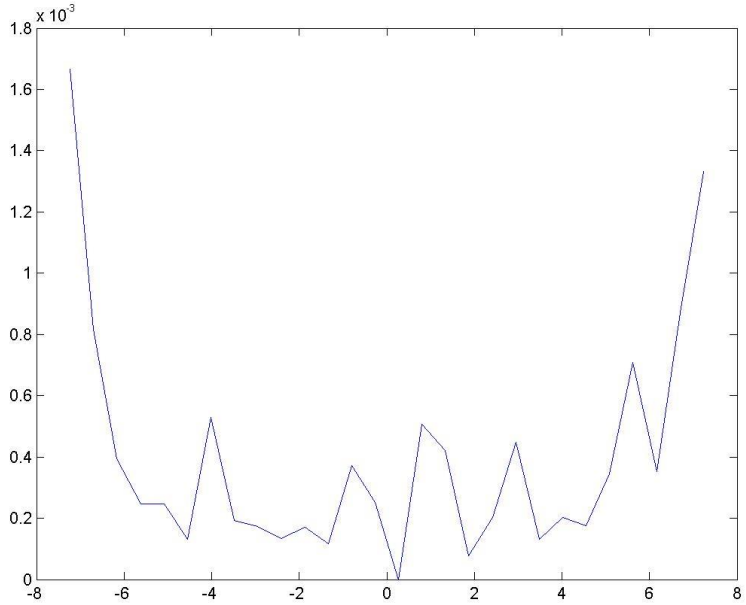

Figure C.75: Dose depth curve for (r, 0,0), Design H, double beam irradiation.

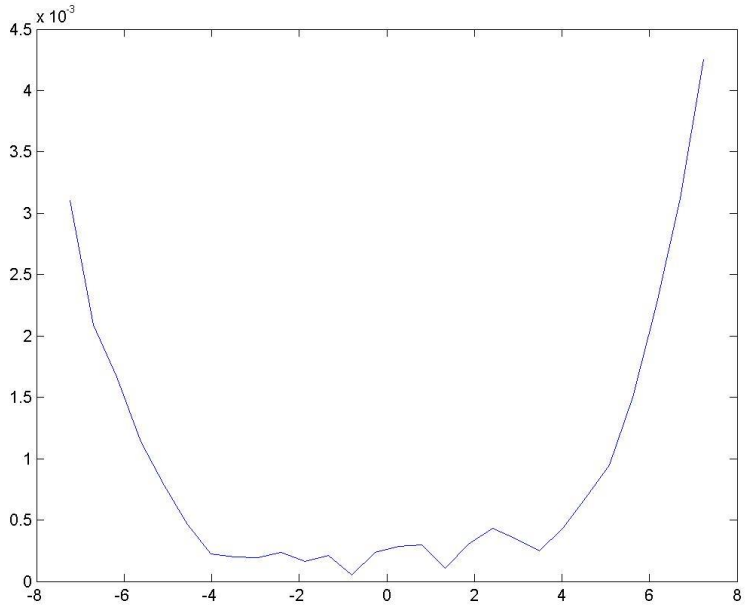

Figure C.76: Dose depth curve for (r,90,0), Design H, double beam irradiation with a 90° rotation about the vertical axis.

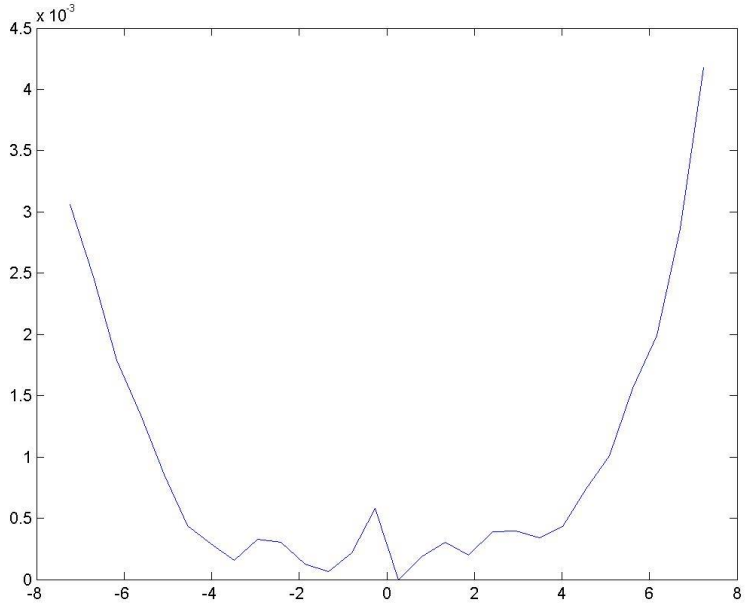

Figure C.77: Dose depth curve for (r,90,90), Design H, double beam irradiation with a 90° rotation about the vertical axis..

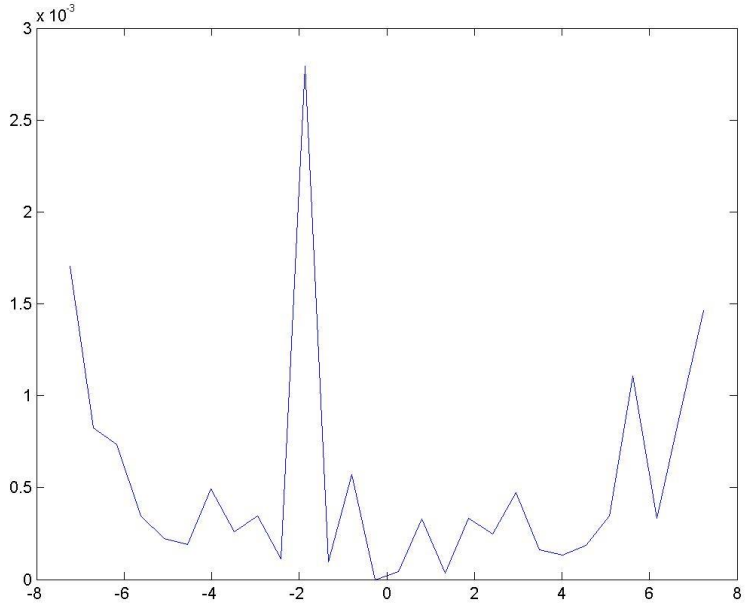

Figure C.78: Dose depth curve for (r, 0,0), Design H, double beam irradiation with a 90° rotation about the vertical axis.

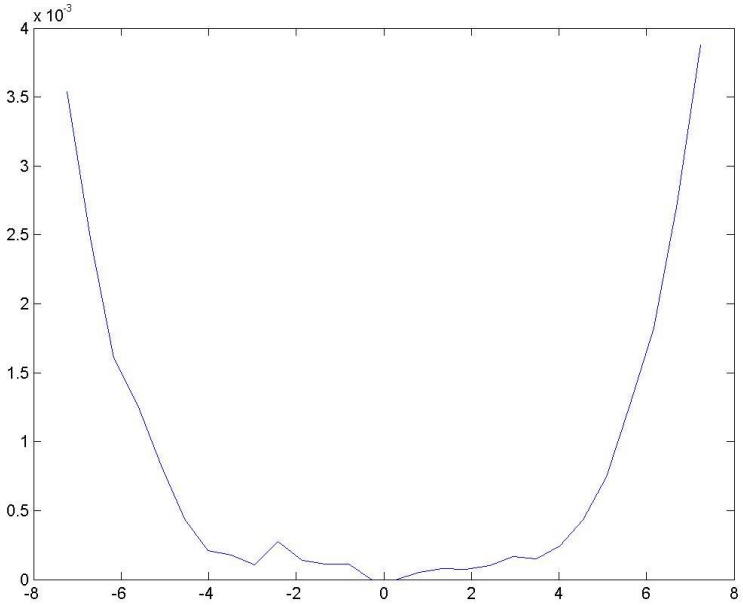

Figure C.79: Dose depth curve for (r,90,0), Design I, single beam irradiation.

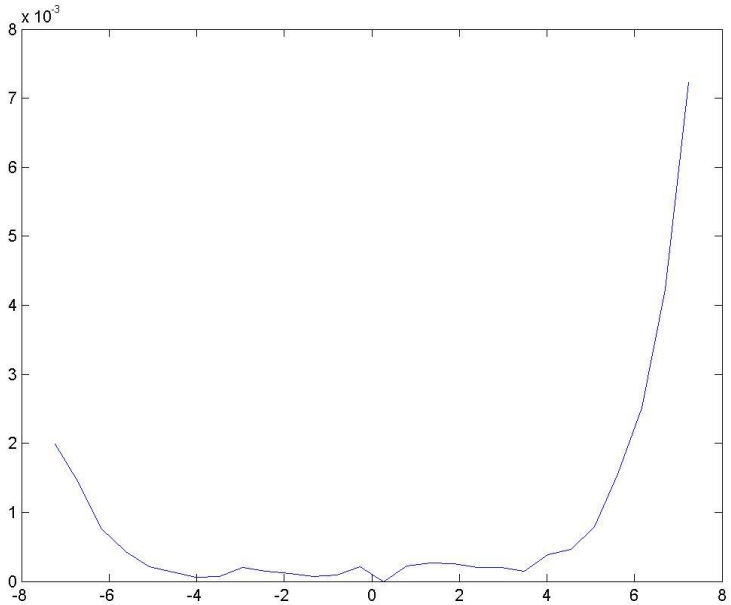

Figure C.80: Dose depth curve for (r,90,90), Design I, single beam irradiation.

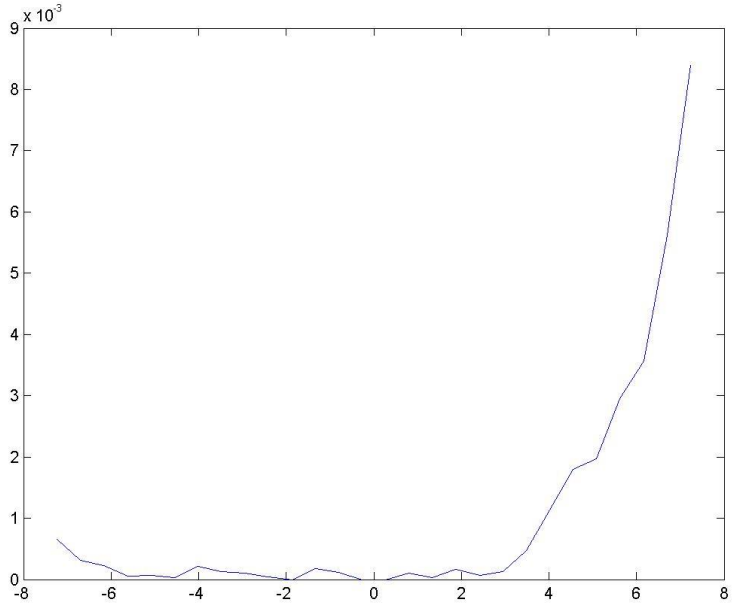

Figure C.81: Dose depth curve for (r, 0,0), Design I, single beam irradiation.

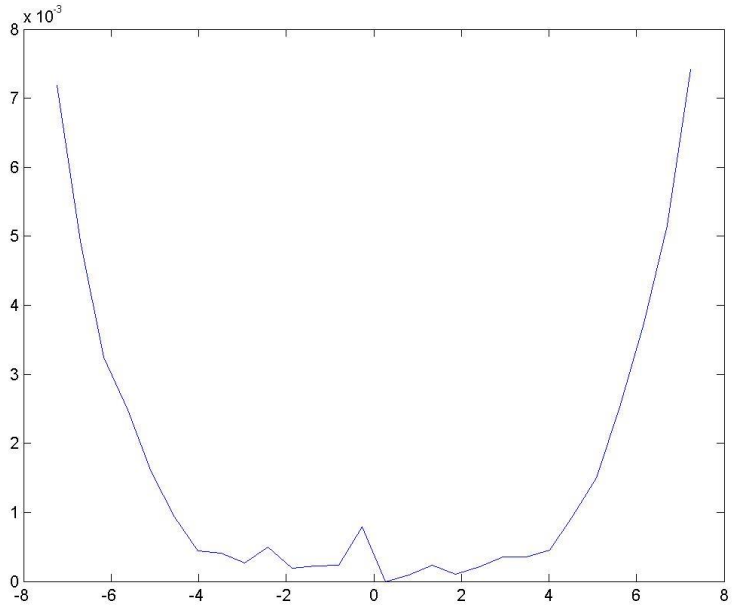

Figure C.82: Dose depth curve for (r,90,0), Design I, double beam irradiation.

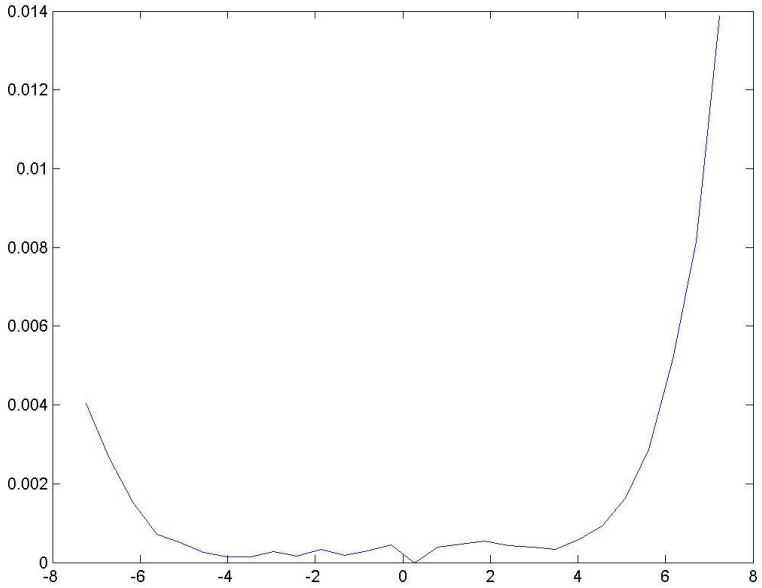

Figure C.83: Dose depth curve for (r,90,90), Design I, double beam irradiation.

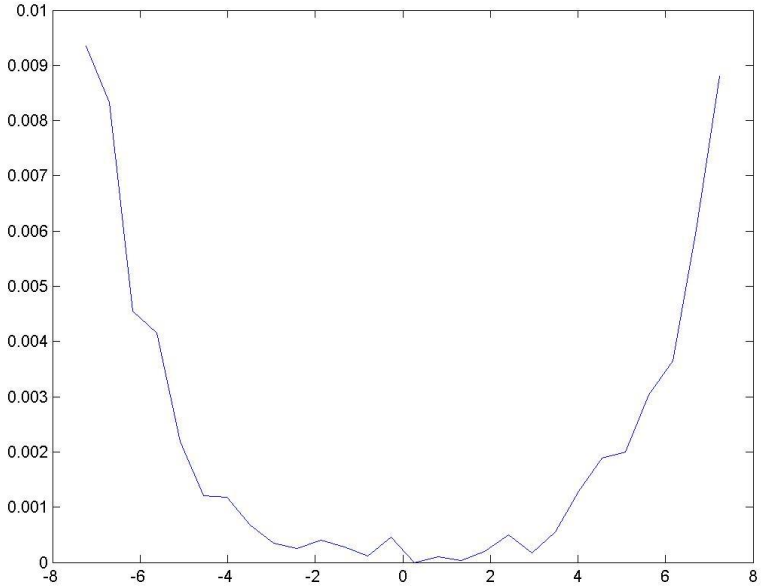

Figure C.84: Dose depth curve for (r, 0,0), Design I, double beam irradiation.

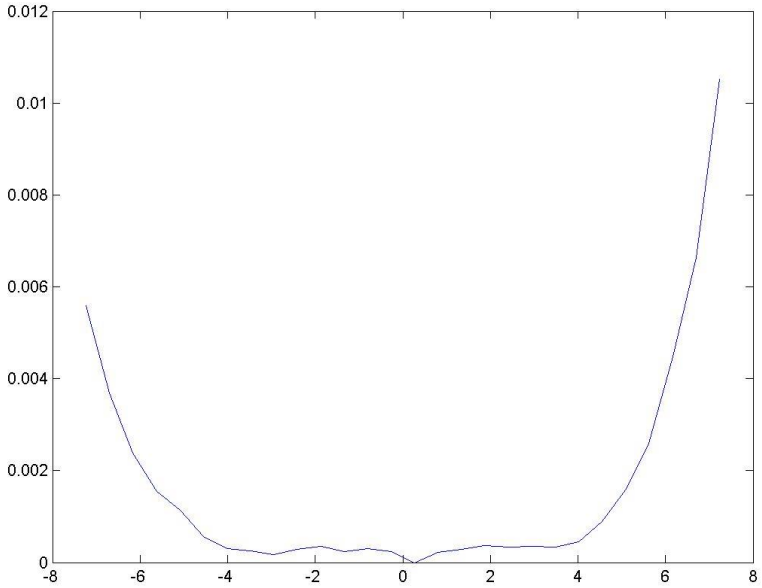

Figure C.85: Dose depth curve for (r,90,0), Design I, double beam irradiation with a 90° rotation about the vertical axis.

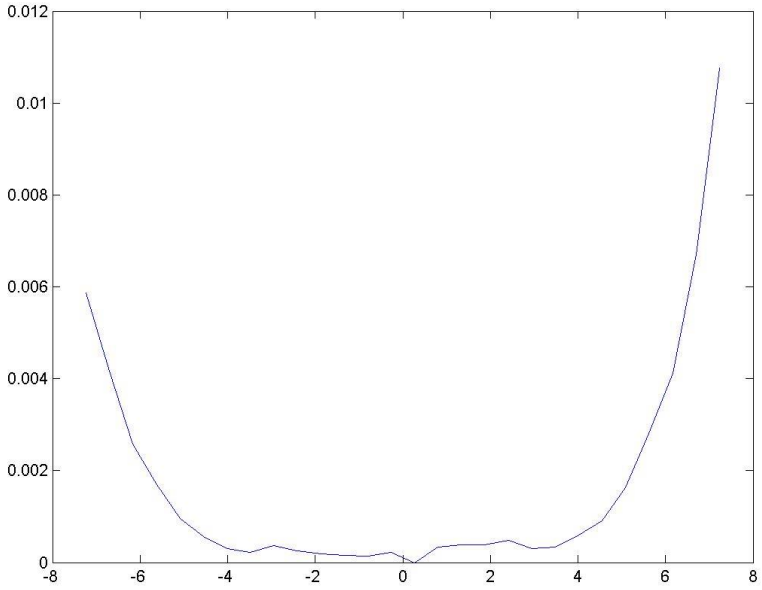

Figure C.86: Dose depth curve for (r,90,90), Design I, double beam irradiation with a 90° rotation about the vertical axis.

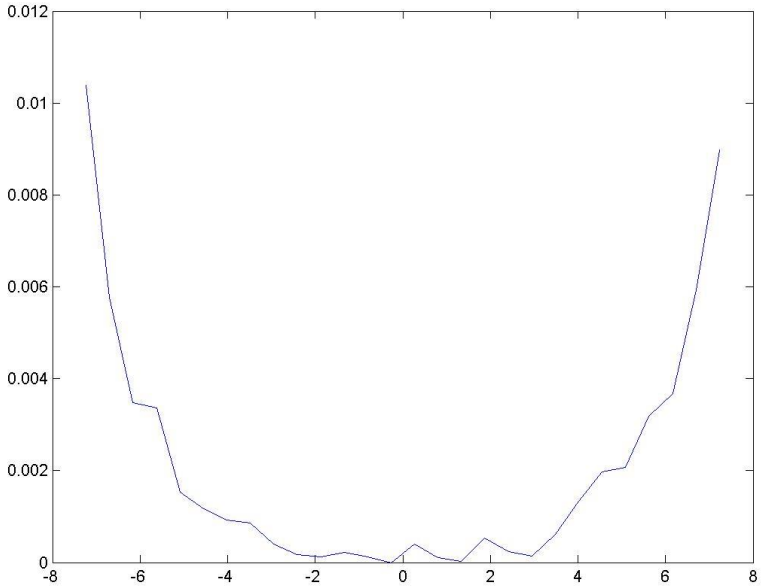

Figure C.87: Dose depth curve for (r, 0,0), Design I, double beam irradiation with a 90° rotation about the vertical axis.

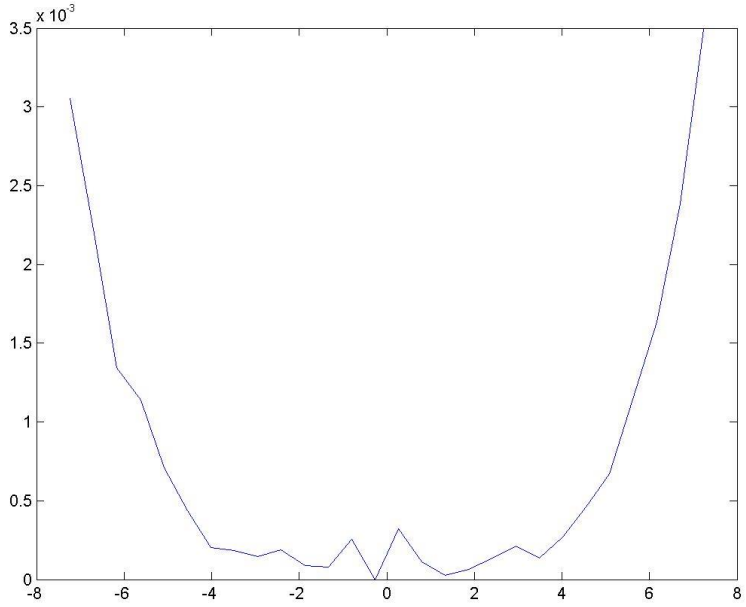

Figure C.88: Dose depth curve for (r,90,0), Design J, single beam irradiation.

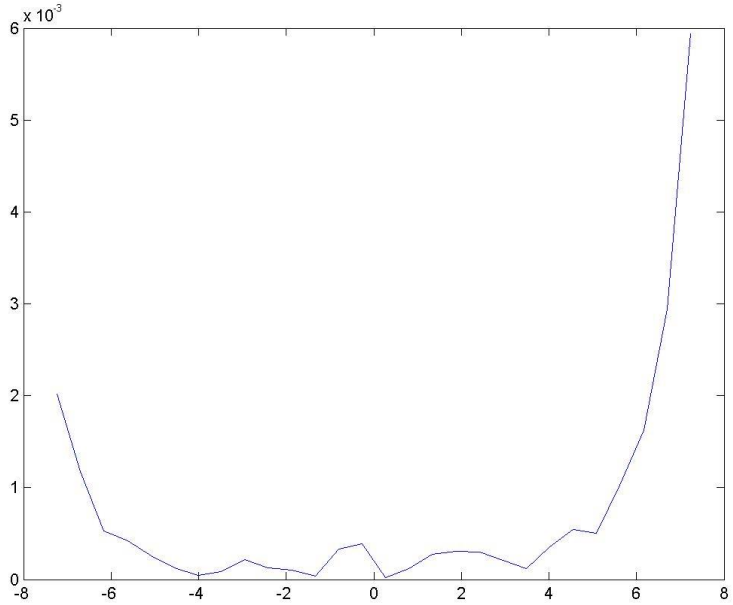

Figure C.89: Dose depth curve for (r,90,90), Design J, single beam irradiation.

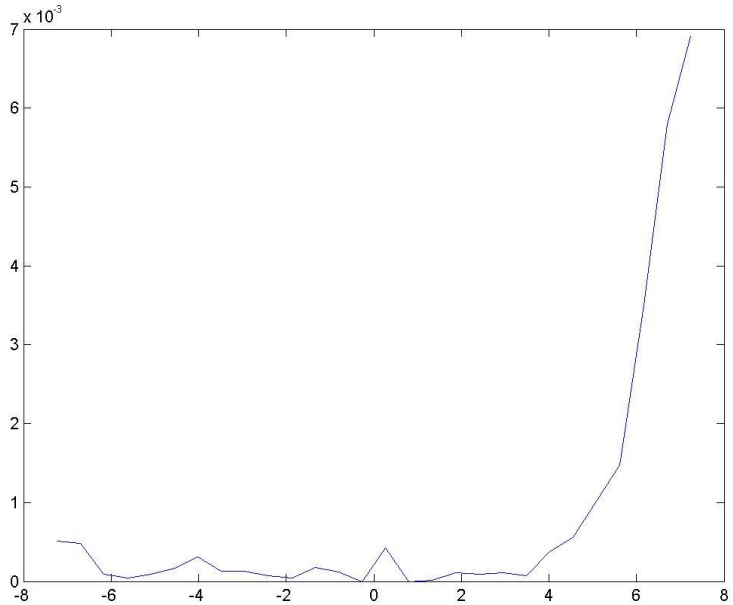

Figure C.90: Dose depth curve for (r, 0,0), Design J, single beam irradiation.

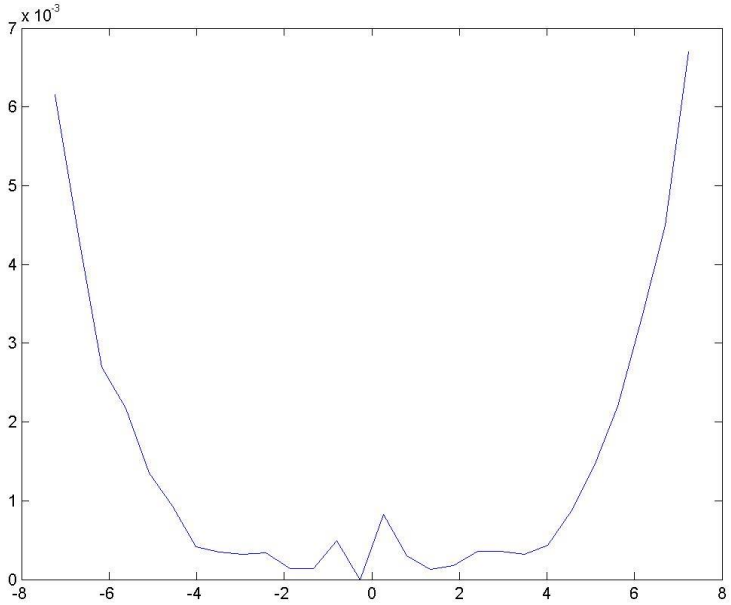

Figure C.91: Dose depth curve for (r,90,0), Design J, double beam irradiation.

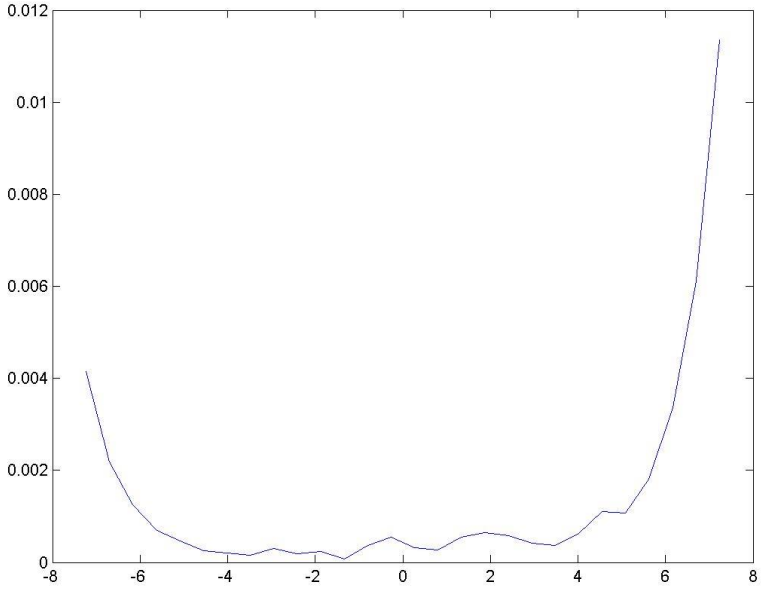

Figure C.92: Dose depth curve for (r,90,90), Design J, double beam irradiation.

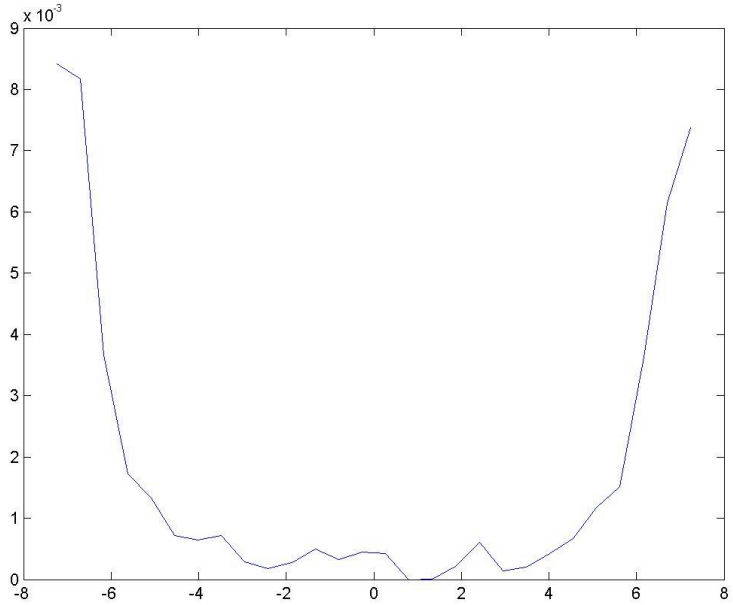

Figure C.93: Dose depth curve for (r, 0,0), Design J, double beam irradiation.

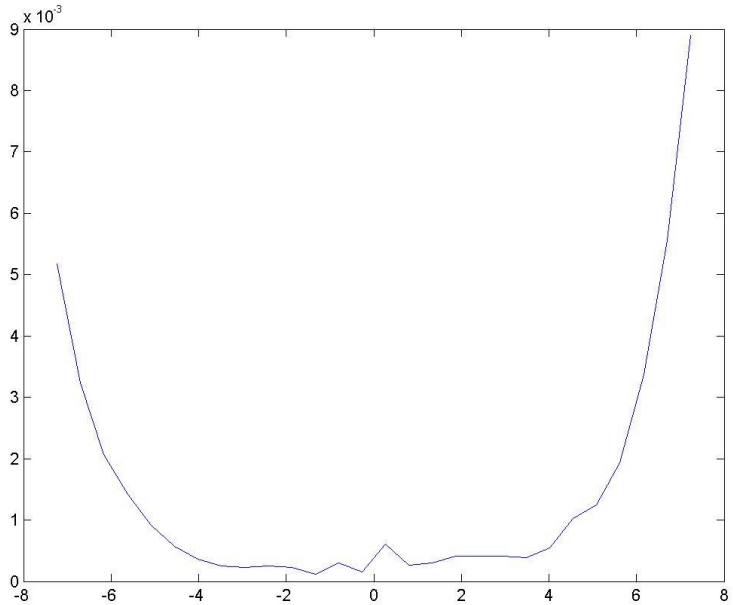

Figure C.94: Dose depth curve for (r,90,0), Design J, double beam irradiation with a 90° rotation about the vertical axis.

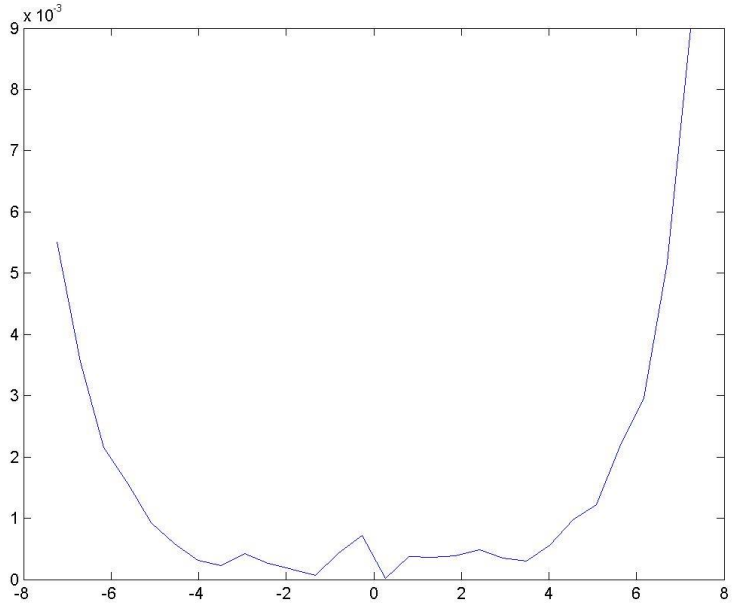

Figure C.95: Dose depth curve for (r,90,90), Design J, double beam irradiation with a 90° rotation about the vertical axis..

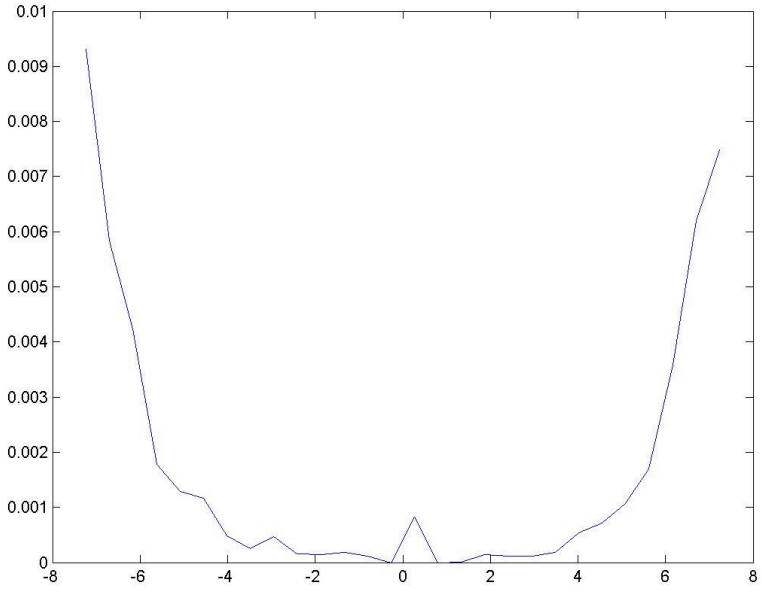

Figure C.96: Dose depth curve for (r, 0,0), Design J, double beam irradiation with a 90° rotation about the vertical axis.

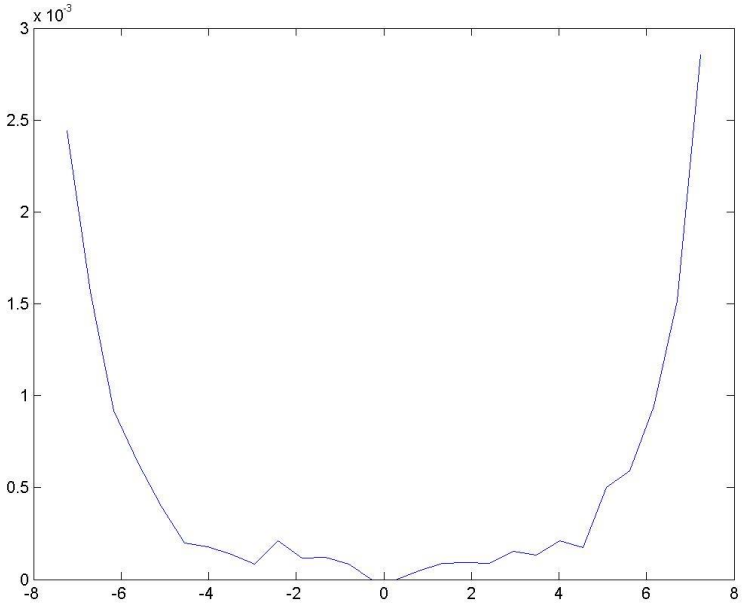

Figure C.97: Dose depth curve for (r,90,0), Design K, single beam irradiation.

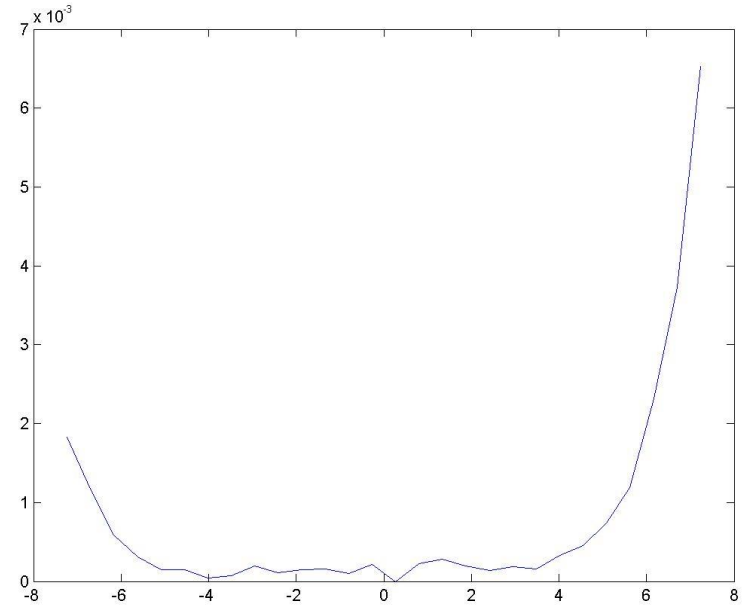

Figure C.98: Dose depth curve for (r,90,90), Design K, single beam irradiation.

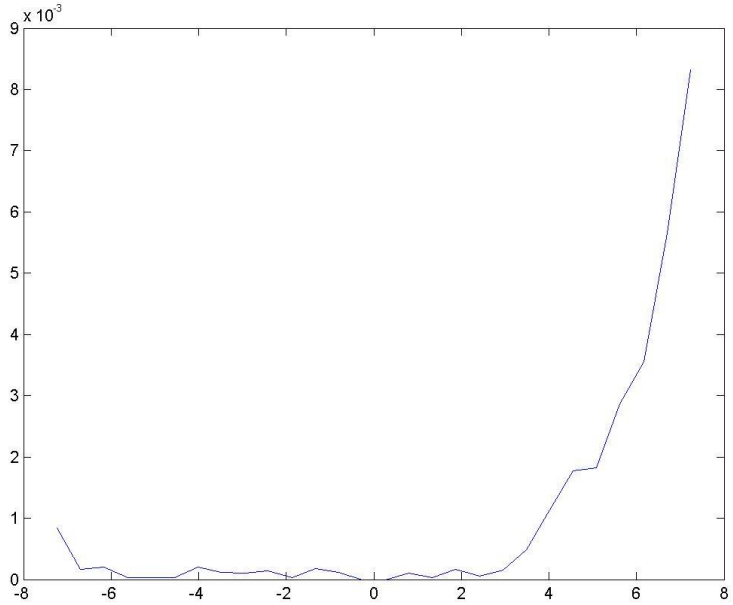

Figure C.99: Dose depth curve for (r, 0,0), Design K, single beam irradiation.

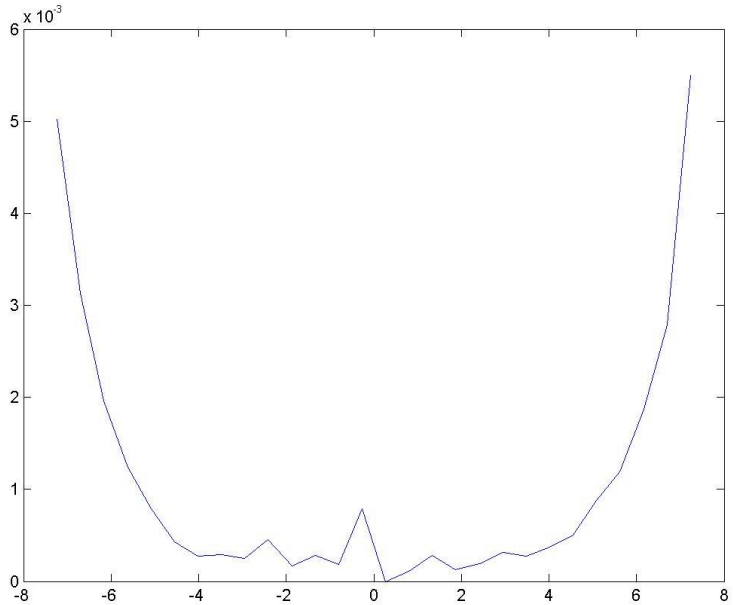

Figure C.100: Dose depth curve for (r,90,0), Design K, double beam irradiation.

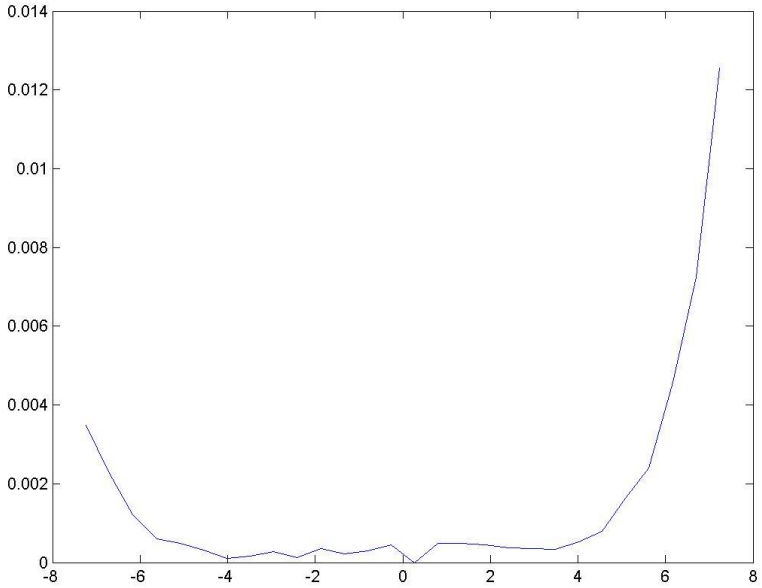

Figure C.101: Dose depth curve for (r,90,90), Design K, double beam irradiation.

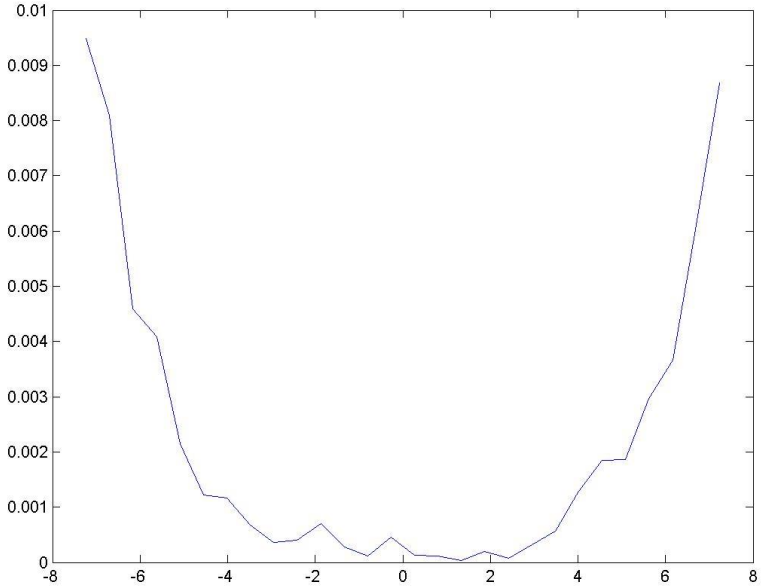

Figure C.102: Dose depth curve for (r, 0,0), Design K, double beam irradiation.

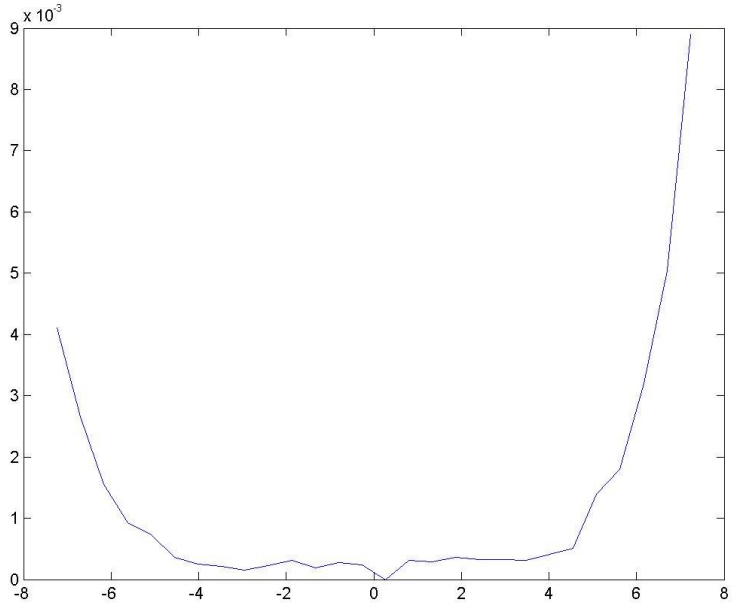

Figure C.103: Dose depth curve for (r,90,0), Design K, double beam irradiation with a 90° rotation about the vertical axis.

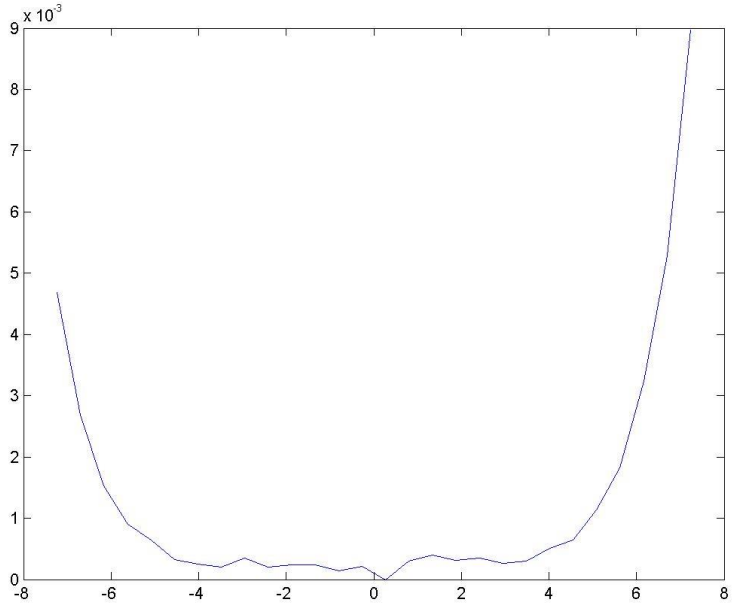

Figure C.104: Dose depth curve for (r,90,90), Design K, double beam irradiation with a 90° rotation about the vertical axis.

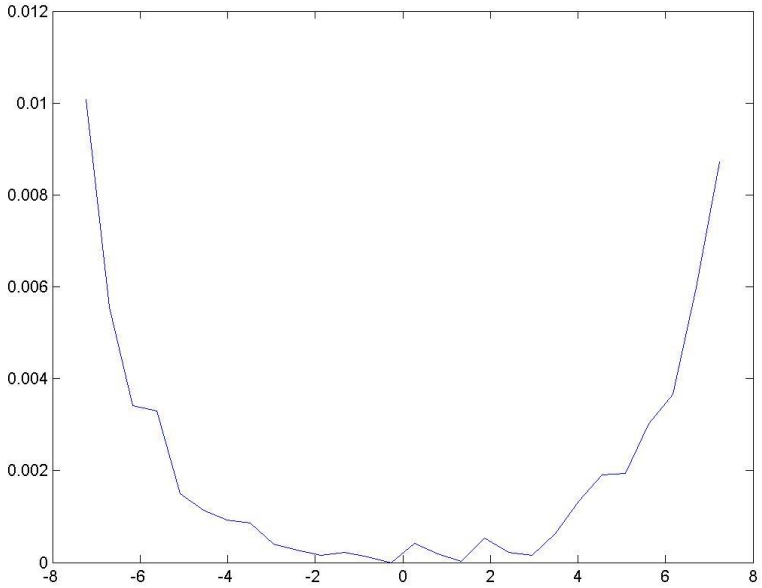

Figure C.105: Dose depth curve for (r, 0,0), Design K, double beam irradiation with a 90° rotation about the vertical axis.

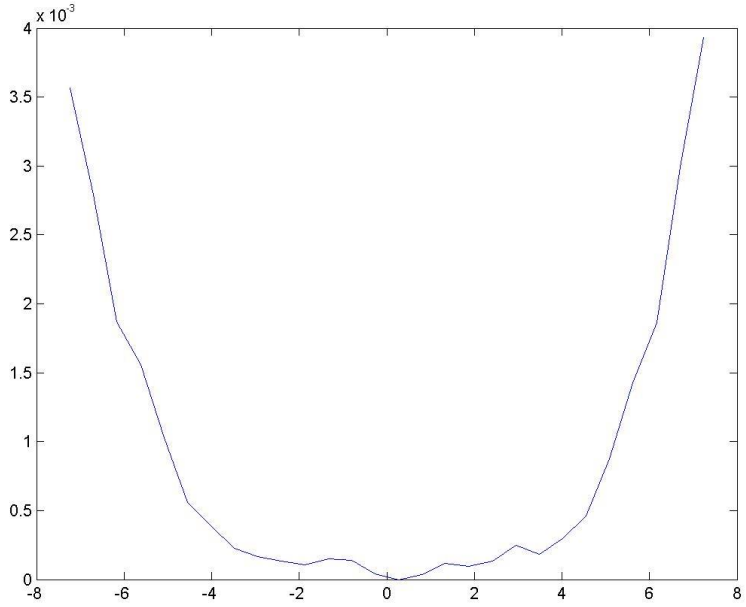

Figure C.106: Dose depth curve for (r,90,0), Design L, single beam irradiation.

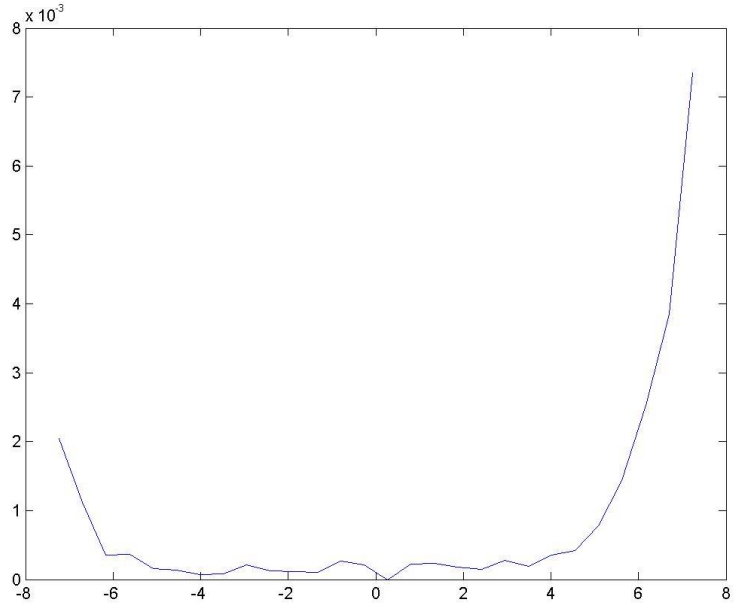

Figure C.107: Dose depth curve for (r,90,90), Design L, single beam irradiation.

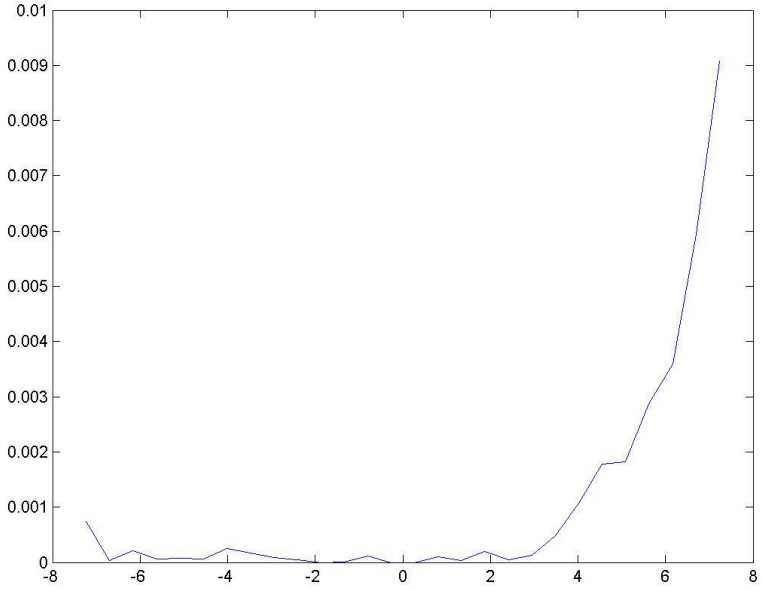

Figure C.108: Dose depth curve for (r, 0,0), Design L, single beam irradiation.

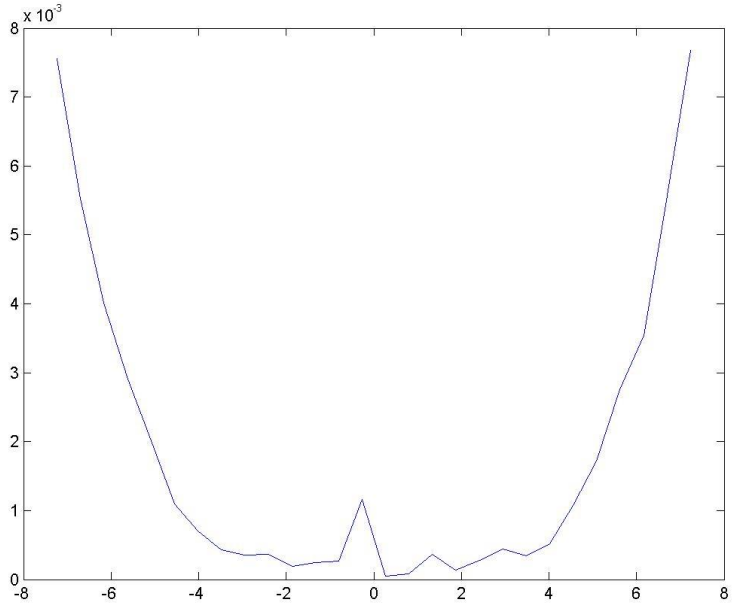

Figure C.109: Dose depth curve for (r,90,0), Design L, double beam irradiation.

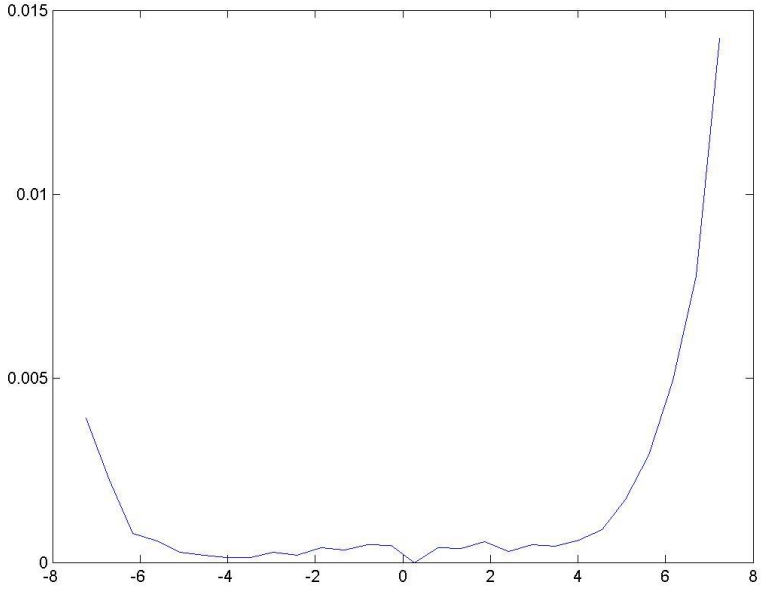

Figure C.110: Dose depth curve for (r,90,90), Design L, double beam irradiation.

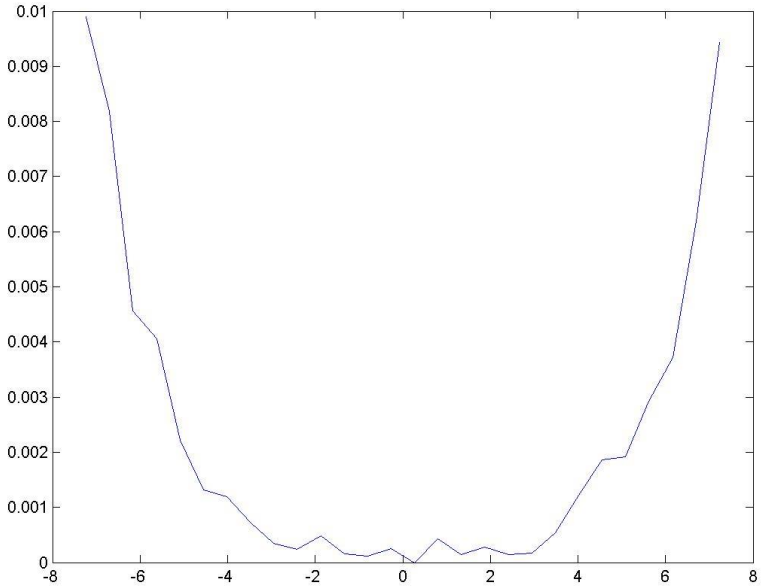

Figure C.111: Dose depth curve for (r, 0,0), Design L, double beam irradiation.

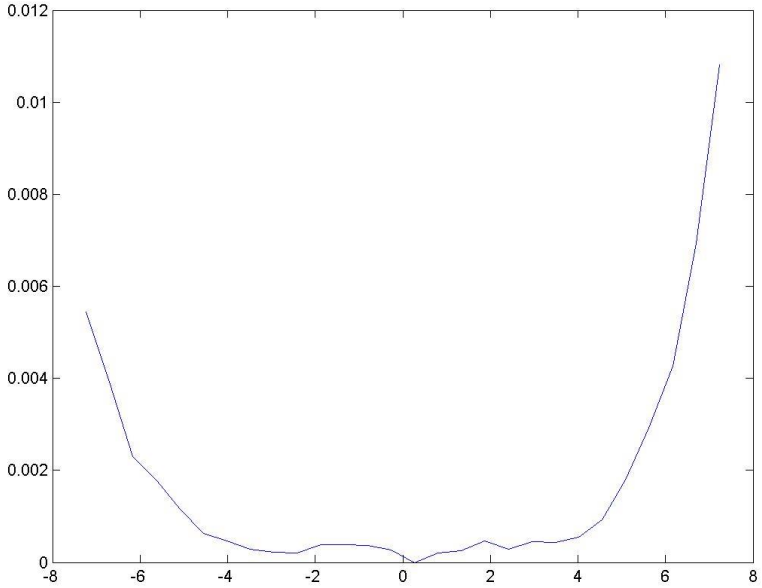

Figure C.112: Dose depth curve for (r,90,0), Design L, double beam irradiation with a 90° rotation about the vertical axis.

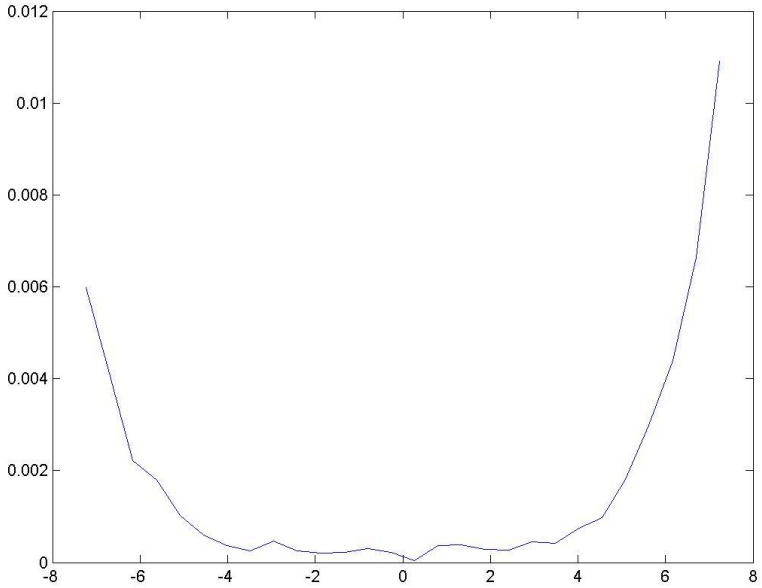

Figure C.113: Dose depth curve for (r,90,90), Design L, double beam irradiation with a 90° rotation about the vertical axis..

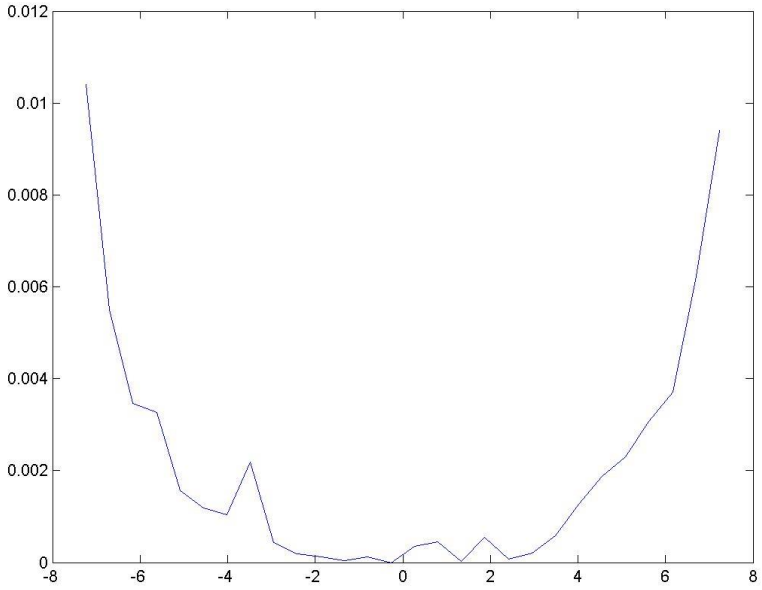

Figure C.114: Dose depth curve for (r, 0,0), Design L, double beam irradiation with a 90° rotation about the vertical axis.

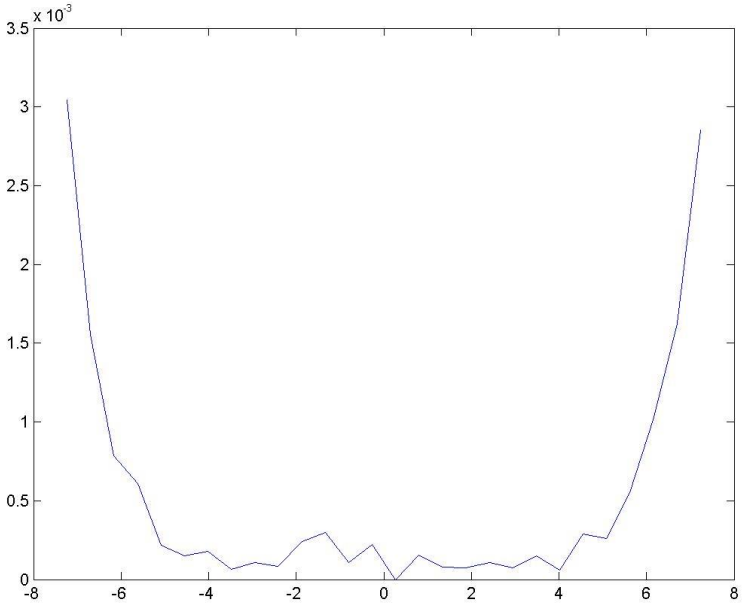

Figure C.115: Dose depth curve for (r,90,0), Design M, single beam irradiation.

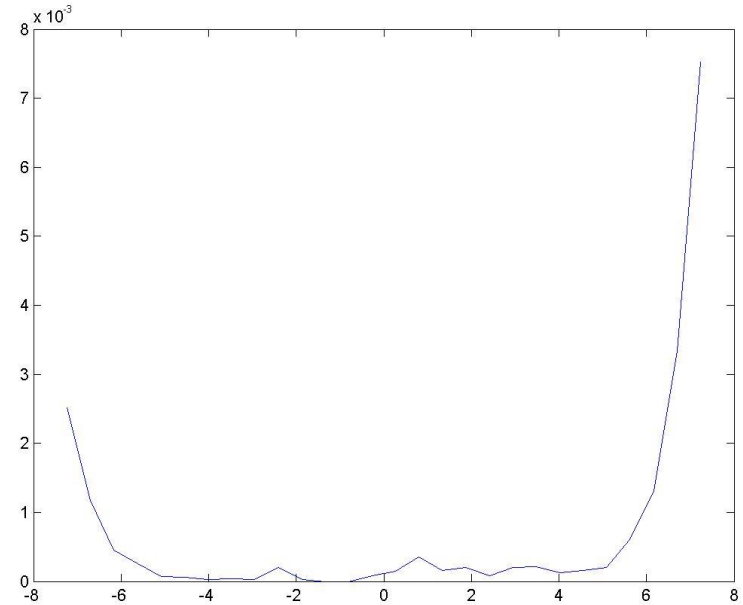

Figure C.116: Dose depth curve for (r,90,90), Design M, single beam irradiation.

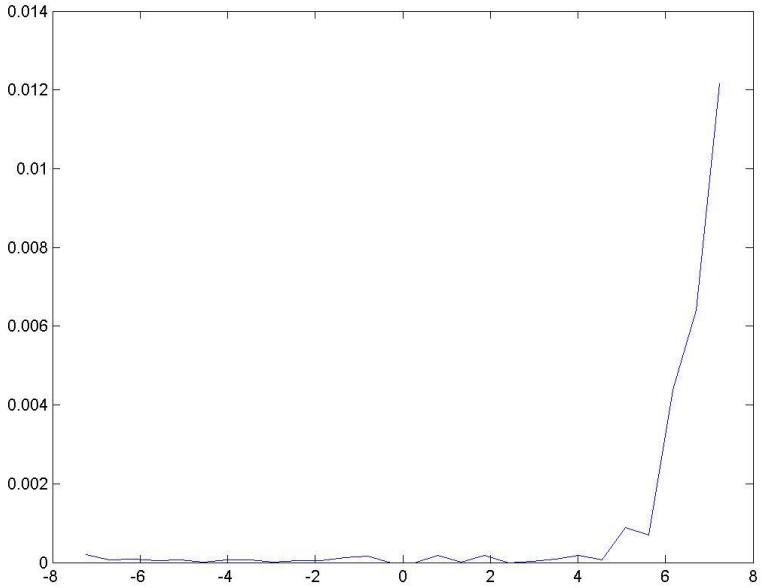

Figure C.117: Dose depth curve for (r, 0,0), Design M, single beam irradiation.

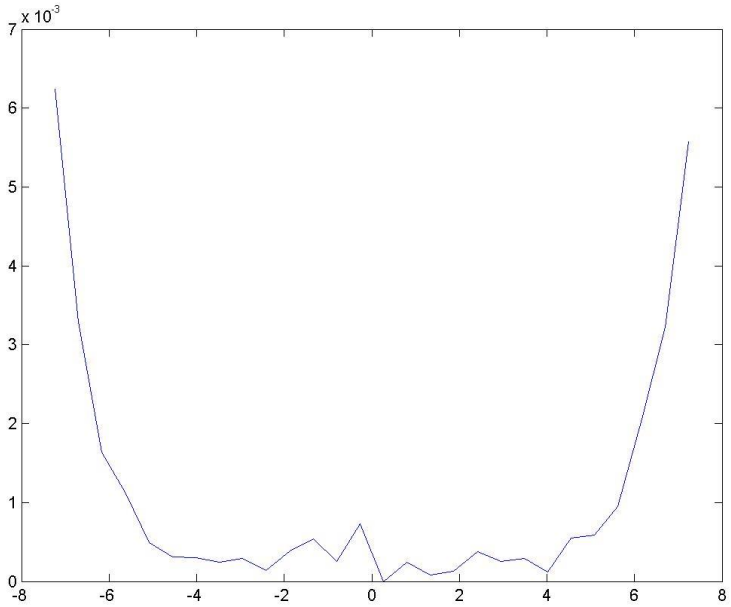

Figure C.118: Dose depth curve for (r,90,0), Design M, double beam irradiation.

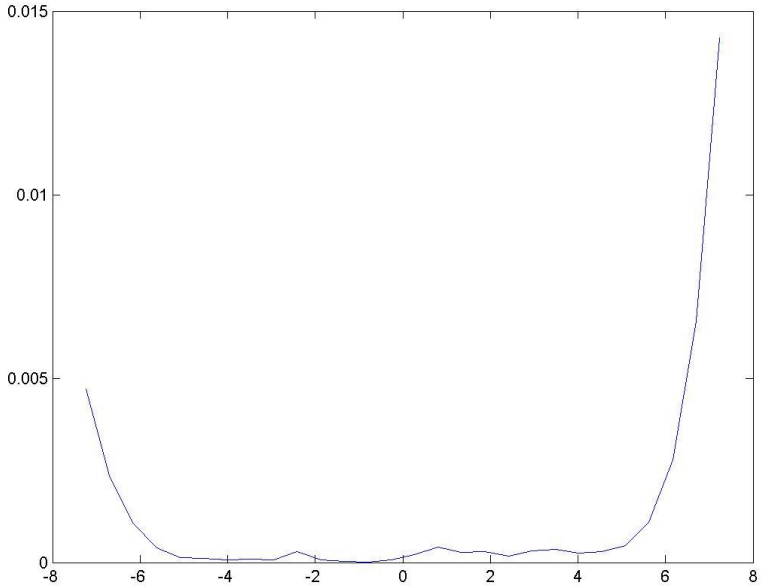

Figure C.119: Dose depth curve for (r,90,90), Design M, double beam irradiation.

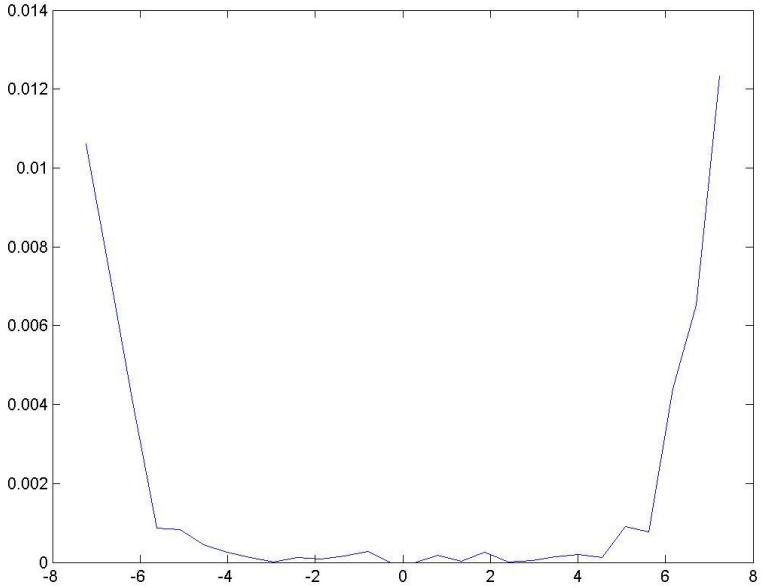

Figure C.120: Dose depth curve for (r, 0,0), Design M, double beam irradiation.

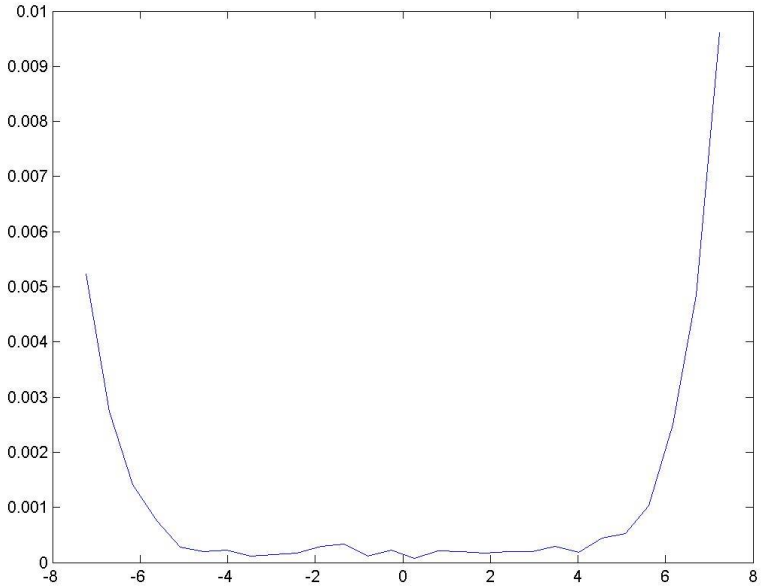

Figure C.121: Dose depth curve for (r,90,0), Design M, double beam irradiation with a 90° rotation about the vertical axis.

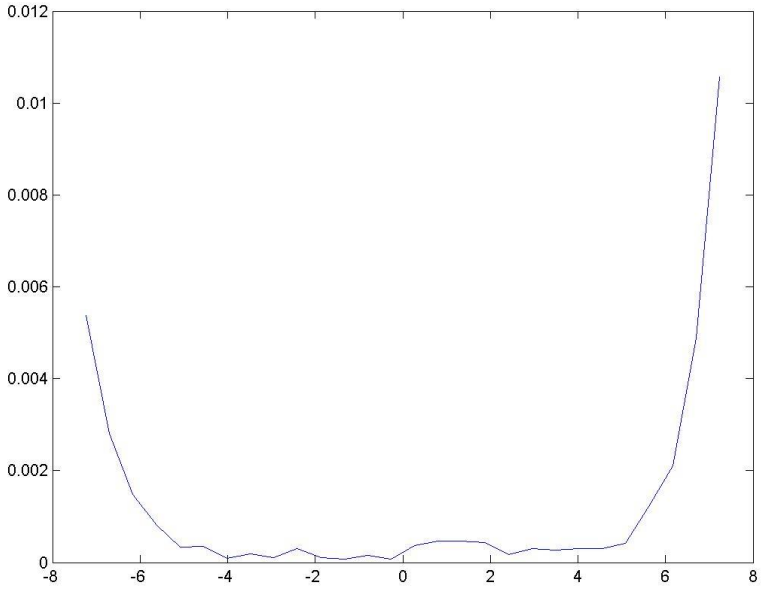

Figure C.122: Dose depth curve for (r,90,90), Design M, double beam irradiation with a 90° rotation about the vertical axis.

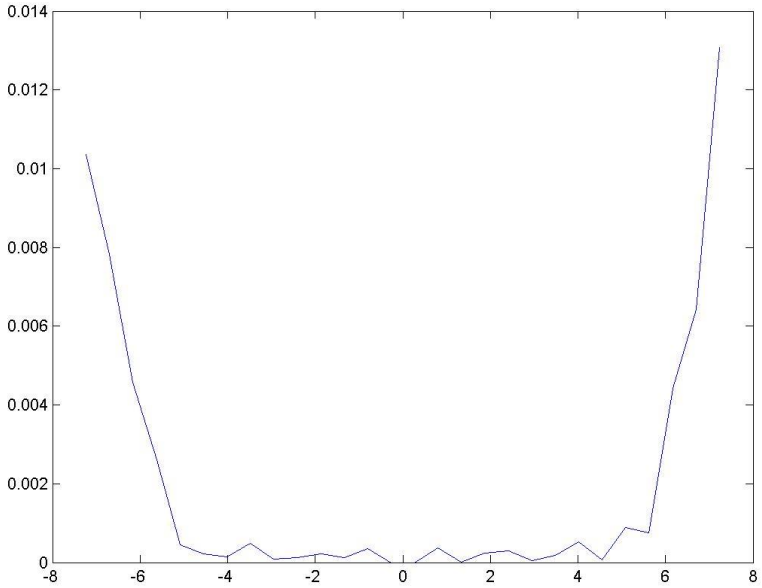

Figure C.123: Dose depth curve for (r, 0,0), Design M, double beam irradiation with a 90° rotation about the vertical axis.

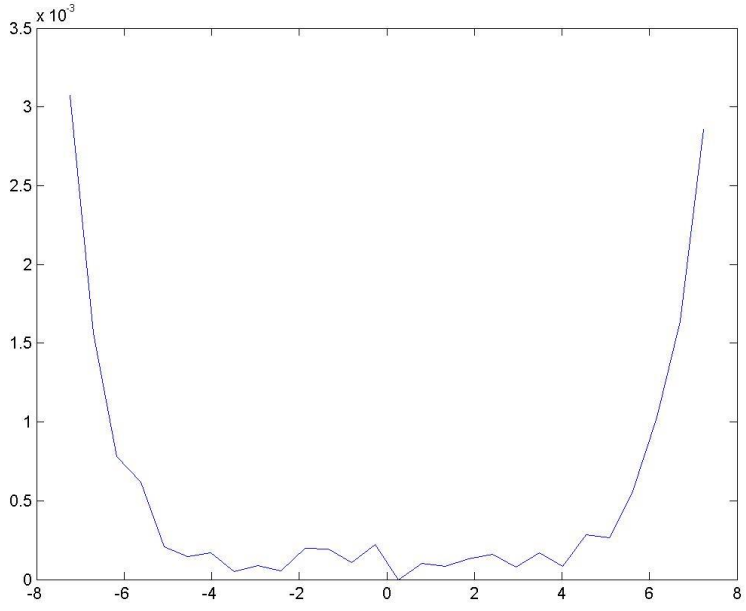

Figure C.124: Dose depth curve for (r,90,0), Design N, single beam irradiation.

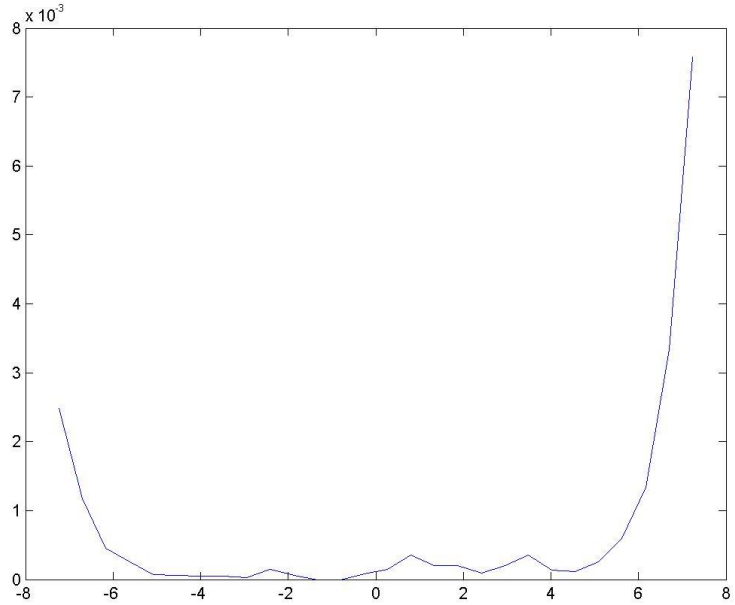

Figure C.125: Dose depth curve for (r,90,90), Design N, single beam irradiation.

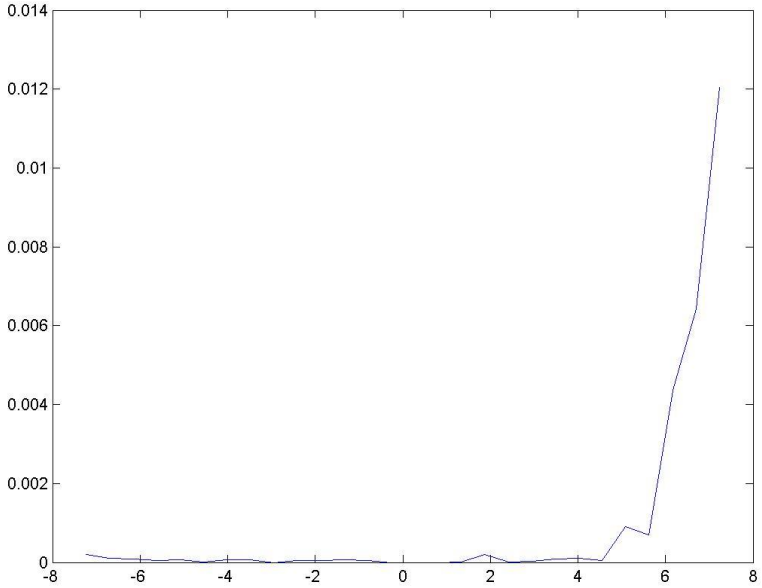

Figure C.126: Dose depth curve for (r, 0,0), Design N, single beam irradiation.

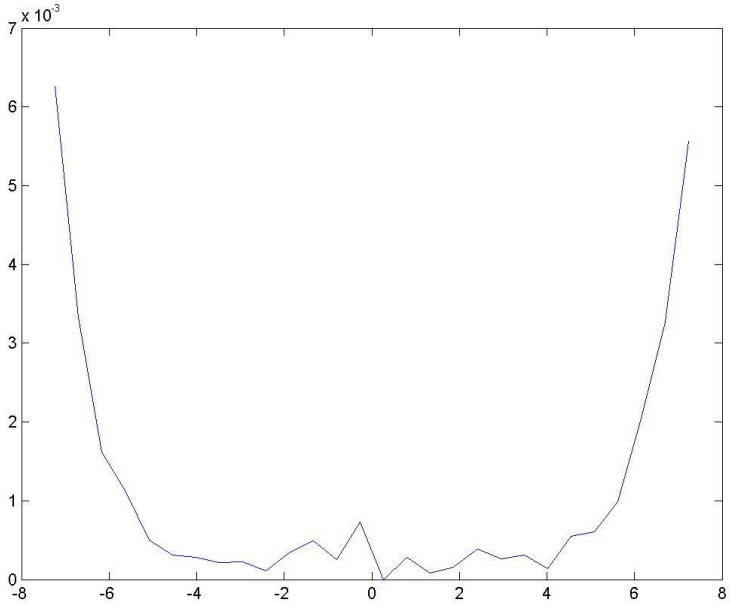

Figure C.127: Dose depth curve for (r,90,0), Design N, double beam irradiation.

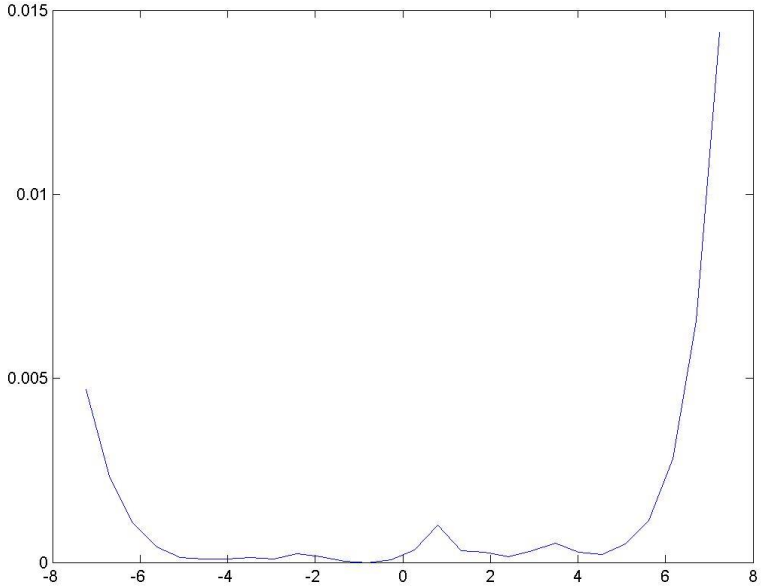

Figure C.128: Dose depth curve for (r,90,90), Design N, double beam irradiation.

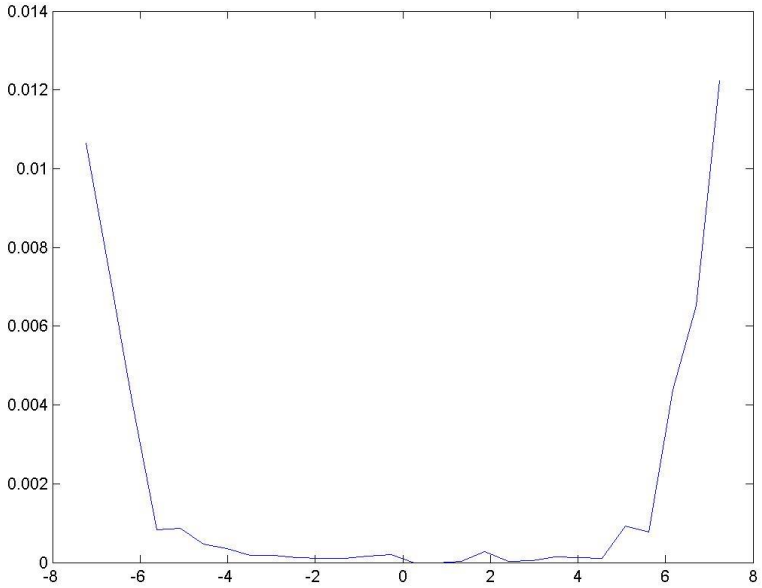

Figure C.129: Dose depth curve for (r, 0,0), Design N, double beam irradiation.

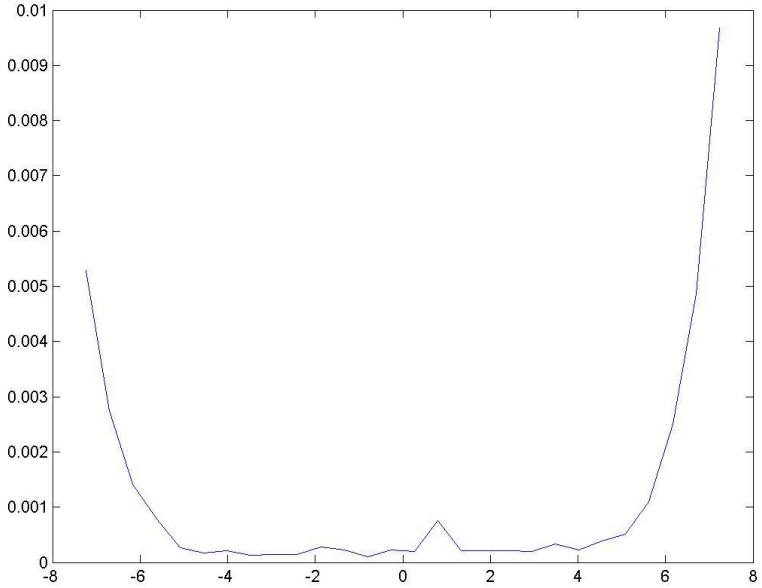

Figure C.130: Dose depth curve for (r,90,0), Design N, double beam irradiation with a 90° rotation about the vertical axis.

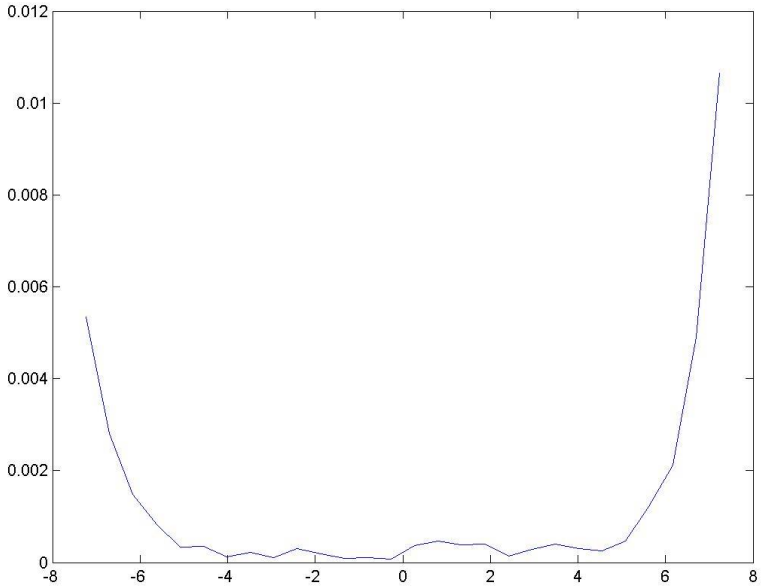

Figure C.131: Dose depth curve for (r,90,90), Design N, double beam irradiation with a 90° rotation about the vertical axis..

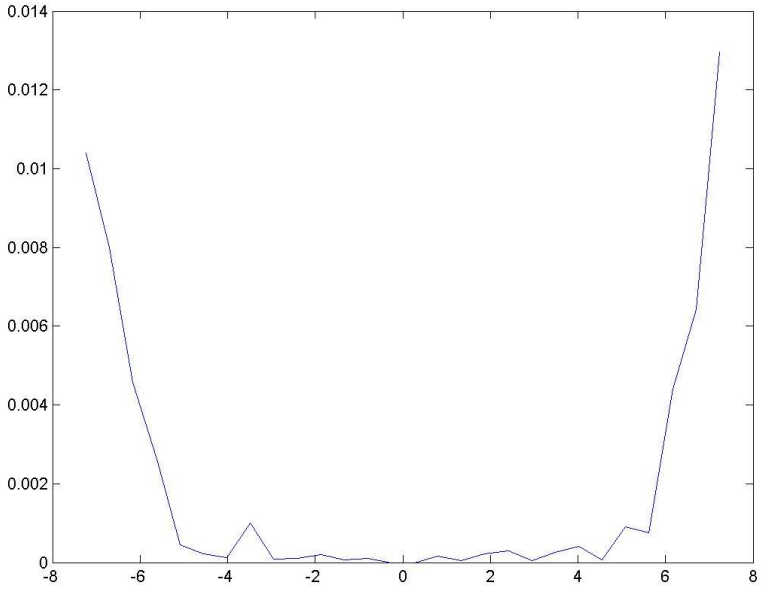

Figure C.132: Dose depth curve for (r, 0,0), Design N, double beam irradiation with a 90° rotation about the vertical axis.

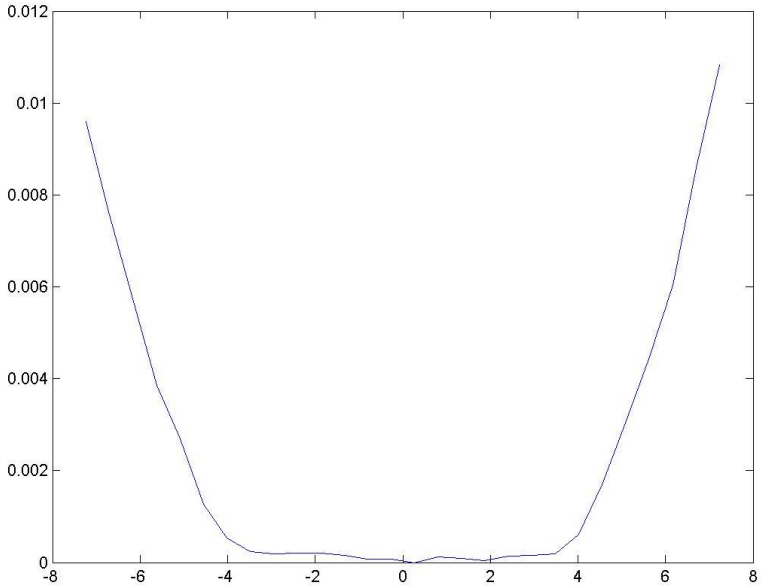

Figure C.133: Dose depth curve for (r,90,0), Design O, single beam irradiation.

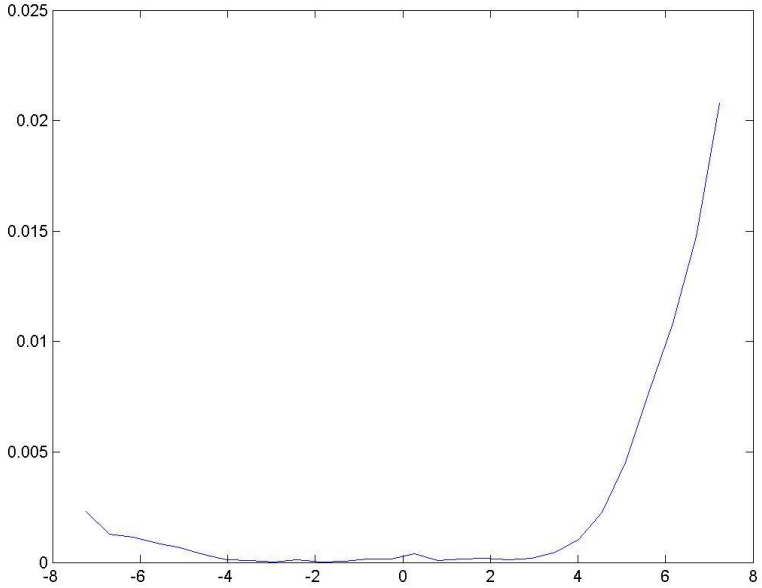

Figure C.134: Dose depth curve for (r,90,90), Design O, single beam irradiation.

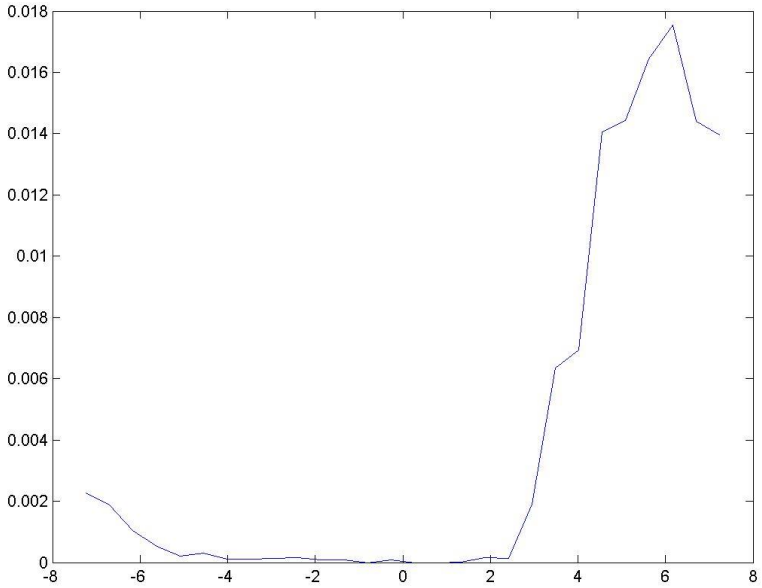

Figure C.135: Dose depth curve for (r, 0,0), Design O, single beam irradiation.

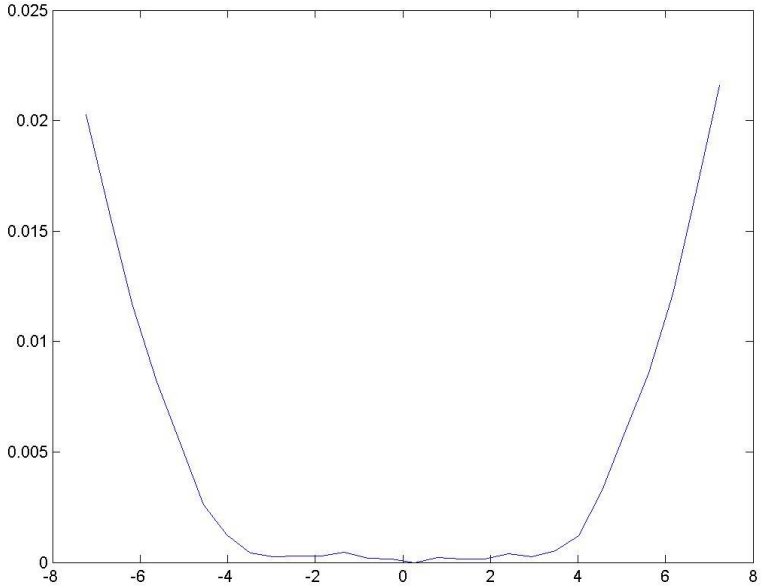

Figure C.136: Dose depth curve for (r,90,0), Design O, double beam irradiation.

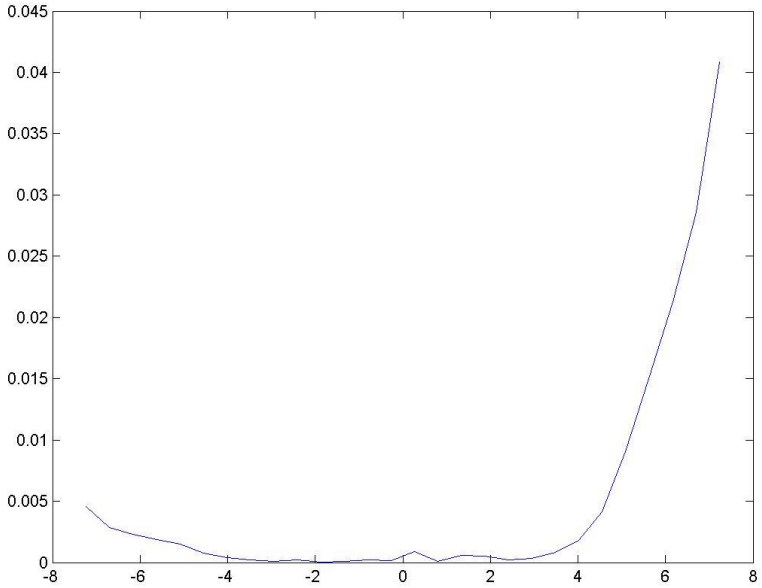

Figure C.137: Dose depth curve for (r,90,90), Design O, double beam irradiation.

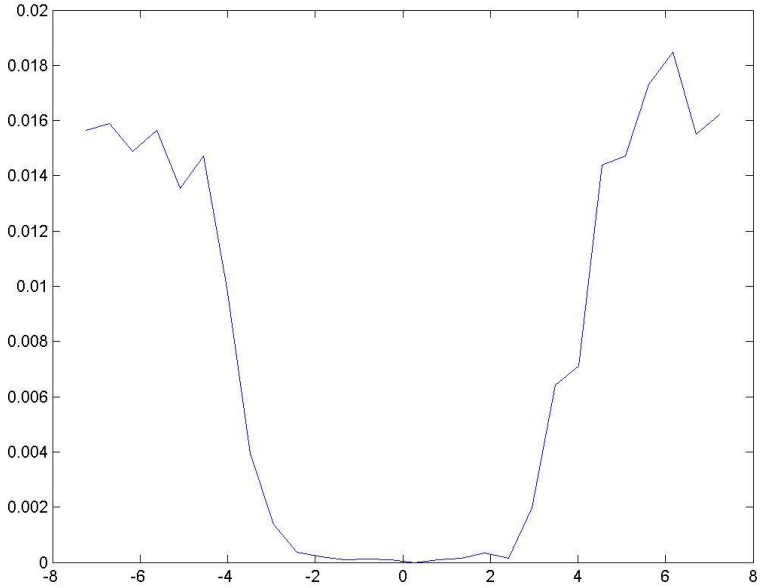

Figure C.138: Dose depth curve for (r, 0,0), Design O, double beam irradiation.

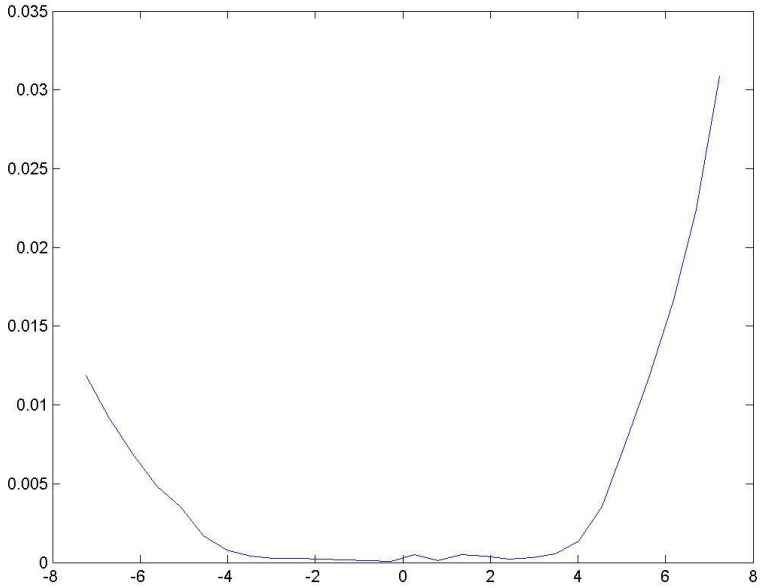

Figure C.139: Dose depth curve for (r,90,0), Design O, double beam irradiation with a 90° rotation about the vertical axis.

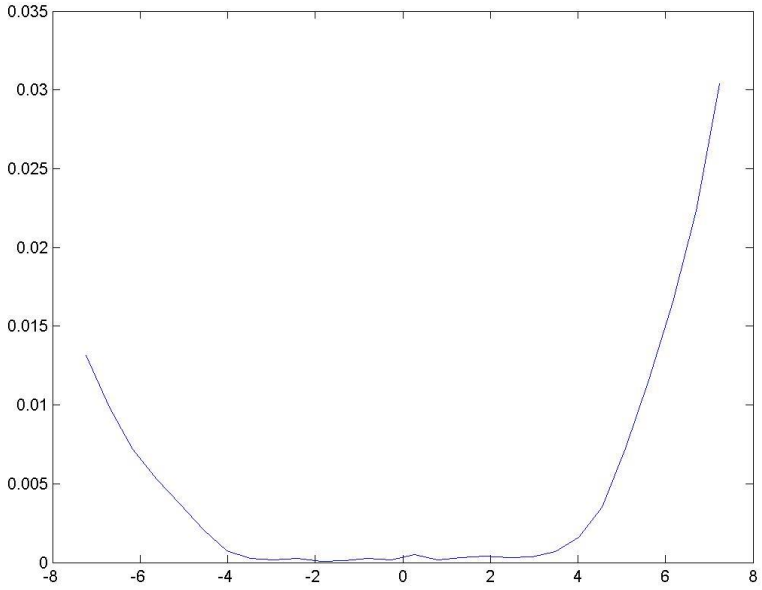

Figure C.140: Dose depth curve for (r,90,90), Design O, double beam irradiation with a 90° rotation about the vertical axis.

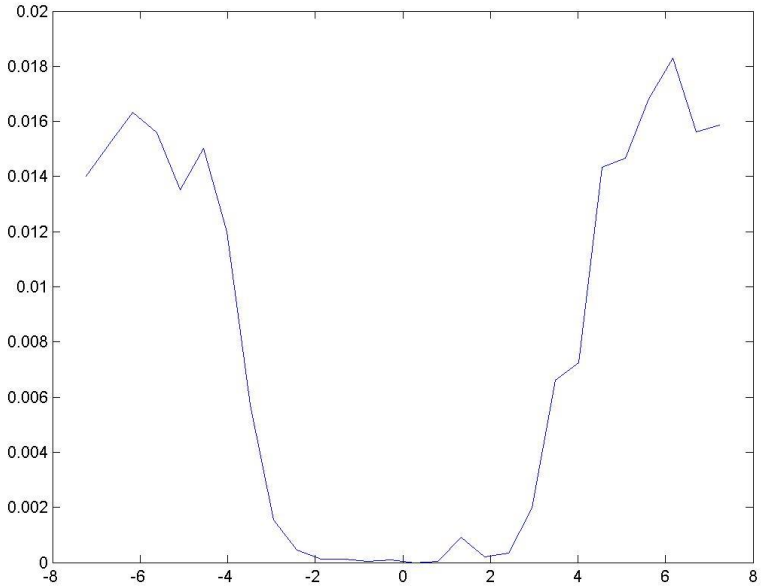

Figure C.141: Dose depth curve for (r, 0,0), Design O, double beam irradiation with a 90° rotation about the vertical axis.

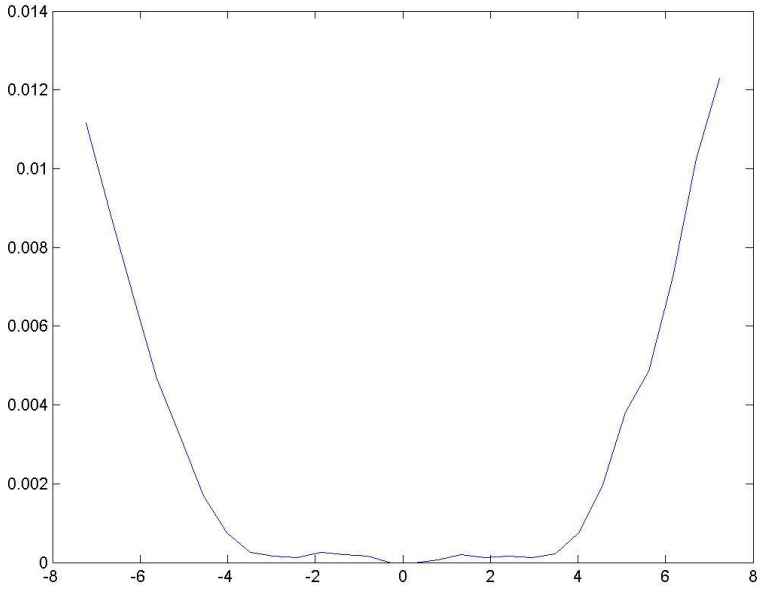

Figure C.142: Dose depth curve for (r,90,0), Design P, single beam irradiation.

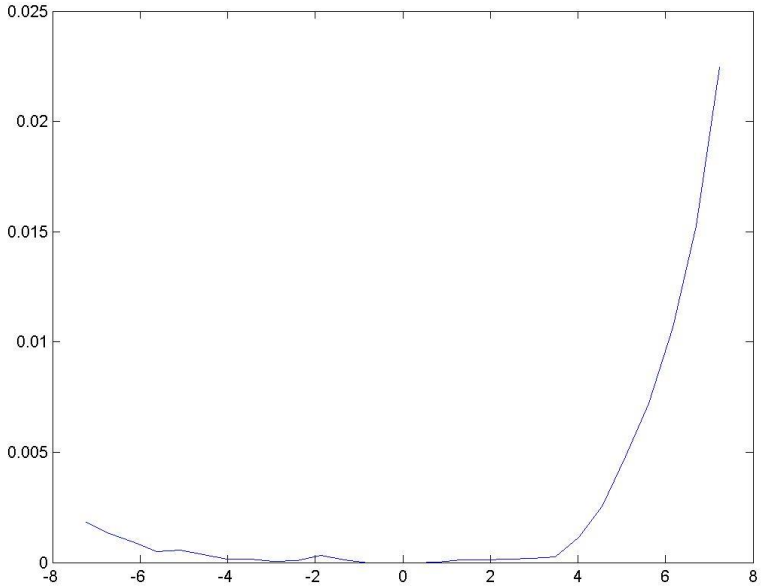

Figure C.143: Dose depth curve for (r,90,90), Design P, single beam irradiation.

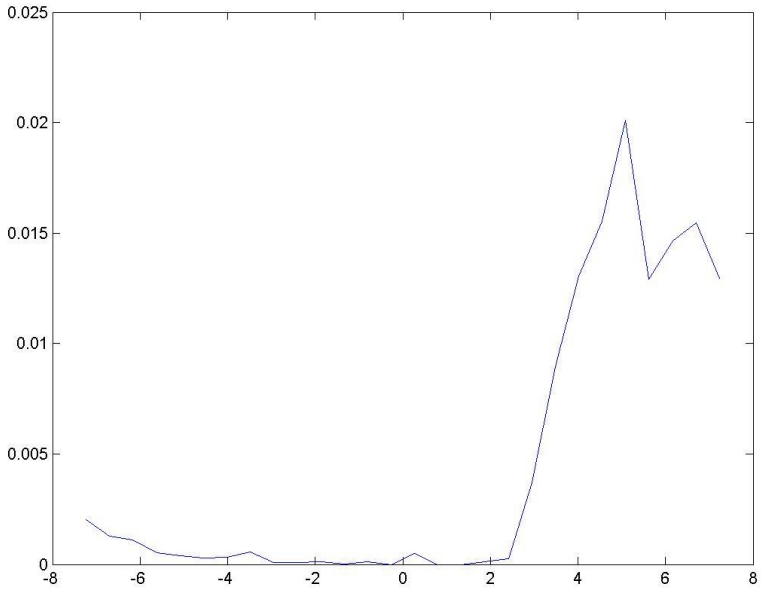

Figure C.144: Dose depth curve for (r, 0,0), Design P, single beam irradiation.

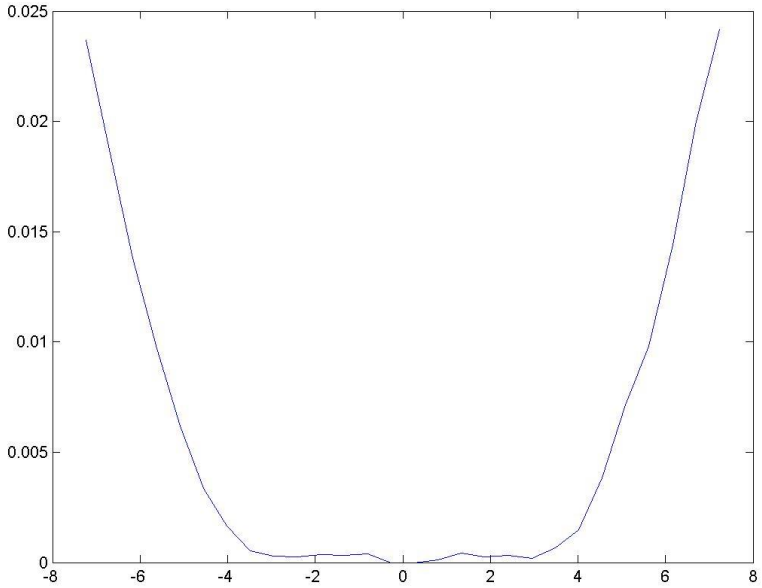

Figure C.145: Dose depth curve for (r,90,0), Design P, double beam irradiation.

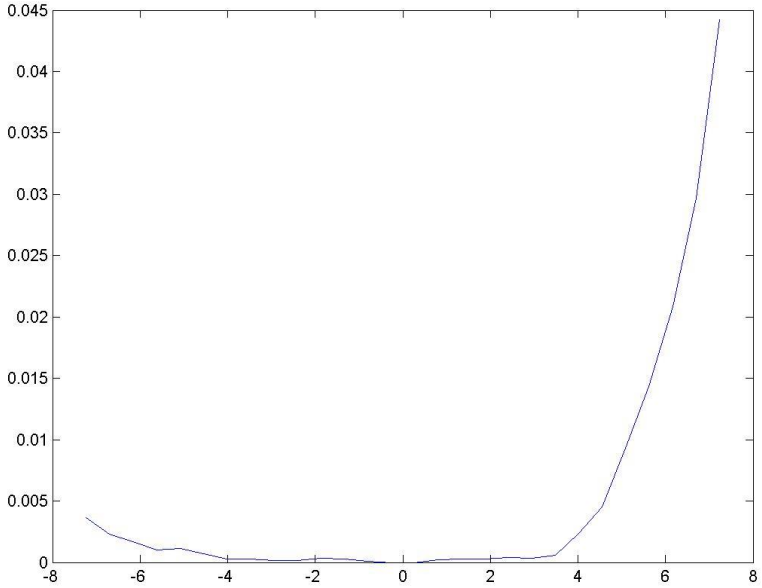

Figure C.146: Dose depth curve for (r,90,90), Design P, double beam irradiation.

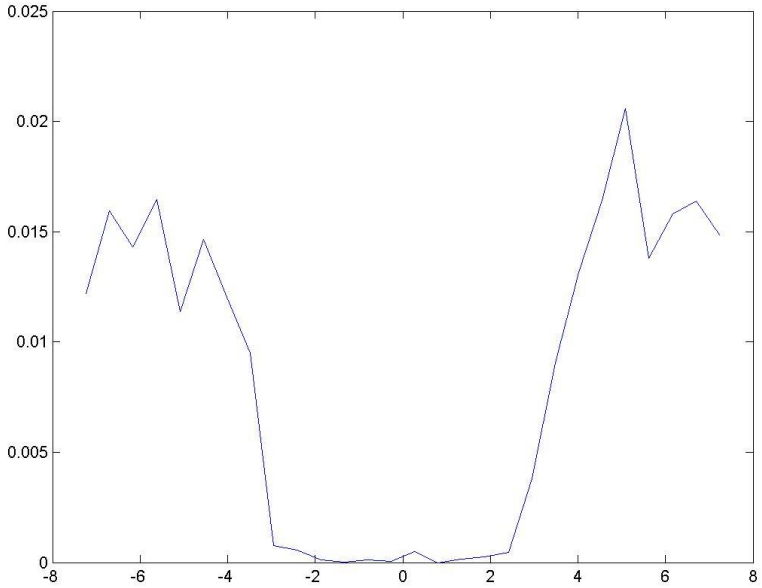

Figure C.147: Dose depth curve for (r, 0,0), Design P, double beam irradiation.

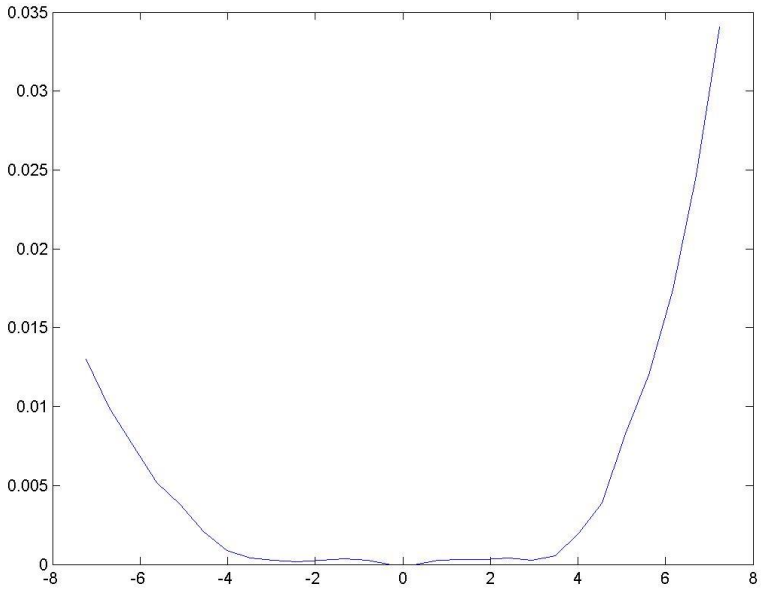

Figure C.148: Dose depth curve for (r,90,0), Design P, double beam irradiation with a 90° rotation about the vertical axis.

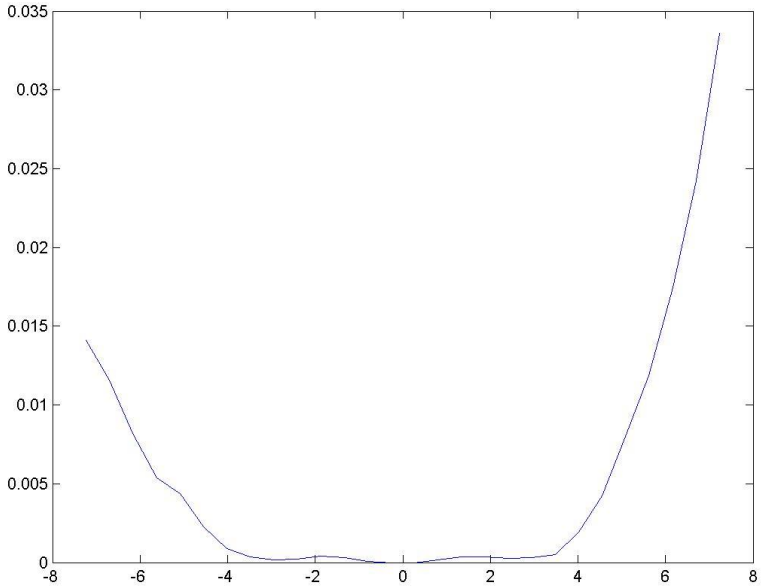

Figure C.149: Dose depth curve for (r,90,90), Design P, double beam irradiation with a 90° rotation about the vertical axis..

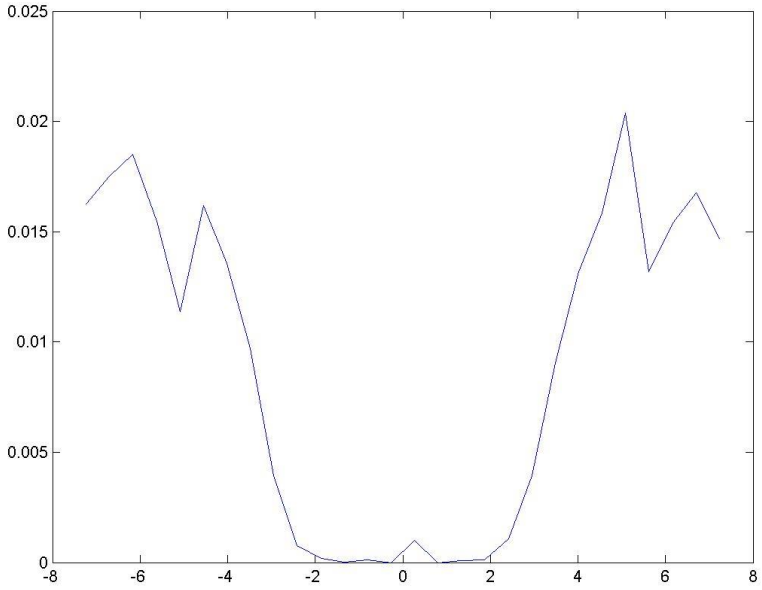

Figure C.150: Dose depth curve for (r, 0,0), Design P, double beam irradiation with a 90° rotation about the vertical axis.

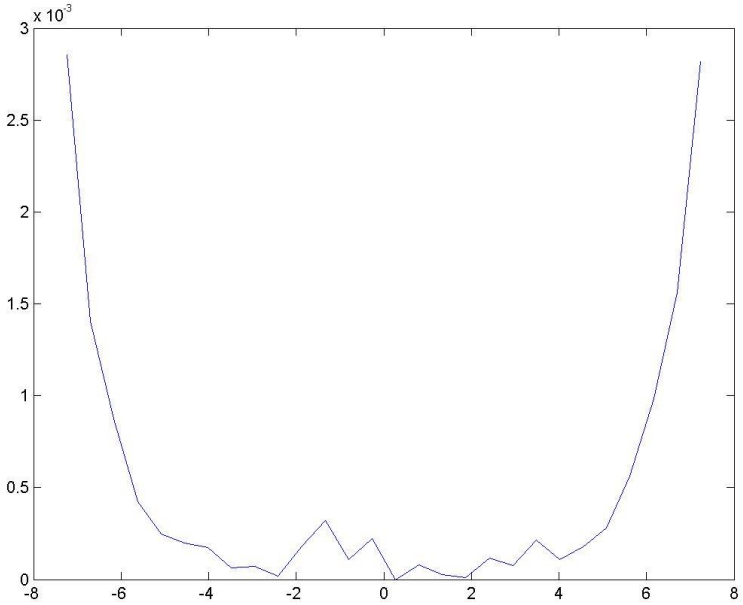

Figure C.151: Dose depth curve for (r,90,0), Design Q, single beam irradiation.

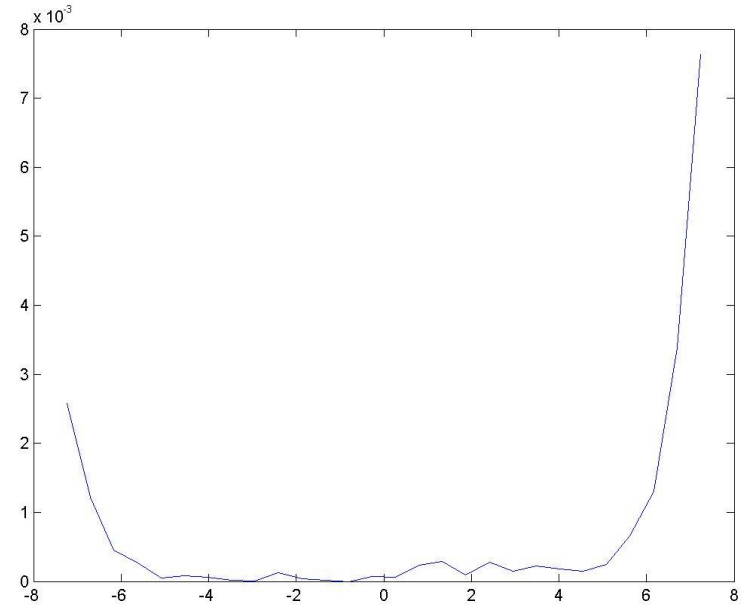

Figure C.152: Dose depth curve for (r,90,90), Design Q, single beam irradiation.

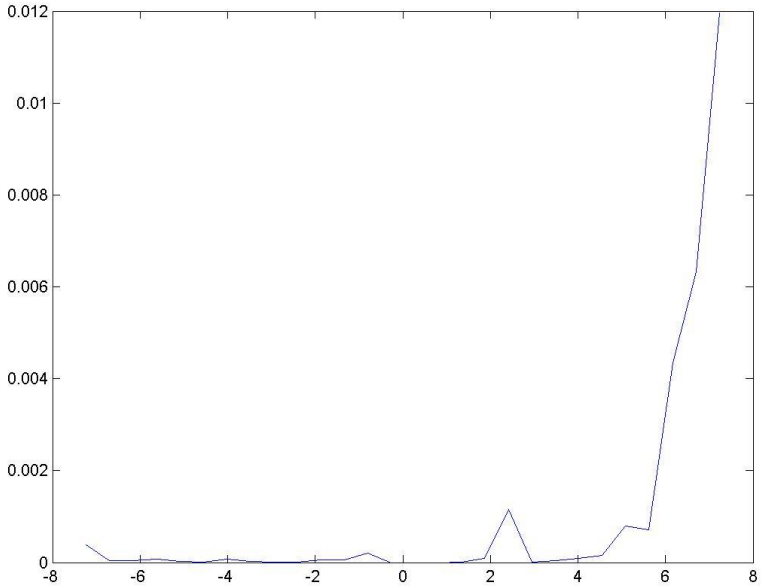

Figure C.153: Dose depth curve for (r, 0,0), Design Q, single beam irradiation.

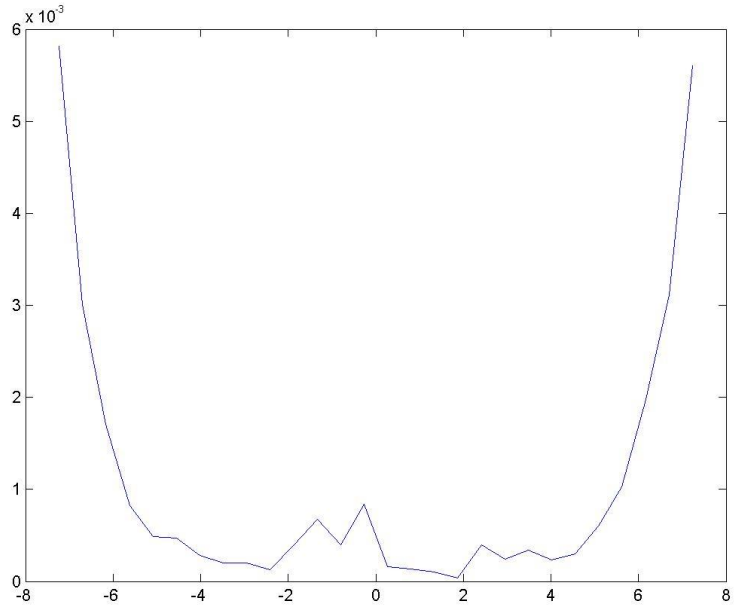

Figure C.154: Dose depth curve for (r,90,0), Design Q, double beam irradiation.

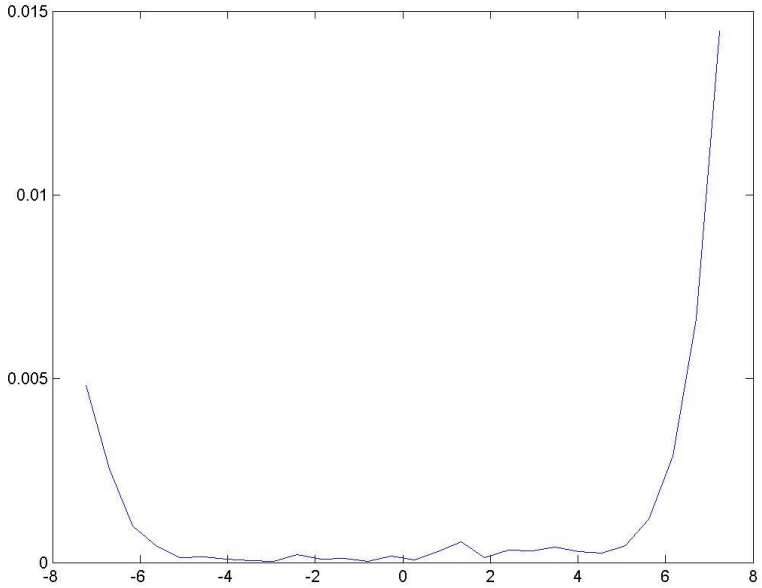

Figure C.155: Dose depth curve for (r,90,90), Design Q, double beam irradiation.

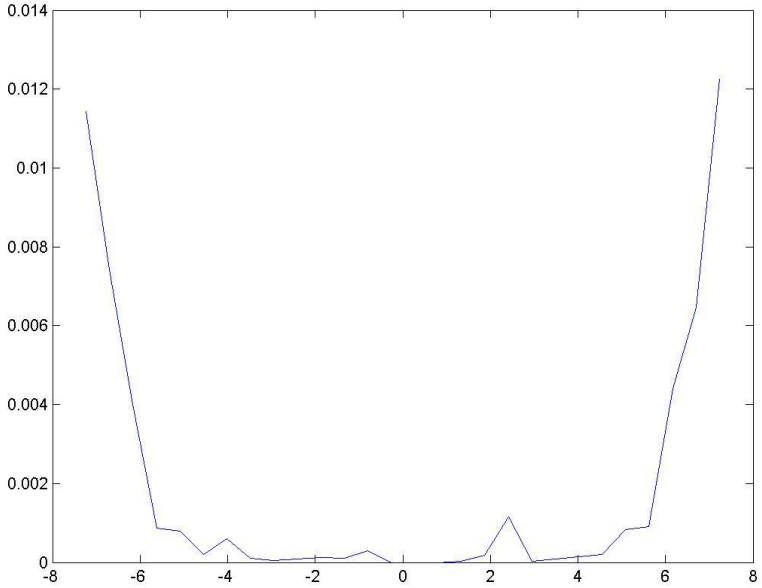

Figure C.156: Dose depth curve for (r, 0,0), Design Q, double beam irradiation.

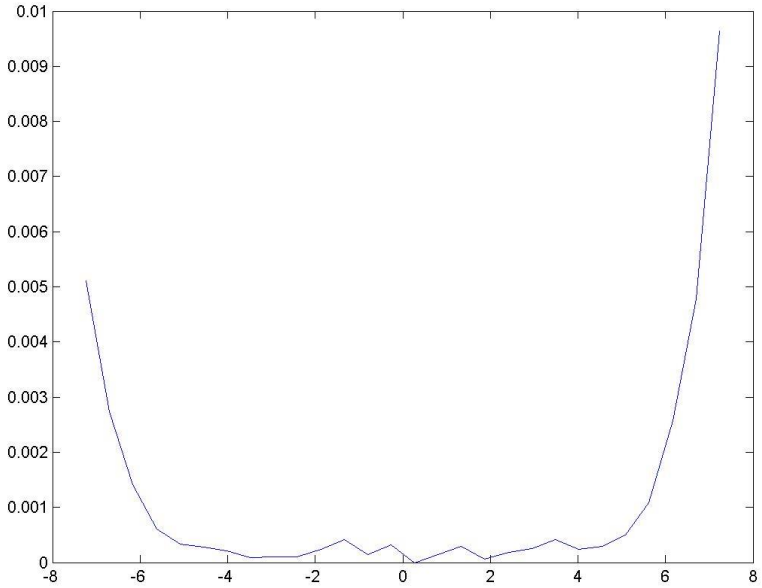

Figure C.157: Dose depth curve for (r,90,0), Design Q, double beam irradiation with a 90° rotation about the vertical axis.

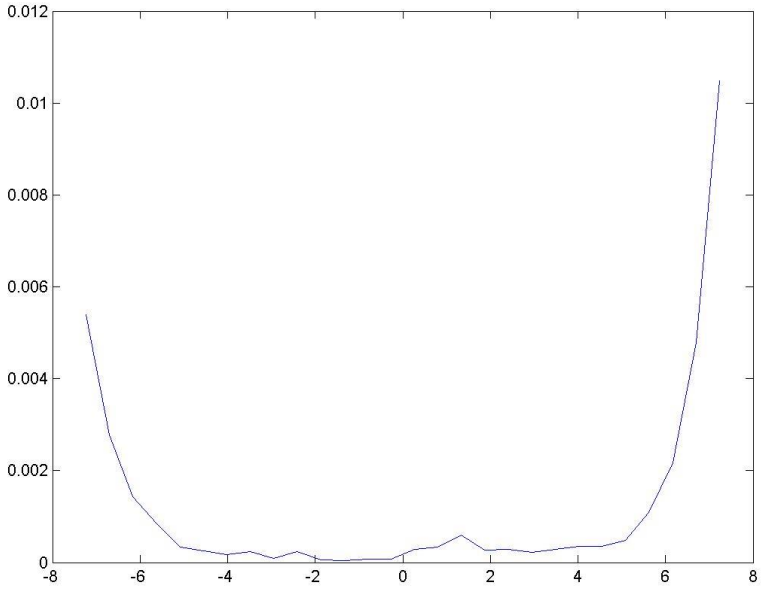

Figure C.158: Dose depth curve for (r,90,90), Design Q, double beam irradiation with a 90° rotation about the vertical axis.

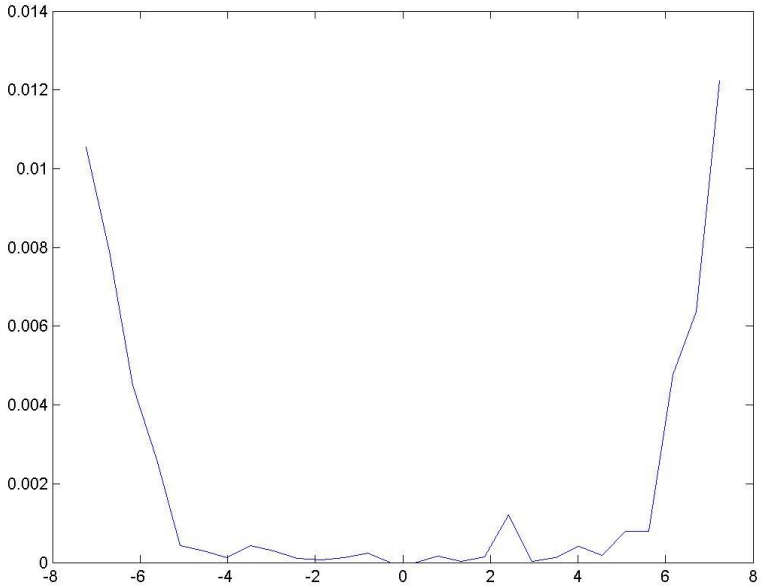

Figure C.159: Dose depth curve for (r, 0,0), Design Q, double beam irradiation with a 90° rotation about the vertical axis.

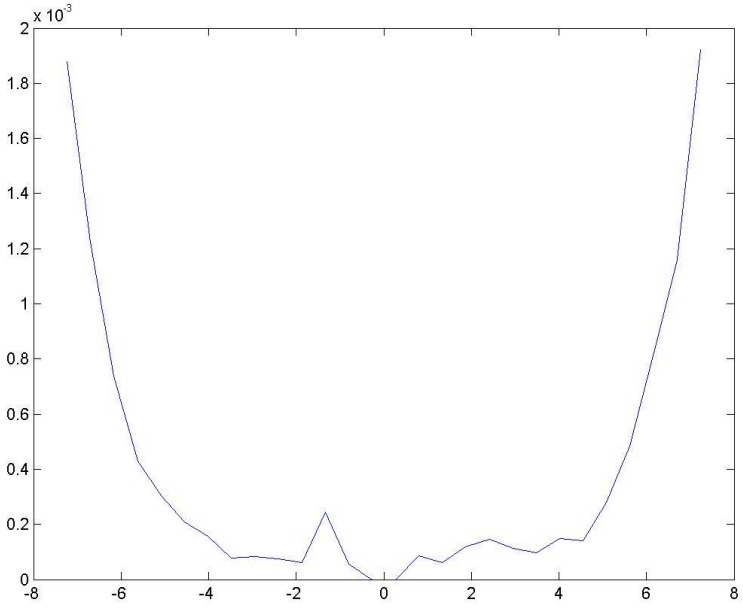

Figure C.160: Dose depth curve for (r,90,0), Design R, single beam irradiation.

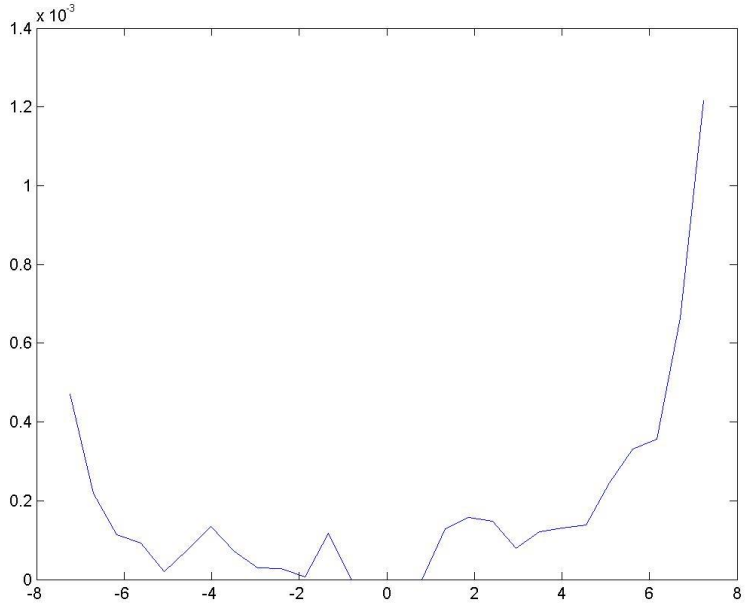

Figure C.161: Dose depth curve for (r,90,90), Design R, single beam irradiation.

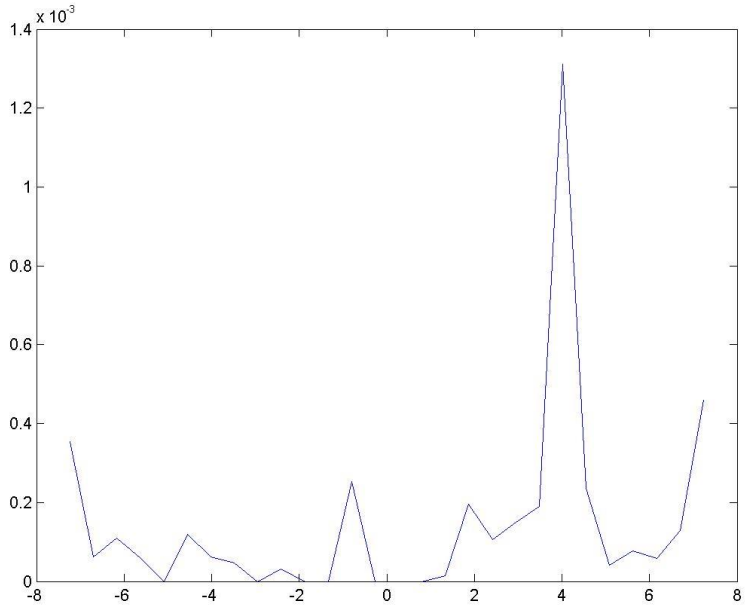

Figure C.162: Dose depth curve for (r, 0,0), Design R, single beam irradiation.

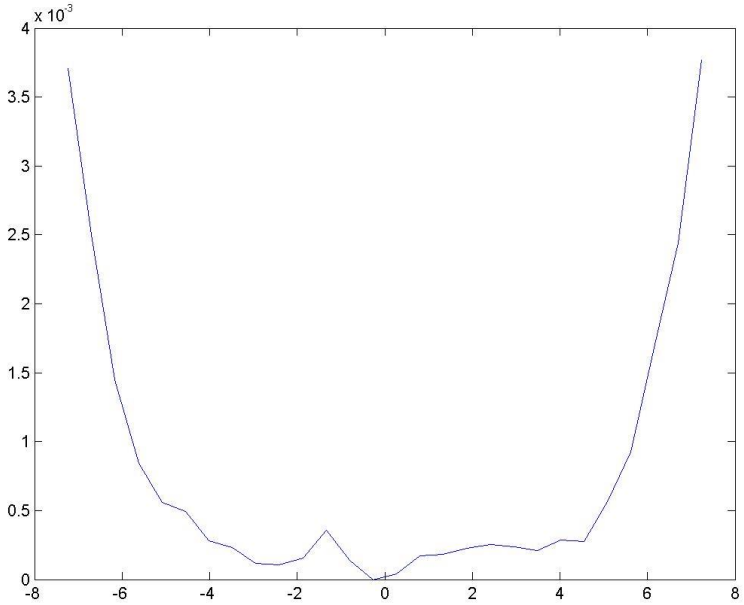

Figure C.163: Dose depth curve for (r,90,0), Design R, double beam irradiation.

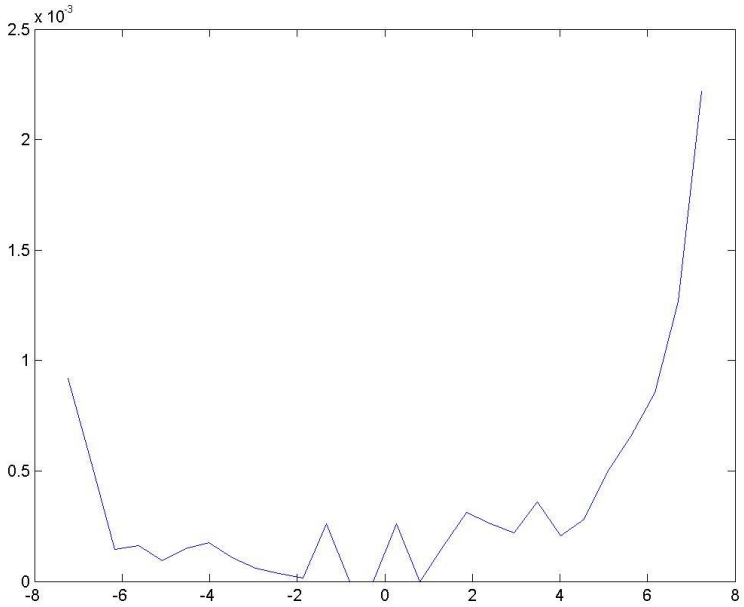

Figure C.164: Dose depth curve for (r,90,90), Design R, double beam irradiation.

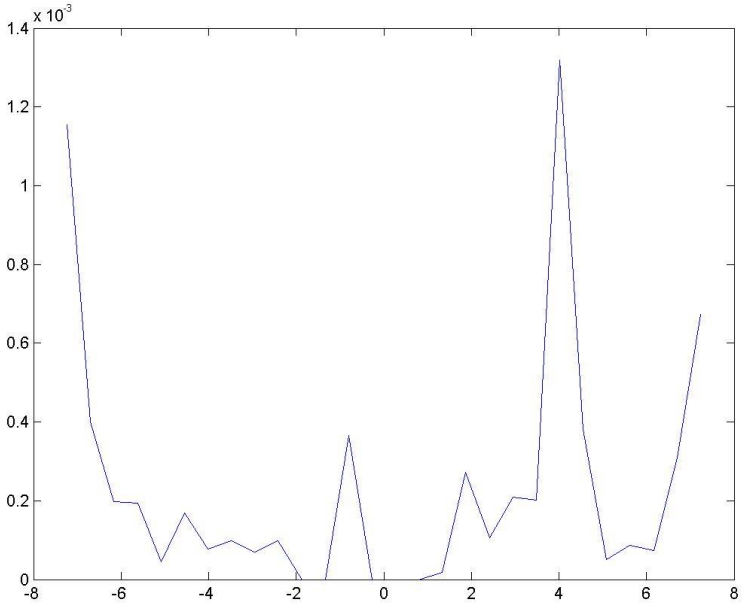

Figure C.165: Dose depth curve for (r, 0,0), Design R, double beam irradiation.

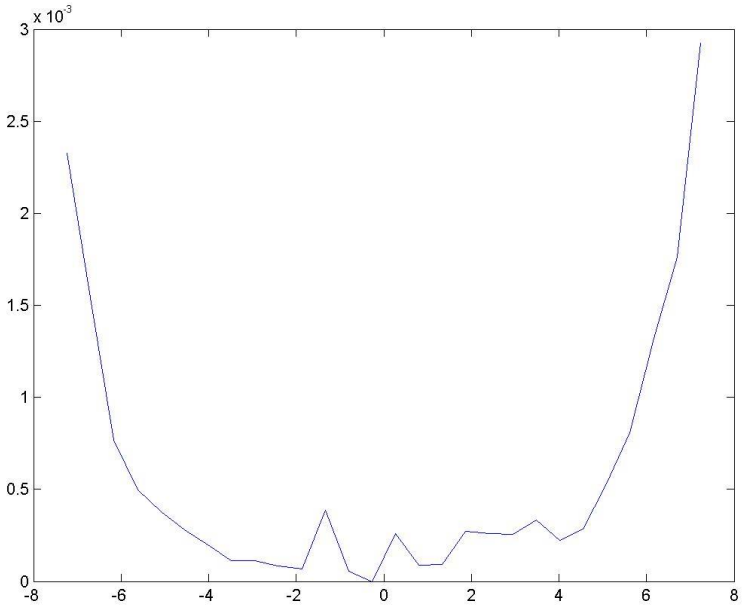

Figure C.166: Dose depth curve for (r,90,0), Design R, double beam irradiation with a 90° rotation about the vertical axis.

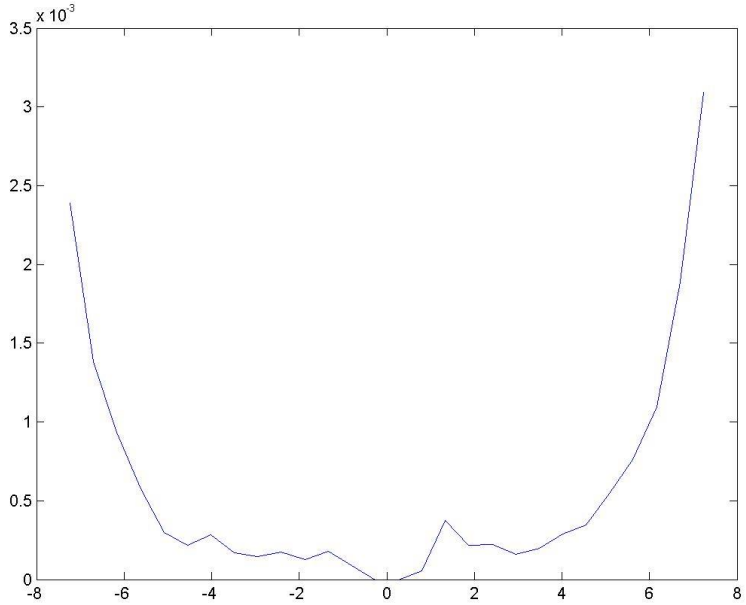

Figure C.167: Dose depth curve for (r,90,90), Design R, double beam irradiation with a 90° rotation about the vertical axis..

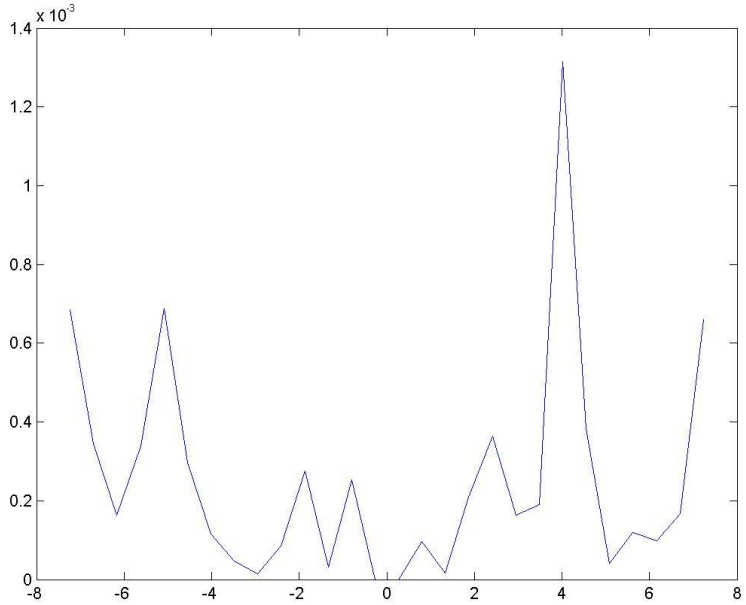

Figure C.168: Dose depth curve for (r, 0,0), Design R, double beam irradiation with a 90° rotation about the vertical axis.

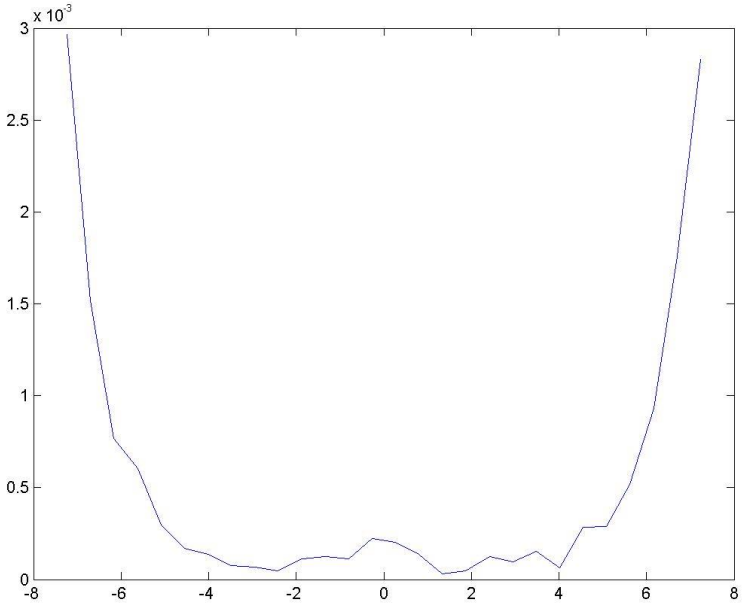

Figure C.169: Dose depth curve for (r,90,0), Design S, single beam irradiation.

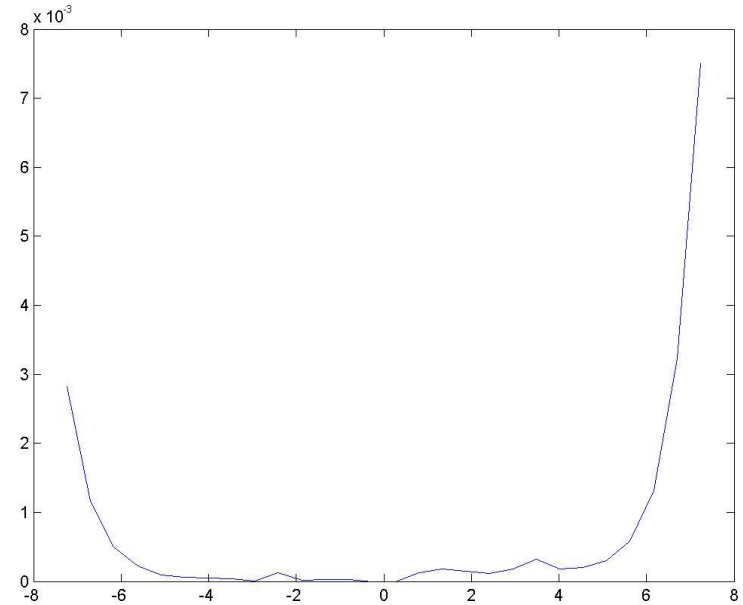

Figure C.170: Dose depth curve for (r,90,90), Design S, single beam irradiation.

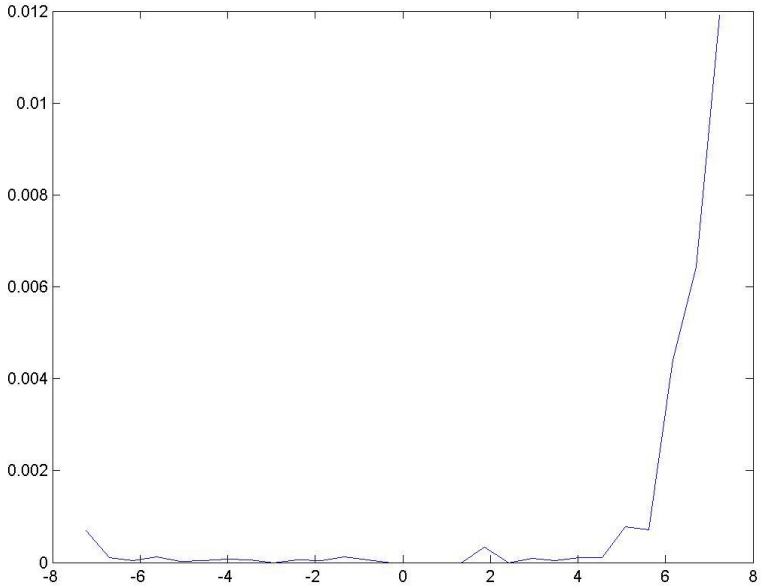

Figure C.171: Dose depth curve for (r, 0,0), Design S, single beam irradiation.

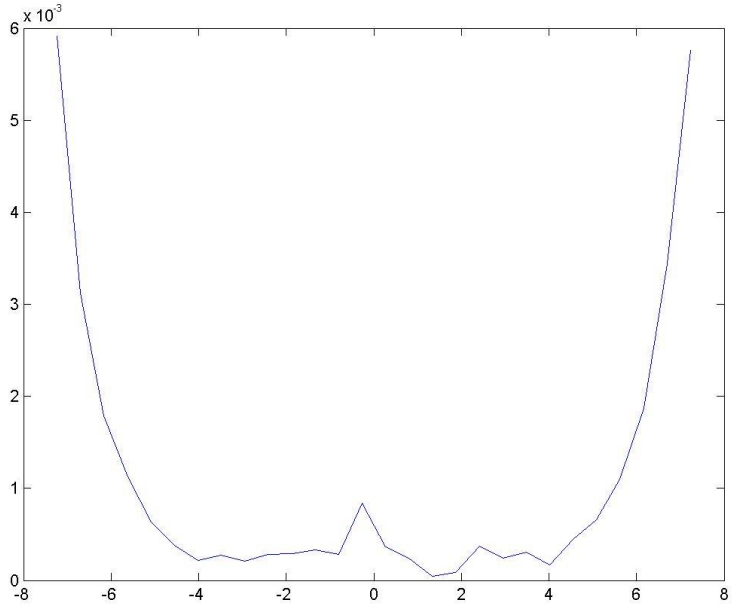

Figure C.172: Dose depth curve for (r,90,0), Design S, double beam irradiation.

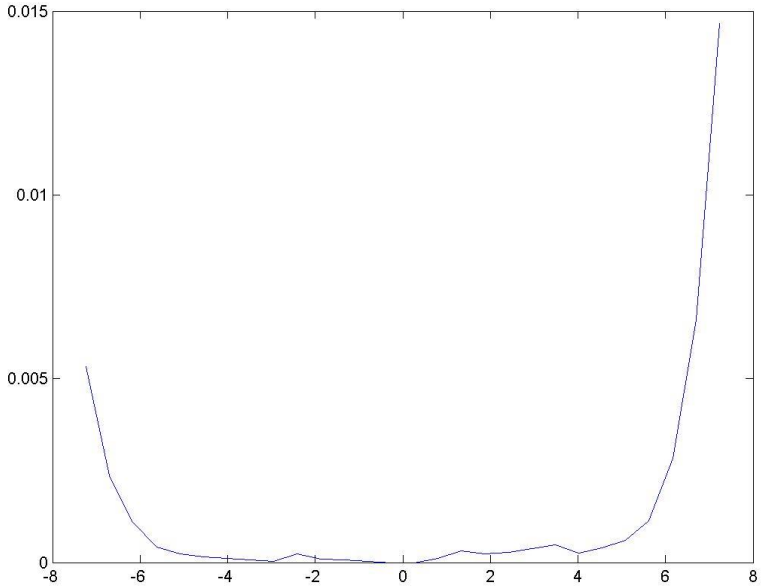

Figure C.173: Dose depth curve for (r,90,90), Design S, double beam irradiation.

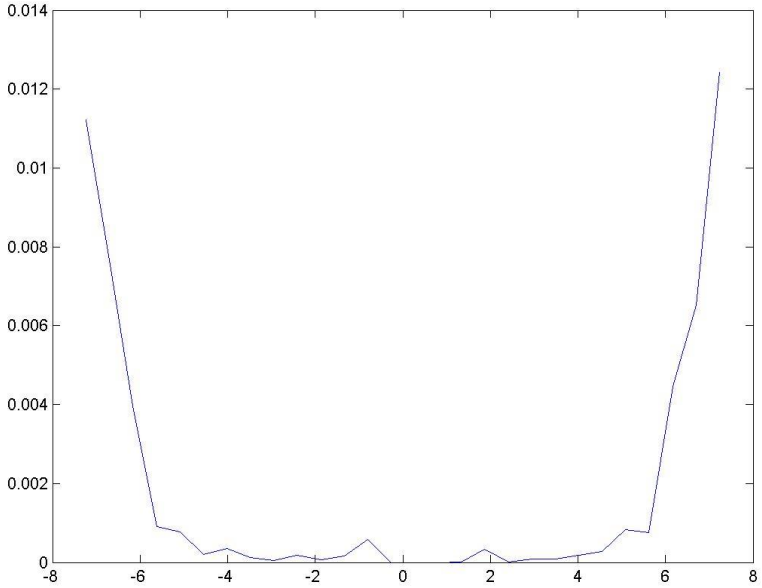

Figure C.174: Dose depth curve for (r, 0,0), Design S, double beam irradiation.

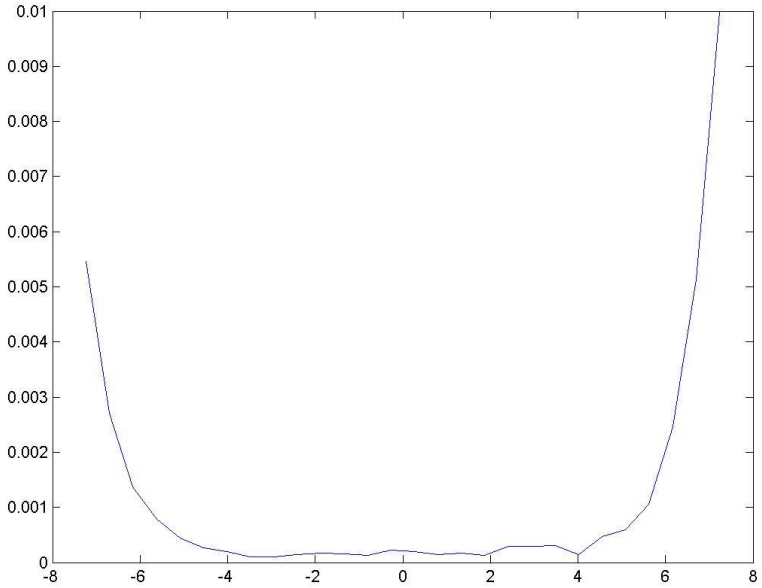

Figure C.175: Dose depth curve for (r,90,0), Design S, double beam irradiation with a 90° rotation about the vertical axis.

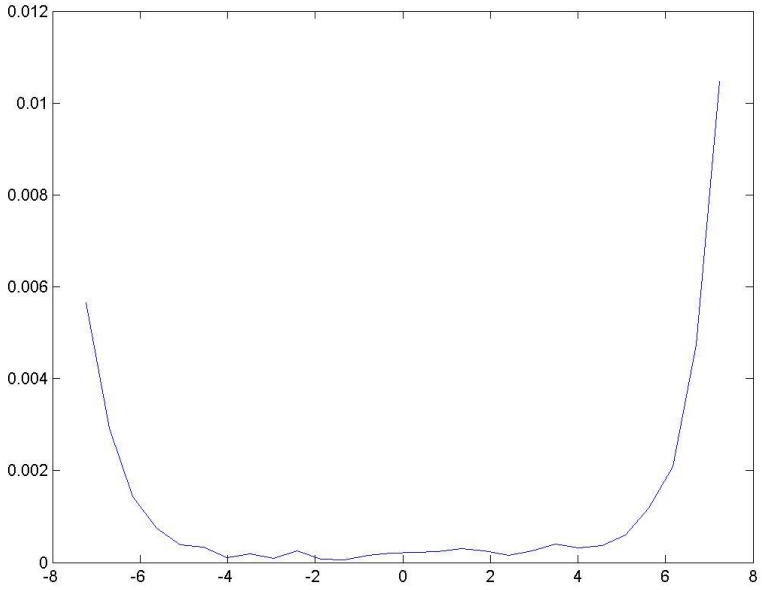

Figure C.176: Dose depth curve for (r,90,90), Design S, double beam irradiation with a 90° rotation about the vertical axis.

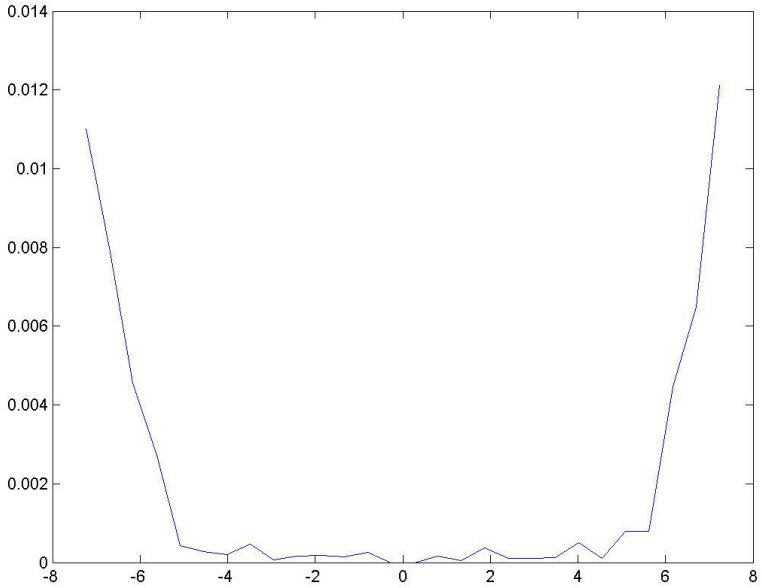

Figure C.177: Dose depth curve for (r, 0,0), Design S, double beam irradiation with a 90° rotation about the vertical axis.

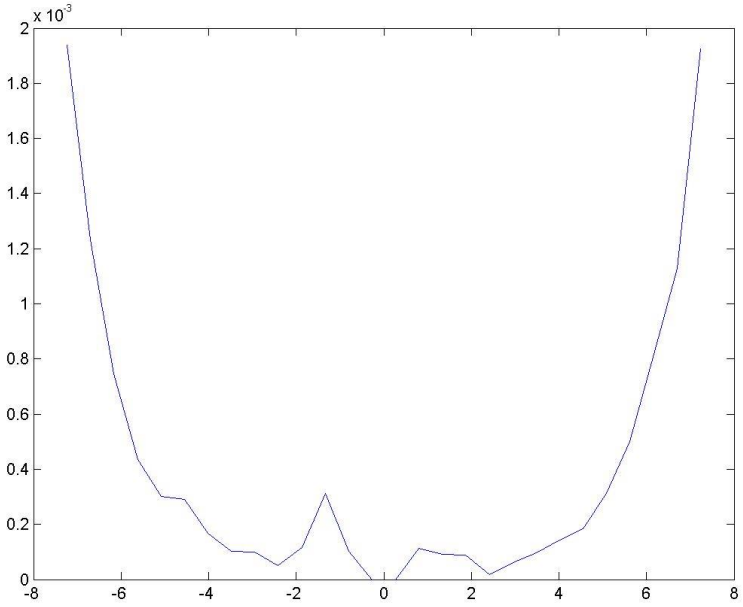

Figure C.178: Dose depth curve for (r,90,0), Design T, single beam irradiation.

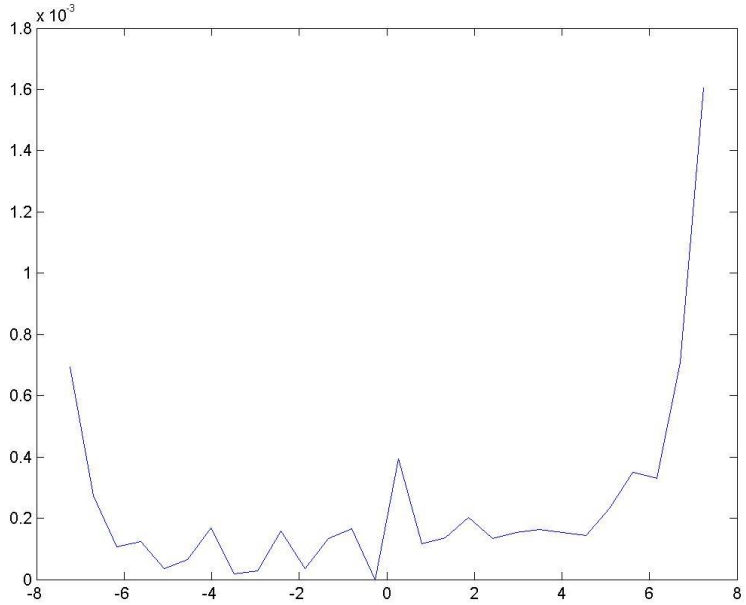

Figure C.179: Dose depth curve for (r,90,90), Design T, single beam irradiation.

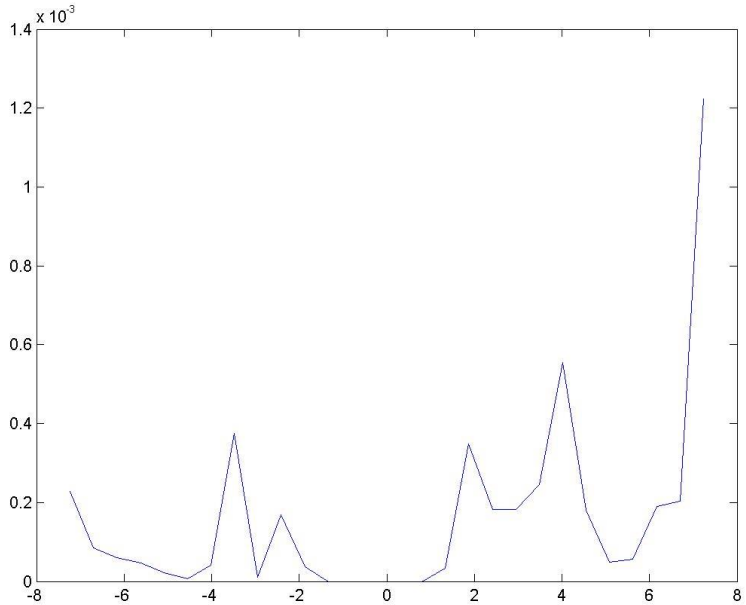

Figure C.180: Dose depth curve for (r, 0,0), Design T, single beam irradiation.

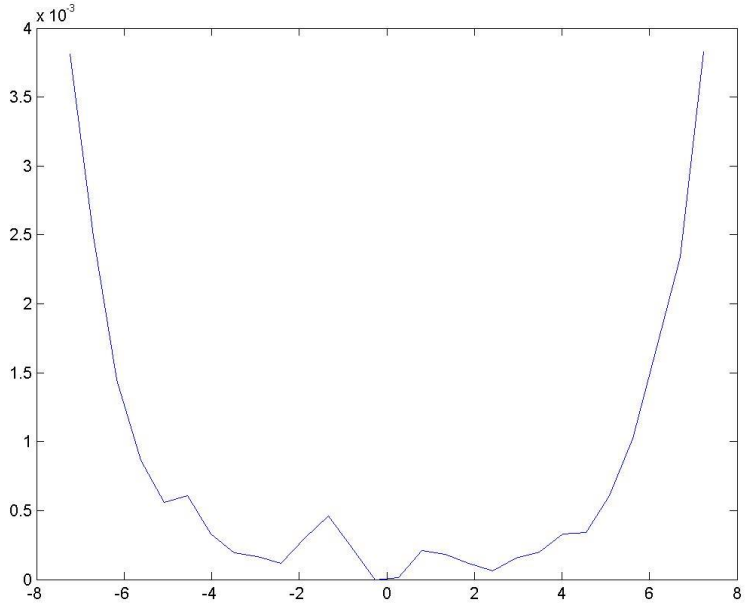

Figure C.181: Dose depth curve for (r,90,0), Design T, double beam irradiation.

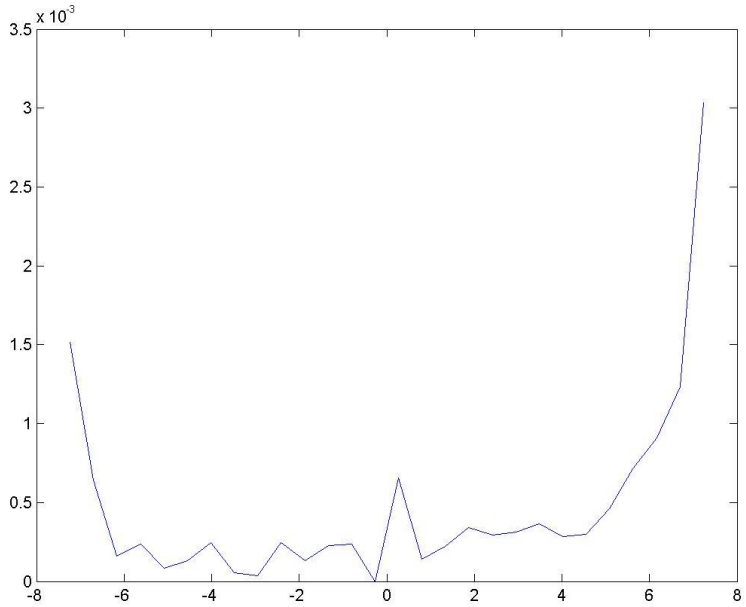

Figure C.182: Dose depth curve for (r,90,90), Design T, double beam irradiation.

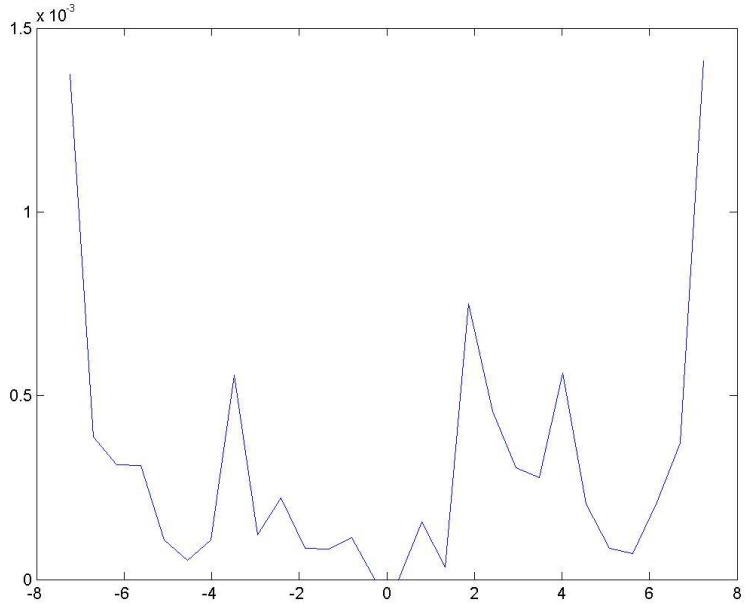

Figure C.183: Dose depth curve for (r, 0,0), Design T, double beam irradiation.

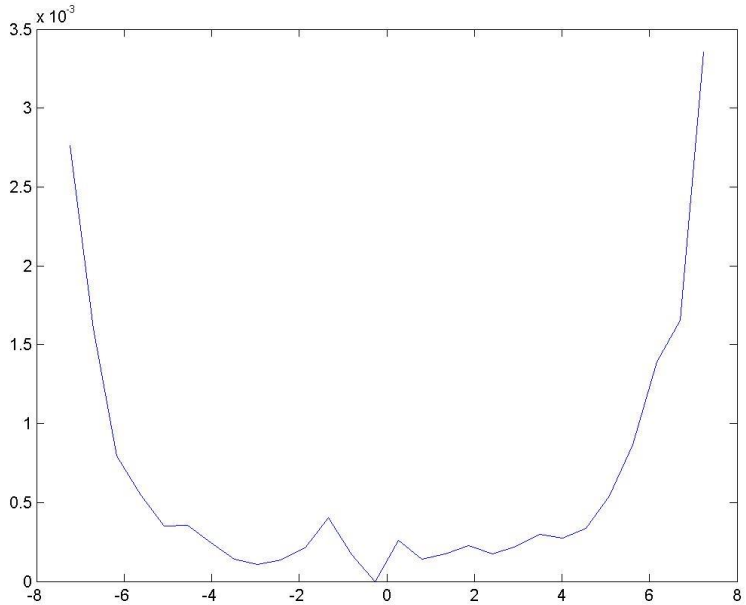

Figure C.184: Dose depth curve for (r,90,0), Design T, double beam irradiation with a 90° rotation about the vertical axis.

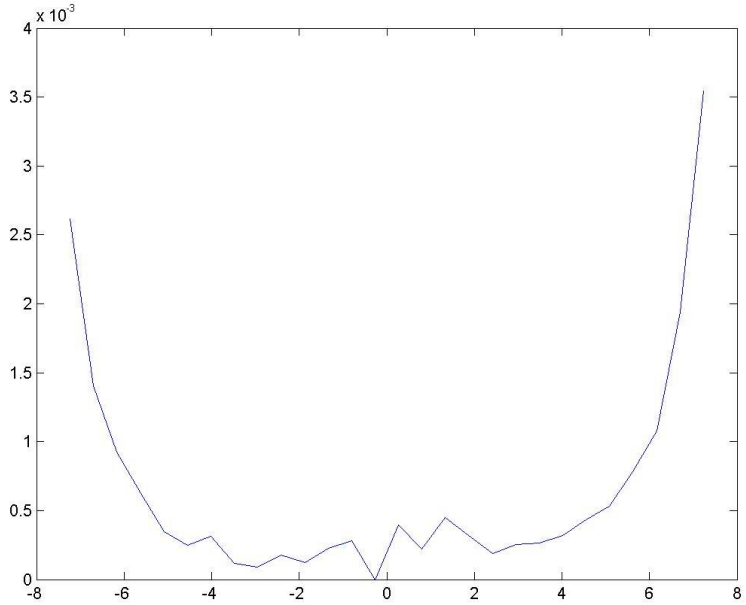

Figure C.185: Dose depth curve for (r,90,90), Design T, double beam irradiation with a 90° rotation about the vertical axis..

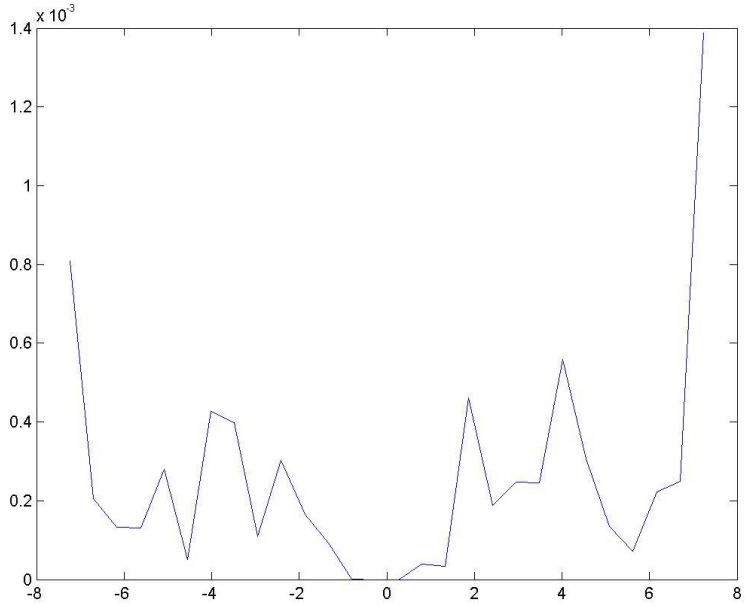

Figure C.186: Dose depth curve for (r, 0,0), Design T, double beam irradiation with a 90° rotation about the vertical axis.

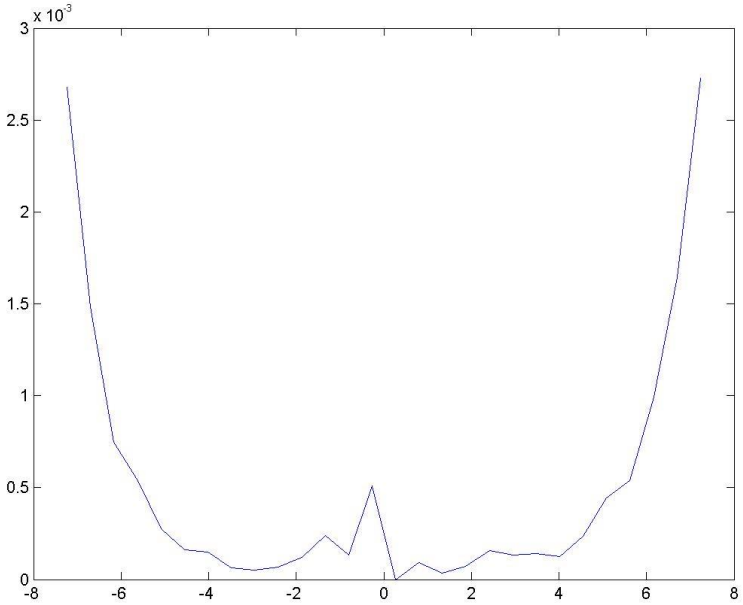

Figure C.187: Dose depth curve for (r,90,0), Design U, single beam irradiation.

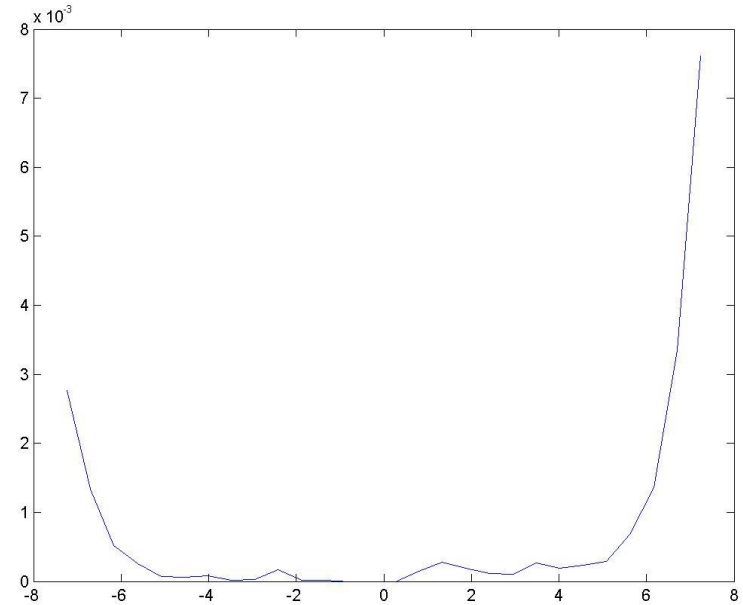

Figure C.188: Dose depth curve for (r,90,90), Design U, single beam irradiation.

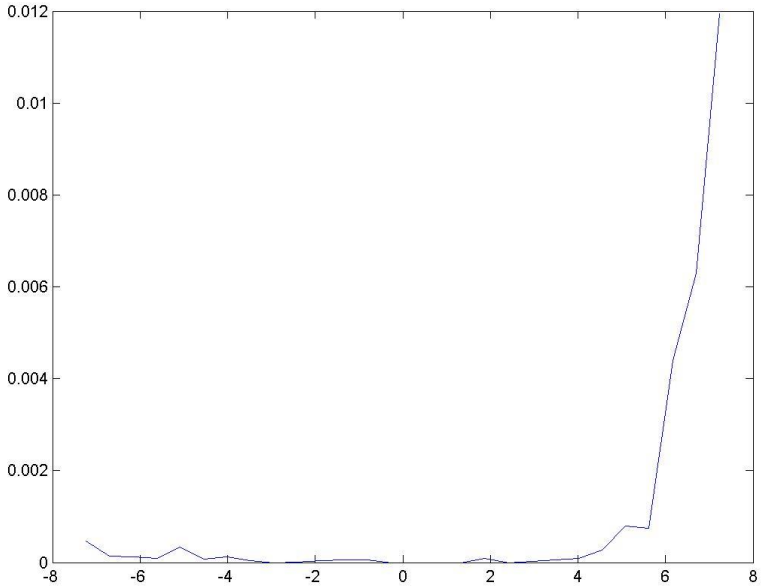

Figure C.189: Dose depth curve for (r, 0,0), Design U, single beam irradiation.

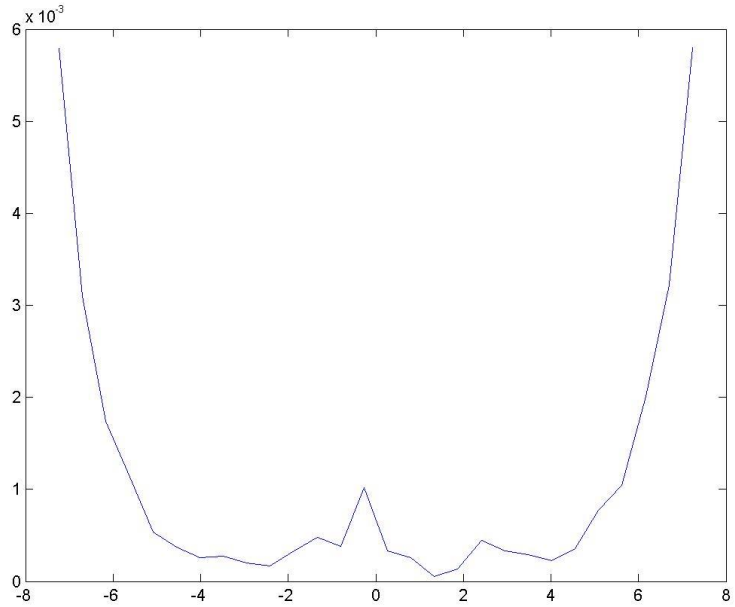

Figure C.190: Dose depth curve for (r,90,0), Design U, double beam irradiation.

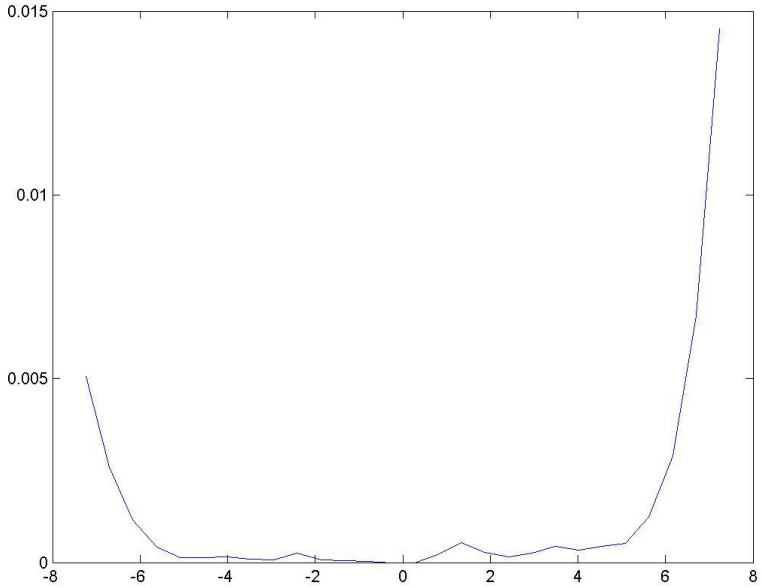

Figure C.191: Dose depth curve for (r,90,90), Design U, double beam irradiation.

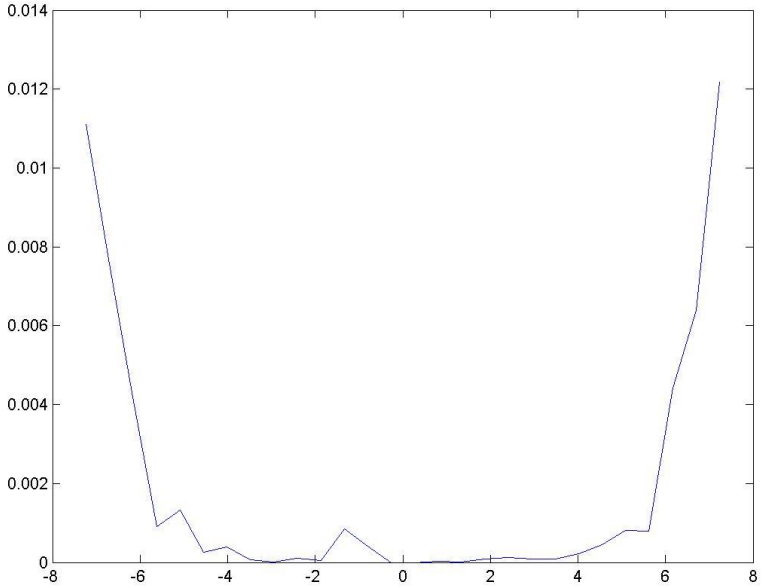

Figure C.192: Dose depth curve for (r, 0,0), Design U, double beam irradiation.

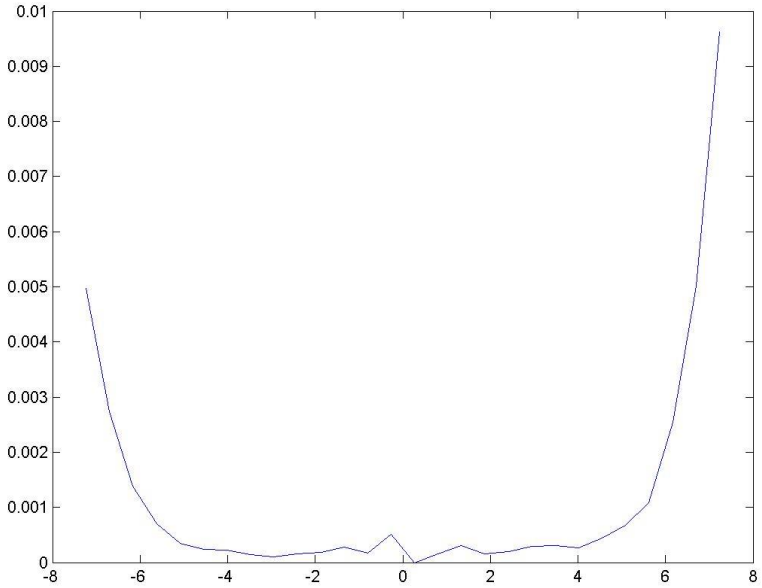

Figure C.193: Dose depth curve for (r,90,0), Design U, double beam irradiation with a 90° rotation about the vertical axis.

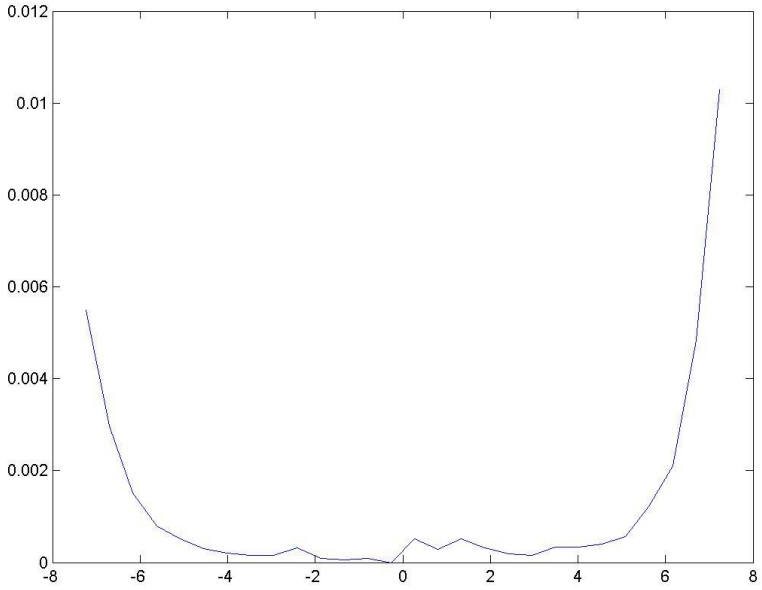

Figure C.194: Dose depth curve for (r,90,90), Design U, double beam irradiation with a 90° rotation about the vertical axis.

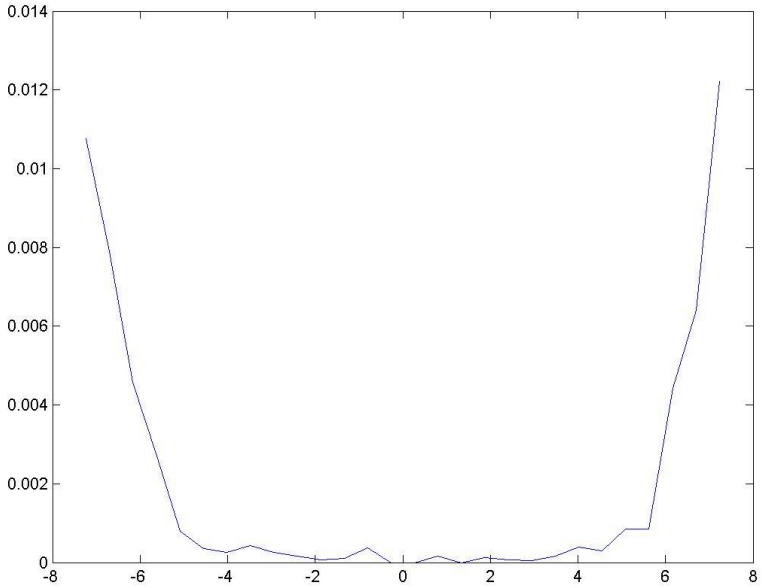

Figure C.195: Dose depth curve for (r, 0,0), Design U, double beam irradiation with a 90° rotation about the vertical axis.

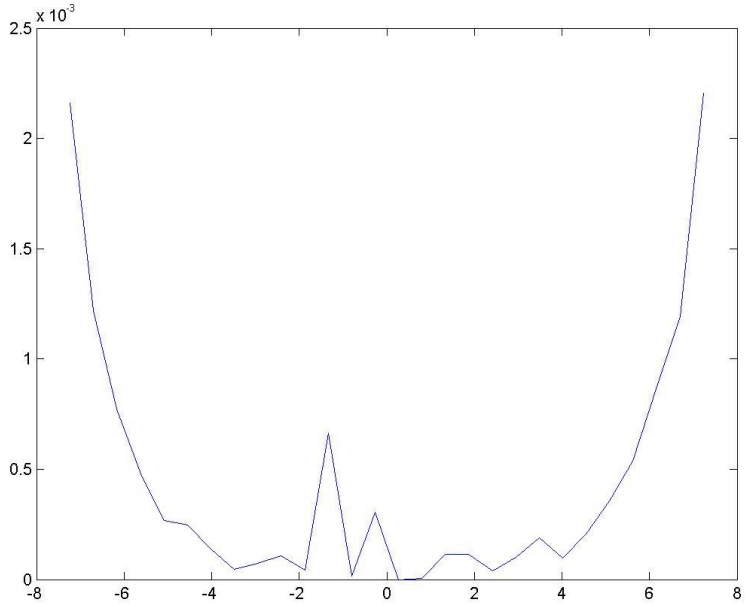

Figure C.196: Dose depth curve for (r,90,0), Design V, single beam irradiation.

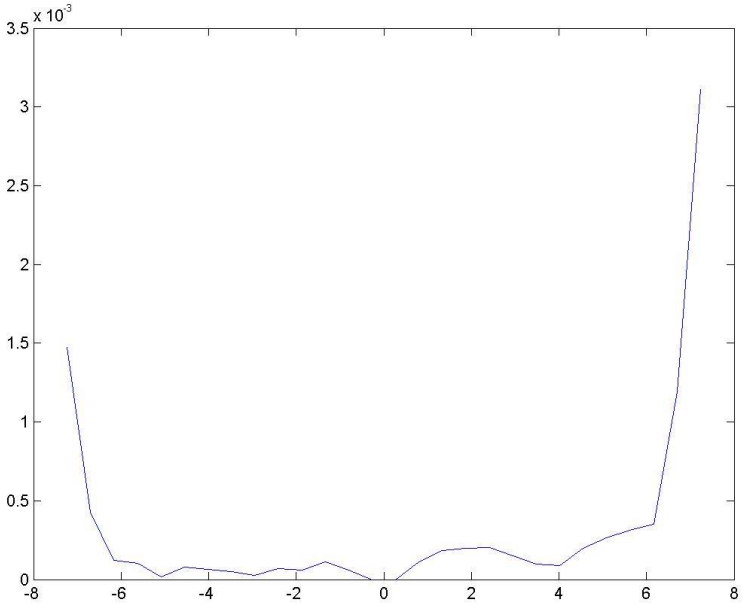

Figure C.197: Dose depth curve for (r,90,90), Design V, single beam irradiation.

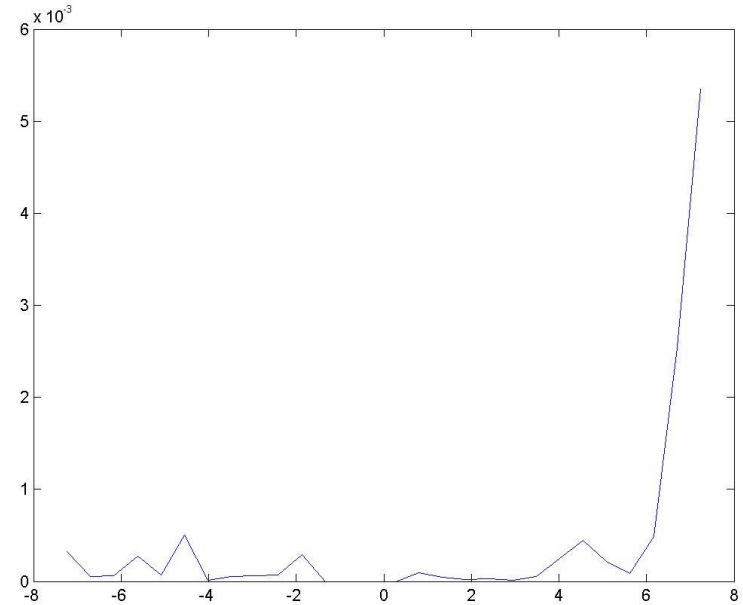

Figure C.198: Dose depth curve for (r, 0,0), Design V, single beam irradiation.

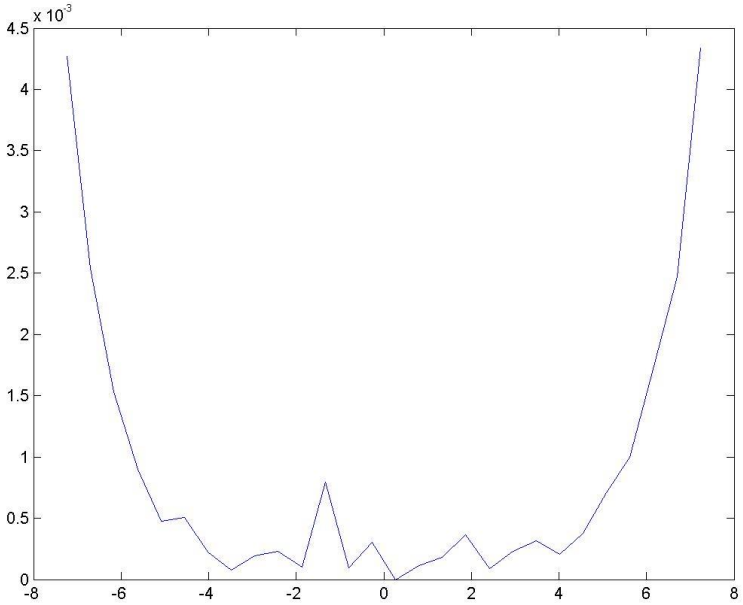

Figure C.199: Dose depth curve for (r,90,0), Design V, double beam irradiation.

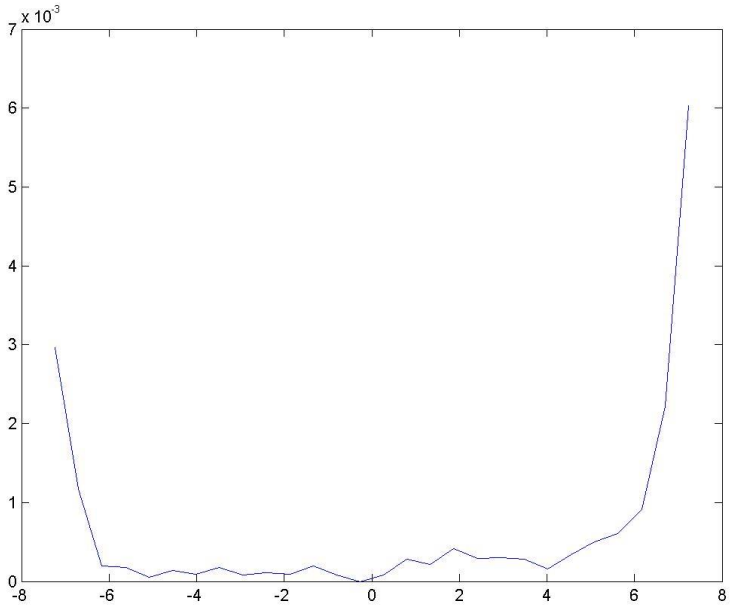

Figure C.200: Dose depth curve for (r,90,90), Design V, double beam irradiation.

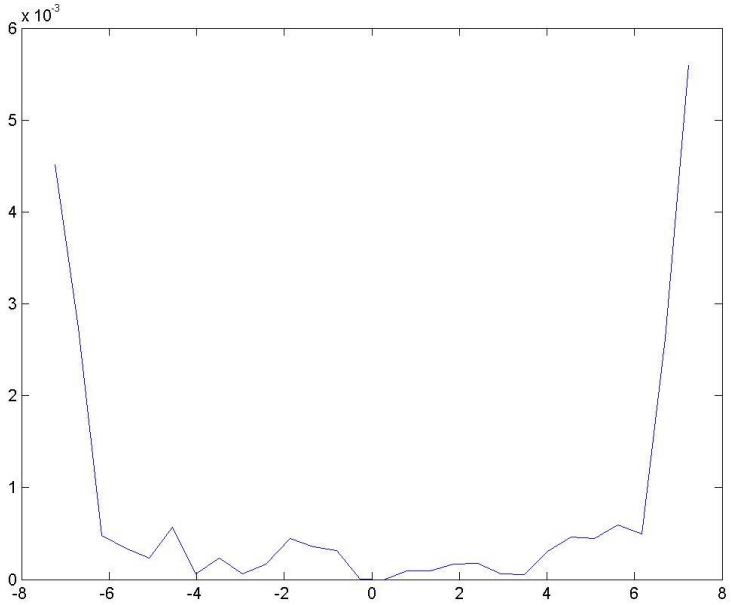

Figure C.201: Dose depth curve for (r, 0,0), Design V, double beam irradiation.

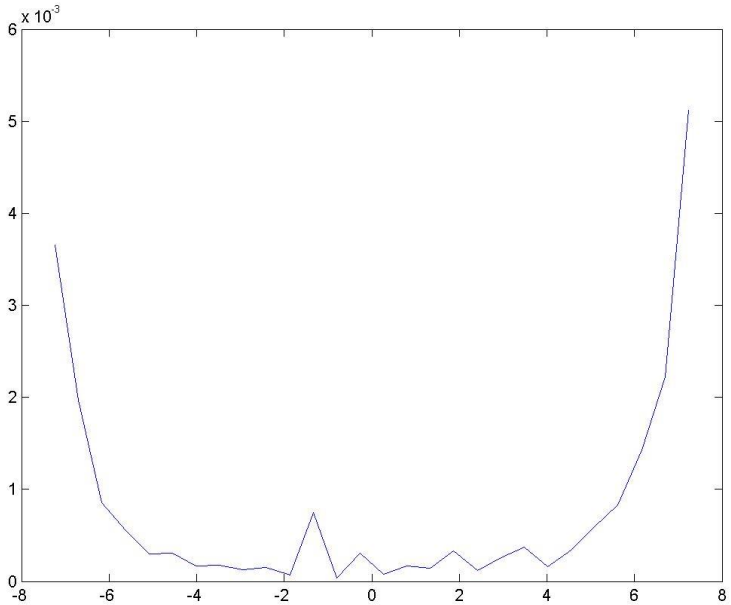

Figure C.202: Dose depth curve for (r,90,0), Design V, double beam irradiation with a 90° rotation about the vertical axis.

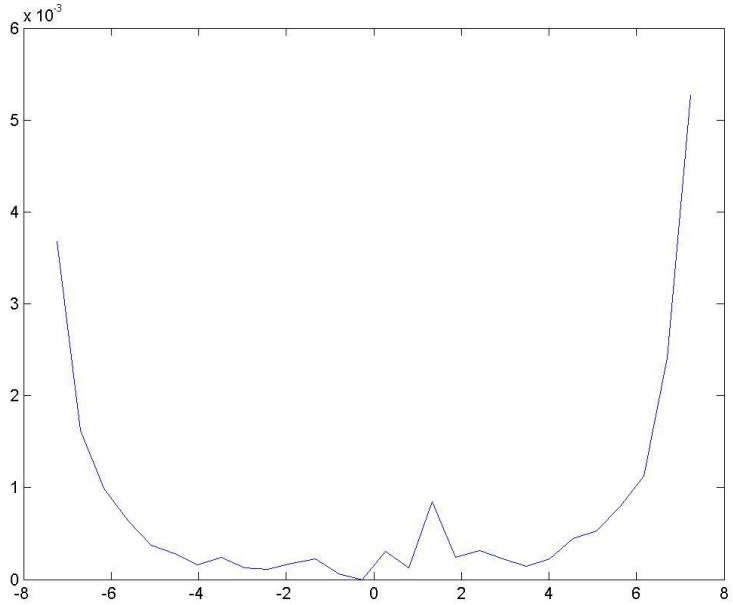

Figure C.203: Dose depth curve for (r,90,90), Design V, double beam irradiation with a 90° rotation about the vertical axis..

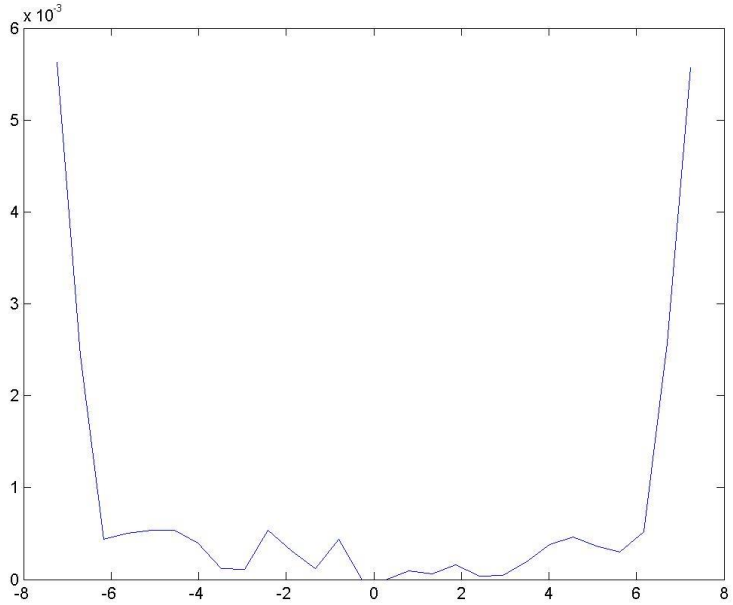

Figure C.204: Dose depth curve for (r, 0,0), Design V, double beam irradiation with a 90° rotation about the vertical axis.

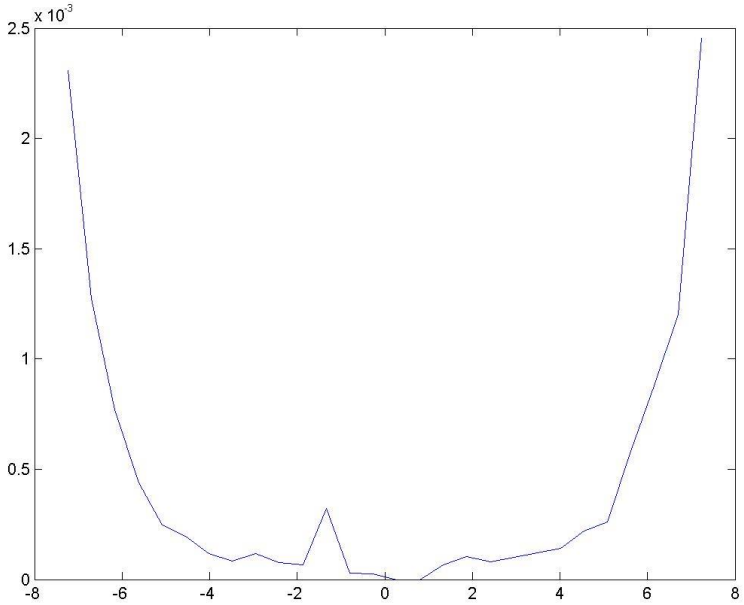

Figure C.205: Dose depth curve for (r,90,0), Design W, single beam irradiation.

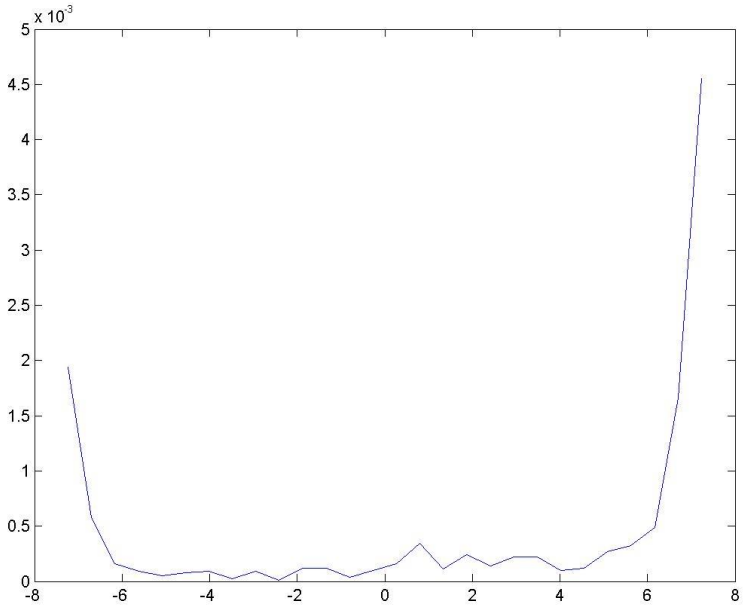

Figure C.206: Dose depth curve for (r,90,90), Design W, single beam irradiation.

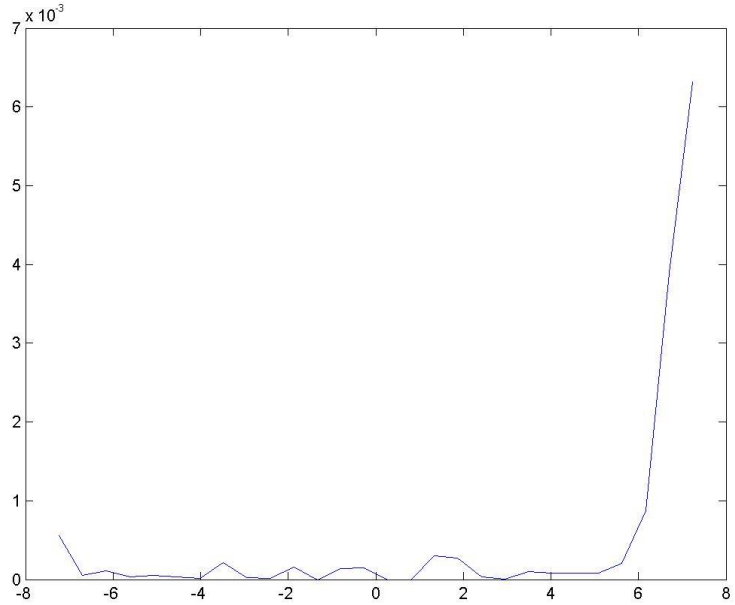

Figure C.207: Dose depth curve for (r, 0,0), Design W, single beam irradiation.

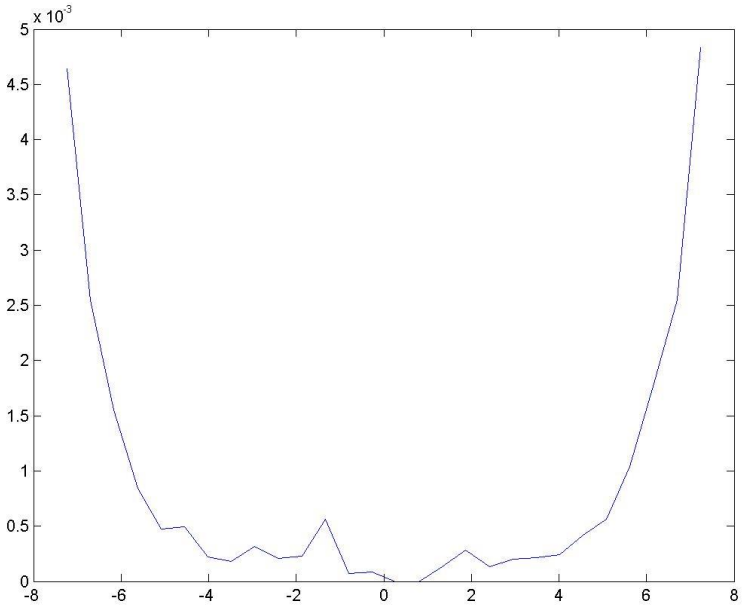

Figure C.208: Dose depth curve for (r,90,0), Design W, double beam irradiation.

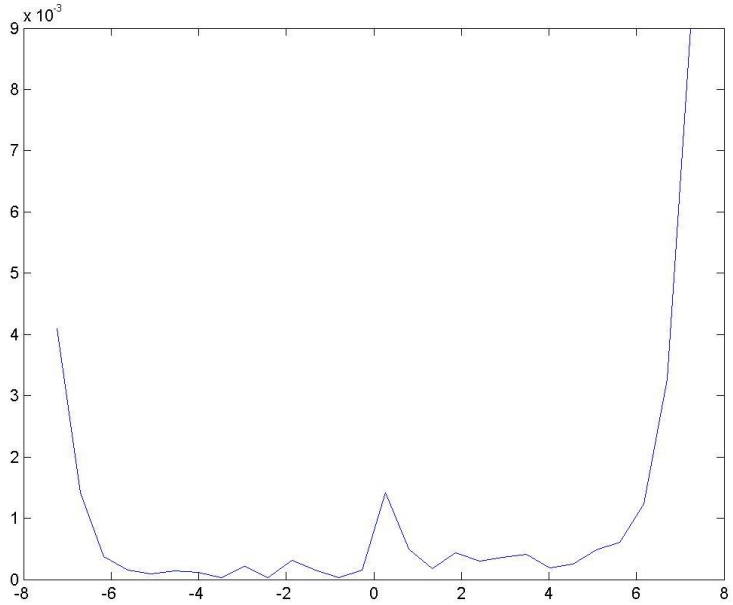

Figure C.209: Dose depth curve for (r,90,90), Design W, double beam irradiation.

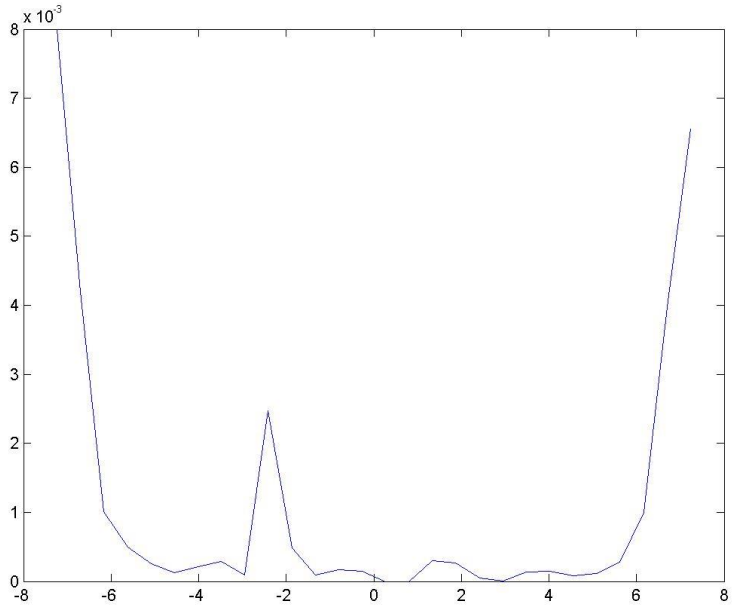

Figure C.210: Dose depth curve for (r, 0,0), Design W, double beam irradiation.

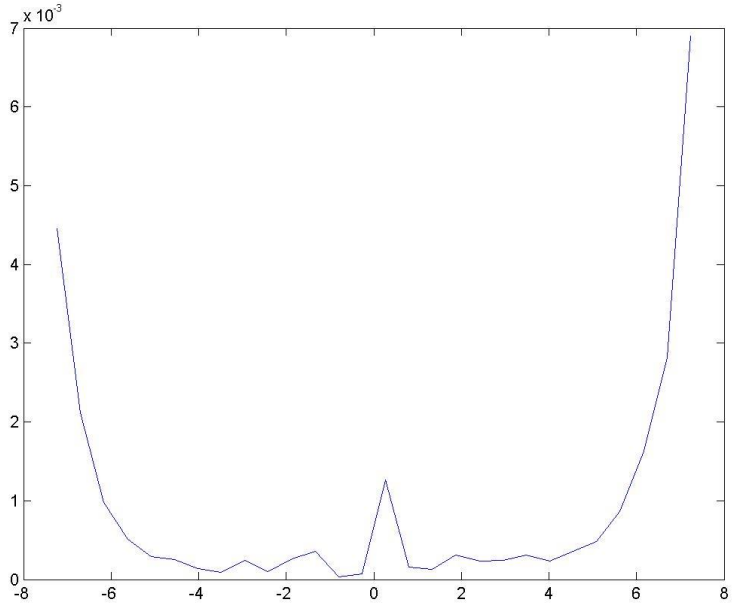

Figure C.211: Dose depth curve for (r,90,0), Design W, double beam irradiation with a 90° rotation about the vertical axis.

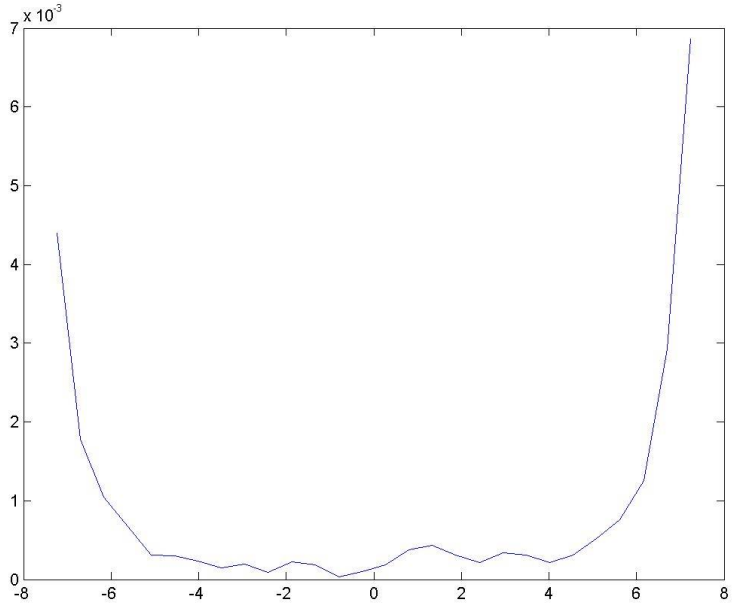

Figure C.212: Dose depth curve for (r,90,90), Design W, double beam irradiation with a 90° rotation about the vertical axis.

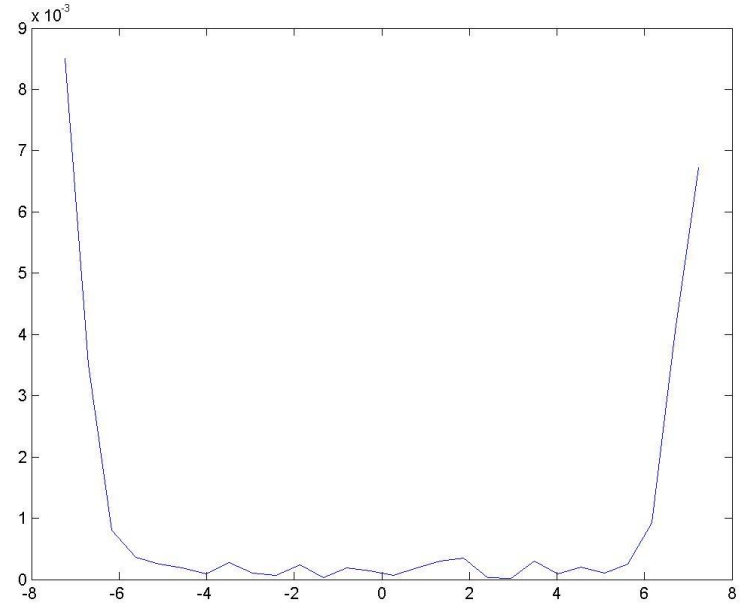

Figure C.213: Dose depth curve for (r, 0,0), Design W, double beam irradiation with a 90° rotation about the vertical axis.

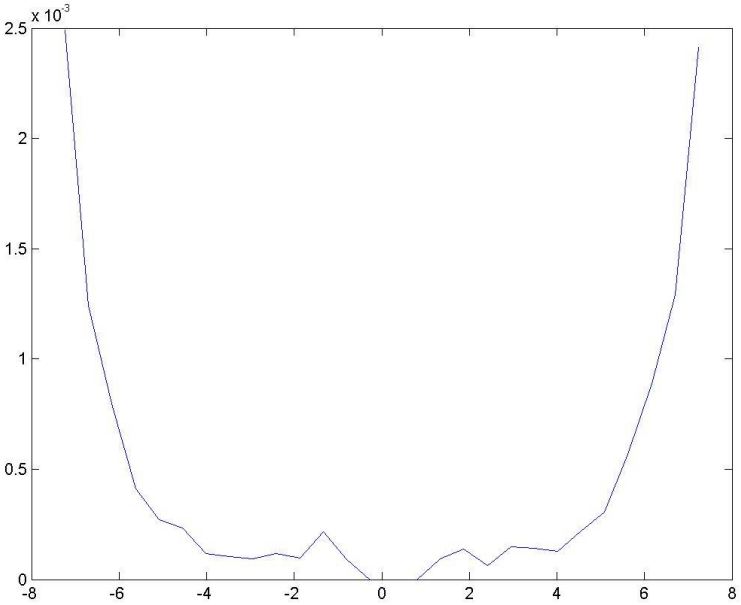

Figure C.214: Dose depth curve for (r, 90,0), Design X, single beam irradiation.

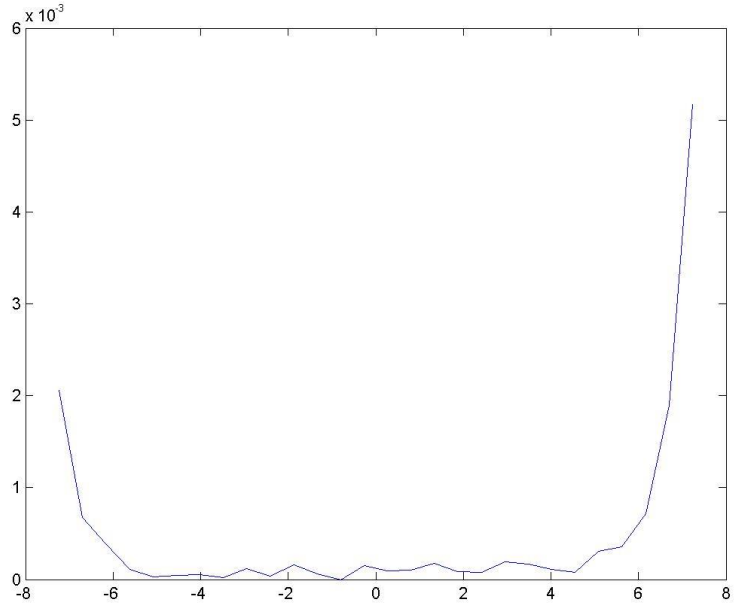

Figure C.215: Dose depth curve for (r,90,90), Design X, single beam irradiation.

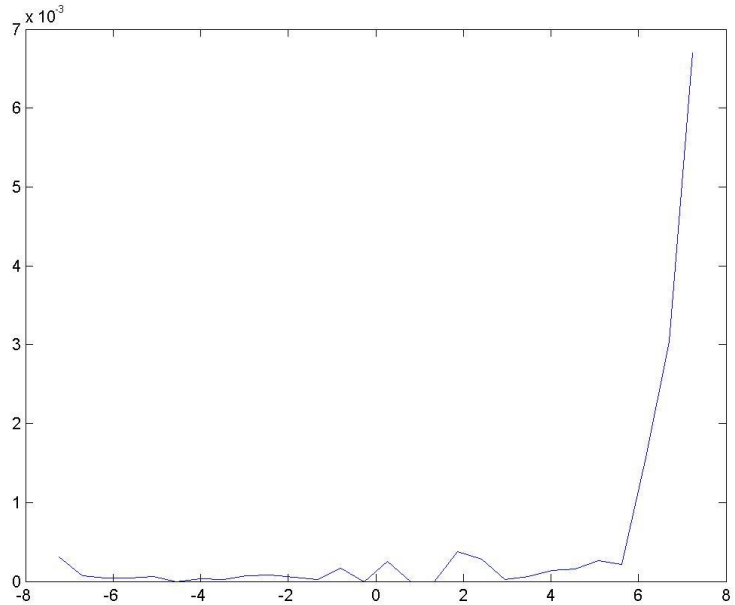

Figure C.216: Dose depth curve for (r,0,0), Design X, single beam irradiation.

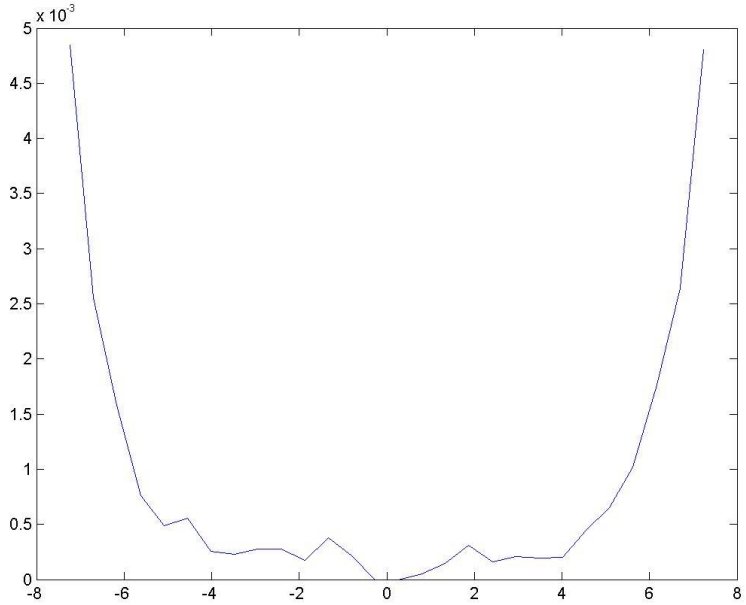

Figure C.217: Dose depth curve for (r, 90,0), Design X, double beam irradiation.

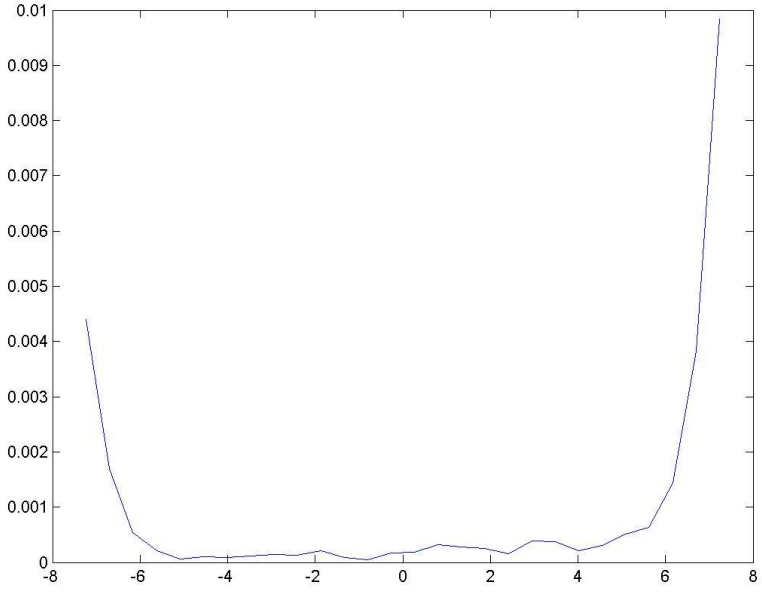

Figure C.218: Dose depth curve for (r,90,90), Design X, double beam irradiation.

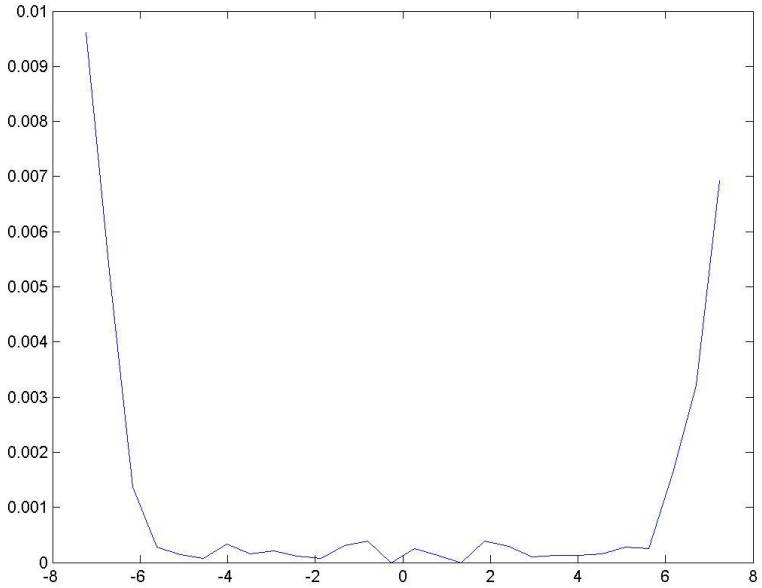

Figure C.219: Dose depth curve for (r,0,0), Design X, double beam irradiation.

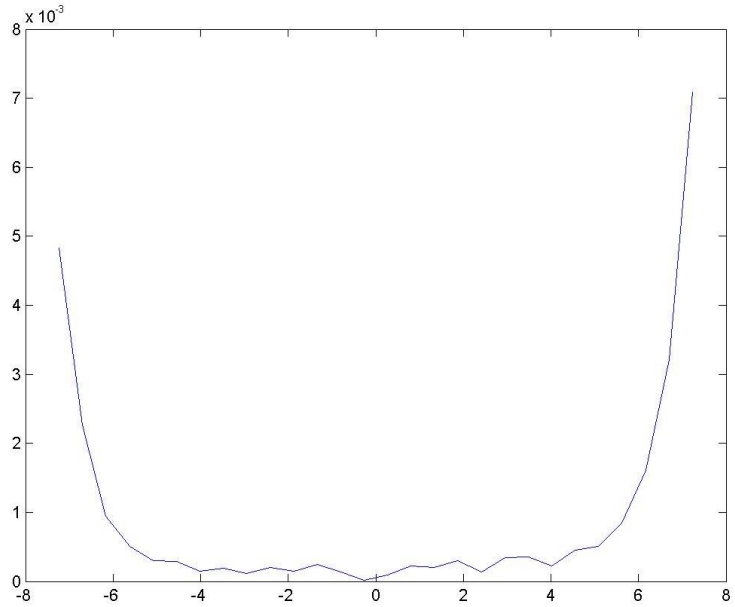

Figure C.220: Dose depth curve for (r, 90,0), Design X, double beam irradiation with a 90° rotation about the vertical axis.

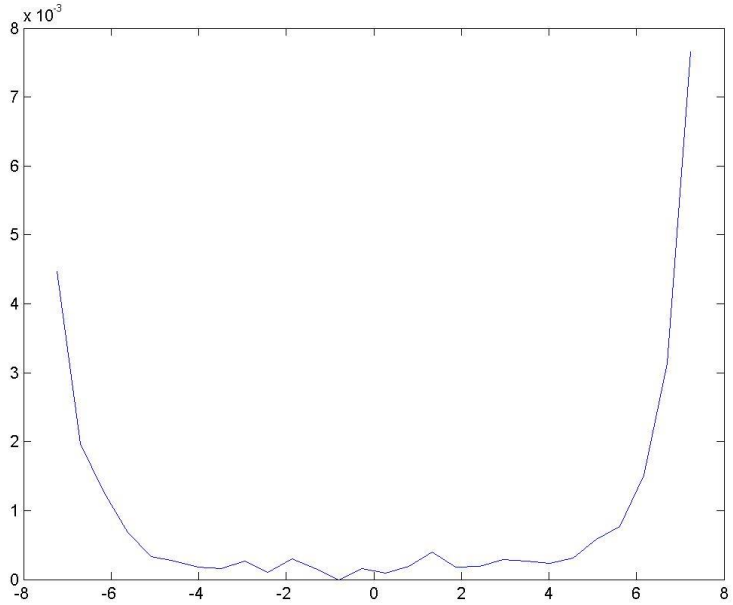

Figure C.221: Dose depth curve for (r,90,90), Design X, double beam irradiation with a 90° rotation about the vertical axis.

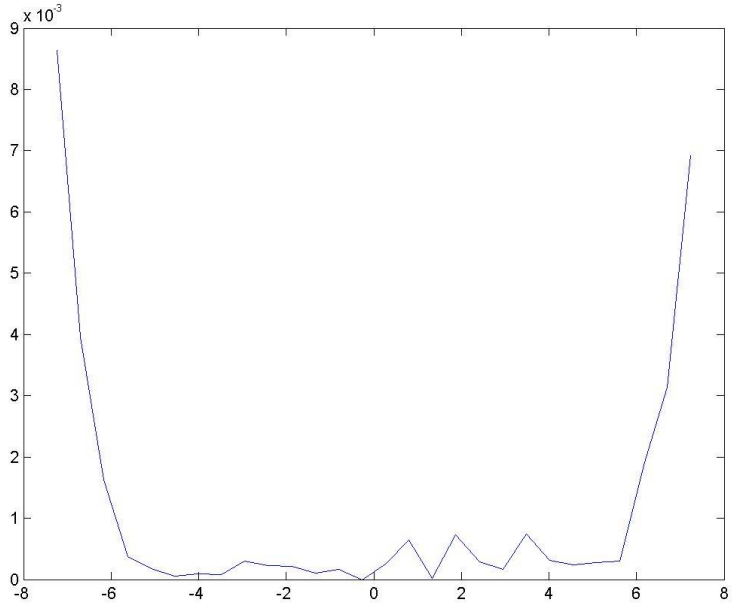

Figure C.222: Dose depth curve for (r,0,0), Design X, double beam irradiation with a 90° rotation about the vertical axis.

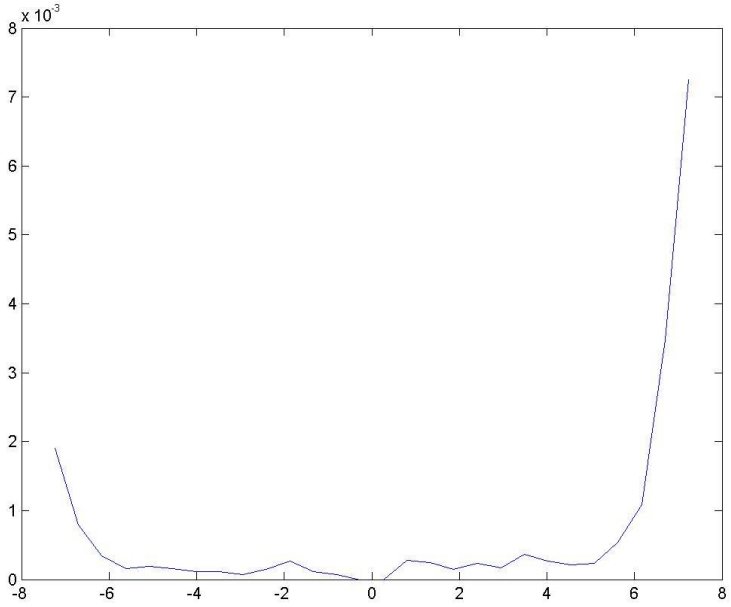

Figure C.223: Dose depth curve for (r,45,0), Design X, double beam irradiation with a 90° rotation about the vertical axis.

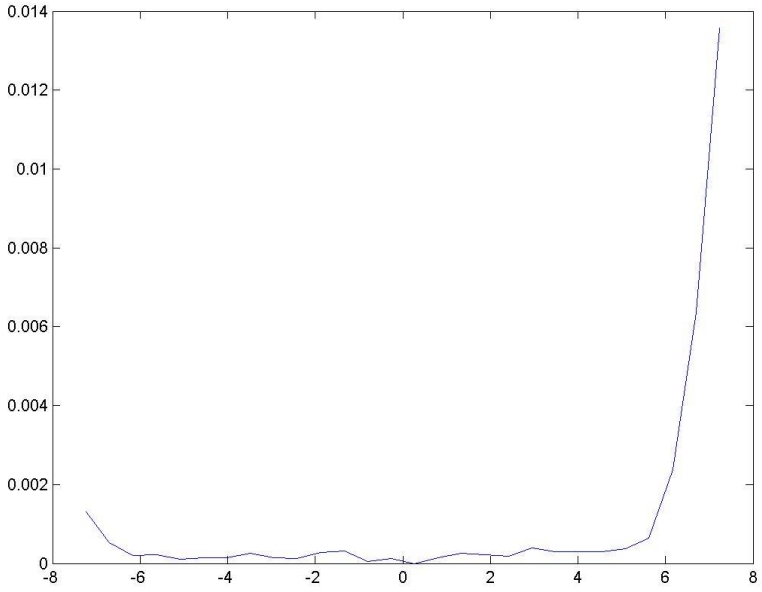

Figure C.224: Dose depth curve for (r,45,45), Design X, double beam irradiation with a 90° rotation about the vertical axis.

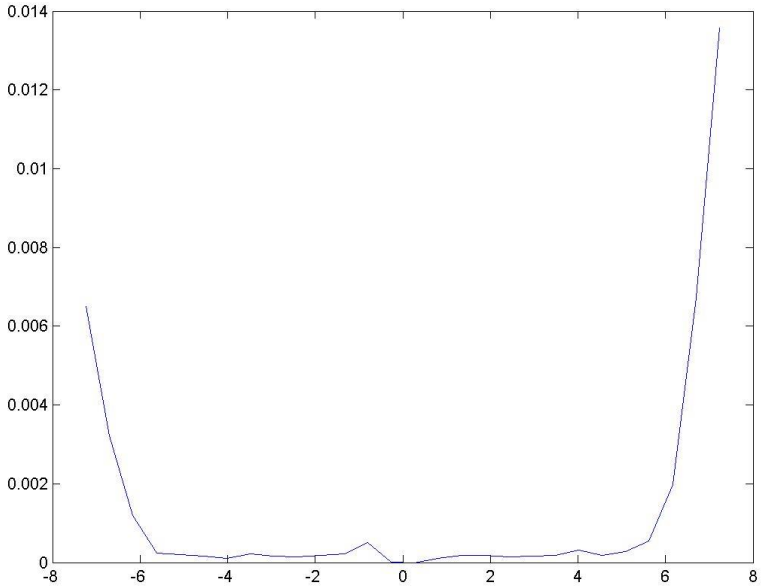

Figure C.225: Dose depth curve for (r,45,90), Design X, double beam irradiation with a 90° rotation about the vertical axis.

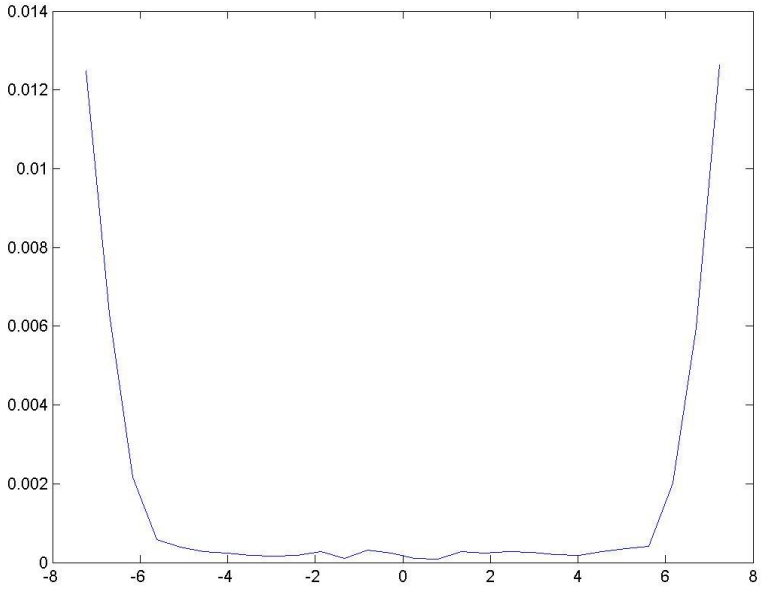

Figure C.226: Dose depth curve for (r,45,135), Design X, double beam irradiation with a 90° rotation about the vertical axis.

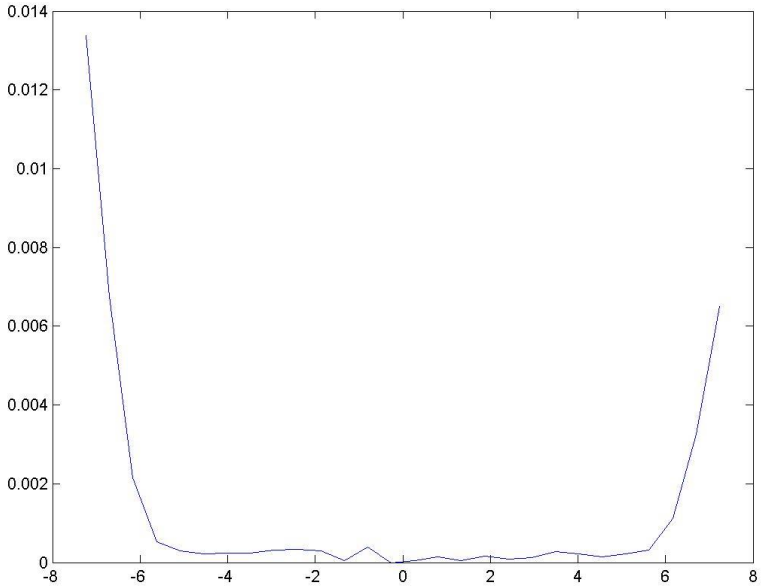

Figure C.227: Dose depth curve for (r,45,180), Design X, double beam irradiation with a 90° rotation about the vertical axis.

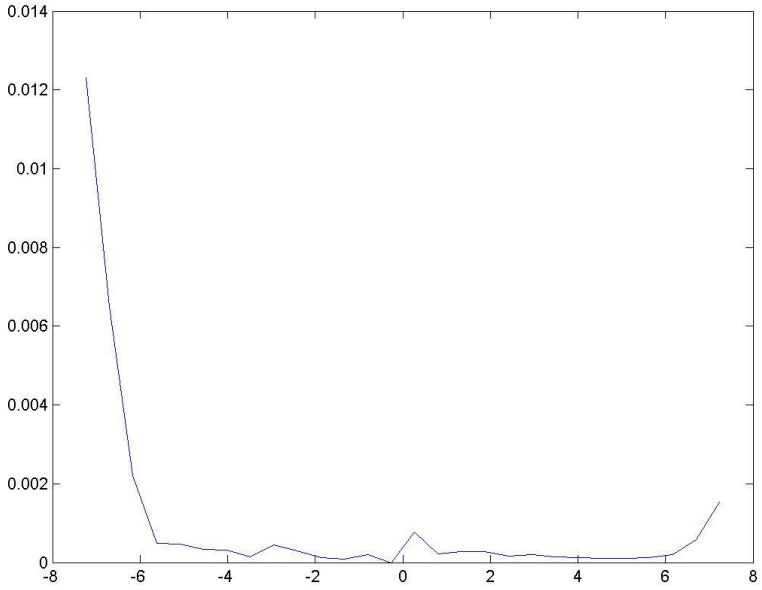

Figure C.228: Dose depth curve for (r,45,225), Design X, double beam irradiation with a 90° rotation about the vertical axis.

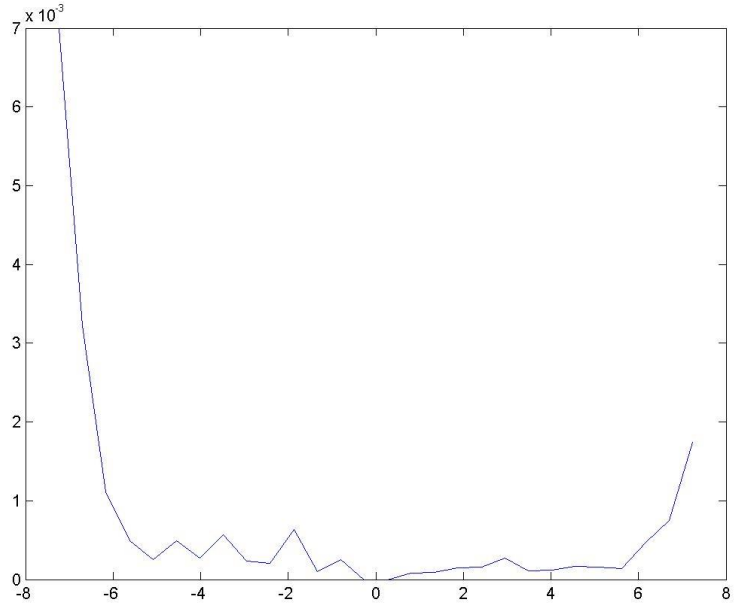

Figure C.229: Dose depth curve for (r,45,270), Design X, double beam irradiation with a 90° rotation about the vertical axis.

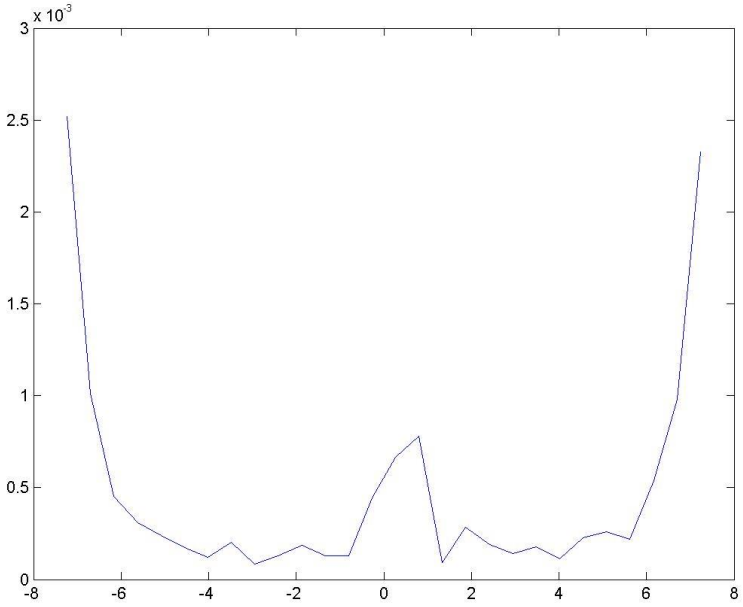

Figure C.230: Dose depth curve for (r,45,315), Design X, double beam irradiation with a 90° rotation about the vertical axis.

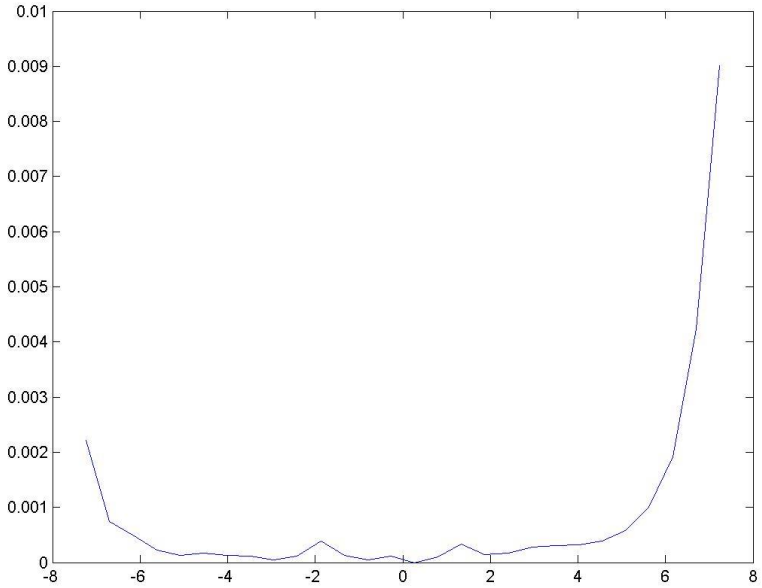

Figure C.231: Dose depth curve for (r,90,45), Design X, double beam irradiation with a 90° rotation about the vertical axis.

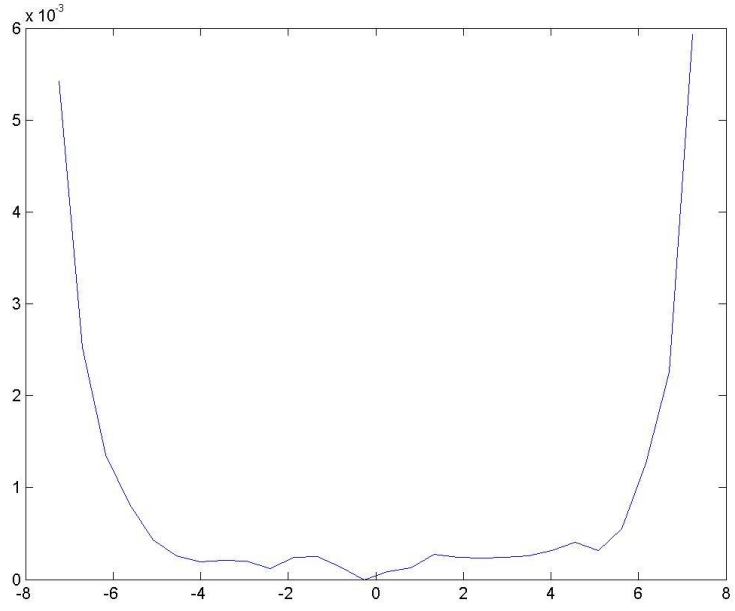

Figure C.232: Dose depth curve for (r,90,135), Design X, double beam irradiation with a 90° rotation about the vertical axis.

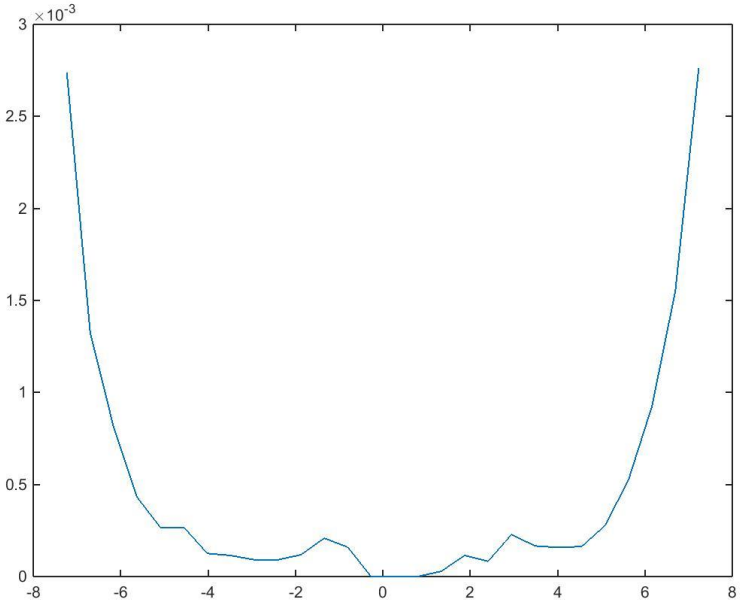

Figure C.233: Dose depth curve for (r,90,0), Design Y, single beam irradiation.

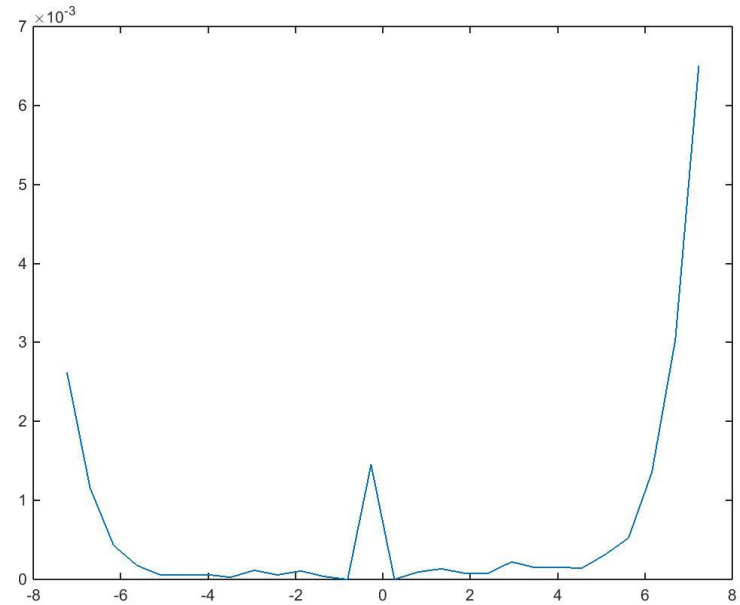

Figure C.234: Dose depth curve for (r,90,90), Design Y, single beam irradiation.

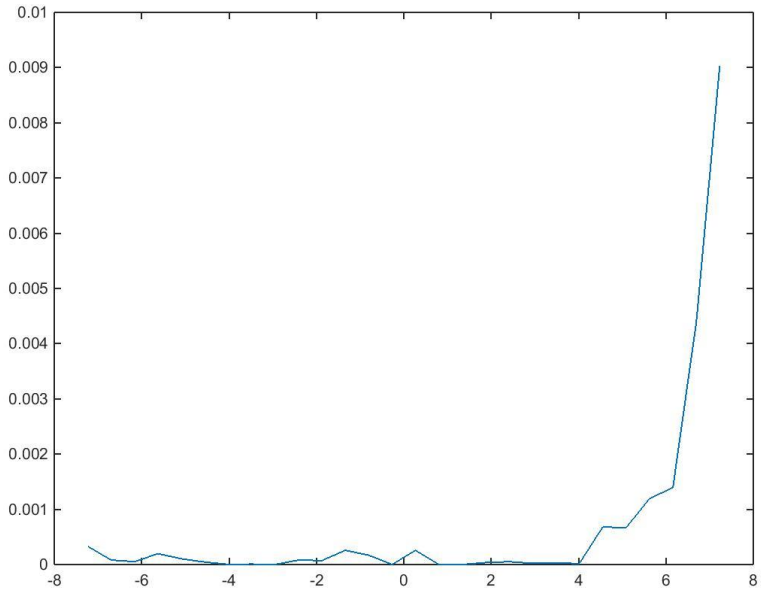

Figure C.235: Dose depth curve for (r, 0,0), Design Y, single beam irradiation.

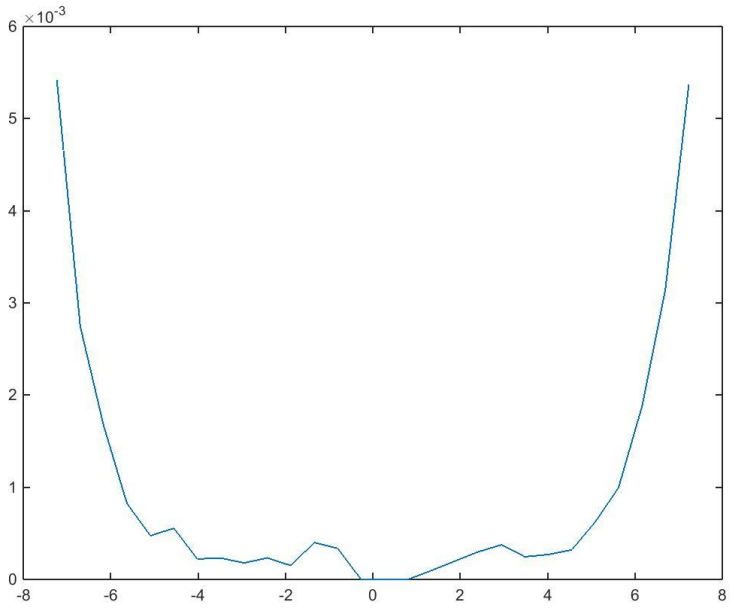

Figure C.236: Dose depth curve for (r,90,0), Design Y, double beam irradiation.

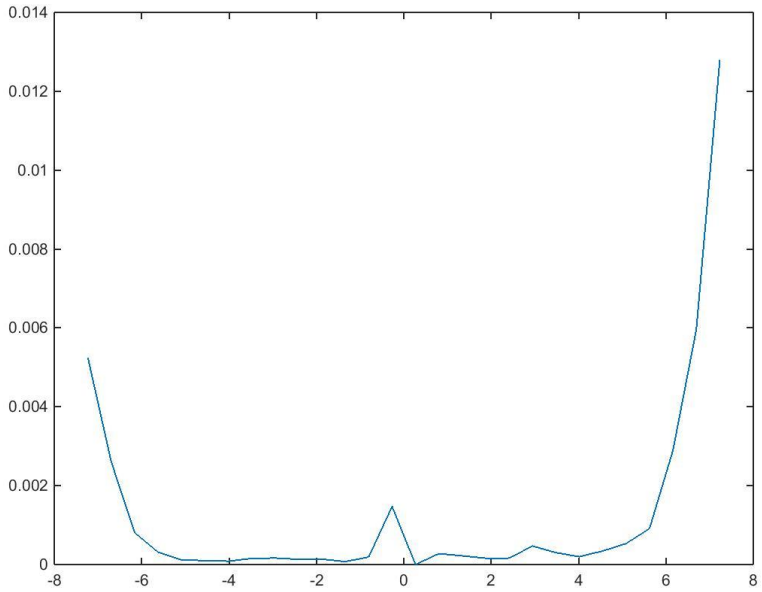

Figure C.237: Dose depth curve for (r,90,90), Design Y, double beam irradiation.

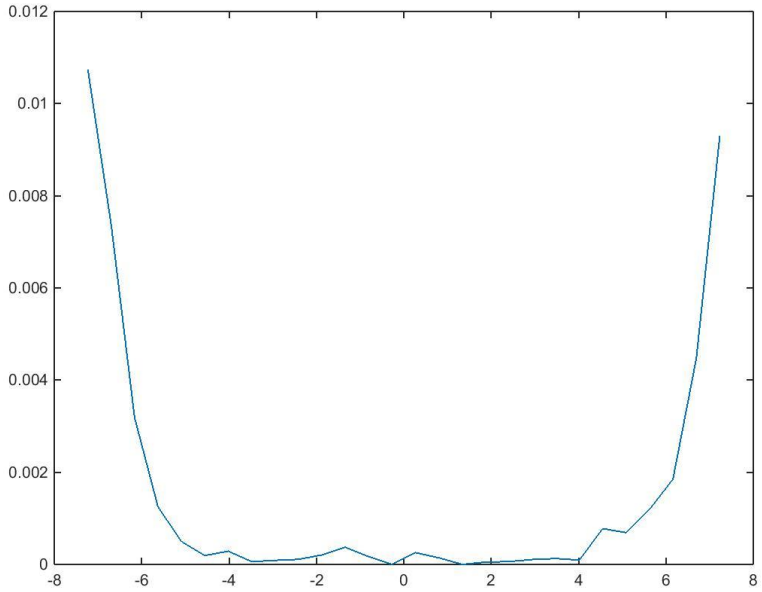

Figure C.238: Dose depth curve for (r, 0,0), Design Y, double beam irradiation.

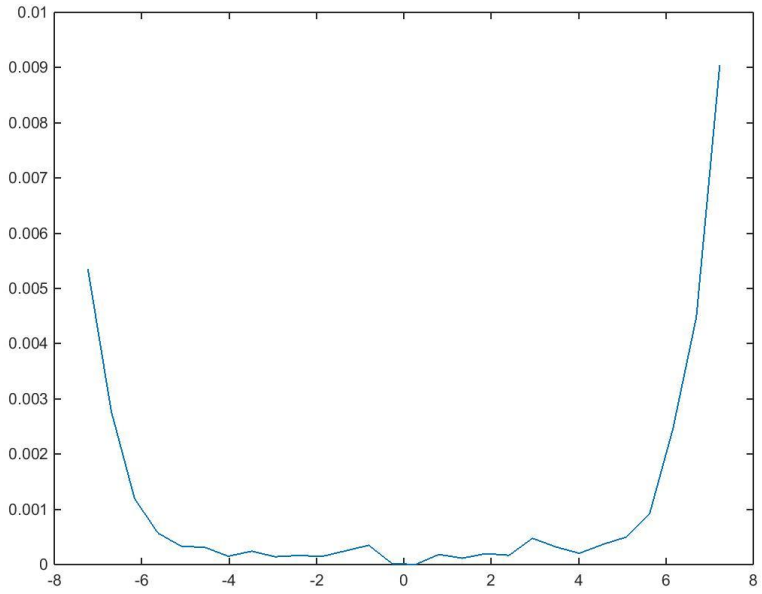

Figure C.239: Dose depth curve for (r,90,0), Design Y, double beam irradiation with a 90° rotation about the vertical axis.

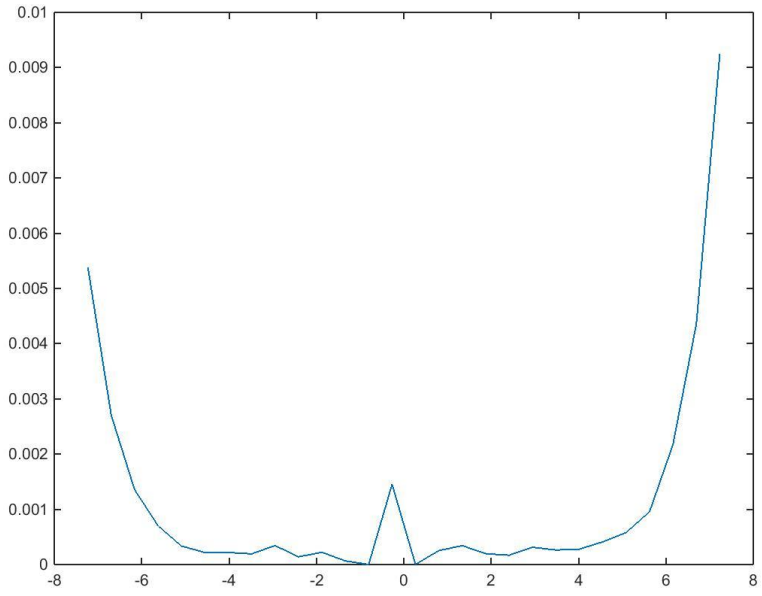

Figure C.240: Dose depth curve for (r,90,90), Design Y, double beam irradiation with a 90° rotation about the vertical axis.

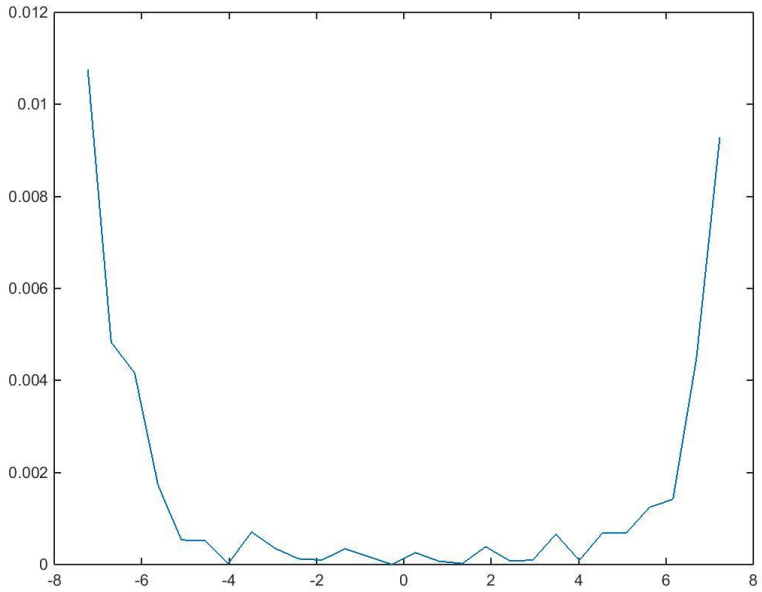

Figure C.241: Dose depth curve for (r, 0,0), Design Y, double beam irradiation with a 90° rotation about the vertical axis.

APPENDIX D

MCNPX DECKS

```
c
c 8/31/14 Design X Location 0
c
c ******************************************
c CELL CARDS
c ******************************************
   1  1  -0.998207   -1                              imp:p,e=1
   2  1  -0.998207   -2                              imp:p,e=1
c   3  1  -0.998207   -3                              imp:p,e=1
c   4  1  -0.998207   -4                              imp:p,e=1
   5  1  -0.998207   -5                              imp:p,e=1
c
  10  4  -2.698900  -10     fill=1                      imp:p,e=1     $upper plate
  11  4  -2.698900  -11 #40 #50                        imp:p,e=1     $lower plate
  40  4  -2.698900   20 -22 23 -24  40 -41  fill=5          imp:p,e=1     $side plate
  50  like 40 but TRCL 402                                              $side plate
c
  99  3  -0.001205  -999 #1 #2 #5 10 #11
                  #40  #50                      imp:p,e=1
                                              imp:p,e=1
c
 100  3  -0.001205  -100 -26 25                    u=3  imp:p,e=1
 101 like 100 but TRCL 101
 102 like 101 but TRCL 102
 103 like 100 but TRCL 103
 104 like 100 but TRCL 104
 105 like 100 but TRCL 105
 106 like 100 but TRCL 106
 107 like 100 but TRCL 107
 108 like 100 but TRCL 108
 109 like 100 but TRCL 109
 110 like 100 but TRCL 110
 111 like 100 but TRCL 111
 112 like 100 but TRCL 112
 113 like 100 but TRCL 113
 114 like 100 but TRCL 114
c
 200  3  -0.001205  -200 -26 25                    u=3  imp:p,e=1
 201 like 200 but TRCL 201
 202 like 200 but TRCL 202
```

```
 203 like 200 but TRCL 203
 204 like 200 but TRCL 204
 205 like 200 but TRCL 205
 206 like 200 but TRCL 206
 207 like 200 but TRCL 207
 208 like 200 but TRCL 208
 209 like 200 but TRCL 209
 210 like 200 but TRCL 210
 211 like 200 but TRCL 211
 212 like 200 but TRCL 212
 213 like 200 but TRCL 213
 214 like 200 but TRCL 214
c
 300  4  -2.698900  (#100 #101 #102 #103 #104 #105 #106
                #107 #108 #109 #110 #111 #112 #113
                #200 #201 #202 #203 #204 #205 #206
                #207 #208 #209 #210 #211 #212 #213
                #114 #214)                    u=3  imp:p,e=1
 301  4  -2.698900     23  -24 -300  301
                lat=1  fill=0:0 -10:10 0:0 1 3 18R 1
                                          u=1  imp:p,e=1
c
 401  4  -2.698900    401 -410                    u=9  imp:p,e=1
 402  3  -0.001205   -401 -410                    u=9  imp:p,e=1
c
 410  0            -451   fill=7                 u=5  imp:p,e=1
 411  4  -2.698900    451  -450                    u=5  imp:p,e=1
c
 450  4  -2.698900   -460  461 -462  463
                lat=1  fill=-9:10 -14:14 0:0 9 579R
                                          u=7  imp:p,e=1
c
 999  0            999                          imp:p,e=0


c
c ****************************************
c SURFACE CARDS
c ****************************************
c Note: these are changed depending on the desired cantaloupe stop
   1  SPH   0   0 0    7.5
   2  SPH   0 -30 0    7.5
c   3  SPH   0 -15 0    7.5
c   4  SPH   0  15 0    7.5
   5  SPH   0  30 0    7.5
```

```
c
  10  RPP   -10   10     -15   15       8.5  10.05
  11  RPP    -9    9     -15   15     -10    -9
  12  RPP   -10   10      -2    2      10    13
  13  RPP    -9    9      -2    2     -11   -10
c
  20  PZ   -10
  22  PZ    10
  23  PY   -15
  24  PY    15
  25  PZ     8
  26  PZ    11
c
  40  P   -10   0  -3  110
  41  P   -10   0  -3  140
c
  50  P   -10   0   3 -110
  51  P   -10   0   3 -140
c
 100  RCC   0    0.125 11.125  0  6 -6  .176777
 200  RCC   0   -0.125 11.125  0 -6 -6  .176777
 300  PX    0.5
 301  PX   -0.5
c
 401  401  SPH    0 0 0.1667    0.5
c
 410  401  RPP   -3    3    -3     3   -4 2
c
 450  401  RPP  -12   12   -15.5  15.5 -3 1
 451  401  RPP   -9.5  8.5 -14.5  14.5 -3 0.5
c
 460  401  PX    0.5
 461  401  PX   -0.5
 462  401  PY    0.5
 463  401  PY   -0.5
c
 999  SPH    0 0 0   100

c
c ****************************************
c SOURCE DEFINITION
c ****************************************
SDEF PAR=3 ERG=10 x=d1 y=d2 z=15 DIR=1 VEC=0 0 -1
SI1 -35 35
```

```
SP1   0  1
SI2  -1  1
SP2   0  1
c
CUT:e j .05
c
c ******************************************
c TALLY CARDS
c ******************************************
TR2       0  -30     0
TR3       0  -15     0
TR4       0   15     0
TR5       0   30     0
c
TR101  0   1   0
TR102  0   2   0
TR103  0   3   0
TR104  0   4   0
TR105  0   5   0
TR106  0   6   0
TR107  0   7   0
TR108  0   8   0
TR109  0   9   0
TR110  0  10   0
TR111  0  11   0
TR112  0  12   0
TR113  0  13   0
TR114  0  14   0
TR201  0  -1   0
TR202  0  -2   0
TR203  0  -3   0
TR204  0  -4   0
TR205  0  -5   0
TR206  0  -6   0
TR207  0  -7   0
TR208  0  -8   0
TR209  0  -9   0
TR210  0 -10   0
TR211  0 -11   0
TR212  0 -12   0
TR213  0 -13   0
TR214  0 -14   0
c
TR401    -11 0 0   3 0 -10  0  1 0
```

```
TR402      0 0 0  -1 0   0  0 -1 0
c
tmesh
   SMESH11:e  pedep
   CORA11     0   13i    7.5
   CORB11     1  178i  180
   CORC11     1  358i  360
c   SMESH21:e  pedep trans 2
c   CORA21     0   13i    7.5
c   CORB21     1  178i  180
c   CORC21     1  358i  360
c   SMESH31:e  pedep trans 3
c   CORA31     0   13i    7.5
c   CORB31     1  178i  180
c   CORC31     1  358i  360
c   SMESH41:e  pedep trans 4
c   CORA41     0   13i    7.5
c   CORB41     1  178i  180
c   CORC41     1  358i  360
c   SMESH51:e  pedep trans 5
c   CORA51     0   13i    7.5
c   CORB51     1  178i  180
c   CORC51     1  358i  360
endmd
c
c mplot   tally 11   free ik
c
c ******************************************
c DATA CARDS
c ******************************************
MODE P E
NPS 1e7
c
c Energy deposition tally in the 4 plates
F16:P,E 10
F46:P,E 40
F56:P,E 50
F26:P,E 11
c
c ******************************************
c MATERIAL CARDS
c ******************************************
c --- Water     0.998207
m1    1000     -0.111894
```

```
      8000     -0.888106
c
c --- SS-302    7.860000
m2     6000     -0.001400
      14000     -0.009300
      15000     -0.000420
      16000     -0.000280
      24000     -0.180000
      25000     -0.018600
      26000     -0.700000
      28000     -0.090000
c
c --- Air       0.001205
m3     6000     -0.000124
       7000     -0.755268
       8000     -0.231781
      18000     -0.012827
c
c --- Aluminum  2.698900
m4    13000     -1.000000
```